UNIVERSITY OF AMSTERDAM

UvA-DARE (Digital Academic Repository)

Zooming in on leukocyte extravasation

Discovering new pathways with innovative technologies

van Steen, A.C.I.

Publication date
2022

Document Version
Final published version

Link to publication

Citation for published version (APA):
van Steen, A. C. I. (2022). *Zooming in on leukocyte extravasation: Discovering new pathways with innovative technologies*.

General rights
It is not permitted to download or to forward/distribute the text or part of it without the consent of the author(s) and/or copyright holder(s), other than for strictly personal, individual use, unless the work is under an open content license (like Creative Commons).

Disclaimer/Complaints regulations
If you believe that digital publication of certain material infringes any of your rights or (privacy) interests, please let the Library know, stating your reasons. In case of a legitimate complaint, the Library will make the material inaccessible and/or remove it from the website. Please Ask the Library: https://uba.uva.nl/en/contact, or a letter to: Library of the University of Amsterdam, Secretariat, Singel 425, 1012 WP Amsterdam, The Netherlands. You will be contacted as soon as possible.

UvA-DARE is a service provided by the library of the University of Amsterdam (https://dare.uva.nl)

Download date:11 Nov 2022

ZOOMING IN ON LEUKOCYTE EXTRAVASATION

Discovering new pathways with innovative technologies

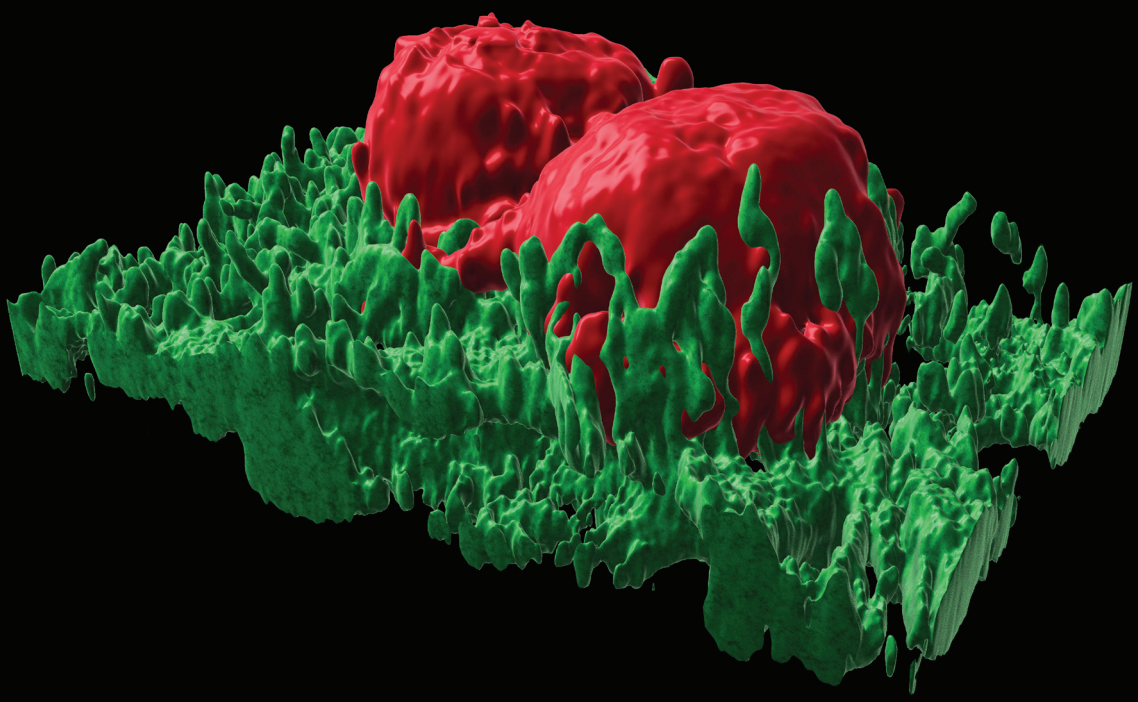

ACI VAN STEEN

Zooming in on leukocyte extravasation

Discovering new pathways with innovative technologies

A.C.I. van Steen

Cover: A.C.I. van Steen
Lay-out: Ilse Modder | www.ilsemodder.nl
Printing / binding: Gildeprint, Enschede

© 2022, A.C.I. van Steen
All rights reserved. No part of this publication may be reproduced, stored in a retrieval system, or transmitted, in any form or by any means, electronic, mechanical, photocopying, recording or otherwise, without prior written permission from the author.

Zooming in on leukocyte extravasation

Discovering new pathways with innovative technologies

ACADEMISCH PROEFSCHRIFT

ter verkrijging van de graad van doctor
aan de Universiteit van Amsterdam
op gezag van de Rector Magnificus
prof. dr. ir. P.P.C.C. Verbeek
ten overstaan van een door het College voor Promoties ingestelde commissie,
in het openbaar te verdedigen in de Agnietenkapel
op maandag 14 november 2022, te 14.00 uur

door Abraham Christoffel Ignatius van Steen
geboren te Haarlem

Promotiecommissie

Promotor:	prof. dr. J.D. van Buul	Universiteit van Amsterdam
Copromotor:	dr. M.A. Nolte	ZonMw
Overige leden:	prof. dr. T.W.J. Gadella	Universiteit van Amsterdam
	prof. dr. C.J.M. de Vries	Universiteit van Amsterdam
	prof. dr. E.A.J. Reits	Universiteit van Amsterdam
	prof. dr. R.A. Boon	Vrije Universiteit Amsterdam
	dr. S. Huveneers	AMC-UvA
	prof. dr. J.M.J. den Toonder	Eindhoven University of Technology

Faculteit der Natuurwetenschappen, Wiskunde en Informatica

CONTENTS

Chapter 1	General Introduction	9
Chapter 2	Actin remodeling of the endothelium during transendothelial migration of leukocytes	25
Chapter 3	Endothelial ICAM-1 adhesome recruits CD44 for optimal transcellular migration of human cytotoxic T lymphocytes	47
Chapter 4	The endothelial diapedesis synapse regulates transcellular migration of human T lymphocytes in a CX3CL1- and SNAP23-dependent manner	73
Chapter 5	Overlapping membrane at endothelial junctions form tunnels during neutrophil transmigration	113
Chapter 6	Transendothelial migration induces differential migration dynamics of leukocytes in tissue matrix	139
Chapter 7	Defective Neutrophil Transendothelial Migration and Lateral Motility in ARPC1B Deficiency Under Flow Conditions	169
Chapter 8	Discussion	189
Appendices	Summary	208
	Nederlandse samenvatting	210
	List of publications	213
	Acknowledgements	214

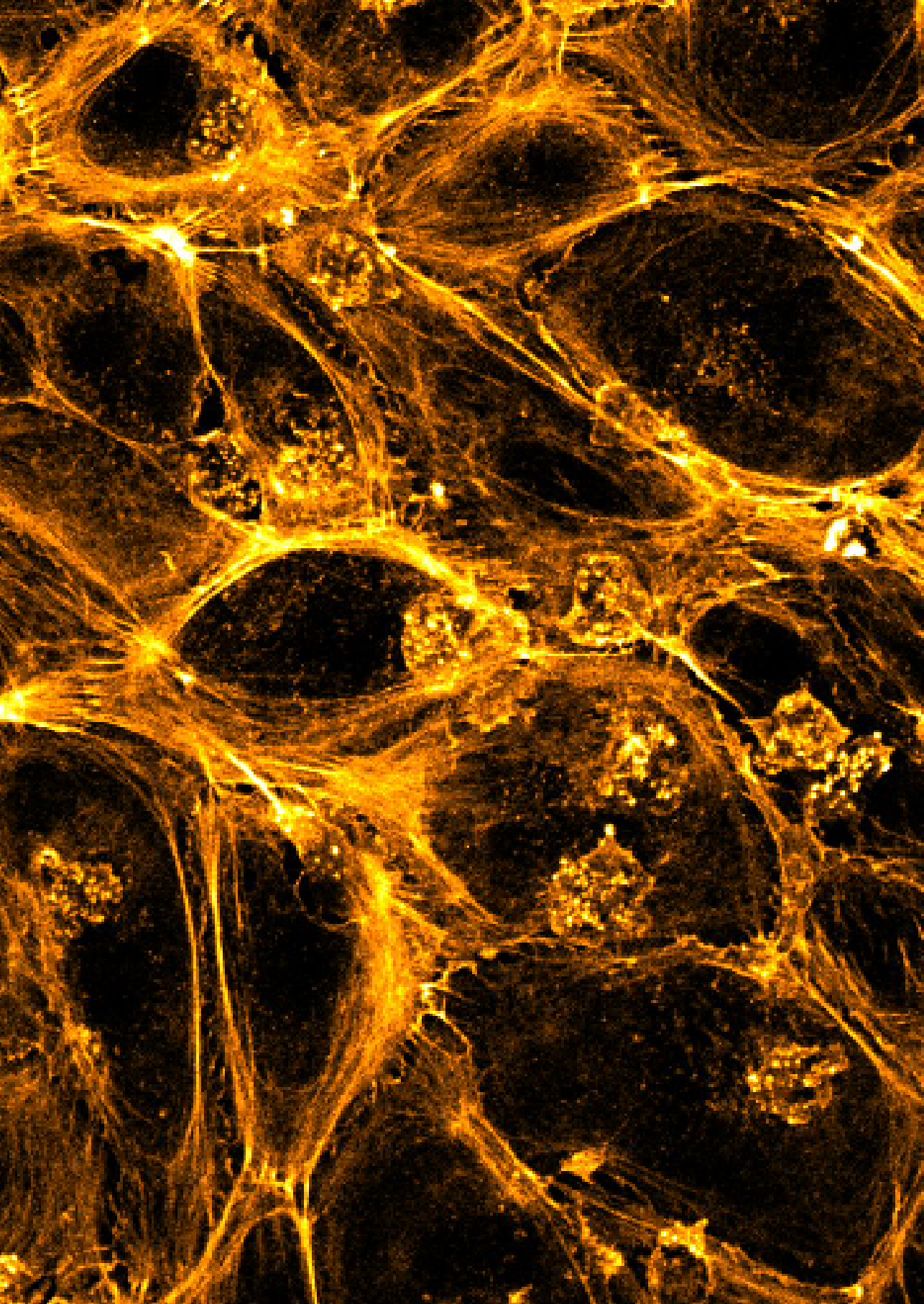

CHAPTER 1

General introduction

THE ENDOTHELIUM

Blood vessels are a crucial part of the human anatomy and allow transport of nutrients, cells, oxygen, and signaling molecules throughout the body, connecting all organs while maintaining hemostasis. This complicated task is mostly performed by the innermost layer of the blood vessels which consists of a monolayer of endothelial cells on a basement membrane. The endothelium provides a selective barrier between the tissues and the circulation. Different organs have different requirements for vascular permeability in which we can appreciate the versatility of the endothelium. The brain is a very delicate organ that is carefully separated from the bloodstream; therefore it requires a tightly regulated barrier that is very impermeable for most blood-derived components. The liver on the other hand filters toxins out of the blood and therefore needs a much more permeable barrier to allow for proper filtering by the tissue (Aird, 2007). The endothelium, therefore, adapts to these different requirements, leading to the formation of different specialized vascular beds. (Figure 1)

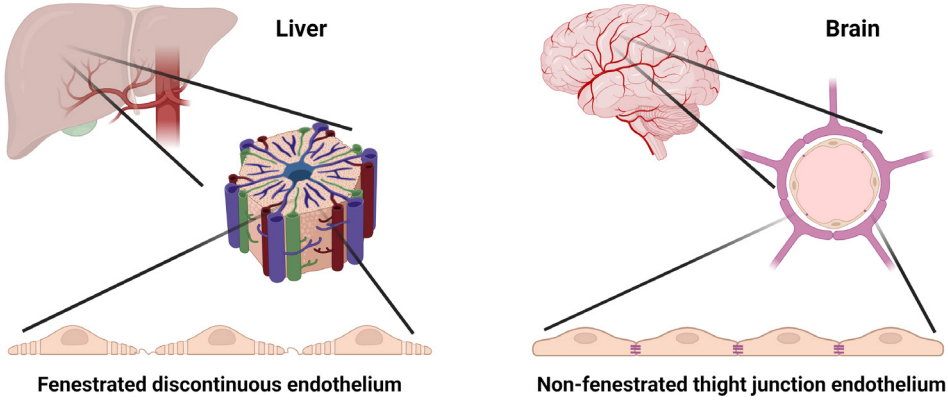

Figure 1. Endothelium adapts to the specific demands of organs, giving rise to specialized vascular beds. The liver filters blood and requires the endothelium to allow for rapid exchange of proteins leading to a discontinuous fenestrated endothelium. The blood brain barrier requires an impermeable barrier to protect the delicate brain which is provided by an impermeable barrier with tight junctions to prevent leakage.

INFLAMMATION

The vascular system is challenged when leukocytes need to migrate through this barrier into the surrounding tissue to eliminate invading pathogens. The barrier must allow leukocytes to cross while maintaining the barrier function. Leukocyte transendothelial migration (TEM) forms the basis for immune surveillance and pathogen clearance and hence plays a pivotal role in many (patho)physiological processes. The process of endothelial inflammation is induced by inflammatory stimuli such as tumor necrosis factor alpha (TNF),

lipopolysaccharides (LPS), or interleukin 1 beta (IL-1β). These signaling molecules are produced by immune activation of tissue-resident cells or derived from pathogens (Girbl et al., 2018a; Middleton et al., 2002a; Speyer & Ward, 2011a). Subsequently, the endothelium is activated, bringing it to a so-called inflamed state. This leads to a wide range of structural and protein expression changes in the endothelial cells. For example, actin stress fibers are induced, leading to increased contractility and stiffness of the endothelium (Chhabra & Higgs, 2007; Wójciak-Stothard et al., 1998).

Additional changes in the endothelium that are triggered by the inflammatory stimuli include the upregulation of adhesion molecules, such as endothelial selectin (E-selectin, CD62E), intercellular adhesion molecule 1 (ICAM-1, CD54), and vascular cell adhesion molecule 1 (VCAM-1, CD106) (McEver, 2015). Finally, the endothelium starts producing signaling molecules, such as cytokines, chemokines, and other pro-inflammatory mediators (Speyer & Ward, 2011b).

LEUKOCYTE TEM CASCADE

Under normal physiological conditions, most leukocytes do not interact with the endothelial cells that line the vessel wall. In this project we limit the scope to leukocyte extravasation upon inflammation however, it is worth noticing that several leukocyte subsets undergo non-inflammation-driven TEM. For example the extravasation of naïve T and B cells towards lymph nodes or effector memory T cells patrolling tissues in steady-state (Ariotti et al., 2012; Lewis et al., 2008; Schnoor et al., 2015). Upon inflammation and the subsequent changes that are induced in the endothelium, as described above, leukocytes start to roll and tether to the endothelial cell monolayers. The highly specialized process consists of a multi-step TEM cascade discussed in depth in Chapter 2 (Butcher, 1991). (Figure 2)

Briefly, inflamed endothelial cells express P-selectin and E-selectin which interact with P-selectin glycoprotein ligand-1 (PSGL-1) on the leukocytes to slow down the leukocytes and cause them to roll over the endothelium. This interaction has a catch-bond character, which means it becomes stronger when there is more force applied to the bond, in this case, shear stress from the blood flow (Marshall et al., 2003). During close contact from selectin-mediated rolling, the leukocytes can sense with their chemokine receptors the chemokines presented on the endothelium. Chemokines are small secreted signaling molecules that induce migration in other cells via signaling through g protein coupled receptors (GPCR). A large number of different chemokines exist as well as a large number of chemokine receptors providing this signaling system with great specificity (Hughes & Nibbs, 2018). Chemokines on the endothelium can either be produced by the endothelium itself or by inflammatory cells underlying the endothelium; in case of the latter, the extracellular chemokines can then be scavenged by the endothelium, transported from the basal side to the apical side in a process

called transcytosis, and presented on the apical surface of the endothelium (Minten et al., 2014). Scavenged chemokines are presented on the surface by scavenging receptors, such as atypical chemokine receptor 1 (ACKR-1 also known as Duffy antigen receptor, DARC), or by specific parts of the glycocalyx (Girbl et al., 2018b; Middleton et al., 2002b, 2002c). The glycocalyx of the endothelium is a layer of carbohydrate-rich molecules lining the endothelial lumen outside of the cell membrane which performs a variety of different functions such as sensing shear stress (Reitsma et al., 2007). Their ability to bind and present chemokines also prevents these soluble mediators from washing away from the inflamed site by the blood flow. These chemokines further activate the leukocyte and induces the next step: firm adhesion of the leukocyte to the endothelium (Alon & Feigelson, 2012).

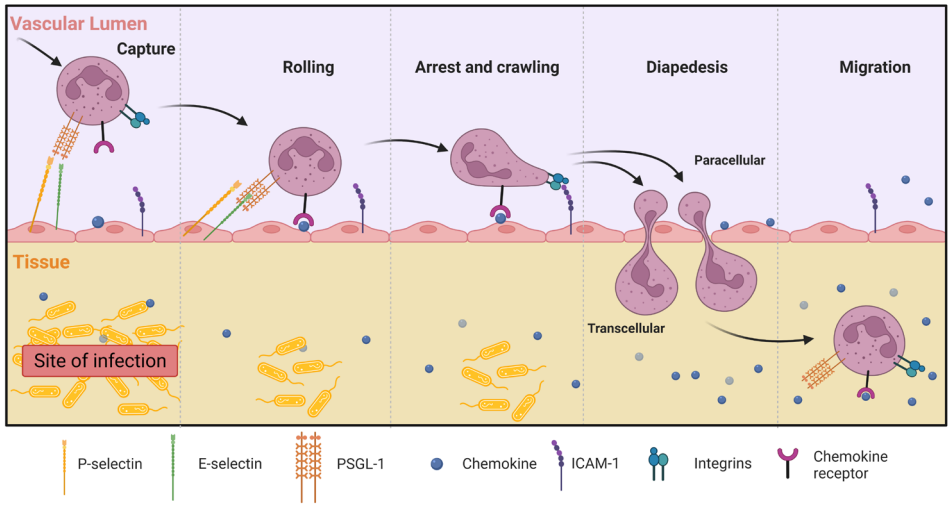

Figure 2. Schematic representation of the leukocyte TEM cascade. Leukocytes are captured from the bloodstream by endothelial selectins, which brings them in close contact with the endothelium. There they start rolling along the vessel wall, which allows chemokines on the endothelium to activate the leukocyte integrins. Integrins form high-affinity bonds with CAM molecules such as ICAM-1 on the endothelium slowing the rolling speed and leading to arrest. After arrest, the leukocyte polarizes and crawls to a suitable diapedesis site where diapedesis occurs via the transcellular or paracellular route. When the leukocyte has crossed the endothelium it detaches from the vessel and migrates into the perivascular tissue.

Leukocyte subsets express various integrins on their surface such as very late antigen-4 (VLA4), lymphocyte function associated antigen-1 (LFA-1), and macrophage antigen-1 (MAC-1) (Berlin et al., 1995; Chesnutt et al., 2006; Dunne et al., 2002). Integrins are adhesion molecules that undergo confirmational changes upon activation which sharply increases their affinity to the adhesion molecules on the endothelium such as ICAM-1 and VCAM-1 (Campbell et al., 1998; Shamri et al., 2005). The high affinity interaction between activated leukocyte integrins and their endothelial ligands provide the strong adhesion forces

required to arrest the leukocyte. Specific chemokines presented by the endothelium are very potent in activating leukocyte integrins like CXCL12, CCL21, CXCL1, CCL2, and CCL25 and have therefore been named “arrest chemokines” (Alon & Feigelson, 2012; Ley, 2003). After arrest the leukocyte can polarize and start crawling over the endothelium towards a suitable site to traverse the endothelium.

Cell adhesion molecule clustering

ICAM-1 and VCAM-1 play an important role in the TEM cascade. They are both members of the immunoglobulin-like (Ig-like) cell adhesion molecule (CAM) family, and they are both strongly upregulated upon inflammation. Before the leukocyte starts penetrating the endothelial monolayer, ICAM-1 is clustered by the leukocyte leading to the activation of downstream signaling pathways in the endothelium recruiting a larger protein complex, called the **ICAM-1-adhesome** (van Buul et al., 2010). This complex consists of a variety of actin adapter proteins. These actin adapter proteins provide a rigid actin-based structure that supports the adhesion and crawling of the leukocytes (Schaefer & Hordijk, 2015; Schimmel et al., 2018). Furthermore, an endothelial membrane structure surrounding the leukocyte, also known as the transmigratory cup, or docking structure, is induced via RhoG signaling downstream of ICAM-1(Barreiro et al., 2002; Carman & Springer, 2004; van Buul et al., 2007). This structure is involved in limiting vascular leakage during transmigration (Heemskerk et al., 2016).

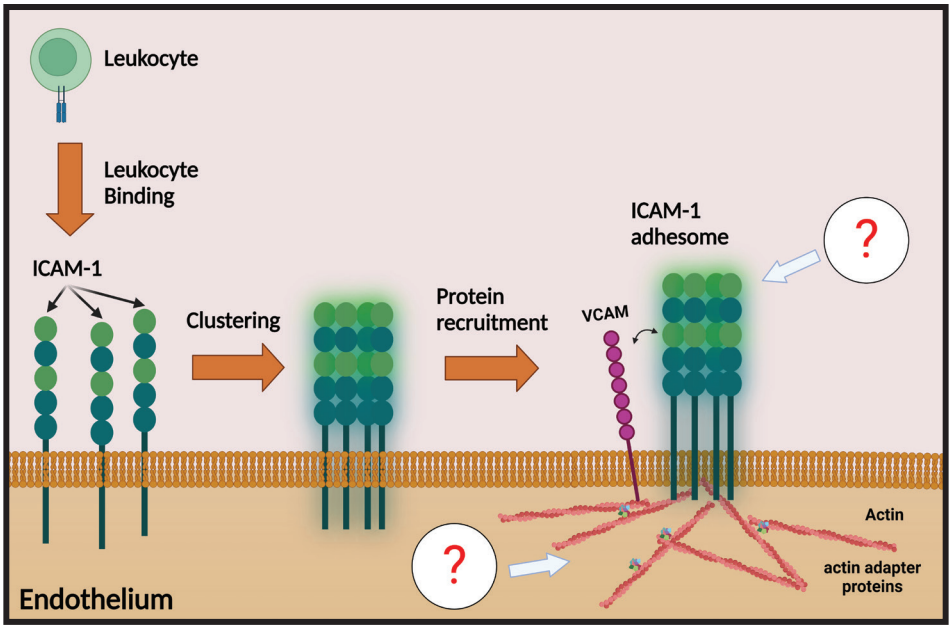

Figure 3. ICAM-1 is clustered by leukocyte integrins upon binding. This activates intracellular G proteins leading to the recruitment of a large number of different membrane and intracellular molecules. This ICAM-1 clustering adhesome contains actin and various actin adapter proteins as well as VCAM.

DIAPEDESIS

The final stage of the leukocyte TEM cascade is the actual migration of the leukocyte through the endothelium. A leukocyte can go through the endothelium in two ways: through the cell-to-cell junctions between two adjacent endothelial cells, called the paracellular route, or immediately through the cell body of an endothelial cell, called the transcellular route.

Paracellular route: Leukocyte extravasation primarily occurs in postcapillary venules, where junctions between endothelial cells are formed by adherens junctions that allow for the transient opening of the barrier to allow leukocytes to pass (Feng et al., 1998; McDonald, 1994). Adherens junctions are formed by vascular endothelial cadherin (VE-cadherin/CD144), platelet endothelial cell adhesion molecule 1 (PECAM-1/CD31), as well as various junctional adhesion molecules (JAMs) (Dejana & Vestweber, 2013; Vestweber, 2015). It is believed that these junctional protein complexes need to be disassembled to allow a leukocyte to pass. The disassembling may be induced upon signaling derived from the adhering leukocyte or by physical forces from the leukocyte forcing the junction to open and allowing the leukocyte to cross in a paracellular manner (Barzilai et al., 2017; Dejana & Vestweber, 2013). Although most leukocytes prefer to cross the endothelium in a paracellular manner, it is still not clear how the junctional proteins are removed from the junction regions. This remains a topic of debate in the field.

Transcellular route: There is much less known about the transcellular route of migration. Our group recently showed that specific chemokines like fractalkine/CX3CL1 may trigger local transcellular migration of T-cell subsets, i.e., effector memory T-cells, whereas other subsets, i.e., central memory T-cells prefer the paracellular migration route (Schoppmeyer et al., 2022). Further work from our group and other groups showed that preference for the route of transmigration depends on leukocyte subset, inflammation, and vascular bed (Abadier et al., 2015; Carman et al., 2007; Heemskerk et al., 2016; Martinelli et al., 2014).

After crossing the endothelium, the leukocytes enter the final step of the TEM cascade: the crossing of the basal membrane and migration into the tissue. This sounds like a trivial step, though recent findings show that delicate signaling interplay is also required to successfully complete this step. Aging can lead to an over presentation of chemokines which dysregulates neutrophils after diapedesis, leading to reverse transmigration back into the bloodstream where they induce damage in remote organs (Barkaway et al., 2021).

LEUKOCYTE EXTRAVASATION IS A RAPID LOCAL EVENT

The complete process of transmigration typically takes a neutrophil less than one minute from the beginning to the end of the process (Kempers et al., 2021). Within this timespan, all different steps of the TEM cascade are completed, including signaling activation of integrins, recruitment of the ICAM-1 adhesome and dissociation and recovery of the endothelial junction integrity. Besides all the steps of this process occurring in a strict and properly timed sequence, this process is also locally regulated, as opening of the endothelial barrier occurs only at the specific location where leukocytes cross. All processes are locally regulated and sequential but do occur in different sites in the blood vessel, selectin binding takes place under flow inside the lumen while migration into the tissue takes place at the interface between the endothelium and the tissue. Ideally, one wishes to capture all these events in one experimental assay. This has been notoriously difficult to achieve, because of technical limitations. Using a Transwell system, most focus is on the number of leukocytes that have crossed the endothelium. The advantages of this system are its simplicity, which is also its disadvantage, as it lacks the presence of flow and the option to allow microscopy analysis. The introduction of the so-called flow chamber allowed to study of the role of flow on TEM as well as microscopy imaging; however, it does not have the option for leukocytes to continue migrating after diapedesis, as these chambers have a glass bottom.

In vivo studies offer an alternative to *in vitro* models, however, these come with considerable ethical and technical challenges (Russell & Burch, 1959). Imaging leukocyte extravasation in mice comes with great challenges such as mounting the animal under a microscope, heartbeat and breathing induced movement, extra tissue obstructing the view, and fewer possibilities to manipulate the system. Furthermore, experiments in mice are time-consuming and expensive compared to in vitro experiments. Furthermore, mice are different from humans and biological pathways in mice, although often similar at first glance are often difficult to translate to humans (Leenaars et al., 2019).

Recent emphasis has been on the development of a so-called *vessel-on-a-chip*. In the section below, I will briefly discuss the advances made in this field. To overcome the aforementioned pitfalls of current techniques, the field of leukocyte extravasation has been looking for assays to study such a spatiotemporally regulated process in detail. An ideal model would allow researchers to study the complete TEM cascade from the initial rolling processes in the bloodstream until the migration through the extravascular “tissue”. In this ideal experimental set-up, the endothelium would have to grow on a substrate of physiological stiffness that can be enhanced with additional cell types such as neurons or pericytes. Moreover, the model should be convenient to image, for example by confocal microscopy, allowing researchers to capture local and fast events.

BLOOD VESSEL-ON-A-CHIP

Organ-on-a-chip is a broad term used for models that mimics specific functions of organs in a microenvironment *in vitro* setting. Over the past decade this field and specifically the blood vessel on a chip (BVOAC) field have been making rapid progress. A wide variety of methods have been developed to create BVOAC with varying degrees of complexity, and possible applications.(Pollet & den Toonder, 2020) These vessels can generally be separated into 2 different types: hydrogel-based systems in which a lumen is created in a hydrogel, and systems based on stiff substrates such as membranes and tissue culture plastic (Farahat et al., 2012; Kim et al., 2016; Sobrino et al., 2016; Wong et al., 2012; Zervantonakis et al., 2012; Zheng et al., 2012). Other differences can be seen in the possibilities to perfuse the BVOAC, the complexity of the system and the reproducibility. A commercially available BVOAC device is the 2 lane Organoplate developed by Mimetas, which is specifically designed for screening purposes. (van Duinen et al., 2017) This system can be seeded with a multichannel pipette and its simple geometry leads to reproducible results. A downside to this system is that the BVOAC is surrounded on 3 sides by tissue culture plastic, reducing the physiological relevance. The LumeNext model does have the endothelium completely embedded in a hydrogel, making the conditions closer to physiological situation in vivo and has 6 devices on a chip (Jiménez-Torres et al., 2016). However continuous perfusion of the LumeNext devices is not possible and the production method as well as BVOAC creation protocols are difficult leading larger variances between BVOAC.

SCOPE OF THIS THESIS

In this thesis, we aim to get a better understanding of the leukocyte TEM cascade. We do this by exploring the pathways induced by leukocyte induced ICAM-1 clustering on inflamed endothelium. Simultaneously we aim to develop new *in vitro* tools to study the TEM cascade by deploying BVOAC systems to develop a leukocyte TEM assay. This two-pronged approach both zooms in on the detailed signaling involved in this process as well as zooming out to study the integral process.

Chapter 2 concentrates on how the endothelial actin cytoskeleton contributes to leukocyte transendothelial migration upon inflammation. In this review we focus on the diapedesis step of extravasation and how this final step can be differentiated into sub-steps. Moreover, we discuss the differences in regulation of the paracellular and transcellular migration using different assays.

Chapter 3 zooms in on the effects of ICAM-1 clustering upon leukocyte transmigration and we perform a proteomic analysis of the proteins recruited to the ICAM-1-adhesome.

We select CD44 as one of the top hits and show how this protein plays a key role in the regulation of ICAM-1 and extravasation of cytotoxic T-lymphocytes (CTLs).

In **Chapter 4,** we focus on SNAP23, one of the positive hits from the ICAM-1-adhesome and show that it plays a crucial role in transcellular diapedesis of CTLs. In this chapter we find that local SNAP-23-mediated release of chemokines is a crucial step in transcellular diapedesis. Blocking this release or reducing SNAP23 expression by RNAi approach inhibits the transcellular migration route of CTLs.

Chapter 5 explores the details of junctional architecture and describes overlapping parts of the plasma membrane between two neighboring endothelial cells. These overlapping membranes typically occur at junction regions and guide paracellular transmigration of neutrophils. Furthermore, this study describes how neutrophils traverse these overlapping membrane junctions by the formation of a transient TEM tunnel.

In **Chapter 6,** we take a different approach: we have set up a new method to study leukocyte migration as an integral process. We generate a BVOAC as a leukocyte extravasation model and use this to study the TEM cascade as a whole: from rolling, capturing from the bloodstream, crossing the endothelium and migration into the perivascular “tissue”.

Chapter 7 applies this novel BVOAC assay to characterize the migration defect in neutrophils of a patient with a deletion of the ARPC1B gene. This study demonstrates the strengths of our model as a new tool to study leukocyte extravasation.

In **Chapter 8,** we discuss the research findings from this thesis and put this in broader perspective. We discuss the implications of the newly described members of the ICAM-1-adhesome described in **Chapter 3** and **4** as well as their functions. The implications of overlapping membranes and the transient tunnels neutrophils create together with the overlapping membranes of the endothelium during transmigration, as described in **Chapter 5**, opens a new paradigm on the endothelial junction, which is explored in more detail in this chapter. Furthermore, we discuss the future of *in vitro* leukocyte extravasation studies and possibilities created by our new model described in **Chapter 6**. Finally, we discuss the findings and possible leads based on the patient data from **Chapter 7**.

REFERENCES

Abadier, M., Haghayegh Jahromi, N., Cardoso Alves, L., Boscacci, R., Vestweber, D., Barnum, S., Deutsch, U., Engelhardt, B., & Lyck, R. (2015). Cell surface levels of endothelial ICAM-1 influence the transcellular or paracellular T-cell diapedesis across the blood-brain barrier. *European Journal of Immunology*, *45*(4), 1043–1058. https://doi.org/10.1002/EJI.201445125

Aird, W. C. (2007). Phenotypic heterogeneity of the endothelium: II. Representative vascular beds. *Circulation Research*, *100*(2), 174–190. https://doi.org/10.1161/01.RES.0000255690.03436.ae

Alon, R., & Feigelson, S. W. (2012). Chemokine-triggered leukocyte arrest: force-regulated bi-directional integrin activation in quantal adhesive contacts. *Current Opinion in Cell Biology*, *24*(5), 670–676. https://doi.org/10.1016/J.CEB.2012.06.001

Ariotti, S., Beltman, J. B., Chodaczek, G., Hoekstra, M. E., van Beek, A. E., Gomez-Eerland, R., Ritsma, L., van Rheenen, J., Marée, A. F. M., Zal, T., de Boer, R. J., Haanen, J. B. A. G., & Schumacher, T. N. (2012). Tissue-resident memory CD8+ T cells continuously patrol skin epithelia to quickly recognize local antigen. *Proceedings of the National Academy of Sciences of the United States of America*, *109*(48), 19739–19744. https://doi.org/10.1073/PNAS.1208927109/SUPPL_FILE/SM08.MOV

Barkaway, A., Rolas, L., Joulia, R., Bodkin, J., Lenn, T., Owen-Woods, C., Reglero-Real, N., Stein, M., Vázquez-Martínez, L., Girbl, T., Poston, R. N., Golding, M., Saleeb, R. S., Thiriot, A., von Andrian, U. H., Duchene, J., Voisin, M. B., Bishop, C. L., Voehringer, D., … Nourshargh, S. (2021). Age-related changes in the local milieu of inflamed tissues cause aberrant neutrophil trafficking and subsequent remote organ damage. *Immunity*, *54*(7), 1494-1510.e7. https://doi.org/10.1016/J.IMMUNI.2021.04.025

Barreiro, O., Yáñez-Mó, M., Serrador, J. M., Montoya, M. C., Vicente-Manzanares, M., Tejedor, R., Furthmayr, H., & Sánchez-Madrid, F. (2002). Dynamic interaction of VCAM-1 and ICAM-1 with moesin and ezrin in a novel endothelial docking structure for adherent leukocytes. *The Journal of Cell Biology*, *157*(7), 1233–1245. https://doi.org/10.1083/JCB.200112126

Barzilai, S., Yadav, S. K., Morrell, S., Roncato, F., Klein, E., Stoler-Barak, L., Golani, O., Feigelson, S. W., Zemel, A., Nourshargh, S., & Alon, R. (2017). Leukocytes Breach Endothelial Barriers by Insertion of Nuclear Lobes and Disassembly of Endothelial Actin Filaments. *Cell Reports*, *18*(3), 685–699. https://doi.org/10.1016/J.CELREP.2016.12.076

Berlin, C., Bargatze, R. F., Campbell, J. J., von Andrian, U. H., Szabo, M. C., Hasslen, S. R., Nelson, R. D., Berg, E. L., Erlandsen, S. L., & Butcher, E. C. (1995). α4 integrins mediate lymphocyte attachment and rolling under physiologic flow. *Cell*, *80*(3), 413–422. https://doi.org/10.1016/0092-8674(95)90491-3

Butcher, E. C. (1991). Leukocyte-endothelial cell recognition: Three (or more) steps to specificity and diversity. *Cell*, *67*(6), 1033–1036. https://doi.org/10.1016/0092-8674(91)90279-8

Campbell, J. J., Hedrick, J., Zlotnik, A., Siani, M. A., Thompson, D. A., & Butcher, E. C. (1998). Chemokines and the Arrest of Lymphocytes Rolling Under Flow Conditions. *Science*, *279*(5349), 381–384. https://doi.org/10.1126/SCIENCE.279.5349.381

Carman, C. v., Sage, P. T., Sciuto, T. E., de la Fuente, M. A., Geha, R. S., Ochs, H. D. D., Dvorak, H. F., Dvorak, A. M., & Springer, T. A. (2007). Transcellular Diapedesis Is Initiated by Invasive Podosomes. *Immunity*, *26*(6), 784. https://doi.org/10.1016/J.IMMUNI.2007.04.015

Carman, C. v., & Springer, T. A. (2004). A transmigratory cup in leukocyte diapedesis both through individual vascular endothelial cells and between them. *The Journal of Cell Biology*, *167*(2), 377–388. https://doi.org/10.1083/JCB.200404129

Chesnutt, B. C., Smith, D. F., Raffler, N. A., Smith, M. L., White, E. J., & Ley, K. (2006). Induction of LFA-1-dependent neutrophil rolling on ICAM-1 by engagement of E-selectin. *Microcirculation*, *13*(2), 99–109. https://doi.org/10.1080/10739680500466376

Chhabra, E. S., & Higgs, H. N. (2007). The many faces of actin: matching assembly factors with cellular structures. *Nature Cell Biology 2007 9:10*, *9*(10), 1110–1121. https://doi.org/10.1038/ncb1007-1110

Dejana, E., & Vestweber, D. (2013). The Role of VE-Cadherin in Vascular Morphogenesis and Permeability Control. *Progress in Molecular Biology and Translational Science*, *116*, 119–144. https://doi.org/10.1016/B978-0-12-394311-8.00006-6

Dunne, J. L., Ballantyne, C. M., Beaudet, A. L., & Ley, K. (2002). Control of leukocyte rolling velocity in TNF-α–induced inflammation by LFA-1 and Mac-1. *Blood*, *99*(1), 336–341. https://doi.org/10.1182/BLOOD.V99.1.336

Farahat, W. A., Wood, L. B., Zervantonakis, I. K., Schor, A., Ong, S., Neal, D., Kamm, R. D., & Asada, H. H. (2012). Ensemble Analysis of Angiogenic Growth in Three-Dimensional Microfluidic Cell Cultures. *PLOS ONE*, *7*(5), e37333. https://doi.org/10.1371/JOURNAL.PONE.0037333

Feng, D., Nagy, J. A., Pyne, K., Dvorak, H. F., & Dvorak, A. M. (1998). Neutrophils emigrate from venules by a transendothelial cell pathway in response to FMLP. *The Journal of Experimental Medicine*, *187*(6), 903–915. https://doi.org/10.1084/JEM.187.6.903

Girbl, T., Lenn, T., Perez, L., Rolas, L., Barkaway, A., Thiriot, A., del Fresno, C., Lynam, E., Hub, E., Thelen, M., Graham, G., Alon, R., Sancho, D., von Andrian, U. H., Voisin, M. B., Rot, A., & Nourshargh, S. (2018a). Distinct Compartmentalization of the Chemokines CXCL1 and CXCL2 and the Atypical Receptor ACKR1 Determine Discrete Stages of Neutrophil Diapedesis. *Immunity*, *49*(6), 1062-1076.e6. https://doi.org/10.1016/J.IMMUNI.2018.09.018

Girbl, T., Lenn, T., Perez, L., Rolas, L., Barkaway, A., Thiriot, A., del Fresno, C., Lynam, E., Hub, E., Thelen, M., Graham, G., Alon, R., Sancho, D., von Andrian, U. H., Voisin, M. B., Rot, A., & Nourshargh, S. (2018b). Distinct Compartmentalization of the Chemokines CXCL1 and CXCL2 and the Atypical Receptor ACKR1 Determine Discrete Stages of Neutrophil Diapedesis. *Immunity*, *49*(6), 1062-1076.e6. https://doi.org/10.1016/J.IMMUNI.2018.09.018

Heemskerk, N., Schimmel, L., Oort, C., van Rijssel, J., Yin, T., Ma, B., van Unen, J., Pitter, B., Huveneers, S., Goedhart, J., Wu, Y., Montanez, E., Woodfin, A., & van Buul, J. D. (2016). F-actin-rich contractile endothelial pores prevent vascular leakage during leukocyte diapedesis through local RhoA signalling. *Nature Communications 2016 7:1*, *7*(1), 1–17. https://doi.org/10.1038/ncomms10493

Hughes, C. E., & Nibbs, R. J. B. (2018). A guide to chemokines and their receptors. *The Febs Journal*, *285*(16), 2944. https://doi.org/10.1111/FEBS.14466

Jiménez-Torres, J. A., Peery, S. L., Sung, K. E., & Beebe, D. J. (2016). LumeNEXT: A Practical Method to Pattern Luminal Structures in ECM Gels. *Advanced Healthcare Materials*, *5*(2), 198–204. https://doi.org/10.1002/ADHM.201500608

Kempers, L., Sprenkeler, E. G. G., van Steen, A. C. I., van Buul, J. D., & Kuijpers, T. W. (2021). Defective Neutrophil Transendothelial Migration and Lateral Motility in ARPC1B Deficiency Under Flow Conditions. *Frontiers in*

Immunology, *12*. https://doi.org/10.3389/FIMMU.2021.678030

Kim, S., Chung, M., Ahn, J., Lee, S., & Jeon, N. L. (2016). Interstitial flow regulates the angiogenic response and phenotype of endothelial cells in a 3D culture model. *Lab on a Chip*, *16*(21), 4189–4199. https://doi.org/10.1039/C6LC00910G

Leenaars, C. H. C., Kouwenaar, C., Stafleu, F. R., Bleich, A., Ritskes-Hoitinga, M., de Vries, R. B. M., & Meijboom, F. L. B. (2019). Animal to human translation: A systematic scoping review of reported concordance rates. *Journal of Translational Medicine*, *17*(1), 1–22. https://doi.org/10.1186/S12967-019-1976-2/FIGURES/11

Lewis, M., Tarlton, J. F., & Cose, S. (2008). Memory versus naive T-cell migration. *Immunology and Cell Biology*, *86*(3), 226–231. https://doi.org/10.1038/SJ.ICB.7100132

Ley, K. (2003). Arrest chemokines. *Microcirculation (New York, N.Y. : 1994)*, *10*(3–4), 289–295. https://doi.org/10.1038/SJ.MN.7800194

Marshall, B. T., Long, M., Piper, J. W., Yago, T., McEver, R. P., & Zhu, C. (2003). Direct observation of catch bonds involving cell-adhesion molecules. *Nature 2003 423:6936*, *423*(6936), 190–193. https://doi.org/10.1038/nature01605

Martinelli, R., Zeiger, A. S., Whitfield, M., Sciuto, T. E., Dvorak, A., van Vliet, K. J., Greenwood, J., & Carman, C. v. (2014). Probing the biomechanical contribution of the endothelium to lymphocyte migration: Diapedesis by the path of least resistance. *Journal of Cell Science*, *127*(17), 3720–3734. https://doi.org/10.1242/JCS.148619/VIDEO-7

McDonald, D. M. (1994). Endothelial gaps and permeability of venules in rat tracheas exposed to inflammatory stimuli. *Https://Doi.Org/10.1152/Ajplung.1994.266.1.L61*, *266*(1 10-1). https://doi.org/10.1152/AJPLUNG.1994.266.1.L61

McEver, R. P. (2015). Selectins: initiators of leucocyte adhesion and signalling at the vascular wall. *Cardiovascular Research*, *107*(3), 331–339. https://doi.org/10.1093/CVR/CVV154

Middleton, J., Patterson, A. M., Gardner, L., Schmutz, C., & Ashton, B. A. (2002a). Leukocyte extravasation: chemokine transport and presentation by the endothelium. *Blood*, *100*(12), 3853–3860. https://doi.org/10.1182/BLOOD.V100.12.3853

Middleton, J., Patterson, A. M., Gardner, L., Schmutz, C., & Ashton, B. A. (2002b). Leukocyte extravasation: chemokine transport and presentation by the endothelium. *Blood*, *100*(12), 3853–3860. https://doi.org/10.1182/BLOOD.V100.12.3853

Middleton, J., Patterson, A. M., Gardner, L., Schmutz, C., & Ashton, B. A. (2002c). Leukocyte extravasation: chemokine transport and presentation by the endothelium. *Blood*, *100*(12), 3853–3860. https://doi.org/10.1182/BLOOD.V100.12.3853

Minten, C., Alt, C., Gentner, M., Frei, E., Deutsch, U., Lyck, R., Schaeren-Wiemers, N., Rot, A., & Engelhardt, B. (2014). DARC shuttles inflammatory chemokines across the blood–brain barrier during autoimmune central nervous system inflammation. *Brain*, *137*(5), 1454–1469. https://doi.org/10.1093/BRAIN/AWU045

Pollet, A. M. A. O., & den Toonder, J. M. J. (2020). Recapitulating the Vasculature Using Organ-On-Chip Technology. *Bioengineering 2020, Vol. 7, Page 17*, *7*(1), 17. https://doi.org/10.3390/BIOENGINEERING7010017

Reitsma, S., Slaaf, D. W., Vink, H., van Zandvoort, M. A. M. J., & Oude Egbrink, M. G. A. (2007). The endothelial glycocalyx: composition, functions, and visualization. *Pflugers Archiv : European Journal of Physiology*, *454*(3), 345–359. https://doi.org/10.1007/S00424-007-0212-8

Russell, W. M. S., & Burch, R. L. (1959). *The principles of humane experimental technique*. Methuen.

Schaefer, A., & Hordijk, P. L. (2015). Cell stiffness-induced mechanosignaling – a key driver of leukocyte transendothelial migration. *J Cell Sci*, jcs.163055. https://doi.org/10.1242/JCS.163055

Schimmel, L., van der Stoel, M., Rianna, C., van Stalborch, A.-M., de Ligt, A., Hoogenboezem, M., Tol, S., van Rijssel, J., Szulcek, R., Bogaard, H. J., Hofmann, P., Boon, R., Radmacher, M., de Waard, V., Huveneers, S., & van Buul, J. D. (2018). Stiffness-Induced Endothelial DLC-1 Expression Forces Leukocyte Spreading through Stabilization of the ICAM-1 Adhesome. *Cell Reports*, *24*(12), 3115–3124. https://doi.org/10.1016/J.CELREP.2018.08.045

Schnoor, M., Alcaide, P., Voisin, M. B., & van Buul, J. D. (2015). Crossing the Vascular Wall: Common and Unique Mechanisms Exploited by Different Leukocyte Subsets during Extravasation. *Mediators of Inflammation*, *2015*. https://doi.org/10.1155/2015/946509

Schoppmeyer, R., van Steen, A. C. I., Kempers, L., Timmerman, A. L., Nolte, M. A., Hombrink, P., van Buul Correspondence, J. D., & van Buul, J. D. (2022). The endothelial diapedesis synapse regulates transcellular migration of human T lymphocytes in a CX3CL1- and SNAP23-dependent manner. *CellReports*, *38*, 110243. https://doi.org/10.1016/j.celrep.2021.110243

Shamri, R., Grabovsky, V., Gauguet, J. M., Feigelson, S., Manevich, E., Kolanus, W., Robinson, M. K., Staunton, D. E., von Andrian, U. H., & Alon, R. (2005). Lymphocyte arrest requires instantaneous induction of an extended LFA-1 conformation mediated by endothelium-bound chemokines. *Nature Immunology 2005 6:5*, *6*(5), 497–506. https://doi.org/10.1038/ni1194

Sobrino, A., Phan, D. T. T., Datta, R., Wang, X., Hachey, S. J., Romero-López, M., Gratton, E., Lee, A. P., George, S. C., & Hughes, C. C. W. (2016). 3D microtumors in vitro supported by perfused vascular networks. *Scientific Reports 2016 6:1*, *6*(1), 1–11. https://doi.org/10.1038/srep31589

Speyer, C. L., & Ward, P. A. (2011a). Role of Endothelial Chemokines and Their Receptors during Inflammation. *Http://Dx.Doi.Org/10.3109/08941939.2010.521232*, *24*(1), 18–27. https://doi.org/10.3109/08941939.2010.521232

Speyer, C. L., & Ward, P. A. (2011b). Role of Endothelial Chemokines and Their Receptors during Inflammation. *Http://Dx.Doi.Org/10.3109/08941939.2010.521232*, *24*(1), 18–27. https://doi.org/10.3109/08941939.2010.521232

van Buul, J. D., Allingham, M. J., Samson, T., Meller, J., Boulter, E., García-Mata, R., & Burridge, K. (2007). RhoG regulates endothelial apical cup assembly downstream from ICAM1 engagement and is involved in leukocyte trans-endothelial migration. *The Journal of Cell Biology*, *178*(7), 1279. https://doi.org/10.1083/JCB.200612053

van Buul, J. D., van Rijssel, J., van Alphen, F. P. J., Hoogenboezem, M., Tol, S., Hoeben, K. A., van Marle, J., Mul, E. P. J., & Hordijk, P. L. (2010). Inside-Out Regulation of ICAM-1 Dynamics in TNF-α-Activated Endothelium. *PLoS ONE*, *5*(6), e11336. https://doi.org/10.1371/journal.pone.0011336

van Duinen, V., van den Heuvel, A., Trietsch, S. J., Lanz, H. L., van Gils, J. M., van Zonneveld, A. J., Vulto, P., & Hankemeier, T. (2017). 96 perfusable blood vessels to study vascular permeability in vitro. *Scientific Reports 2017 7:1*, *7*(1), 1–11. https://doi.org/10.1038/s41598-017-14716-y

Vestweber, D. (2015). How leukocytes cross the vascular endothelium. *Nature Reviews Immunology*, *15*(11), 692–704. https://doi.org/10.1038/nri3908

Wójciak-Stothard, B., Entwistle, A., Garg, R., & Ridley, A. J. (1998). Regulation of TNF-α-induced reorganization of the actin cytoskeleton and cell-cell junctions by Rho, Rac, and Cdc42 in human endothelial cells. *Journal of Cellular Physiology*, *176*(1), 150–165. https://doi.org/https://doi.org/10.1002/(SICI)1097-4652(199807)176:1<150::AID-JCP17>3.0.CO;2-B

Wong, K. H. K., Chan, J. M., Kamm, R. D., & Tien, J. (2012). Microfluidic Models of Vascular Functions. *Http://Dx.Doi.Org/10.1146/Annurev-Bioeng-071811-150052*, *14*, 205–230. https://doi.org/10.1146/ANNUREV-BIOENG-071811-150052

Zervantonakis, I. K., Hughes-Alford, S. K., Charest, J. L., Condeelis, J. S., Gertler, F. B., & Kamm, R. D. (2012). Three-dimensional microfluidic model for tumor cell intravasation and endothelial barrier function. *Proceedings of the National Academy of Sciences of the United States of America*, *109*(34), 13515–13520. https://doi.org/10.1073/PNAS.1210182109/SUPPL_FILE/SM01.MOV

Zheng, Y., Chen, J., Craven, M., Choi, N. W., Totorica, S., Diaz-Santana, A., Kermani, P., Hempstead, B., Fischbach-Teschl, C., López, J. A., & Stroock, A. D. (2012). In vitro microvessels for the study of angiogenesis and thrombosis. *Proceedings of the National Academy of Sciences of the United States of America*, *109*(24), 9342–9347. https://doi.org/10.1073/PNAS.1201240109/SUPPL_FILE/SM03.WMV

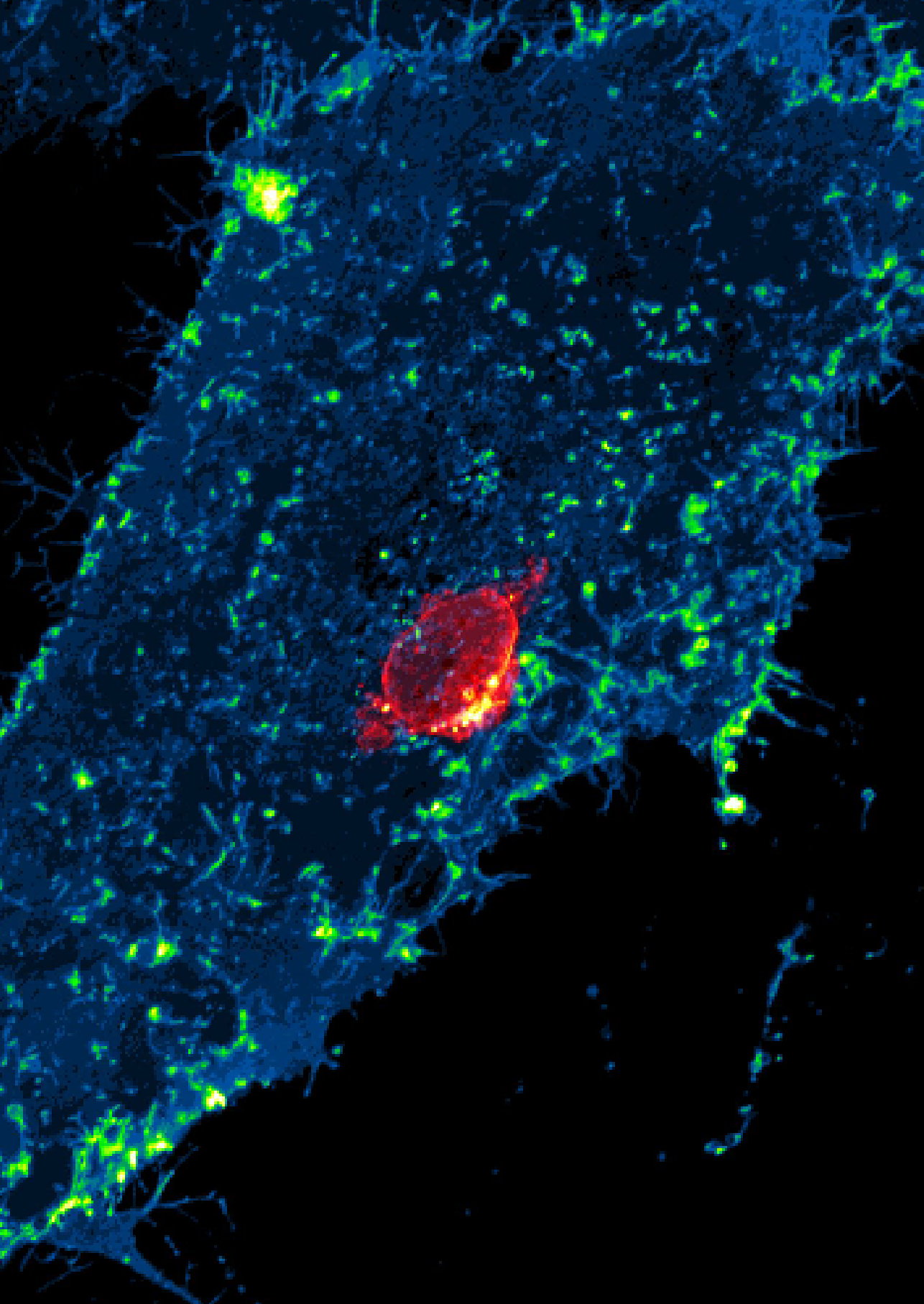

CHAPTER 2

Actin remodeling of the endothelium during transendothelial migration of leukocytes

Abraham C.I. van Steen[1,*]
Werner J. van der Meer[1,2,*]
Imo E. Hoefer[3]
Jaap D. van Buul[1,2,‡]

[1] *Molecular Cell Biology Lab at Dept. Molecular Cellular Haemostasis, Sanquin Research and Landsteiner Laboratory, Amsterdam, the Netherlands*
[2] *Leeuwenhoek Centre for Advanced Microscopy (LCAM), Section Molecular Cytology, Swammerdam Institute for Life Sciences (SILS), University of Amsterdam, the Netherlands*
[3] *Laboratory of Clinical Chemistry and Hematology, UMC Utrecht, Utrecht, the Netherlands*

Atherosclerosis 315 (2020): 102-110

ABSTRACT

For leukocytes crossing the vessel wall to solve inflammation, the endothelium acts as customs control. In the past years, progress has been made on the molecular mechanisms that are used by both the leukocytes and endothelium to allow efficient crossing, although not all the exact rules these vascular customs play by are completely understood. In this review, we focus on the contribution of the endothelium to the process of leukocyte extravasation and summarize the different molecular mechanisms involved in efficient leukocyte passage and prevention of local leakage at the same time. We will highlight the dynamic regulation of the endothelial actin cytoskeleton, which under the influence of different stimuli is a key player in leukocyte transendothelial migration.

INTRODUCTION

Leukocytes traversing the endothelial barrier at the correct site is an essential step in the inflammatory response. Leukocyte transendothelial migration (TEM) is an essential step in many pathophysiological processes, including - but not limited to - allograft rejection, tumor immunotherapies, rheumatoid arthritis and atherosclerosis. Therefore, many studies have focused on strategies to limit or prevent unwanted leukocyte migration and accumulation by intervening with molecular factors involved in TEM. The TEM process was first described in a three-step model [1], which was later refined into a multistep cascade model [2,3]. This cascade can be divided into three major events; rolling over the endothelium, firm adhesion, and finally diapedesis (Fig. 1). The diapedesis can occur through either the endothelial cell body (transcellular transmigration) or through the endothelial cell-cell junction (paracellular transmigration) [4–6]. Inflammatory stimuli steer TEM by activating molecular signaling pathways that trigger the endothelium to upregulate adhesion molecules and promote signaling pathways that govern the actin cytoskeleton dynamics to facilitate efficient leukocyte TEM, for example by the induction of actin stress fibers. For a general introduction to the actin cytoskeleton, dynamics and regulation by various adaptor proteins, we recommend an extensive review by Pollard [7]. These molecular signaling processes give rise to various inflammation-specific actin-rich cellular structures such as stress fibers, protrusions, docking structures and local rings. This review will give an overview of the actin-related processes in the inflamed endothelium that drive leukocyte extravasation.

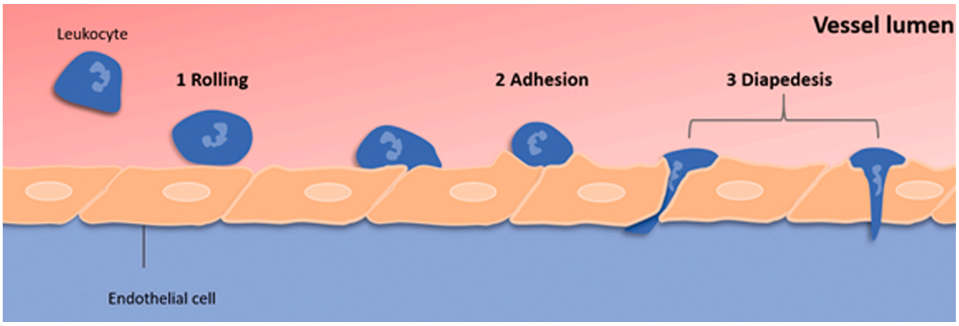

Fig. 1. The three-step model of leukocyte transendothelial migration.
The leukocyte roles on the inflamed endothelium (step 1), slows down and firmly adheres (step 2), and finally crosses the endothelial barrier either through cell-cell junctions (paracellular) or the endothelial cell body (transcellular) (step 3).

INFLAMMATORY SIGNALS

Detection of damage or pathogen associated molecular patterns causes tissues to release pro-inflammatory stimuli such as IFN-γ, IL1-β and TNFα, bringing the endothelium to an inflammatory state that drives TEM and induces vascular permeability. The effects of these inflammatory stimuli on endothelial cells have been extensively studied to reveal the mechanisms that locally trigger TEM. The inflamed state of the endothelium includes upregulation of P- and E-selectins, as well as several adhesion molecules including Inter Cellular Adhesion Molecule 1 and 2 (ICAM-1/CD54, ICAM-2/CD102) and Vascular Cell Adhesion Molecule 1 (VCAM-1/CD106) [8,9]. Beside the upregulation of surface receptors, the inflamed endothelium changes its mechanical properties, for example by the formation of actin stress fibers through the activity of the small Rho GTPase RhoA [10]. This leads to increased cytoskeletal contractility, which enhances vascular permeability [11]. Vascular leakage and leukocyte TEM both occur during inflammation, and for a long time, a connection between the two has been proposed [12]. However, the McDonald group showed that plasma leakage is induced by inflammatory stimuli in rat trachea and is independent of leukocyte TEM [13]. A later study of the same group, found the processes of plasma leakage and leukocyte TEM in rat trachea to occur at separated locations in the vascular bed: plasma leakage occurs upstream from the site of leukocyte TEM [14]. Additionally, TNFα-induced leukocyte TEM did not alter the permeability of micro-vessels [15]. This leads to the conclusion that leukocyte TEM and vascular permeability both occur in response to inflammatory stimuli but are not causally related processes. We will now discuss the different steps of leukocyte TEM, also known as the multistep model. It is important to realize that in this review we will discuss the “normal” inflammatory response. Under various disease conditions such as atherosclerosis other factors such as disturbed flow and modified lipoproteins play a role in altering the “normal” inflammatory process in the endothelium. For further in-formation on these effects, we refer to the comprehensive review by Hahn and Schwartz [16]. As already pointed out by Butcher in the early 90s [1], each individual step is most likely regulated by its own set of mechanistic molecular signals.

ROLLING

Selectins

Initial contact between leukocytes and the inflamed endothelium is mediated by selectins. Upon inflammation, the endothelium upregulates the expression of P- and E-selectins and presents them on the luminal membrane [17]. These selectins interact with P-selectin glycoprotein ligand 1 (PSGL1) expressed by leukocytes [18]. This interaction slows down the leukocyte through the formation of so-called “catch bonds”, bringing the leukocyte in close proximity to the endothelium and initiating a rolling over the endothelium [19]. Catch bonds

are noncovalent bonds of which the lifetime increases as the exerted tension on these bonds increases. This type of interaction between endothelial selectin and PSGL1 results in less leukocyte adhesion in the presence of low shear stress and more leukocyte adhesion in the presence of higher shear stress [20]. In addition to slowing down the leukocyte, selectin interactions with PSGL1 induce the activation of lymphocyte function-associated antigen 1 (LFA-1) integrins on the leukocyte [21], resulting in the transition to the next step: the adhesion, discussed in Section 4.

Finger-like protrusions

Inflamed endothelial monolayers display a typical phenotype: at the luminal side, small dynamic finger-like membrane protrusions can be detected [22,23]. These endothelial membrane protrusions have been visualized in multiple research articles [24]. Electron microscopy has shown that the chemokine IL-8 is presented at the tip of these protrusions [25]. Glycosaminoglycans present on the EC surface have been reported to immobilize chemokines at the luminal membrane [26]. In addition to presenting chemokines 1, these protrusions may serve as templates for the formation of firm adhesion structures, thereby mediating the transition of the rolling to a firm adhesion step in the leukocyte TEM cascade. Since these protrusions play such an important role in leukocyte extravasation, we find it necessary to discuss them in detail.

In cell biology, such finger-like protrusions are categorized in multiple groups, two of which are named microvilli and filopodia. These structures are defined as thin membrane protrusions driven by parallel F-actin bundles [27]. Microvilli do not adhere to any extra-cellular component but instead extend into a lumen, whereas filopodia probe and adhere to a substrate or a neighboring cell. Filopodia function as directional sensors for migrating cells [28], and are driven by the activity of small Rho GTPases and the molecular motor proteins of the myosin family [27]. A myosin family member that is crucial for the organization of a filopodia, both the formation and the transport of proteins into these structures, is Myosin-X [29,30].

Myosin-X induces the formation of filopodia by reorganizing actin at the cell cortex. The motor function, not the cargo trafficking ability of Myosin-X, is crucial for this induction [31]. Surprisingly, Myosin-X overexpression in Cos7 monkey cells leads to the formation of dorsal filopodia in a Cdc42-dependent manner [30]. These typical dorsal filopodia are found not to adhere to any substrate or other cells [30]. In the endothelium, inflammatory signals such as TNF-α upregulate Myosin-X expression and activate the small membrane bound Rho-GTPase Cdc42 [32]. This activation leads to a reorganization of the actin cytoskeleton [33]. Cdc42 reorganizes the actin cytoskeleton through p21-activated Kinase 4 (PAK4), which has been identified as a downstream effector of Cdc42 [34]. As a result, PAK4-induced actin reorganization, together with Myosin-X activity, leads to the formation of finger-like protrusions at the luminal membrane of endothelial cells upon inflammation. Interestingly,

these micro-villi like structures show Myosin-X localization at the very tip and are enriched in ICAM-1 [33]. The Myosin-X localization leads us to draw the conclusion that these structures are in fact filopodia, despite their apparent similarity to microvilli. Fig. 2 depicts a schematic overview of such an inflammation induced endothelial filopodium.

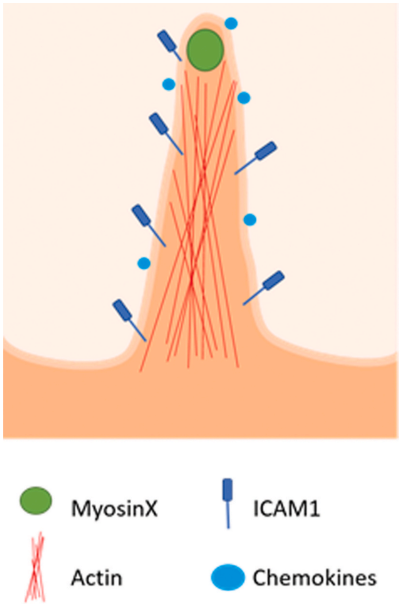

Fig. 2. Inflammation-induced endothelial filopodium.
Inflammatory stimuli activate the membrane-bound Cdc42, recruiting Myosin-X and the actin cytoskeleton. This results in the formation of filopodia at the luminal membrane. Myosin-X and ICAM-1 are found in these filopodia, and heparan sulphates at the EC surface immobilize chemokines.

Chemokines

Chemokines are chemoattractant cytokines, which guide leukocytes across the endothelium, towards the source of inflammation. These chemokines are small molecules secreted by tissue cells, and then taken up by the basolateral membrane of endothelial cells and transcytosed to be presented at the apical membrane and filopodia [25]. However, endothelial cells can also produce chemokines themselves [35,36]. As blood flow would instantly flush away any gradient of soluble chemokines, it was hypothesized that these molecules had to be anchored at the luminal membrane of the endothelium. Glycosaminoglycans on the surface of endothelial cells were found to mediate immobilization of chemokines [26,37,38]. Another source of chemokines has been found in chemokine rich vesicles surrounding actin stress fibers [39]. These vesicles are presented to crawling leukocytes upon contact, which leads to a very local and controlled presentation of chemokines by the endothelium upon signals received from the crawling leukocytes. As the leukocytes are steered by these chemokines

across the endothelium, they encounter cues to guide them further into the inflamed tissue. Different chemokines have been shown to activate different leukocyte integrins [40]. An example of how this affects migration is present in the work by the Kubes lab, where they studied the integrin dependency of chemotaxis towards fMLP and IL-8 [41]. They discovered that the leukocyte integrin Mac1 is the dominant integrin during chemotaxis towards fMLP, whereas LFA1 integrin was more involved in movement towards an IL-8 gradient. Furthermore, when neutrophils are presented with both chemoattractants, they will preferentially migrate towards the source of fMLP regardless of the concentration of the chemoattractants. It was concluded that Mac1-mediated crawling allows leukocytes to directly move towards the target, if it is present. In the absence of Mac-1-sensitive chemoattractants, the LFA-1-sensitive chemoattractants will steer crawling towards these chemoattractants leading to a hierarchy in chemoattractant signals. Based on this and many other works, it is overall accepted that chemokines presented on the endothelial surface mediate the transition from neutrophil rolling to the adhesion and crawling step. So, in accordance with the TEM cascade, chemokine regulation should be placed between step 1 and 2.

Interestingly, it was recently reported that chemokines are not necessarily restricted to the rolling to adhesion transition. The group of Nourshargh showed that different chemokines play a role in the full TEM cascade. For the first part, the endothelium exposes CXCL1 on its luminal surface [35]. This results in the transition from rolling to adhesion of neutrophils on the endothelium, followed by the release of CXCL2 by the neutrophils at junction regions. ACKR-1, also known as DARC, located at junctions, acts as a chemokine presenter, binds to CXCL2 and thereby mediates neutrophil migration through cell-cell junctions. This signaling loop combined with the previously described TEM cascade already highlights the complexity of the TEM process.

ADHESION

The second step in the three-step model of leukocyte TEM is the transition from rolling to firm adhesion (Fig. 1). Integrins LFA1 (CD11a/ CD18), MAC-1 (CD11b/CD18) and VLA-4 (CD29/ CD49d) on the surface of leukocytes interact with ICAM1 and VCAM1 presented by the endothelium [42]. As a result, ICAM1 and VCAM1 are clustered, triggering downstream signaling pathways, including the recruitment of actin adapter proteins [23,43–46]. A study using anti ICAM-1 coated beads as a model for leukocyte binding showed that upon ICAM-1 clustering on the endothelial membrane, α-actinin-4, cortactin and filamin-B were sequentially recruited to ICAM-1 in time, leading to a large protein complex called the ICAM-1 adhesome [44]. Interestingly, endothelial stiffness has been shown to be a major factor in the efficiency of leukocyte TEM: when endothelial cells are cultured on stiff surfaces, this promotes the efficiency of the number of leukocytes that crosses in a Rho/ROCK-dependent manner [47,48].

The stiffness of the substrate upon which endothelial cells grow determines the expression of Deleted in Liver Cancer-1 (DLC-1) [49]. DLC-1 is a Rho-GAP that is upregulated in pathological vascular stiffening such as in atherosclerotic plaques. The absence of DLC-1 results in an impaired ICAM-1 adhesome formation and thereby reduced TEM efficiency.

"Docking structures"

ICAM-1 clustering results in the recruitment of various actin adaptor proteins, as well as an enrichment in ERM molecules [50]. The recruitment of actin regulating proteins results in the formation of a so-called docking structure that extends the endothelial basolateral plane and surrounds the adherent leukocyte [43]. As these structures seem to control the adhesion state of leukocyte, they were referred to as "docking structures". However, other groups have separately described these structures: linking them to transmigration events and naming them "transmigratory cups" or linking them to the shape and describing them as "cup structures" [51,52]. These structures form rapidly upon LFA-1-induced ICAM-1 clustering and are highly depend on the endothelial actin cytoskeleton and intracellular calcium signaling [53]. The current view on the function of these typical membrane structures is that they enlarge the area of contact between the leukocyte and the endothelium, aiding in the efficiency of TEM and limiting the vascular leakage during TEM [54,55].

The formation of this membrane structure is poorly understood, however, there might be a hint in the identification of the finger-like protrusions on the apical membrane of the inflamed endothelium as filopodia. During cell migration, filopodia act as templates for lamellipodia formation [56]. The lamellipodium is a broad membrane protrusion driven by Arp2/3-mediated branched F-actin network. Filopodia act as directional sensors and push the membrane forward by the assembly of F-actin, resulting in the formation of a lamellipodium [56,57]. It is an attractive hypothesis to consider endothelial filopodia as templates for F-actin-rich membrane protrusions to be generated in-between individual filopodia in a similar way. This process results in structures that may aid in the firm adhesion of leukocytes.

Now that the leukocyte is firmly adhered and anchored to the endothelium with the help of an F-actin-rich membrane structure, the third and final step of the TEM cascade is the actual crossing of the endothelium, also known as diapedesis (Fig. 1). In this final step, proteins that normally keep endothelial junctions together, must somehow allow the passage of the leukocyte and therefore transiently dissociate from each other. We will therefore first discuss the regulation of several endothelial cell-cell junction proteins, and their dynamics following leukocyte adhesion prior to the process of diapedesis.

Junctional architecture

Endothelial cells form a dynamic barrier between the bloodstream and surrounding tissues. They control the passage of macromolecules into the underlying tissue via transcellular vesicle

trafficking, as well as via controlled opening and closing of junctions [58]. Tight Junctions (TJs) and Adherens Junctions (AJs) are located throughout the entire endothelial junction as well as proteins that do not localize to TJ or AJ (Fig. 3). The distribution of these junctional proteins is distinctly different from epithelial junctions, where these proteins are located in strict junctional compartments [59]. In the endothelium, TJs mainly regulate paracellular permeability and contain the junctional adhesion molecules A, B and C (JAMs), ESAM, occludin, and claudins, the latter two are connected to the actin cytoskeleton via zona occludens (ZO) 1,2 and 3 [60]. An interesting junctional molecule is ESAM-1, involved in vascular permeability and regulation of the passage of neutrophils [61]. Gene inactivation of ESAM-1 increased vascular permeability in the lung, but not in the heart, skin, and brain [62]. For the other junctional proteins JAM-A and PECAM-1 (CD31), no different effect on barrier permeability was detected, making ESAM-1 unique in its role as an organ-specific regulator of the endothelial barrier.

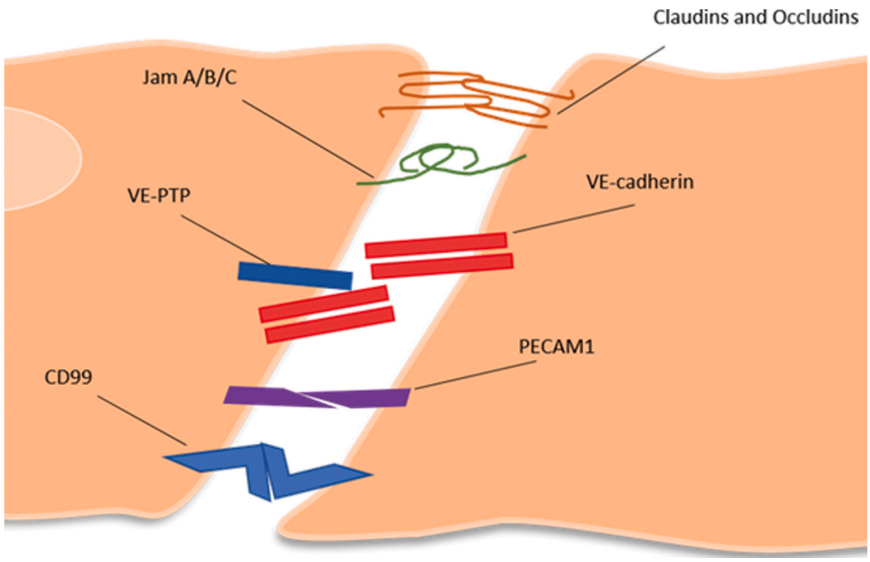

Fig. 3. The molecular components of an endothelial junction.
The endothelial junction is made up by several junctional proteins. Claudins, Occludin and Junctional adhesion molecule A/B/C (Jam A/B/C) make up tight junctions. VE-cadherin stabilised by VE-PTP is the main component of adherens junctions. PECAM-1 and CD99 do not localise specifically to tight or adherens junctions.

AJs consist of Vascular Endothelial cadherin (VE-cadherin/CD144) and provide junctional stability by connecting ECs and regulate tension and cell-cell communication [63]. Upon inflammation, the endothelial actin is remodeled to form stress fibers, the ends of these stress fibers are anchored in AJ [64]. VE-cadherin is linked to the actin cytoskeleton, via interactions with α-and β catenin, which allows the AJ to connect stress fibers from adjacent cells and transmit tension across cell-cell junctions [65]. Under inflammatory conditions, the

remodelling of these junctions leads to the recruitment of various molecules that strengthen the junction, for example vinculin or vascular endothelial protein tyrosine phosphate (VE-PTP) [64–66]. VE-PTP can bind to the extracellular region of VE-cadherin and thereby further enhance its function by promoting the endothelial barrier [66].

Some junctional proteins that do not localize to AJs or TJs are Platelet Endothelial Cell Adhesion Molecule 1 (PECAM-1), ESAM-1, CD99 and CD99L2. PECAM-1 is localized at endothelial junctions, forms homophilic interactions and is expressed by both the endothelium and leukocytes. Antibody blocking of PECAM-1 inhibits leukocyte transmigration, trapping neutrophils between the endothelium and the underlying basement membrane [67]. CD99 is expressed by the endothelium at cell borders, and like PECAM-1, also on leukocytes. Homophilic interactions between endothelial CD99 and leukocytes CD99 are important for diapedesis. Blocking CD99 interaction causes transmigrating leukocytes to get trapped between the endothelium at the basement membrane [67,68]. CD99L2, which is an isoform of CD99, was shown to localize at cell-cell junctions and mediate leukocyte passage [67,69]. Both CD99 and CD99L2 work independently of PECAM-1 and help neutrophils overcome the endothelial basement membrane. During diapedesis, many junctional proteins perform a role at a different moment in the leukocyte crossing event. Therefore, we propose to refine the diapedesis step in three distinct sequential steps: early, mid and late diapedesis [70]. In the next section, we will use these concepts to better frame the processes during the last step of TEM.

DIAPEDESIS

The third and final step of the leukocyte TEM process is the crossing of the endothelium, diapedesis (Fig. 4). During diapedesis, the leukocyte crosses the endothelial barrier via either the paracellular or transcellular route. During paracellular diapedesis, the leukocyte crosses the endothelium through a cell-cell junction, in between two or three adjacent endothelial cells [71]. When migrating transcellularly, leukocytes move through the body of an endothelial cell, often close to the junction where the luminal and apical membrane are in close proximity [72]. It is interesting to realize that the protruding membrane structure, as discussed previously, is observed in both routes of transmigration [51]. Why a leukocyte prefers the transcellular or paracellular route is still an open question. It has been established that the preference of a leukocyte for either route of transmigration is specific for different leukocyte subsets. However, the same leukocyte can have a different preference for a route depending on the organ where transmigration occurs. An overview of the preference for the different routes of transmigration based on both leukocyte subsets, vascular bed or model and inflammatory stimulus is shown in Table 1, which is an updated version of a previously published table by Sage and Carman [73]. For example, in vivo experiments conducted on the skin show a high percentage of transcellular migration

(Table 1). Although the process of transcellular migration is less well understood, many of the same adhesion molecules that are known to be involved in paracellular migration have also been reported to be involved in transcellular migration [72,74]. PECAM-1, CD99 and JAM-A were found in the encapsulating membrane structure around transcellularly migrating leukocytes. Surprisingly, when studying paracellular migration of T- lymphocytes, it was found that blocking the junctional protein PECAM-1 with antibodies also prevented transcellular migration events [75].

In general, the paracellular route is the most frequently observed route both in vivo and in vitro. Therefore, its molecular mechanisms have been more extensively studied. Here we will discuss the process of paracellular diapedesis in more detail by dividing it into three steps: early, mid and late diapedesis (Fig. 4B).

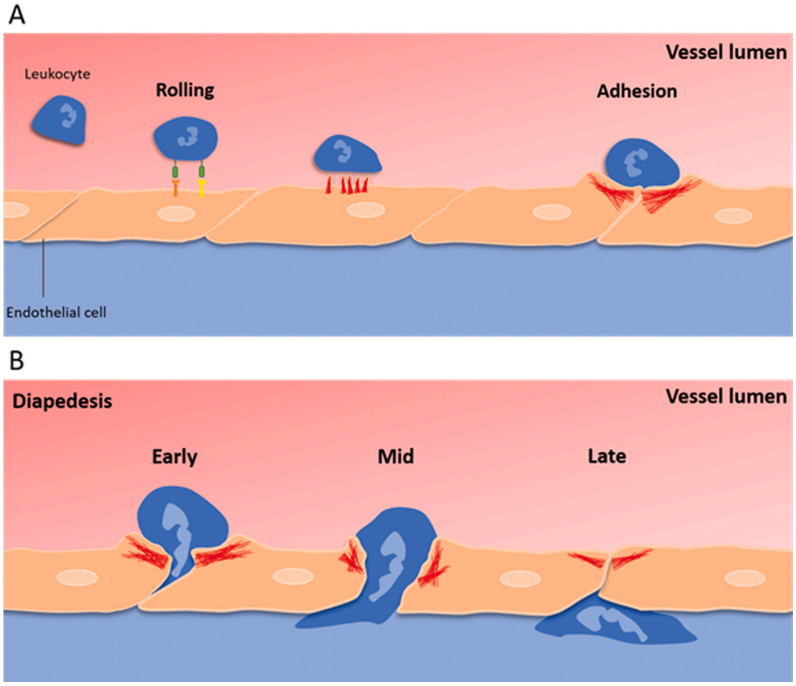

Fig. 4. The leukocyte transmigration cascade.
(A) PSGL1 on the leukocyte forming catch-bonds with E- and P-selectins on the endothelium is the first interaction between the leukocyte and the endothelium. This interaction induces activation of LFA-1 on the leukocyte, which interacts with ICAM-1 presented on dorsal endothelial filopodia and slows down the leukocyte, transitioning to the adhesion step and ICAM-1 clustering. This results in an actin rich membrane structure around the transmigrating leukocyte. (B) Early diapedesis is characterized by the leukocyte that inserts its protrusion with a leading lobe of the nucleus into the junction, forming the start of the endothelial gap. During middiapedesis, the leukocyte pushes its nucleus through the endothelial gap, where RhoA induced Myosin–II–mediated contractility, together with a de novo formed Factin ring to ensure no plasma leakage. Finally, during late diapedesis, the leukocyte is underneath the endothelium and detaches from the apical membranes of the endothelial cells. The contractility closes the endothelial gap behind the leukocyte.

Table 1. Percentage of transmigration routes taken by leukocytes in different species, tissues, cell types and under different inflammatory stimuli. Adapted from Ref. [73].

In vitro/vivo	Species	Cell type/tissue	Leukocyte	Migratory/inflammatory stimuli	Method	Percentage of transmigrational routes	Reference
In vitro	Human	BBB	T lymphocytes	TNF-alpha	TEM	Transcellular migration is observed	[76]
	Human	HUVEC	Monocytes	TNF-alpha, MCP-1	IFM	7% transcellular 93% paracellular	[51]
	Human	HUVEC	Neutrophils	TNF-alpha, PAF	IFM	5% transcellular 95% paracellular	[51]
	Human	HUVEC	T lymphocytes	TNF-alpha, SDF-1	IFM	11% transcellular 89% paracellular	[51]
	Human	HUVEC	Neutrophils	TNF-alpha	TEM	5% transcellular 95% paracellular	[77]
	Human	HCAEC	Monocytes	IL-1beta	IFM	15% transcellular 85% paracellular	[78]
	Human	HDMVEC	T lymphocytes	TNF-alpha	IFM	31% transcellular 69% paracellular	[79]
	Human	HUVEC	T lymphocytes	TNF-alpha	IFM, TEM	9% transcellular 91% paracellular	[79]
	Human	iHUVEC	Neutrophils	TNF-alpha	IFM	10% transcellular 90% paracellular	[80]
	Human	iHUVEC	T lymphocytes	TNF-alpha	IFM	100% paracellular	[80]
	Human	HUVEC	T lymphocytes	TNF-alpha	IFM	10% Transcellular	[75]
	Human	HDMVEC	T lymphocytes	TNF-alpha	IFM, TEM	30% transcellular	[75]
	Human	HLMVEC	T lymphocytes	TNF-alpha	IFM, TEM	30% transcellular	[75]
	Human	Lymphatic	T lymphocytes	TNF-alpha	IFM	30% transcellular	[75]
	Human	HUVEC	Neutrophils	TNF-alpha	AFM	Transcellular migration observed	[81]
	Human	HDMVEC	Neutrophils	TNF-alpha	IFM	73% paracellular 27% transcellular	[82]
	Human	HUVEC	Monocytes	TNF-alpha	IFM	62% paracellular 38% transcellular	[5]
	Human	HUVEC HDMVEC	T lymphocytes	TNF-alpha	IFM	Transcellular transmigration is observed	[83]
	Mouse	BBB pMBMEC	$CD4^+$ T-EM	TNF-alpha IL-1-beta	Live cell imaging	Normal ICAM levels, Mainly paracellular High ICAM, mainly Transcellular	[84]
	Human	HUVEC	Neutrophils	TNF-alpha	Live cell imaging	90% paracellular 10% transcellular	[70]
	Human	HUVEC	Monocytes	TNF-alpha	Live cell imaging	90% paracellular 10% transcellular	[70]
	Human	HDMVEC	Neutrophils	IL-1-beta	Live cell imaging	100% paracellular	[85]
	Human	HDMVEC	Peripheral blood T-cells	IL-1-beta	Live cell imaging	80% paracellular 20% transcellular	[85]
	Human	HDMVEC	T effector	IL-1-beta	Live cell imaging	50% paracellular 50% transcellular	[85]
	Mouse	BBB pMBMEC	$CD4^+$ Tcells	TNF-alpha IFN-gamma	Live cell imaging	51% paracellular 49% transcellular	[86]
In vivo	Rat	Mesentery	Neutrophils, Eosinophils, Monocytes	Mechanical trauma	TEM	Transcellular migration observed	[87]
	Dog	Pancreas	Leukocytes	Ischemia	TEM	Transcellular migration observed	[88]
	Dog	Pancreas	Leukocytes	Ischemia	TEM	Transcellular migration observed	[89]
	Human	Skin	Neutrophils	C5a, NAP, IL-1, LTB4	TEM	100% transcellular	[90]
	Mouse	Liver, lung, spleen, kidney, heart	Lymphocytes	IL-2	TEM	Transcellular migration observed	[91]
	Guinea pig	Skin	Neutrophils, eosinophils	fMLP	Serial TEM	91% transcellular 9% paracellular	[92]
	Mouse	Skin	Neutrophils	fMLP	Serial TEM	83% transcellular 17% paracellular	[93]
	Mouse	Cremaster muscle	Neutrophils	MIP-2 (CXCL2)	Live cell imaging	14% transcellular 86% paracellular	[94]
	Mouse	Cremaster muscole	Neutrophils	MIP-2 (CXCL2)	Live cell imaging	14% transcellular 86% paracellular	[95]
	Mouse	Cremaster muscle	Neutrophils	IL-1β, fMLP, I-R	Live cell imaging	10% transcellular 90% paracellular	[96]
	Mouse	Cremaster muscle	Neutrophil	IL-1β	Live cell imaging	10% transcellular 90% paracellular	[97]

BBB: blood brain barrier, fMLP: formyl-metFormylmethionyl-leucyl-phenylalanine, LTB4: leukotriene B4, MCP-1: monocyte chemoattractant protein-1, MIP-2: macrophage inflammatory protine-2, NAP: neutrophil activating peptide, PAF: platelet activating factor, HUVEC: human umbilical vein endothelial cells, pMBMEC: primary mouse brain microvascular endothelial cell, HDMVEC: human dermal microvascular endothelial cells, HLMVEC: human lung microvascular endothelial cells, HCAEC: human coronary artery endothelial cells TEM: transmission electron microscopy, SEM: scanning electron microscopy.

Early diapedesis

Early diapedesis is defined as the moment when leukocytes start to breach the endothelium (Fig. 4B) [70]. Leukocyte adhesion to the endothelium tells the endothelium to prepare the cell-cell junctions to open up for diapedesis. Leukocyte integrin-induced clustering of ICAM-1 triggers the beginning of diapedesis in two different ways: firstly, leukocyte docking to inflamed ECs leads to the dissociation of VE-PTP from VE-cadherin, reducing the adhesive and bridging function of VE-cadherin, resulting in loosening of the endothelial cell-cell junction [66]. This mode of action was elegantly illustrated by Nottebaum and colleagues, who additionally showed that leukocytes only induced VE-PTP dissociation from VE-cadherin in the TNFα-stimulated endothelium and not in resting ECs. In a follow up study, they demonstrated that leukocyte docking induces signaling via the SRC homology 2-containing protein-tyrosine phosphatase 2 (SHP2), resulting in dephosphorylation of the Y731 tyrosine residue of VE-cadherin allowing the adaptin protein complex 2 (AP2) to bind. This then leads to enhanced endocytosis of VE-cadherin [98]. Secondly, ICAM-1 clustering leads to an increase of cytoplasmic Ca2+, which may be needed for phosphorylating myosin light chain kinase (MLCK) [99]. The leukocyte inserts an actin-rich protrusion into the loosened endothelial junction. This protrusion forms a subendothelial lamellipodium, and the nucleus is deformed so that a leading lobe can be pushed in-between the two endothelial cells [85]. Interestingly, in vivo studies showed that the close relative of ICAM-1, ICAM-2, mediates early diapedesis. Using ICAM-2-deficient mice, the authors showed that transmigrating leukocytes are stopped during the process of TEM at the luminal membrane [100].

Mid diapedesis

Mid diapedesis is defined as the step where the transmigration pore is opened and the leukocyte is halfway through [70]. Recent literature indicates that the leukocyte is pushing the major part of its nucleus through the endothelial pore [85]. At this point, it is suggested that ICAM-1 clustering induces local activation of RhoA via the Guanine Exchange Factors (GEFs) Ect2 and LARG. The site of transmigration has been shown to be rich in actin stress fibers that locally interact upon ICAM-1 clustering by a leukocyte [79]. RhoA induces Myosin-II contraction via ROCK2b as well as mediating the formation of a de novo F- actin ring around the endothelial pore, limiting plasma leakage during diapedesis [70]. These findings seem at first contradictory to the dogma, as RhoA activity was believed to be involved in the opening of endothelial pores. However, the latter study showed that depletion of RhoA activity in ECs resulted in vascular leakage during leukocyte diapedesis but did not reduce leukocyte transmigration in any way. Depletion of endothelial RhoB and C did not have any effect on the number of leukocytes that cross the endothelium [55]. A FRET-based RhoA biosensor revealed the spatiotemporal activity of RhoA activation to occur at the edge of the gap, only during mid-diapedesis. No RhoA activity was detected during early diapedesis, indicating that the leukocyte breaches the endothelial junction independent of any RhoA activity. Thus, the findings that RhoA was activated upon leukocyte TEM were

correct, however, the interpretation of these results that this would lead to opening of cell-cell junctions, as it occurs during thrombin or histamine treatment [101], had to be revised. We now recognize that RhoA activity is required to limit local fluid losses during leukocyte TEM, which has since then also been confirmed by other research groups, leading to the establishment of a new dogma in the field [54,102].

As the leukocyte moves through the endothelial junction, homophilic interactions of both CD99 and PECAM-1 on both the endothelium and leukocyte trigger intracellular signals in the endothelium. This in turn can lead to the formation of vesicles that are recruited to the junctional EC membrane. These vesicles are believed to be part of a membrane compartment referred to as the Lateral Border Recycling Compartment (LBRC) and they increase the membrane surface area at the site of leukocyte interaction [103]. LBRC mediates paracellular and transcellular migration [104]. Interestingly, lack of endothelial JAM-A results in the arrest of leukocytes at the endothelial junction, in-between the endothelial cells, thus at the mid-diapedesis stage [100]. Why this happens is currently unclear. A possible explanation is that JAM-A is located halfway the junction and therefore is needed at that particular part of the diapedesis stage, as it is a ligand for LFA-1 [105]. Also blockade of CD99 results in an arrest of leukocyte TEM at the mid- diapedesis state [106,107]. CD99, as JAM-A, is located halfway the EC junction and CD99 forms a homophilic interaction with CD99 on the leukocyte part. It is proposed that this interaction is required to complete the diapedesis step. Lack of endothelial CD99 may result in a failure for leukocyte to continue their way through the endothelial cell-cell junction.

Late Diapedesis

Late diapedesis is defined as the moment when the leukocyte has crossed the endothelium and the endothelial pore is closing [55]. Besides closing the transmigration gap using a contractile ring, several endothelial junction proteins play a role in enabling the leukocyte to leave the endothelium and migrate into the tissue. The junctional proteins PECAM1 and CD99 facilitate the penetration of the basement membrane, as blocking or genetic interference with these proteins traps the leukocyte in-between the endothelium and the underlying basement membrane [67].

Once a leukocyte is underneath the endothelium, it encounters pericytes and the basement membrane. Pericytes surround the endothelium and affect endothelial cell proliferation, junctional permeability and many other factors concerning vessel integrity [108]. These pericytes form a secondary barrier for leukocytes transmigrating into inflamed tissues. In-between, neighboring pericytes gap areas are observed, which are enlarged under stimulation of TNFα and IL-1β [109]. Neutrophils prefer to use these enlarged gaps between pericytes as location for breaching of the pericyte layer. Recently, it was shown that neutrophil elastase plays a non-redundant role in supporting neutrophil breaching of the venular basement

membrane [110]. Interestingly, many of these gaps colocalize with basement membrane regions that show reduced levels of matrix proteins, such as collagen type IV, laminin-8 and laminin-10 [111]. These regions of the basement membrane might therefore be more easily breached by transmigrating leukocytes, allowing for the passage into the inflamed tissues. Additionally, it was reported that the endothelial cell basement protein laminin 511 promotes endothelial barrier function by stabilizing VE-cadherin at junctions [112]. At the same time, it is involved in downregulating CD99L2. Both actions were correlated with reduced neutrophil TEM. Binding of endothelial cells to laminin 511, but not laminin 411 or non-endothelial laminin 111, increased the barrier function and inhibited neutrophil TEM. These data suggest that the basement membrane protein laminin 511 regulates leukocyte extravasation both directly and indirectly by modulating endothelial barrier properties.

From a three-step model to a cascade model

In this review, we used the well-accepted three-step model of leukocyte TEM (Fig. 1) to discuss how the endothelium, activated by inflammatory stimuli, is involved in this process. We particularly focused on how the actin cytoskeleton of the endothelium is remodeled and how the various actin-controlled structures that originate from the endothelium allow efficient TEM. As mentioned above, TEM is crucially involved in the daily immune surveillance but also in many disorders and diseases and thus represents an interesting target for therapeutic intervention. The multistep TEM cascade principally provides a plethora of points of attack that may be suitable to inhibit leukocyte TEM. However, clinical applications specifically targeting factors of the TEM cascade are scarce. This may partly be due to its complexity and possible redundancy of single proteins by other proteins during functional knockdowns. Questions that remain open: what determines the preference for paracellular or transcellular migration? Also, is it that specific actin-mediated endothelial structures are dysfunctional in diseased settings and how can two endothelial cells form a tight ring of F-actin to limit leakage during normal TEM events? Regardless, TEM is a complex process but this complexity also provides new opportunities. Our growing knowledge of its molecular players and mechanisms will likely yield new insights that render TEM a promising target for future applications.

Financial support

This work was supported by LSBR grant # 1649 and ZonMW NWO Vici grant # 91819632.

Declaration of competing interest

The authors declared they do not have anything to disclose regarding conflict of interest with respect to this manuscript.

REFERENCES

[1] E.C. Butcher, Leukocyte-endothelial cell recognition: three (or more) steps to specificity and diversity, Cell 67 (6) (20-Dec-1991) 1033–1036.

[2] T.A. Springer, Traffic signals for lymphocyte recirculation and leukocyte emigration: the multistep paradigm, Cell 76 (2) (28-Jan-1994) 301–314.

[3] T.M. Carlos, J.M. Harlan, Leukocyte-endothelial adhesion molecules, Blood 84 (7) (Oct. 1994) 2068–2101.

[4] R. Gorina, R. Lyck, D. Vestweber, B. Engelhardt, β 2 integrin–mediated crawling on endothelial ICAM-1 and ICAM-2 is a prerequisite for transcellular neutrophil diapedesis across the inflamed blood–brain barrier, J. Immunol. 192 (1) (Jan. 2014) 324–337.

[5] Z. Mamdouh, A. Mikhailov, W.A. Muller, Transcellular migration of leukocytes is mediated by the endothelial lateral border recycling compartment, J. Exp. Med. 206 (12) (Nov. 2009) 2795–2808.

[6] S. Nourshargh, R. Alon, Leukocyte migration into inflamed tissues, Immunity 41 (5) (20-Nov-2014) 694–707 Cell Press.

[7] T.D. Pollard, Actin and actin-binding proteins, Cold Spring Harb. Perspect. Biol. 8 (8) (Aug. 2016).

[8] Y. Longbiao, H. Setiadi, X. Lijun, Z. Laszik, F.B. Taylor, R.P. McEver, Divergent inducible expression of P-selectin and E-selectin in mice and primates, Blood 94 (11) (Dec. 1999) 3820–3828.

[9] J.D. van Buul, P.L. Hordijk, Endothelial signalling by Ig-like cell adhesion molecules, Transfus. Clin. Biol. 15 (1–2) (Feb. 2008) 3–6.

[10] B. Wójciak-Stothard, A. Entwistle, R. Garg, A.J. Ridley, Regulation of TNF-α-induced reorganization of the actin cytoskeleton and cell-cell junctions by Rho, Rac, and Cdc42 in human endothelial cells, J. Cell. Physiol. 176 (1) (Jul. 1998)150–165.

[11] J.D. van Buul, I. Timmerman, Small Rho GTPase-mediated actin dynamics at endothelial adherens junctions, Small GTPases 7 (1) (2016) 21–31.

[12] P. He, Leucocyte/endothelium interactions and microvessel permeability: coupled or uncoupled? Cardiovasc. Res. 87 (2) (2010) 281–290 Oxford University Press.

[13] D.M. McDonald, Endothelial gaps and permeability of venules in rat tracheas exposed to inflammatory stimuli, Am. J. Physiol. Lung Cell Mol. Physiol. 266 (110–1) (1994).

[14] P. Baluk, P. Bolton, A. Hirata, G. Thurston, D.M. McDonald, Endothelial gaps and adherent leukocytes in allergen-induced early- and late-phase plasma leakage in rat airways, Am. J. Pathol. 152 (6) (Jun. 1998) 1463–1476.

[15] M. Zeng, H. Zhang, C. Lowell, P. He, Tumor necrosis factor-α-induced leukocyte adhesion and microvessel permeability, Am. J. Physiol. Cell Physiol. 283 (6) (Dec. 2002) H2420–H2430.

[16] C. Hahn, M.A. Schwartz, Mechanotransduction in vascular physiology and atherogenesis, Nat. Rev. Mol. Cell Biol. 10 (1) (Jan. 2009) 53–62.

[17] K. Ebnet, D. Vestweber, Molecular mechanisms that control leukocyte extravasation: the selectins and the chemokines, Histochem. Cell Biol. 112 (1) (1999) 1–23.

[18] R.P. McEver, Selectins: initiators of leucocyte adhesion and signalling at the vascular wall, Cardiovasc. Res. 107 (3) (Aug. 2015) 331–339.

[19] D.A. Hammer, Leukocyte adhesion: what's the catch? Curr. Biol. 15 (3) (08-Feb- 2005) Cell Press.

[20] B.T. Marshall, M. Long, J.W. Piper, T. Yago, R.P. McEver, C. Zhu, Direct observation of catch bonds involving cell-

adhesion molecules, Nature 423 (6936) (May 2003) 190–193.

[21] Y. Kuwano, O. Spelten, H. Zhang, K. Ley, A. Zarbock, Rolling on E- or P-selectin induces the extended but not high-affinity conformation of LFA-1 in neutrophils, Blood 116 (4) (Jul. 2010) 617–624.

[22] H.-M. Oh, et al., RKIKK motif in the intracellular domain is critical for spatial and dynamic organization of ICAM-1: functional implication for the leukocyte adhesion and transmigration, Mol. Biol. Cell 18 (6) (Jun. 2007) 2322–2335.

[23] J.D. van Buul, et al., Inside-out regulation of ICAM-1 dynamics in TNF-alpha-activated endothelium, PloS One 5 (6) (Jun. 2010) e11336.

[24] M. Walski, S. Chlopicki, R. Celary-Walska, M. Frontczak-Baniewicz, Ultrastructural alterations of endothelium covering advanced atherosclerotic plaque in human carotid artery visualised by scanning electron microscope, J.Physiol. Pharmacol. 53 (4 I) (2002) 713–723.

[25] J. Middleton, et al., Transcytosis and surface presentation of IL-8 by venular endothelial cells, Cell 91 (3) (Oct. 1997) 385–395.

[26] A.J. Hoogewerf, et al., Glycosaminoglycans mediate cell surface oligomerization of chemokines, Biochemistry 36 (44) (Nov. 1997) 13570–13578.

[27] E.S. Chhabra, H.N. Higgs, The many faces of actin: matching assembly factors with cellular structures, Nat. Cell Biol. 9 (10) (Oct-2007) 1110–1121.

[28] J.Q. Zheng, J.J. Wan, M.M. Poo, Essential role of filopodia in chemotropic turning of nerve growth cone induced by a glutamate gradient, J. Neurosci. 16 (3) (Feb.1996) 1140–1149.

[29] G. Jacquemet, H. Hamidi, J. Ivaska, Filopodia in cell adhesion, 3D migration and cancer cell invasion, Curr. Opin. Cell Biol. 36 (01-Oct-2015) 23–31 Elsevier Ltd.

[30] A.B. Bohil, B.W. Robertson, R.E. Cheney, Myosin-X is a molecular motor that functions in filopodia formation, Proc. Natl. Acad. Sci. U. S. A 103 (33) (Aug.2006) 12411–12416.

[31] H. Tokuo, K. Mabuchi, M. Ikebe, The motor activity of myosin-X promotes actin fiber convergence at the cell periphery to initiate filopodia formation, J. Cell Biol. 179 (2) (Oct. 2007) 229–238.

[32] J. Van Rijssel, et al., The Rho-GEF Trio regulates a novel pro-inflammatory pathway through the transcription factor Ets2, Biol. Open 2 (6) (Jun. 2013) 569–579.

[33] J. Kroon, et al., Inflammation-sensitive myosin-X functionally supports leukocyte extravasation by cdc42-mediated ICAM-1-rich endothelial filopodia formation, J. Immunol. 200 (5) (2018) 1790–1801.

[34] A. Abo, PAK4, a novel effector for Cdc42Hs, is implicated in the reorganization of the actin cytoskeleton and in the formation of filopodia, EMBO J. 17 (22) (Nov. 1998) 6527–6540.

[35] T. Girbl, et al., Distinct compartmentalization of the chemokines CXCL1 and CXCL2 and the atypical receptor ACKR1 determine discrete stages of neutrophil diapedesis, Immunity 49 (6) (Dec. 2018) 1062–1076 e6.

[36] C. Whittall, O. Kehoe, S. King, A. Rot, A. Patterson, J. Middleton, “, A chemokine self-presentation mechanism involving formation of endothelial surface microstructures, J. Immunol. 190 (4) (Feb. 2013) 1725–1736.

[37] J. Middleton, A.M. Patterson, L. Gardner, C. Schmutz, B.A. Ashton, Leukocyte extravasation: chemokine transport and presentation by the endothelium, Blood 100 (12) (01-Dec-2002) 3853–3860.

[38] G.J. Graham, T.M. Handel, A.E.I. Proudfoot, Leukocyte adhesion: reconceptualizing chemokine presentation by glycosaminoglycans, Trends Immunol. 40 (6) (01-Jun-2019) 472–481 Elsevier Ltd.

[39] Z. Shulman, et al., Transendothelial migration of lymphocytes mediated by intraendothelial vesicle stores rather

than by extracellular chemokine depots, Nat. Immunol. 13 (1) (Jan. 2012) 67–76.

[40] A.E.I. Proudfoot, M. Uguccioni, Modulation of chemokine responses: synergy and cooperativity, Front. Immunol. 7 (2016) MAY. Frontiers Media S.A..

[41] B. Heit, P. Colarusso, P. Kubes, Fundamentally different roles for LFA-1, Mac-1 and α 4-integrin in neutrophil chemotaxis, J. Cell Sci. 118 (22) (Nov. 2005) 5205–5220.

[42] N. Reglero-Real, B. Marcos-Ramiro, J. Millán, Endothelial membrane reorganization during leukocyte extravasation, Cell. Mol. Life Sci. 69 (18) (Sep-2012) 3079–3099.

[43] O. Barreiro, et al., Dynamic interaction of VCAM-1 and ICAM-1 with moesin and ezrin in a novel endothelial docking structure for adherent leukocytes, J. Cell Biol. 157 (7) (Jun. 2002) 1233–1245.

[44] A. Schaefer, et al., Actin-binding proteins differentially regulate endothelial cell stiffness, ICAM-1 function and neutrophil transmigration, J. Cell Sci. 127 (20) (2014) 4470–4482.

[45] C. Amos, et al., Cross-linking of brain endothelial intercellular adhesion molecule (ICAM)-1 induces association of ICAM-1 with detergent-insoluble cytoskeletal fraction, Arterioscler. Thromb. Vasc. Biol. 21 (5) (May 2001) 810–816.

[46] J.D. Van Buul, P.L. Hordijk, Signaling in leukocyte transendothelial migration, Arterioscler. Thromb. Vasc. Biol. 24 (5) (May-2004) 824–833.

[47] J. Huynh, et al., Age-related intimal stiffening enhances endothelial permeability and leukocyte transmigration, Sci. Transl. Med. 3 (112) (Dec. 2011).

[48] K.M. Stroka, H. Aranda-Espinoza, Endothelial cell substrate stiffness influences neutrophil transmigration via myosin light chain kinase-dependent cell contraction, Blood 118 (6) (Aug. 2011) 1632–1640.

[49] L. Schimmel, et al., Stiffness-induced endothelial DLC-1 expression forces leukocyte spreading through stabilization of the ICAM-1 adhesome, Cell Rep. 24 (12) (Sep. 2018) 3115–3124.

[50] M. Schnoor, Endothelial actin-binding proteins and actin dynamics in leukocyte transendothelial migration, J. Immunol. 194 (8) (Apr. 2015) 3535–3541.

[51] C.V. Carman, T.A. Springer, A transmigratory cup in leukocyte diapedesis both through individual vascular endothelial cells and between them, J. Cell Biol. 167 (2) (Oct. 2004) 377–388.

[52] J.D. van Buul, et al., RhoG regulates endothelial apical cup assembly downstream from ICAM1 engagement and is involved in leukocyte transendothelial migration, J. Cell Biol. 178 (7) (Sep. 2007) 1279–1293.

[53] C. V Carman, C. -D. Jun, A. Salas, T.A. Springer, Endothelial cells proactively form microvilli-like membrane projections upon intercellular adhesion molecule 1 engagement of leukocyte LFA-1, J. Immunol. 171 (11) (Dec. 2003) 6135–6144.

[54] D. Vestweber, How leukocytes cross the vascular endothelium, Nat. Rev. Immunol. 15 (11) (Nov. 2015) 692–704.

[55] L. Schimmel, A. de Ligt, S. Tol, V. de Waard, J.D. van Buul, Endothelial RhoB and RhoC are dispensable for leukocyte diapedesis and for maintaining vascular integrity during diapedesis, Small GTPases (Jan. 2018) 1–8.

[56] H.E. Johnson, S.J. King, S.B. Asokan, J.D. Rotty, J.E. Bear, J.M. Haugh, F-actin bundles direct the initiation and orientation of lamellipodia through adhesion-based signaling, J. Cell Biol. 208 (4) (Feb. 2015) 443–455.

[57] M. Krause, A. Gautreau, Steering cell migration: lamellipodium dynamics and the regulation of directional persistence, Nat. Rev. Mol. Cell Biol. 15 (9) (2014) 577–590 Nature Publishing Group.

[58] A.M. Dvorak, S. Kohn, E.S. Morgan, P. Fox, J.A. Nagy, H.F. Dvorak, The vesiculo-vacuolar organelle (VVO): a distinct endothelial cell structure that provides a transcellular pathway for macromolecular extravasation, J. Leukoc. Biol. 59 (1) (1996) 100–115.

[59] S. Citi, D. Guerrera, D. Spadaro, J. Shah, Epithelial junctions and Rho family GTPases: the zonular signalosome, Small GTPases 5 (4) (Dec. 2014).

[60] S. Garrido-Urbani, P.F. Bradfield, B.A. Imhof, Tight junction dynamics: the role of junctional adhesion molecules (JAMs), Cell Tissue Res. 355 (3) (2014) 701–715 Springer Verlag.

[61] F. Wegmann, et al., ESAM supports neutrophil extravasation, activation of Rho, and VEGF-induced vascular permeability, J. Exp. Med. 203 (7) (Jul. 2006) 1671–1677.

[62] C.N. Duong, et al., Interference with ESAM (endothelial cell-selective adhesion molecule) plus vascular endothelial-cadherin causes immediate lethality and lung-specific blood coagulation, Arterioscler. Thromb. Vasc. Biol. 40 (2) (Feb. 2020) 378–393.

[63] E. Dejana, Endothelial cell-cell junctions: happy together, Nat. Rev. Mol. Cell Biol. 5 (4) (Apr-2004) 261–270.

[64] S. Huveneers, et al., Vinculin associates with endothelial VE-cadherin junctions to control force-dependent remodeling, J. Cell Biol. 196 (5) (2012) 641–652.

[65] J. Millán, et al., Adherens junctions connect stress fibres between adjacent endothelial cells, BMC Biol. 8 (1) (Aug. 2010) 11.

[66] A.F. Nottebaum, et al., VE-PTP maintains the endothelial barrier via plakoglobin and becomes dissociated from VE-cadherin by leukocytes and by VEGF, J. Exp. Med. 205 (12) (Nov. 2008) 2929–2945.

[67] M.G. Bixel, et al., CD99 and CD99L2 act at the same site as, but independently of PECAM-1 during leukocyte diapedesis, Blood 116 (7) (Aug. 2010) 1172–1184.

[68] R.L. Watson, et al., Endothelial CD99 signals through soluble adenylyl cyclase and PKA to regulate leukocyte transendothelial migration, J. Exp. Med. 212 (7) (2015) 1021–1041.

[69] R. Seelige, et al., Cutting edge: endothelial-specific gene ablation of CD99L2 impairs leukocyte extravasation in vivo, J. Immunol. 190 (3) (Feb. 2013) 892–896.

[70] N. Heemskerk, et al., F-actin-rich contractile endothelial pores prevent vascular leakage during leukocyte diapedesis through local RhoA signalling, Nat. Commun. 7 (2016).

[71] W.A. Muller, Transendothelial migration: unifying principles from the endothelial perspective, Immunol. Rev. 273 (1) (01-Sep-2016) 61–75 Blackwell Publishing Ltd.

[72] C.V. Carman, Mechanisms for transcellular diapedesis: probing and pathfinding by 'invadosome-like protrusions, J. Cell Sci. 122 (17) (Sep. 2009) 3025–3035.

[73] P.T. Sage, C.V. Carman, Settings and mechanisms for transcellular diapedesis, Front. Biosci. 14 (13) (Jun. 2009) 5066–5083.

[74] C.V. Carman, T.A. Springer, Transcellular migration: cell-cell contacts get intimate, Curr. Opin. Cell Biol. 20 (5) (Oct-2008) 533–540.

[75] C. V Carman, et al., Transcellular diapedesis is initiated by invasive podosomes, Immunity 26 (6) (Jun. 2007) 784–797.

[76] D. Wong, R. Prameya, K. Dorovini-Zis, In vitro adhesion and migration of T lymphocytes across monolayers of human brain microvessel endothelial cells: regulation by ICAM-1, VCAM-1, E-selectin and PECAM-1, J. Neuropathol. Exp. Neurol. 58 (2) (Feb. 1999) 138–152.

[77] G. Cinamon, V. Shinder, R. Shamri, R. Alon, Chemoattractant signals and beta 2 integrin occupancy at apical endothelial contacts combine with shear stress signals to promote transendothelial neutrophil migration, J. Immunol. 173 (12) (Dec. 2004) 7282–7291.

[78] A.M. Ferreira, C.J. McNeil, K.M. Stallaert, K.A. Rogers, M. Sandig, Interleukin-1beta reduces transcellular monocyte diapedesis and compromises endothelial adherens junction integrity, Microcirculation 12 (7) (2005) 563–579.

[79] J. Millán, L. Hewlett, M. Glyn, D. Toomre, P. Clark, A.J. Ridley, Lymphocyte transcellular migration occurs through recruitment of endothelial ICAM-1 to caveola- and F-actin-rich domains, Nat. Cell Biol. 8 (2) (Feb. 2006) 113–123.

[80] L. Yang, R.M. Froio, T.E. Sciuto, A.M. Dvorak, R. Alon, F.W. Luscinskas, ICAM-1 regulates neutrophil adhesion and transcellular migration of TNF-alpha-activated vascular endothelium under flow, Blood 106 (2) (Jul. 2005) 584–592.

[81] C. Riethmuller, I. Nasdala, D. Vestweber, Nanosurgery at the leukocyte-endothelial docking site, Pflugers Archiv European Journal of Physiology 456 (1) (Apr-2008) 71–81.

[82] S. Marmon, M. Cammer, C.S. Raine, M.P. Lisanti, Transcellular migration of neutrophils is a quantitatively significant pathway across dermal microvascular endothelial cells, Exp. Dermatol. 18 (1) (Jan. 2009) 88–90.

[83] Z. Shulman, et al., Lymphocyte crawling and transendothelial migration require chemokine triggering of high-affinity LFA-1 integrin, Immunity 30 (3) (Mar. 2009) 384–396.

[84] M. Abadier, et al., Cell surface levels of endothelial ICAM-1 influence the transcellular or paracellular T-cell diapedesis across the blood-brain barrier, Eur. J.Immunol. 45 (4) (Apr. 2015) 1043–1058.

[85] S. Barzilai, et al., Leukocytes breach endothelial barriers by insertion of nuclear lobes and disassembly of endothelial actin filaments, Cell Rep. 18 (3) (Jan. 2017) 685–699.

[86] I. Wimmer, et al., PECAM-1 Stabilizes Blood-Brain Barrier Integrity and Favors Paracellular T-Cell Diapedesis Across the Blood-Brain Barrier During Neuroinflammation, Front. Immunol. 10 (2019) 711.

[87] V.T. Marchesi, H.W. Florey, Electron micrographic observations on the emigration of leucocyt, Q. J. Exp. Physiol. Cogn. Med. Sci. 45 (4) (Oct. 1960) 343–348.

[88] J.R. Williamson, J.W. Grisham, Leucocytic emigration from inflamed capillaries, Nature 188 (4757) (1960) 1203.

[89] J.R. Williamson, J.W. Grisham, Electron microscopy of leukocytic margination and emigration in acute inflammation in dog pancreas, Am. J. Pathol. 39 (Aug. 1961) 239–256.

[90] C. Schubert, E. Christophers, O. Swensson, T. Isei, Transendothelial cell diapedesis of neutrophils in inflamed human skin, Arch. Dermatol. Res. 281 (7) (1989) 475–481.

[91] S. Fujita, R.K. Puri, Z.X. Yu, W.D. Travis, V.J. Ferrans, An ultrastructural study of in vivo interactions between lymphocytes and endothelial cells in the pathogenesis of the vascular leak syndrome induced by interleukin-2, Cancer 68 (10) (Nov. 1991) 2169–2174.

[92] D. Feng, J.A. Nagy, K. Pyne, H.F. Dvorak, A.M. Dvorak, Neutrophils emigrate from venules by a transendothelial cell pathway in response to FMLP, J. Exp. Med. 187 (6) (Mar. 1998) 903–915.

[93] O. Hoshi, T. Ushiki, Scanning Electron Microscopic Studies on the Route of Neutrophil Extravasation in the Mouse after Exposure to the Chemotactic Peptide N-formyl-Methionyl-Leucyl-Phenylalanine (fMLP), Arch. Histol. Cytol. 62 (3) (1999) 253–260.

[94] M. Phillipson, B. Heit, P. Colarusso, L. Liu, C.M. Ballantyne, P. Kubes, Intraluminal crawling of neutrophils to emigration sites: a molecularly distinct process from adhesion in the recruitment cascade, J. Exp. Med. 203 (12) (Nov. 2006) 2569–2575.

[95] M. Phillipson, J. Kaur, P. Colarusso, C.M. Ballantyne, P. Kubes, Endothelial domes encapsulate adherent neutrophils and minimize increases in vascular permeability in paracellular and transcellular emigration, PLoS One 3 (2) (Feb. 2008).

[96] A. Woodfin, et al., The junctional adhesion molecule JAM-C regulates polarized transendothelial migration of neutrophils in vivo, Nat. Immunol. 12 (8) (Aug. 2011) 761–769.

[97] K. Halai, J. Whiteford, B. Ma, S. Nourshargh, A. Woodfin, ICAM-2 facilitates luminal interactions between neutrophils and endothelial cells in vivo, J. Cell Sci. 127 (3) (Feb. 2014) 620–629.

[98] F. Wessel, et al., Leukocyte extravasation and vascular permeability are each controlled in vivo by different tyrosine residues of VE-cadherin, Nat. Immunol. 15(3) (Mar. 2014) 223–230.

[99] E.A. Hixenbaugh, Z.M. Goeckeler, N.N. Papaiya, R.B. Wysolmerski, S.C. Silverstein, A.J. Huang, Stimulated neutrophils induce myosin light chain phosphorylation and isometric tension in endothelial cells, Am. J. Physiol. 273 (2 Pt 2) (Aug. 1997) H981–H988.

[100] A. Woodfin, M.B. Voisin, B.A. Imhof, E. Dejana, B. Engelhardt, S. Nourshargh, Endothelial cell activation leads to neutrophil transmigration as supported by the sequential roles of ICAM-2, JAM-A, and PECAM-1, Blood 113 (24) (2009) 6246–6257.

[101] G.P. Van Nieuw Amerongen, R. Draijer, M.A. Vermeer, V.W.M. Van Hinsbergh, Transient and prolonged increase in endothelial permeability induced by histamine and thrombin: role of protein kinases, calcium, and RhoA, Circ. Res. 83 (11) (Nov. 1998) 1115–1123.

[102] W.A. Muller, Localized signals that regulate transendothelial migration, Curr. Opin. Immunol. 38 (Feb. 2016) 24–29.

[103] Z. Mamdouh, X. Chen, L.M. Plerini, F.R. Maxfield, W.A. Muller, Targeted recycling of PECAM from endothelial surface-connected compartments during diapedesis, Nature 421 (6924) (Feb. 2003) 748–753.

[104] Z. Mamdouh, A. Mikhailov, W.A. Muller, Transcellular migration of leukocytes is mediated by the endothelial lateral border recycling compartment, J. Exp. Med. 206 (12) (Nov. 2009) 2795–2808.

[105] G. Ostermann, K.S.C. Weber, A. Zernecke, A. Schröder, C. Weber, JAM-I is a ligand of the β2 integrin LFA-I involved in transendothelial migration of leukocytes, Nat. Immunol. 3 (2) (2002) 151–158.

[106] D. Goswami, et al., Endothelial CD99 supports arrest of mouse neutrophils in venules and binds to neutrophil PILRs, Blood 129 (13) (Mar. 2017) 1811–1822.

[107] A.R. Schenkel, Z. Mamdouh, X. Chen, R.M. Liebman, W.A. Muller, CD99 plays a major role in the migration of monocytes through endothelial junctions, Nat. Immunol. 3 (2) (Feb. 2002) 143–150.

[108] D. Shepro, N.M.L. Morel, Pericyte physiology, FASEB (Fed. Am. Soc. Exp. Biol.) J. 7 (11) (1993) 1031–1038.

[109] D. Proebstl, et al., Pericytes support neutrophil subendothelial cell crawling and breaching of venular walls in vivo, J. Exp. Med. 209 (6) (Jun. 2012) 1219–1234.

[110] M.-B. Voisin, et al., Neutrophil elastase plays a non-redundant role in remodeling the venular basement membrane and neutrophil diapedesis post-ischemia/reperfusion injury, J. Pathol. 248 (1) (May 2019) 88–102.

[111] S. Wang, et al., Venular basement membranes contain specific matrix protein low expression regions that act as exit points for emigrating neutrophils, J. Exp. Med. 203 (6) (Jun. 2006) 1519–1532.

[112] J. Song, et al., Endothelial basement membrane laminin 511 contributes to endothelial junctional tightness and thereby inhibits leukocyte transmigration, Cell Rep. 18 (5) (Jan. 2017) 1256–1269.

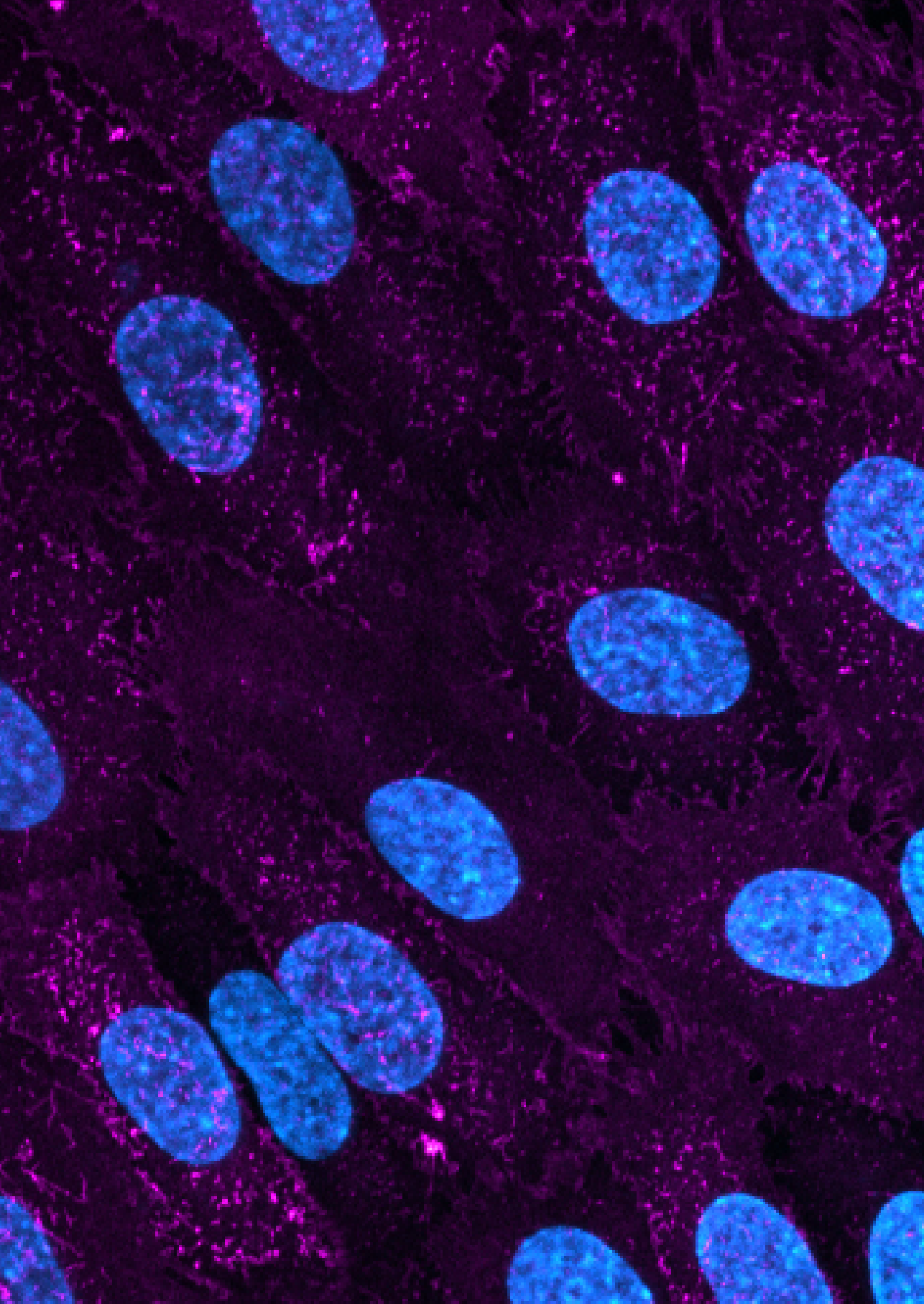

CHAPTER 3

Endothelial ICAM-1 adhesome recruits CD44 for optimal transcellular migration of human cytotoxic T lymphocytes

Abraham C.I. van Steen[1,*]
Sander Joosten[2,3,4]
Floris van Alphen[5]
Maartje van den Biggelaar[5]
Martijn A. Nolte[6]
Marcel Spaargaren[2,3,4]
Jaap D. van Buul[1,7,8,*]
Rouven Schoppmeyer[1,7]

[1] Department of Molecular Hematology, Sanquin Research, Amsterdam, The Netherlands.

[2] Department of Pathology, Amsterdam UMC location University of Amsterdam, Meibergdreef 9, Amsterdam, The Netherlands.

[3] Lymphoma and Myeloma Center Amsterdam (LYMMCARE), Amsterdam, The Netherlands

[4] Cancer Center Amsterdam (CCA), Cancer Biology and Immunology, Target & Therapy Discovery, Amsterdam, The Netherlands

[5] Department of Molecular Hematology, Core Facility, Sanquin Research, Amsterdam, The Netherlands.

[6] Core Facility, Dept. Molecular Hematology, Sanquin Research, Amsterdam, The Netherlands.

[7] Leeuwenhoek Centre for Advanced Microscopy (LCAM), section Molecular Cytology at Swammerdam Institute for Life Sciences (SILS) at University of Amsterdam, The Netherlands.

[8] Department of Medical Biochemistry, Amsterdam UMC location AMC, Amsterdam, the Netherlands.

Submitted Aug. 2022

SUMMARY

The endothelial lining of blood vessels is covered with a thin polysaccharide coat called the glycocalyx. This layer of polysaccharides contains hyaluronan that forms a protective coat on the endothelial surface. Upon inflammation, leukocytes leave the circulation and enter inflamed tissue by crossing inflamed endothelial cells, mediated by adhesion molecules such as ICAM-1/CD54. To what extent the glycocalyx participates in the regulation of leukocyte transmigration is not clear. During extravasation, leukocyte integrins cluster ICAM-1, resulting in the recruitment of a number of intracellular proteins and subsequent downstream effects in the endothelial cells. Using an unbiased proteomics approach, we identified the full ICAM-1 adhesome and identified 93 new subunits of the ICAM-1 adhesome. Interestingly, we found the glycoprotein CD44 as part of the glycocalyx to be recruited to clustered ICAM-1 specifically. Our data demonstrate that CD44 binds hyaluronan to the endothelial surface, where it locally concentrates and presents chemokines that are essential for leukocytes to cross the endothelial lining. Together, we discover a link between ICAM-1 clustering and hyaluronan-mediated chemokine presentation by recruiting hyaluronan to sites of leukocyte adhesion via CD44.

INTRODUCTION

Inflammation is characterized by a local influx of leukocytes from the circulation into the inflamed tissue. Leukocytes typically leave the circulation by rolling on, adhering to, and finally transmigrating across the endothelial monolayers, the cells lining the inner layer of the blood vessels. This process is also known as transendothelial migration (TEM). In the initial adhesion stages, adhesion molecules like ICAM-1 (CD54) are crucially involved. ICAM-1 mediates the firm adhesion of the leukocyte and the endothelium by binding to β2-integrins on immune cells (Dustin & Springer, 1988). Upon leukocyte binding to endothelial cells, ICAM-1 is clustered in a ring-like fashion and induces intracellular signals into the endothelium (Alcaide et al., 2009; van Buul et al., 2007, 2010). These signals support the efficient migration of the immune cells across the endothelium. However, also external signals may be recruited to the ICAM-1 clustering platform (Haymet et al., 2021). We showed that specific membrane structures, called lipid rafts, are induced upon ICAM-1 clustering (van Buul et al., 2010). Preventing the formation of lipid rafts upon ICAM-1 clustering reduced the efficiency of neutrophils to cross the endothelial monolayer.

And although many details have been unraveled in recent years (Liu et al., 2012; Nourshargh et al., 2010; Vestweber, 2015), there are still open questions that deserve an answer. One of these questions involves the role of the glycocalyx in leukocyte TEM. The glycocalyx is a coat of various polysaccharides at the endothelial cells' luminal side (Reitsma et al., 2007). This fragile extracellular structure is a porous, hair-like, regularly organized coat, whose thickness is estimated as 0.5 to 5 μm under physiological conditions and consists of glycosaminoglycans (GAGs) and proteoglycans (Becker et al., 2015; van den Berg et al., 2003). These glycan structures include hyaluronan (also known as hyaluronic acid, HA), a large molecular weight (MDa) glycosaminoglycan, which is highly hygroscopic and forms a porous hydrogel.

Under healthy conditions, HA shields the vessel wall from shear stresses, promotes barrier integrity, and reduces leukocyte and platelet adhesion (Becker et al., 2015; Haymet et al., 2021). However, plasma HA was found to be elevated under various clinical conditions, including ischemia, sepsis, and inflammation(Yagmur et al., 2012). It has also been suggested that HA can support leukocyte extravasation by mediating chemokine presentation on the endothelial surface, although solid proof is missing (Butler et al., 2009).

The glycoprotein CD44 is well recognized for its role as a receptor for hyaluronan (Naor et al., 1997). CD44 is present on a wide variety of cell types, including leukocytes and endothelial cells (Ilangumaran et al., 2010). CD44 comes in a variety of over 20 different isoforms, with CD44 hematopoietic, also known as CD44s (standard), being the most abundant form (Naor et al., 1997). It was shown that CD44 on endothelial cell surfaces supports T cell and

neutrophil rolling (Mylvaganam et al., 2020). Together, CD44 and hyaluronan may mediate several physiological and pathophysiological processes, including inflammatory responses (Camp et al., 1993; Dogné & Flamion, 2020). However, how these two molecules are directly connected to leukocyte TEM is not known.

Using mass spectrometry, we identified the full ICAM-1 adhesome and found that CD44 is recruited to leukocyte-induced ICAM-1 clustering sites. Silencing endothelial CD44 resulted in impaired migration of human cytotoxic T-lymphocytes (CTLs) across primary human endothelial cells under physiological flow conditions. In addition, CD44 silencing also reduced the lateral mobility of ICAM-1 in the endothelial membrane, essential for optimal leukocyte adhesion. Enzymatic removal of endothelial-expressed HA resulted in not only reduced CTL transmigration but also in increased lateral mobility of ICAM-1.

In summary, we provide evidence that ICAM-1 clustering by adhering CTL results in CD44 recruitment and silencing of CD44, or removal of the HA coat, impairs CTL transmigration. Our data reveal a novel link between ICAM-1clustering and HA-mediated chemokine presentation by recruiting CD44 to sites of leukocyte adhesion.

RESULTS

Leukocytes like T-Lymphocytes use their β2-integrin LFA-1 to bind endothelial ICAM-1, and thereby adhere to and efficiently cross the endothelial monolayer. Upon binding, ICAM-1 is clustered, resulting in the recruitment of several actin adapter proteins (van Buul et al., 2007). To reveal the various proteins recruited to ICAM-1 upon clustering, we identified for the first time the proteins recruited to ICAM-1 clustering sites on endothelial cells, also called the ICAM-1 adhesome (Schimmel et al., 2018). For this, we used anti-ICAM-1 antibody-coated leukocyte-sized beads (from hereon called ICAM-1 beads) that we allowed to adhere to the endothelium. This approach resulted in the recruitment of endothelial ICAM-1 and the clustering of intracellular proteins to ICAM-1, called the ICAM-1 adhesome. The condition where we induce clustering of ICAM-1 in living cells is called the “clustered” condition. In the other condition, called the “unclustered condition, cells are lysed before adding the beads, allowing proteins to bind the ICAM-1 beads, but inhibiting the recruitment of the ICAM-1 adhesome. After lysis, ICAM-1-bead bound proteins (the ICAM-1 adhesome) were isolated from cell lysate by magnetic separation. Next, we analyzed the composition of the bead-bound proteins using mass spectrometry (**Figure 1A**). Among the known interactors of clustered ICAM-1, e.g., Filamin A (van Rijssel et al., 2012), we found in total 93 proteins to interact with ICAM-1 upon clustering. Among those, CD44 was found to be present in the ICAM-1 adhesome (**Figures 1B and 1C**). Interestingly, matrix metalloprotease 14 (MMP-14), a protein known to bind and cleave CD44 was also prominently detected (Cho et al., 2012;

Kajita et al., 2001; Mori et al., 2002). The alfa and beta subunits of sprectrin, an intracellular scaffolding protein known to interact with CD44 were also detected (Mylvaganam et al., 2020; Y. Wang et al., 2014). Finally, a string network showing proteins enriched in the unclustered condition comprised predominantly mitochondrial and nuclear proteins, as found in the string analysis network for this population (**Supplemental figure 1A).** The complete list of the ICAM-1 adhesome discovered by mass spectroscopy can be found in the supplemental materials (**Supplemental Figure 1B**).

We confirmed the interaction of CD44 with clustered ICAM-1 using Western blotting (**Figures 2A**). As a negative control, we added the anti-ICAM-1 antibody-coated beads to the endothelial cells' lysates, preventing them from clustering ICAM-1. These controls showed that the beads precipitated ICAM-1, but not the proteins known to be recruited upon clustering like filamin and CD44 (**Figure 2A**). Many proteins in the adhesome are dependent on actin polymerization like filamin B and α-actinin (Schaefer et al., 2014). Therefore, we checked if the interaction between ICAM-1 and CD44 was dependent on the actin cytoskeleton by pretreating the endothelium with the actin polymerizing inhibitor Cytochalasin B. Whereas the interaction of ICAM-1 with Filamin A depends on actin polymerization (Schaefer et al., 2014), we found that CD44-ICAM-1 interaction did not, indicating that the interaction was not simply a member of the actin adapter protein interactome (**Figure 2A**).

As CD44 is expressed in various isoforms (**Figure 2B**) (Naor et al., 1997), we set out to determine the prominent isoforms in endothelial cells and studied the influence of inflammation on isoform expression. Using the nested PCR technique (Zeilstra et al., 2014), we measured the different splice variants present in the endothelium (**Figure 2C**). We found predominant expression of the CD44s variant and low expression of CD44v10, CD44v6-10, CD44v3 and CD44v6 (**Figure 2B**). We did not find any difference in the expression of the isoforms between control and inflamed, i.e., TNF-treated endothelial cells (**Figure 2C**). Immunofluorescence labeling of HUVEC showed that under inflammatory conditions, ICAM-1 and CD44 co-localized on endothelial filopodia (**Figure 2D**). These small finger-like structures are induced by inflamed endothelial cells to present adhesion molecules to adherent leukocytes (Kroon et al., 2018).

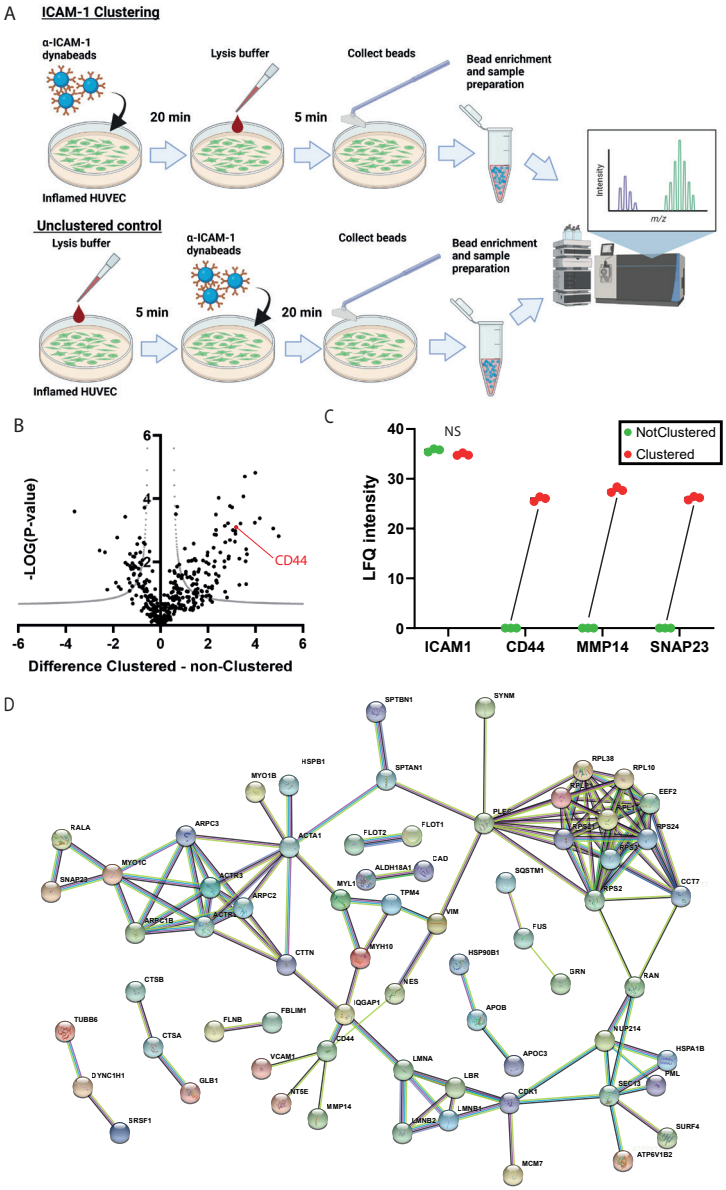

Figure 1. Proteomic analysis of ICAM-1 adhesome recruited after ICAM-1 clustering reveals 93 proteins enriched.

(A) ICAM-1 clustering was induced in 20h (10ng/mL) TNF-stimulated HUVEC by α-ICAM-1 antibody coated dynabeads. In "Clustered" conditions, beads were added to live HUVECs for 30 min. After 30 minutes, HUVEC were lysed on ice, and total cell lysate (TCL) was collected. In "Unclustered" conditions, HUVEC were lysed, and beads were added to the lysate for 30 minutes. TCL for both conditions was used as input control. The remaining lysate was cleared using magnetic bead washing and digested for proteomic analysis. (B) Vulcano plot of identified proteins. Proteomic analysis of clustered and unclustered samples identified 374 proteins. 132 proteins were significantly enriched, 93 in the clustered condition and 39 in the unclustered condition. (C) LFQ intensity plot of ICAM-1, CD44, MMP14, and SNAP-23. LFQ intensity of selected proteins shows ICAM-1 has similar levels in clustered and unclustered conditions. CD44, MMP14, and SNAP-23 are below the detection limit in unclustered samples and detected in all clustered samples. This indicates CD44,

MMP-14, and SNAP-23 bind ICAM-1 only after clustering. (D) String analysis of proteins enriched in clustered samples. This network represents proteins enriched in the clustered condition and therefore represents the recruited ICAM-1 adhesome.

To study if CD44 plays an essential role in CTL extravasation, we depleted CD44 from endothelial cells (**Supplemental Figure 2A**). Important to note is that the antibody we used to test for CD44 protein expression recognized the constant region of CD44 and therefore recognized all isoforms, which includes CD44s. We allowed CTLs to cross inflamed endothelial cells under physiological flow conditions. CD44 silencing did not affect adhesion numbers (**Figure 3A**) but reduced the number of CTLs showing polarization and migration after adhesion to the endothelial monolayer (**Figure 3B). Moreover,** we found that the number of CTLs that crossed endothelial monolayers deficient for CD44 was significantly reduced (**Figure 3C**). Interestingly, we also measured a shift from transcellular to paracellular events when endothelial cells were depleted for CD44 (**Figure 3D**). As adhesion and crawling depends on ICAM-1 mobility (12), we started to assess if CD44 is involved in the mobility of ICAM-1. To study this, we used Fluorescence Recovery after Photobleaching (FRAP) with HUVEC overexpressing ICAM-1-GFP (**Figure 3E**).

Depletion of CD44 resulted in a significant increase of the ICAM-1 mobility in the endothelial plasma membrane (**Figure 2D**). Also, the plateau value showed a more substantial recovery indicating a larger mobile fraction of ICAM-1 in the absence of CD44 (**Figure 3E**). Due to their importance in leukocyte adhesion and as we found that CD44 localized to ICAM-1-rich filopodia under inflammatory conditions (**Figure 2D**) and regulated ICAM-1 membrane mobility, we questioned if CD44 is involved in the formation of ICAM-1-rich filopodia. Therefore, we quantified the number of filopodia on CD44-silenced endothelial cells (**Figure 3F**). Strikingly, we found that filopodial numbers are drastically reduced in endothelial cells that were silenced for CD44 (**Figure 3F**).

As CD44 is the primary receptor for Hyaluronan (HA), one of the main components of the endothelial glycocalyx (Naor et al., 1997), we next focused on the role of HA in CTL TEM. First, we assessed if HA can be stained on the surface of endothelial cells using an HA-binding protein stain. The results showed the presence of HA on the endothelial monolayer (**Figure 4A**). Furthermore, we found that inhibition of HA by treating endothelial cells with hyaluronidase increased ICAM-1 membrane mobility to the same degree as we found upon depletion of CD44 (**Figure 4B**).

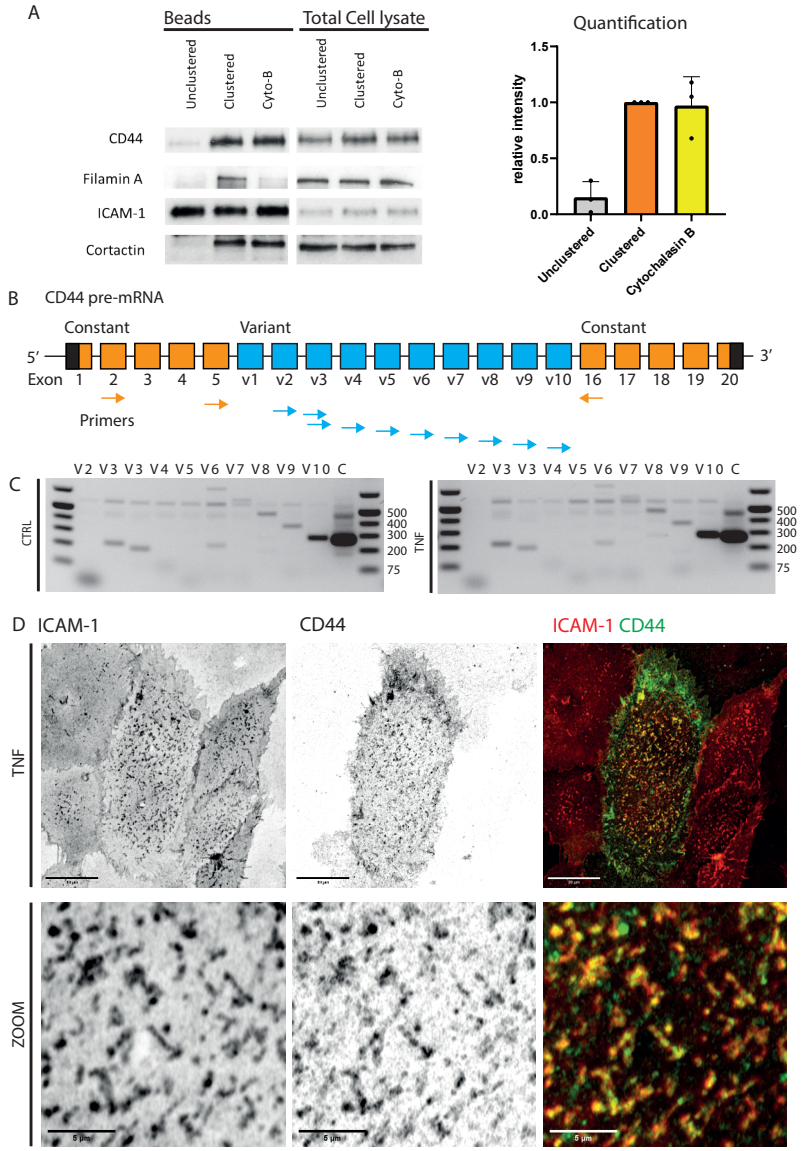

Figure 2. CD44s co-localises with ICAM-1 in finger-like protrusions on inflamed HUVEC; the interaction requires ICAM-1 clustering.
(A) Western blot analysis shows CD44 recruitment to unclustered, clustered, and clustered in cytochalasin-B treated HUVEC. In "Unclustered" conditions, HUVEC were lysed, and beads were added to the lysate for 30 minutes. In "Clustered" and "Cytochalasin B" conditions, beads were added to live HUVECs for 30 min. After 30 minutes, HUVEC were lysed on ice, and TCL was collected. In the "Cytochalasin B" condition, HUVEC were pretreated with 2µM cytochalasin B for 10 minutes. TCL is used as input control. Beads were washed using magnetic bead washing. (B) Schematic of nested PCR for CD44 variant exon usage. (C) CD44 variant exon usage in control and TNF treated (20h, 10ng/mL) HUVEC. HUVECs express CD44s predominantly as well as low expression of CD44v10, CD44v6-10, CD44v3 & CD44v6. TNF treatment does not alter CD44 exon usage. (D) HUVEC were grown in µ-slides, treated with TNF (10ng/mL) for 20 hours, and fixed. Cells were stained for ICAM-1 and CD44.

We next tested the importance of HA in CTL adhesion to and migration across the endothelium by removing HA from the endothelial surface. Endothelial cells were pretreated with TNFα, and subsequently with hyaluronidase, after which CTL TEM was analyzed in a physiological flow system. We found that hyaluronidase treatment significantly reduced CTL adhesion to the endothelium (**Figure 4C**), and CTLs showed reduced polarization and migration phenotype. And consequently, we found that the number of CTLs that crossed the endothelial monolayer was also drastically impaired (**Figure 4E**). As for silencing CD44, we observed a shift towards more paracellular events. These data showed that an intact HA-coat is essential for efficient CTL TEM (**Figure 4F**).

Key molecules for efficient CTL TEM are chemokines (Cinamon et al., 2001; Schreiber et al., 2007). The endothelium can present these chemokines to assist CTL TEM (Middleton et al., 2002). To study if chemokines are linked to the HA coat and are involved in the presentation of chemokines, we assessed which chemokines are released by the endothelium and if enzymatic treatment with hyaluronidase increased the number of chemokines in the endothelial supernatant (**Figure 5A**). Interestingly, the amount of the chemokines that we measured in the supernatant was indeed significantly increased upon hyaluronidase treatment (**Figure 5A**). CXCL1/10 and fractalkine are well recognized for their role in CTL TEM (Fong et al., 1998; Karin, 2020; Schoppmeyer et al., 2022). Heparan sulfate (HS), another main glycosaminoglycan in the endothelial glycocalyx, can bind specific chemokines (Bao et al., 2010; Lortat-Jacob, 2009; D. Wang et al., 2003). When using heparinase to remove HS from the endothelia surface enzymatically, we only detected a slight increase in the amount of CCL5/20/22 and CXCL1 in the supernatant (**Figure 5A**). These data indicate that in particular HA mediates the general presentation of the chemokines tested at the apical surface of the endothelium.

Based on these data, we hypothesized that chemokines are bound to the apical endothelial surface by HA and upon clustering of ICAM-1 by adherent CTL, CD44 is effectively recruited to leukocyte adhesion sites, additively recruiting HA-bound chemokines. This series of events activates the β2-integrins on the CTL to firmly adhere to and migrate across the endothelium. To test our hypothesis, i.e., the binding of chemokines to HA and its recruitment along CD44 via ICAM-1 clustering facilitated CTL TEM, we used supernatant of endothelial cells that were treated with inflammatory stimuli and thus contain HA-binding chemokines. Endothelial cells were incubated with either supernatant of inflamed endothelium or supernatant of non-treated endothelium and analyzed CTL TEM (Schoppmeyer et al., 2022).

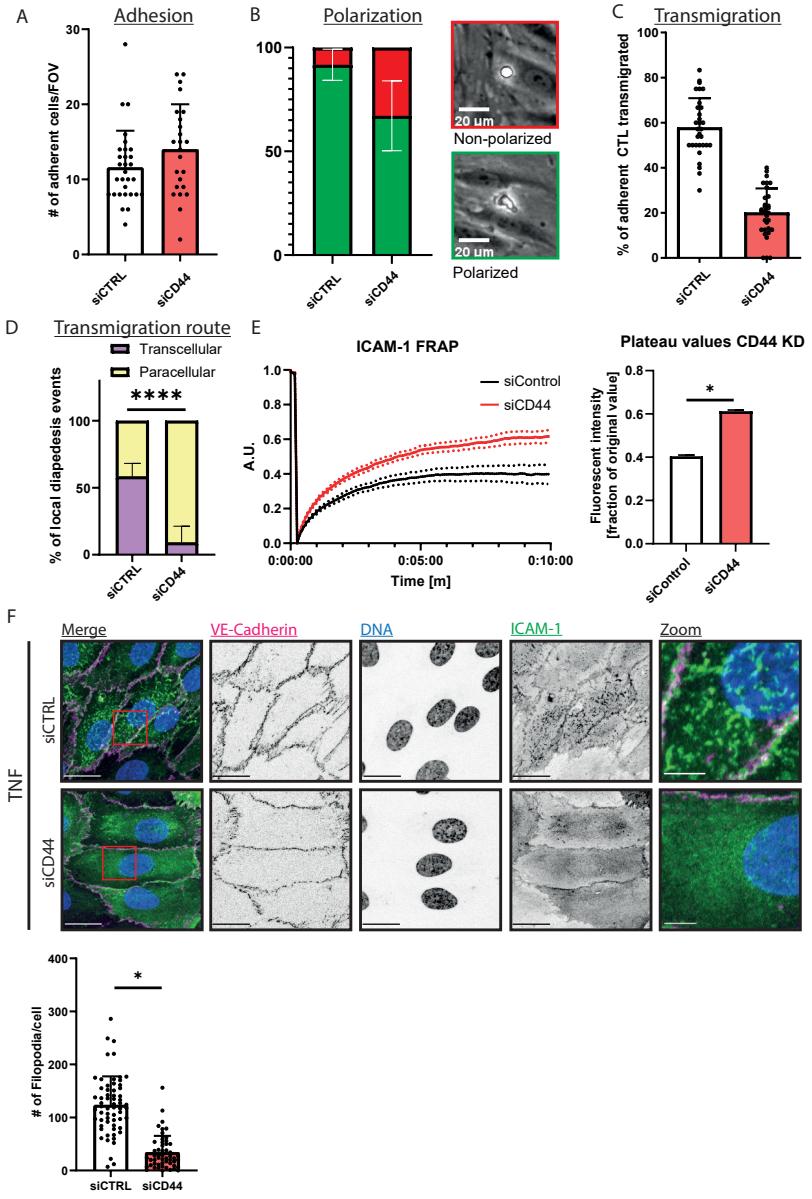

Figure 3. siRNA inhibition of CD44 in HUVEC reduces CTL transmigration under flow efficiency and formation of endothelial finger-like protrusions.

(A) CD44 expression in HUVEC was knocked down using siRNA against CD44 or non-sense siRNA. HUVECs were cultured in a µ-slide (Ibidi) and activated with TNF for 20 h (10ng/mL), after which CTL were flowed over the HUVEC while being imaged every 5 seconds. The number of adhering leukocytes per field of view (FOV) was counted. (B) Quantification of the polarization of adhering CTL. Image inserts show examples of polarized and non-polarized CTL. (C) Percentage of adhering CTL that transmigrated through the endothelial monolayer. (D) ICAM-1-GFP was overexpressed in HUVEC using a lentiviral vector and then transduced with siCTRL or siCD44. HUVEC were cultured in a µ-dish for 2 days after reaching confluency and activated with TNF for 20 h (10ng/mL). A cell region was bleached, and FRAP was measured. Fluorescent intensity is shown as a ratio of fluorescent intensity before bleaching. Plateau values were calculated using the logarithmic plateau fit in

Graphpad Prism. (E) HUVEC were transduced with siRNA against CD44 or non-sense siRNA, treated with TNF for 20 hours, and fixed. HUVEC were stained for VE-cadherin, DNA, and ICAM-1 and imaged. Quantification of filopodia was performed with Imaris software and shown beneath the images.

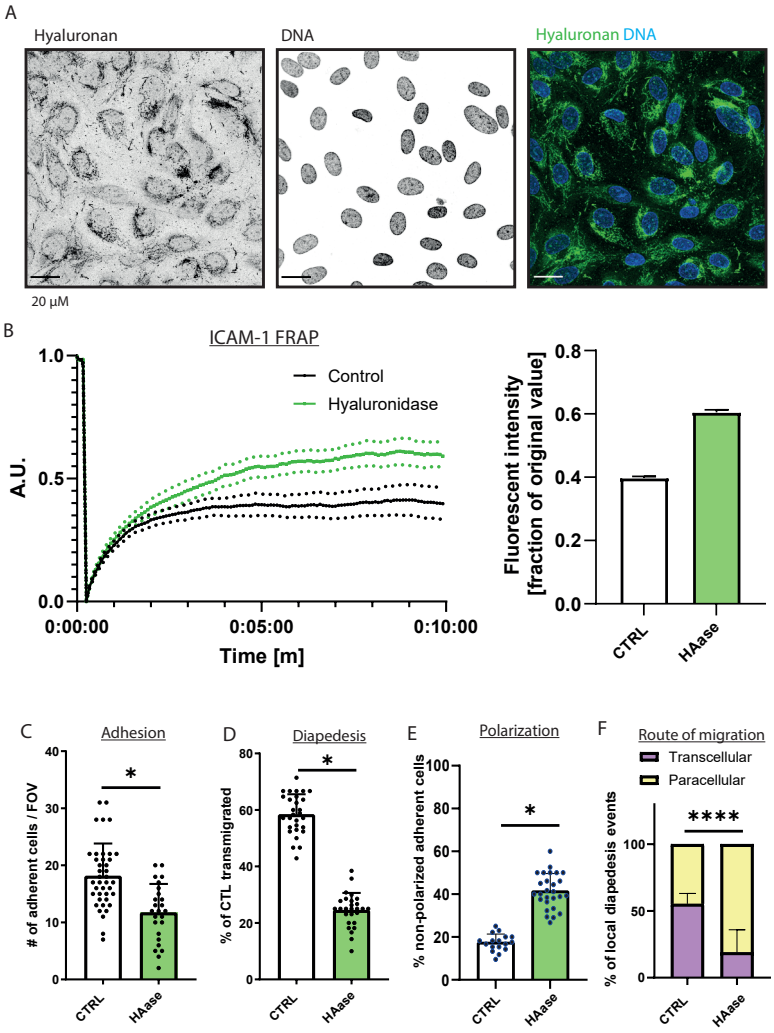

Figure 4. Enzymatic degradation of endothelial HA increases ICAM-1 mobility and inhibits CTL transmigration.

(A) HUVEC were cultured for 3 days after reaching confluency and activated with TNF for 20h before methanol fixation. Cells were stained for HA with biotinylated hyaluronic acid binding protein (HABP) and DNA using Hoechst 33342. (B) ICAM-1-GFP was overexpressed in HUVEC using a lentiviral vector. HUVEC were cultured in a µ-dish for 2 days after reaching confluency and activated with TNF for 20 h (10ng/mL). HUVEC were then treated with hyaluronidase or vehicle. A cell region was bleached, and FRAP was measured. Fluorescent intensity is shown as a ratio of fluorescent intensity before bleaching. Plateau values were calculated using the logarithmic plateau fit in Graphpad Prism. (C) HUVECs were cultured in a µ-slide (Ibidi), activated with TNF for 20 h (10ng/mL), and treated with hyaluronidase, after which CTLs were flowed over the HUVEC while being imaged every 5 seconds. The number of adhering CTL per field of view (C), percentage of adherent CTL that successfully migrated through the endothelium (D), and the number of non-polarizing adhering CTL (E) were quantified.

Interestingly, inflamed supernatant drastically induced transmigration of CTL compared to control supernatant (**Figure 5B**). Treatment with hyaluronidase showed the dependence on HA in this experimental setup (**Figure 5B**).

To proof that CTL TEM depends on HA and not HS, we used CXCL12, as CXCL12 is known to bind to HS and not HA (Panitz et al., 2016) and CTL express the cognate receptor CXCR4 (T. Zhang et al., 2005). CXCL12 was immobilized on the endothelium and CTL TEM was analyzed under flow and inflammatory conditions. We found that endothelial surface that was loaded with CXCL12 promoted CTL TEM (**Figure 5C**). Treating CXCL12-immobilized endothelial cells with hyaluronidase decreased overall transmigration efficiency, however did not affect the CXCL12 mediated increase in CTL TEM. This indicates that CXCL12 promotion of CTL TEM is independent of HA presence on the endothelium.

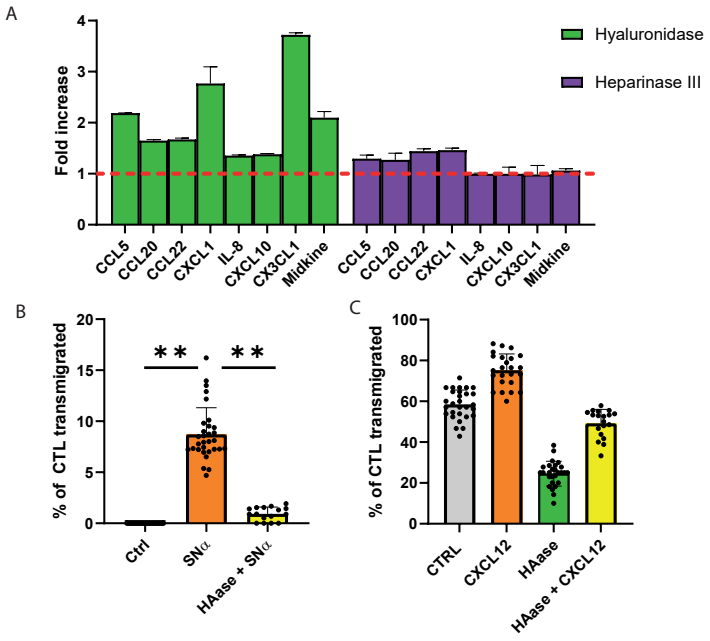

Figure 5. Endothelial HA binds chemokines that can drive CTL transmigration.
(A) HUVEC were cultured in a fibronectin-coated dish and activated with TNF for 20 h. The medium was removed and replaced with a medium containing vehicle, hyaluronidase, or heparinase III. After 2 hours, the supernatant was harvested, and a chemokine screen was performed using the chemokine profiler kit (RnD). Chemokine expression is shown as a ratio of control. The screen was performed once with a technical duplicate; therefore, no statistics were done. (B) HUVEC were cultured in a fibronectin-coated µ-dish, and activated for 15 minutes with TNF. The medium was then changed again, and conditioned supernatant (SN) containing chemokines secreted by activated HUVEC was harvested after 24 hours. Non-inflamed HUVEC in another µ-dish were treated with hyaluronidase or vehicle and then loaded with the conditioned SN. The conditioned SN was washed away, and CTL were added to the non-inflamed HUVEC. The transmigration of CTL was quantified using life-cell microscopy. (C) HUVEC were cultured in a fibronectin-coated µ-dish,

activated with TNF for 20 h, and treated with hyaluronidase or vehicle. Recombinant CXCL12 was loaded on the endothelium for 10 minutes and washed away. Then CTL were added, and transmigration was quantified as % of adherent CTL.

DISCUSSION

Clustering of ICAM-1 and, as a result, the recruitment of several actin adapter proteins has been recognized over recent years to play an important role in several pathways involved in the multistep leukocyte extravasation cascade (Schaefer et al., 2014; Schimmel et al., 2018). Recently, the importance of this complex and the different pathways it controls has led it to be named the ICAM-1 adhesome. Here we have, for the first time, performed an unbiased proteomic analysis of the complete ICAM-1 adhesome in an attempt to map the entire complex. By doing this, we have discovered several proteins not previously linked to ICAM-1 and leukocyte TEM. Furthermore, this screen reveals a potential link between ICAM-1 clustering and glycocalyx function.

The glycocalyx has only recently undergone a change in the perception of its physiological function and importance. Apart from recent reviews on the subject matter regarding transmigration under inflammation conditions, the glycocalyx has been studied only marginally, implicating involvement in chemokine presentation as most chemokines bind either HA or HS (Graham et al., 2019). Limiting adhesion to endothelial cells by blocking adhesion molecule access to bypassing leukocytes and subsequently reducing transmigration and tissue infiltration is a commonly assumed primary function of the glycocalyx (Hu et al., 2021; Iba & Levy, 2019). Studies show that glycocalyx structure and thickness change upon inflammation, and even non-inflammatory-caused alterations of the endothelial glycocalyx can partly mimic inflammatory conditions (Delgadillo et al., 2021; Qu et al., 2021). A considerable hindrance in glycocalyx research, also from our own experience, is the lack of cell biological tools for imaging purposes, the glycocalyx' sensitivity to washing and fixation techniques, and that glycocalyx formation *in vitro* depends on cell type and culture conditions and length.

Enzymatic removal of HS was shown to increase the adhesion of acute promyelocytic leukemia cells on human abdominal aortic endothelial cells (McDonald et al., 2016). The authors attribute increased cell adhesion to a proinflammatory-like phenotype induced by HS removal and consequent exposure and upregulation of ICAM-1 on the endothelial cell surface. As transmigration was analyzed for cancer cells, the described results cannot be directly translated to leukocytes.

For HA, reports are more scarce. In 1997 DeGrendele *et al*. published that in mice, activated (effector) T cells show increased binding to endothelial HA in a CD44-dependent manner,

implying importance in transmigration under inflammatory conditions (DeGrendele et al., 1997). Zhang *et al*. showed shortly after that blocking CD44-HA interaction had an inhibitory effect on immune cell infiltration in a rat organ graft model (W. Zhang et al., 2000). Overall, CD44 (on $CD4^+$ T cells (Brennan et al., 1999) and endothelial cells (Mylvaganam et al., 2020)) has been implicated in participating in the control of transmigration.

We recently showed that specifically, cytotoxic effector $CD8^+$ T cells show high levels of transcellular migration, which relies on the formation of a diapedesis synapse, that itself is not required for paracellular migration of these T cells (Schoppmeyer et al., 2022). Formation of the synapse induces ICAM-1 clustering on endothelial cells at the synapse resulting in the recruitment of SNAP23 to the synapse (Schoppmeyer et al., 2022). These data were confirmed in the ICAM-1 adhesome presented in this study.

Among SNAP23 (Schoppmeyer et al., 2022), we show that CD44 is specifically recruited to clustered ICAM-1, independent of actin polymerization. Of the various CD44 isoforms, we find mainly the full CD44s and the expression profile is unchanged before and after inflammatory stimulation. Using immunofluorescent labeling of endothelial ICAM-1, which also reveals endothelial filopodia, in combination with CD44-labeling, we found CD44 to be co-localized with ICAM-1 on filopodia. These filopodia have been established as important structures mediating the initiation of transmigration of leukocytes.

ICAM-1 expression on cells induces the formation of protrusions which have been shown to depend on Myosin X and which support leukocyte extravasation (Kroon et al., 2018; Oh et al., 2007). Interestingly, CD44 appears essential for the formation of ICAM-1 filopodia on EC, as silencing of CD44 drastically reduced ICAM-1-rich filopodia. In line, silencing of CD44 reduces transmigration efficiency of CTLs without affecting adhesion numbers significantly. Notably, upon silencing CD44, adhering CTLs show less polarization after contact, implying a lack of chemotactic stimulation (Schoppmeyer et al., 2022). Additionally, we found that silencing CD44 increases ICAM-1 membrane mobility which can negatively affect clustering. Recently, Freeman and colleagues (Freeman et al., 2018) showed that CD44 acts as a picket fence by interacting with cortical actin (intracellularly) and HA (extracellularly), limiting receptor membrane motility. When endothelial cells are treated with hyaluronidase, we observed the same increase in ICAM-1 membrane mobility. This implies that restricted ICAM-1 mobility and clustering are mediated by CD44 bound to HA.

When using hyaluronidase to digest the endothelial glycocalyx, CTL transmigration is significantly reduced. We hypothesized that this is due to a lack of initial integrin-activating chemotactic stimulation and decreased filopodia presence. Potentially, chemokines are immobilized at the endothelial surface by HA, and upon ICAM-1 clustering, CD44 is recruited. Potentially this recruitment of CD44 leads to the recruitment of CD44-bound HA,

which binds chemokines, that could further stimulate CTL clustering ICAM-1.

When we analyzed the release of chemokines from the glycocalyx by enzymatically reducing endothelial glycocalyx components HS and HA, we found that digestion of HA significantly increased the levels of a set of endothelial-secreted chemokines over baseline. When applying the same analysis after HS digest, apart from a marginal increase of CXCL1 and CCL20 in the supernatant, which bind to HS (Nonaka et al., 2014; Wang et al., 2003), no other chemokines were released.

Based on the data presented here and previous published data, we postulate that inflammation-induced chemokines in endothelial cells are immobilized at the endothelial cell surface by HA. CD44 enhances ICAM-1 filopodia formation and the presence of CD44 upon ICAM-1 clustering lowers membrane mobility of ICAM-1 and thereby increases its adhesion function and allow more HA-bound chemokines to activate CTLs locally to start migrating across the endothelial monolayer.

DETAILED METHODS

HUVEC cell culture (subculture, and TNFα activation) and CTL recovery culture

Endothelial cells were cultured under sterile conditions in an incubator at 37 °C and 5 % CO_2. HUVEC were cultured in EGM-2 (PromoCell) with the endothelial cell growth supplement and 1% Penicillin/Streptomycin and grown on fibronectin (Sanquin Reagents) coated plastic culture dishes (TPP). Detachment of endothelial cells was done by washing with 37 °C PBS and incubation with Trypsin*EDTA (1 mL per 100 mm dish) until detachment. The reaction was stopped using the same volume of trypsin neutralizing solution (Sigma) as trypsin solution, followed by centrifugation at 250 g for 5 min to change to full medium. HUVEC were stimulated with TNFα (10 ng mL^{-1}) in EGM-2 overnight or for indicated times. CTL were recovered after isolation overnight in RPMI medium at 37 °C and 5 % CO_2 before use in experiments.

Cell treatments

Fluorescent membrane labeling of CTL was done in HEPES buffer (20 mM HEPES,132 mM NaCl, 6 mM KCL, 1 mM $CaCl_2$, 1 mM $MgSO_4$, 1.2 mM K_2HPO_4, 1 g L^{-1} D-glucose, and 0.5 % (w/v) human serum albumin) using 1:6000 diluted Vybrant DiD (Thermo Fisher) for 20 minutes at 37° in an Eppendorf tube. This was followed by a washing step (250 g, 5 min) and resuspension in medium.

To test if chemokines secreted by HUVEC cells are bound to the hyaluronic acid coat, we treated HUVEC with hyaluronidase (400 U mL^{-1}) or heparinase III (0.5 µg mL^{-1}) the chemokine

content in supernatant was compared. Upon hyaluronidase treatment (30 min, 400 U mL^{-1}) more chemokines are released into the supernatant, which was not the case for heparinase III treatment (30 min, 0.5 µg mL).

After overnight stimulation with TNFα the medium was removed and either replaced by fresh medium or fresh medium containing 400 U mL^{-1} hyaluronidase or 0.5 mg mL^{-1} heparinase III. After 30 min the medium was collected, centrifuged at 700 g for 5 min and placed on ice until processing in a chemokine array the same day. Data are from at least 3 donors each.

Supernatant

Supernatant was collected 20h post TNFα addition to HUVEC monolayers. Medium was not exchanged after addition of TNFα and no washing steps were applied before collection. The supernatant was frozen at -20°C when not used right away. Huvec monolayers were loaded with supernatant containing chemokines by removing the medium from a non-stimulated monolayer and incubation the monolayer with the frozen supernatant for 30 min prior to addition of T cells. For adding T cells the supernatant was removed and medium containing T cells was added.

Sample preparation for mass spectrometry analysis

Sample preparation has been performed as previously published (Schillemans et al., 2019). Immunoprecipitated proteins were reduced on-bead in 1M urea (Life technologies),10mM DTT (Thermo Scientific) in 100mM TRIS-HCl pH 7.5 (Life technologies) for 20 minutes at 25°C, followed by alkylation with 50mM iodoacetamide (Life technologies) for 10 minutes at 25°C. Proteins were detached from the beads by incubation with 250ng MS-grade trypsin (Promega) for 2 hours at 25°C. Beads were removed and proteins were further digested for 16 hours at 25°C with 350ng MS-grade trypsin (Promega). Tryptic peptides were desalted and concentrated using in house prepared Empore-C18 StageTips and eluted with 0.5% (v/v) acetic acid in 80 % (v/v) acetonitrile. Sample volume was reduced by SpeedVac and supplemented with 2 % acetonitrile, 0.1% TFA to a final volume of 5 µl. 3 µl of each sample was injected for MS analysis.

Mass spectrometry data acquisition

Tryptic peptides were separated by nanoscale C18 reverse phase chromatography coupled online to an Orbitrap Fusion Tribrid mass spectrometer (Thermo Scientific) via a nanoelectrospray ion source (Nanospray Flex Ion Source, Thermo Scientific). Peptides were loaded on a 20 cm 75–360 µm inner-outer diameter fused silica emitter (New Objective) packed in-house with ReproSil-Pur C18-AQ, 1.9 µm resin (Dr. Maisch GmbH). The column was installed on a Dionex Ultimate3000 RSLC nanoSystem (Thermo Scientific) using a MicroTee union formatted for 360 µm outer diameter columns (IDEX) and a liquid junction. The spray voltage was set to 2.15 kV. Buffer A comprised 0.5 % acetic acid and buffer B of 0.5 % acetic

acid and 80% acetonitrile. Peptides were loaded for 17 min at 300 ml/min at 5% buffer B, equilibrated for 5 minutes at 5% buffer B (17-22 min), and eluted by increasing buffer B from 5-15% (22-87 min) and 15-38% (87-147 min), followed by a 10-minute wash to 90 % and a 5 min regeneration to 5%. Survey scans of peptide precursors from 400 to 1500 *m*/*z* were performed at 120K resolution (at 200 *m*/*z*) with a 4×10^5 ion count target. Tandem mass spectrometry was performed by isolation with the quadrupole with isolation window 1.6, HCD fragmentation with a normalized collision energy of 30, and rapid scan mass spectrometry analysis in the ion trap. The MS^2 ion count target was set to 1.5×10^4, and the max injection time was 35 ms. Only those precursors with charge states 2–7 were sampled for MS^2. The dynamic exclusion duration was set to 30 s with a 10 ppm tolerance around the selected precursor and its isotopes. Monoisotopic precursor selection was turned on. The instrument was run in top speed mode with 3 s cycles. All data were acquired with SII for Xcalibur software.

HUVEC RNA isolation and CD44 RT-PCR analysis

HUVEC were grown in a fibronectin-coated 6-well dish until confluency and stimulated with TNF or vehicle for 20 hours and washed with 37° PBS containing 1 mM $CaCl_2$ and 0.5 mM $MgCl_2$. Cells were then lysed and RNA isolated using the RNeasy Plus Micro Kit (Qiagen, cat. Nr. 74034) according to the manufacturers' instructions. cDNA was created using the SuperScript III (ThermoFisher, cat. Nr. 18080093) according to the manufacturers' instructions. Exon specific RT-PCR of CD44 was then performed as explained previously (Zeilstra et al., 2014).

The following primers were used:

Target	Orientation	Sequence (5'→ 3')
Exon-2	se	GATGGAGAAAGCTCTGAGCATC
Exon-16	as	TTTGCTCCACCTTCTTGACTCC
Exon-5	se	AAGACATCTACCCCAGCAAC
Exon-v2	se	GATGAGCACTAGTGCTACAG
Exon-v3a	se	ACGTCTTCAAATACCATCTC
Exon-v3b	se	TGGGAGCCAAATGAAGAAAA
Exon-v4	se	TCAACCACACCACGGGCTTT
Exon-v5	se	GTAGACAGAAATGGCACCAC
Exon-v6	se	CAGGCAACTCCTAGTAGTAC
Exon-v7	se	CAGCCTCAGCTCATACCAGC
Exon-v8	se	TCCAGTCATAGTATAACGCT
Exon-v9	se	CAGAGCTTCTCTACATCACA
Exon-v10	se	GGTGGAAGAAGAGACCCAAA

ICAM-1-GFP FRAP

Cells were transfected with ICAM-1-GFP using a lentiviral vector described in the methods'

transduction part. Transfected cells were seeded in µ-slide 8 well high dishes (IBIDI) at a density of 5,0*10^4 cells per well. Cells were then cultured for two more days until the experiment, which was performed on day 7. FRAP experiments were performed on an LSM980 with an Airyscan2 module (Zeiss) using a 40x oil immersion objective (NA 1.3). An image was acquired every 5 seconds. After 3 frames, an area was bleached using the interactive bleaching module and 8 iterations at 100% laser power using the 488 nm laser. Recovery was then measured over 10 minutes which was sufficient for recovery to reach plateau values. Analysis was performed in ImageJ, and data was processed in MS Excel. Raw intensity values of the bleached area were converted to relative intensity by subtracting the minimum value from all values and normalizing these corrected values from zero to one to allow for comparison and statistics. One represents the maximum fluorescent intensity which is typically the fluorescent intensity before bleaching, and zero is the minimum intensity which corresponds to the first frame after bleaching. Statistics were calculated using GraphPad Prism. Plateau values were calculated using the logarithmic plateau fit function in GraphPad.

The following methods are used in Chapter 4 and are described there

- Flow channel preparation
- Live imaging transmigration under flow
- PBMC and CTL isolation for *in vitro* experiments
- Image analysis
- Chemical fixation of cells for immunofluorescence labeling
- Immunofluorescence staining of cells for microscopy
- Chemokine analysis
- Statistical analysis
- Virus production
- Coating of polystyrene beads with α-ICAM-1 antibodies
- ICAM-1 pull-out
- Transfection of HUVECs siRNA
- Western blot analysis of ICAM-1 bead pull-out

Keywords

Cytotoxic T cell, transendothelial migration, transcellular, endothelial cells, inflammation, glycosaminoglycans, glycocalyx, CD44, hyaluronic acid, hyaluronan

Acknowledgements

This work was supported by LSBR grant # 1649 (A.C.I.v.S.), and ZonMW NWO Vici grant #91819632 (RS and J.D.v.B.).

Author contributions

A.C.I.v.S., S.J., F.v.A., M.v.d.B., M.S., and R.S. performed experiments, analysed data. A.C.I.v.S., J.D.v.B. and R.S. wrote manuscript. M.A.N. and J.D.v.B. supervised the study.

REFERENCES

Alcaide, P., Auerbach, S., & Luscinskas, F. W. (2009). Neutrophil recruitment under shear flow: it's all about endothelial cell rings and gaps. *Microcirculation (New York, N.Y. : 1994)*, *16*(1), 43–57. https://doi.org/10.1080/10739680802273892

Bao, X., Moseman, E. A., Saito, H., Petryanik, B., Thiriot, A., Hatakeyama, S., Ito, Y., Kawashima, H., Yamaguchi, Y., Lowe, J. B., von Andrian, U. H., & Fukuda, M. (2010). Endothelial Heparan Sulfate Controls Chemokine Presentation in Recruitment of Lymphocytes and Dendritic Cells to Lymph Nodes. *Immunity*, *33*(5), 817–829. https://doi.org/10.1016/J.IMMUNI.2010.10.018

Becker, B. F., Jacob, M., Leipert, S., Salmon, A. H. J., & Chappell, D. (2015). Degradation of the endothelial glycocalyx in clinical settings: searching for the sheddases. *British Journal of Clinical Pharmacology*, *80*(3), 389–402. https://doi.org/10.1111/BCP.12629

Brennan, F. R., O'Neill, J. K., Allen, S. J., Butter, C., Nuki, G., & Baker, D. (1999). CD44 is involved in selective leucocyte extravasation during inflammatory central nervous system disease. *Immunology*, *98*(3), 427–435. https://doi.org/10.1046/J.1365-2567.1999.00894.X

Butler, L. M., Rainger, G. E., & Nash, G. B. (2009). A role for the endothelial glycosaminoglycan hyaluronan in neutrophil recruitment by endothelial cells cultured for prolonged periods. *Experimental Cell Research*, *315*(19), 3433–3441. https://doi.org/10.1016/J.YEXCR.2009.08.012

Camp, R. L., Scheynius, A., Johansson, C., & Puré, E. (1993). CD44 is necessary for optimal contact allergic responses but is not required for normal leukocyte extravasation. *The Journal of Experimental Medicine*, *178*(2), 497–507. https://doi.org/10.1084/JEM.178.2.497

Cho, S. H., Park, Y. S., Kim, H. J., Kim, C. H., Lim, S. W., Huh, J. W., Lee, J. H., & Kim, H. R. (2012). CD44 enhances the epithelial-mesenchymal transition in association with colon cancer invasion. *International Journal of Oncology*, *41*(1), 211–218. https://doi.org/10.3892/IJO.2012.1453

Cinamon, G., Grabovsky, V., Winter, E., Franitza, S., Feigelson, S., Shamri, R., Dwir, O., & Alon, R. (2001). Novel chemokine functions in lymphocyte migration through vascular endothelium under shear flow. *Journal of Leukocyte Biology*, *69*(6), 860–866. https://doi.org/10.1189/JLB.69.6.860

DeGrendele, H. C., Estess, P., & Siegelman, M. H. (1997). Requirement for CD44 in Activated T Cell Extravasation into an Inflammatory Site. *Science*, *278*(5338), 672–675. https://doi.org/10.1126/SCIENCE.278.5338.672

Delgadillo, L. F., Lomakina, E. B., Kuebel, J., & Waugh, R. E. (2021). Changes in endothelial glycocalyx layer protective ability after inflammatory stimulus. *American Journal of Physiology - Cell Physiology*, *320*(2), C216–C224. https://doi.org/10.1152/AJPCELL.00259.2020

Dogné, S., & Flamion, B. (2020). Endothelial Glycocalyx Impairment in Disease: Focus on Hyaluronan Shedding. *The American Journal of Pathology*, *190*(4), 768–780. https://doi.org/10.1016/J.AJPATH.2019.11.016

Dustin, M. L., & Springer, T. A. (1988). Lymphocyte function-associated antigen-1 (LFA-1) interaction with intercellular adhesion molecule-1 (ICAM-1) is one of at least three mechanisms for lymphocyte adhesion to cultured endothelial cells. *The Journal of Cell Biology*, *107*(1), 321–331. https://doi.org/10.1083/JCB.107.1.321

Fong, A. M., Robinson, L. A., Steeber, D. A., Tedder, T. F., Yoshie, O., Imai, T., & Patel, D. D. (1998). Fractalkine and CX3CR1 Mediate a Novel Mechanism of Leukocyte Capture, Firm Adhesion, and Activation under Physiologic Flow. *Journal of Experimental Medicine*, *188*(8), 1413–1419. https://doi.org/10.1084/JEM.188.8.1413

Freeman, S. A., Vega, A., Riedl, M., Collins, R. F., Ostrowski, P. P., Woods, E. C., Bertozzi, C. R., Tammi, M. I., Lidke,

D. S., Johnson, P., Mayor, S., Jaqaman, K., & Grinstein, S. (2018). Transmembrane Pickets Connect Cyto- and Pericellular Skeletons Forming Barriers to Receptor Engagement. *Cell*, *172*(1–2), 305-317.e10. https://doi.org/10.1016/J.CELL.2017.12.023

Graham, G. J., Handel, T. M., & Proudfoot, A. E. I. (2019). Leukocyte Adhesion: Reconceptualizing Chemokine Presentation by Glycosaminoglycans. *Trends in Immunology*, *40*(6), 472–481. https://doi.org/10.1016/J.IT.2019.03.009

Haymet, A. B., Bartnikowski, N., Wood, E. S., Vallely, M. P., McBride, A., Yacoub, S., Biering, S. B., Harris, E., Suen, J. Y., & Fraser, J. F. (2021). Studying the Endothelial Glycocalyx in vitro: What Is Missing? *Frontiers in Cardiovascular Medicine*, *8*. https://doi.org/10.3389/FCVM.2021.647086

Hu, Z., Cano, I., & D'Amore, P. A. (2021). Update on the Role of the Endothelial Glycocalyx in Angiogenesis and Vascular Inflammation. *Frontiers in Cell and Developmental Biology*, *9*, 2431. https://doi.org/10.3389/FCELL.2021.734276/BIBTEX

Iba, T., & Levy, J. H. (2019). Derangement of the endothelial glycocalyx in sepsis. *Journal of Thrombosis and Haemostasis*, *17*(2), 283–294. https://doi.org/10.1111/JTH.14371

Ilangumaran, S., Borisch, B., & Hoessli, D. C. (2010). Signal Transduction via CD44: Role of Plasma Membrane Microdomains. *Https://Doi.Org/10.1080/10428199909169610*, *35*(5–6), 455–469. https://doi.org/10.1080/10428199909169610

Kajita, M., Itoh, Y., Chiba, T., Mori, H., Okada, A., Kinoh, H., & Seiki, M. (2001). Membrane-type 1 matrix metalloproteinase cleaves CD44 and promotes cell migration. *The Journal of Cell Biology*, *153*(5), 893–904. https://doi.org/10.1083/JCB.153.5.893

Karin, N. (2020). CXCR3 Ligands in Cancer and Autoimmunity, Chemoattraction of Effector T Cells, and Beyond. *Frontiers in Immunology*, *11*, 976. https://doi.org/10.3389/FIMMU.2020.00976/BIBTEX

Kroon, J., Schaefer, A., van Rijssel, J., Hoogenboezem, M., van Alphen, F., Hordijk, P., Stroes, E. S. G., Strömblad, S., van Rheenen, J., & van Buul, J. D. (2018). Inflammation-Sensitive Myosin-X Functionally Supports Leukocyte Extravasation by Cdc42-Mediated ICAM-1-Rich Endothelial Filopodia Formation. *Journal of Immunology (Baltimore, Md. : 1950)*, *200*(5), 1790–1801. https://doi.org/10.4049/JIMMUNOL.1700702

Liu, G., Place, A. T., Chen, Z., Brovkovych, V. M., Vogel, S. M., Muller, W. A., Skidgel, R. A., Malik, A. B., & Minshall, R. D. (2012). ICAM-1–activated Src and eNOS signaling increase endothelial cell surface PECAM-1 adhesivity and neutrophil transmigration. *Blood*, *120*(9), 1942–1952. https://doi.org/10.1182/BLOOD-2011-12-397430

Lortat-Jacob, H. (2009). The molecular basis and functional implications of chemokine interactions with heparan sulphate. *Current Opinion in Structural Biology*, *19*(5), 543–548. https://doi.org/10.1016/J.SBI.2009.09.003

McDonald, K. K., Cooper, S., Danielzak, L., & Leask, R. L. (2016). Glycocalyx Degradation Induces a Proinflammatory Phenotype and Increased Leukocyte Adhesion in Cultured Endothelial Cells under Flow. *PLOS ONE*, *11*(12), e0167576. https://doi.org/10.1371/JOURNAL.PONE.0167576

Middleton, J., Patterson, A. M., Gardner, L., Schmutz, C., & Ashton, B. A. (2002). Leukocyte extravasation: chemokine transport and presentation by the endothelium. *Blood*, *100*(12), 3853–3860. https://doi.org/10.1182/BLOOD.V100.12.3853

Mori, H., Tomari, T., Koshikawa, N., Kajita, M., Itoh, Y., Sato, H., Tojo, H., Yana, I., & Seiki, M. (2002). CD44 directs membrane-type 1 matrix metalloproteinase to lamellipodia by associating with its hemopexin-like domain. *The EMBO Journal*, *21*(15), 3949–3959. https://doi.org/10.1093/EMBOJ/CDF411

Mylvaganam, S., Riedl, M., Vega, A., Collins, R. F., Jaqaman, K., Grinstein, S., & Freeman, S. A. (2020). Stabilization

of Endothelial Receptor Arrays by a Polarized Spectrin Cytoskeleton Facilitates Rolling and Adhesion of Leukocytes. *Cell Reports*, *31*(12). https://doi.org/10.1016/J.CELREP.2020.107798

Naor, D., Sionov, R. V., & Ish-Shalom, D. (1997). CD44: structure, function, and association with the malignant process. *Advances in Cancer Research*, *71*, 241–319. https://doi.org/10.1016/S0065-230X(08)60101-3

Nonaka, M., Bao, X., Matsumura, F., Götze, S., Kandasamy, J., Kononov, A., Broide, D. H., Nakayama, J., Seeberger, P. H., & Fukuda, M. (2014). Synthetic di-sulfated iduronic acid attenuates asthmatic response by blocking T-cell recruitment to inflammatory sites. *Proceedings of the National Academy of Sciences of the United States of America*, *111*(22), 8173–8178. https://doi.org/10.1073/PNAS.1319870111/SUPPL_FILE/PNAS.201319870SI.PDF

Nourshargh, S., Hordijk, P. L., & Sixt, M. (2010). Breaching multiple barriers: leukocyte motility through venular walls and the interstitium. *Nature Reviews Molecular Cell Biology 2010 11:5*, *11*(5), 366–378. https://doi.org/10.1038/nrm2889

Oh, H. M., Lee, S. G., Na, B. R., Wee, H., Kim, S. H., Choi, S. C., Lee, K. M., & Jun, C. D. (2007). RKIKK motif in the intracellular domain is critical for spatial and dynamic organization of ICAM-1: Functional implication for the leukocyte adhesion and transmigration. *Molecular Biology of the Cell*, *18*(6), 2322–2335. https://doi.org/10.1091/MBC.E06-08-0744/ASSET/IMAGES/LARGE/ZMK0060781030011.JPEG

Panitz, N., Theisgen, S., Samsonov, S. A., Gehrcke, J. P., Baumann, L., Bellmann-Sickert, K., Köhling, S., Teresa Pisabarro, M., Rademann, J., Huster, D., & Beck-Sickinger, A. G. (2016). The structural investigation of glycosaminoglycan binding to CXCL12 displays distinct interaction sites. *Glycobiology*, *26*(11), 1209–1221. https://doi.org/10.1093/GLYCOB/CWW059

Qu, J., Cheng, Y., Wu, W., Yuan, L., & Liu, X. (2021). Glycocalyx Impairment in Vascular Disease: Focus on Inflammation. *Frontiers in Cell and Developmental Biology*, *9*, 2567. https://doi.org/10.3389/FCELL.2021.730621/BIBTEX

Reitsma, S., Slaaf, D. W., Vink, H., van Zandvoort, M. A. M. J., & Oude Egbrink, M. G. A. (2007). The endothelial glycocalyx: composition, functions, and visualization. *Pflugers Archiv* , *454*(3), 345. https://doi.org/10.1007/S00424-007-0212-8

Schaefer, A., Riet, J. te, Ritz, K., Hoogenboezem, M., Anthony, E. C., Mul, F. P. J., de Vries, C. J., Daemen, M. J., Figdor, C. G., van Buul, J. D., & Hordijk, P. L. (2014). Actin-binding proteins differentially regulate endothelial cell stiffness, ICAM-1 function and neutrophil transmigration. *Journal of Cell Science*, *127*(20), 4470–4482. https://doi.org/10.1242/JCS.154708/VIDEO-4

Schillemans, M., Karampini, E., Hoogendijk, A. J., Wahedi, M., van Alphen, F. P. J., van den Biggelaar, M., Voorberg, J., & Bierings, R. (2019). Interaction networks of Weibel-Palade body regulators syntaxin-3 and syntaxin binding protein 5 in endothelial cells. *Journal of Proteomics*, *205*, 103417. https://doi.org/10.1016/J.JPROT.2019.103417

Schimmel, L., van der Stoel, M., Rianna, C., van Stalborch, A. M., de Ligt, A., Hoogenboezem, M., Tol, S., van Rijssel, J., Szulcek, R., Bogaard, H. J., Hofmann, P., Boon, R., Radmacher, M., de Waard, V., Huveneers, S., & van Buul, J. D. (2018). Stiffness-Induced Endothelial DLC-1 Expression Forces Leukocyte Spreading through Stabilization of the ICAM-1 Adhesome. *Cell Reports*, *24*(12), 3115–3124. https://doi.org/10.1016/J.CELREP.2018.08.045

Schoppmeyer, R., van Steen, A. C. I., Kempers, L., Timmerman, A. L., Nolte, M. A., Hombrink, P., van Buul Correspondence, J. D., & van Buul, J. D. (2022). The endothelial diapedesis synapse regulates transcellular migration of human T lymphocytes in a CX3CL1- and SNAP23-dependent manner. *CellReports*, *38*, 110243. https://doi.org/10.1016/j.celrep.2021.110243

Schreiber, T. H., Shinder, V., Cain, D. W., Alon, R., & Sackstein, R. (2007). Shear flow-dependent integration of apical

and subendothelial chemokines in T-cell transmigration: implications for locomotion and the multistep paradigm. *Blood*, *109*(4), 1381–1386. https://doi.org/10.1182/BLOOD-2006-07-032995

van Buul, J. D., Kanters, E., & Hordijk, P. L. (2007). Endothelial signaling by Ig-like cell adhesion molecules. *Arteriosclerosis, Thrombosis, and Vascular Biology*, *27*(9), 1870–1876. https://doi.org/10.1161/ATVBAHA.107.145821

van Buul, J. D., van Rijssel, J., van Alphen, F. P. J., Hoogenboezem, M., Tol, S., Hoeben, K. A., van Marle, J., Mul, E. P. J., & Hordijk, P. L. (2010). Inside-Out Regulation of ICAM-1 Dynamics in TNF-α-Activated Endothelium. *PLOS ONE*, *5*(6), e11336. https://doi.org/10.1371/JOURNAL.PONE.0011336

van den Berg, B. M., Vink, H., & Spaan, J. A. E. (2003). The endothelial glycocalyx protects against myocardial edema. *Circulation Research*, *92*(6), 592–594. https://doi.org/10.1161/01.RES.0000065917.53950.75

van Rijssel, J., Kroon, J., Hoogenboezem, M., van Alphen, F. P. J., de Jong, R. J., Kostadinova, E., Geerts, D., Hordijk, P. L., & van Buul, J. D. (2012). The Rho-guanine nucleotide exchange factor Trio controls leukocyte transendothelial migration by promoting docking structure formation. *Molecular Biology of the Cell*, *23*(15), 2831–2844. https://doi.org/10.1091/MBC.E11-11-0907/ASSET/IMAGES/LARGE/2831FIG10.JPEG

Vestweber, D. (2015). How leukocytes cross the vascular endothelium. *Nature Reviews. Immunology*, *15*(11), 692–704. https://doi.org/10.1038/NRI3908

Wang, D., Sai, J., & Richmond, A. (2003). Cell Surface Heparan Sulfate Participates in CXCL1-Induced Signaling†. *Biochemistry*, *42*(4), 1071–1077. https://doi.org/10.1021/BI026425A

Wang, Y., Yago, T., Zhang, N., Abdisalaam, S., Alexrakis, G., Rodgers, W., & McEver, R. P. (2014). Cytoskeletal regulation of CD44 membrane organization and interactions with E-selectin. *The Journal of Biological Chemistry*, *289*(51), 35159–35171. https://doi.org/10.1074/JBC.M114.600767

Yagmur, E., Koch, A., Haumann, M., Kramann, R., Trautwein, C., & Tacke, F. (2012). Hyaluronan serum concentrations are elevated in critically ill patients and associated with disease severity. *Clinical Biochemistry*, *45*(1–2), 82–87. https://doi.org/10.1016/J.CLINBIOCHEM.2011.10.016

Zeilstra, J., Joosten, S. P. J., van Andel, H., Tolg, C., Berns, A., Snoek, M., van de Wetering, M., Spaargaren, M., Clevers, H., & Pals, S. T. (2014). Stem cell CD44v isoforms promote intestinal cancer formation in Apc(min) mice downstream of Wnt signaling. *Oncogene*, *33*(5), 665–670. https://doi.org/10.1038/ONC.2012.611

Zhang, T., Somasundaram, R., Berencsi, K., Caputo, L., Rani, P., Guerry, D., Furth, E., Rollins, B. J., Putt, M., Gimotty, P., Swoboda, R., Herlyn, M., & Herlyn, D. (2005). CXC Chemokine Ligand 12 (Stromal Cell-Derived Factor 1α) and CXCR4-Dependent Migration of CTLs toward Melanoma Cells in Organotypic Culture. *The Journal of Immunology*, *174*(9), 5856–5863. https://doi.org/10.4049/JIMMUNOL.174.9.5856

Zhang, W., Gao, L., Qi, S., Liu, D., Xu, D., Peng, J., Daloze, P., Chen, H., & Buelow, R. (2000). Blocking of CD44-hyaluronic acid interaction prolongs rat allograft survival. *Transplantation*, *69*(4), 665–667. https://doi.org/10.1097/00007890-200002270-00032

SUPPLEMENTAL FILES

A

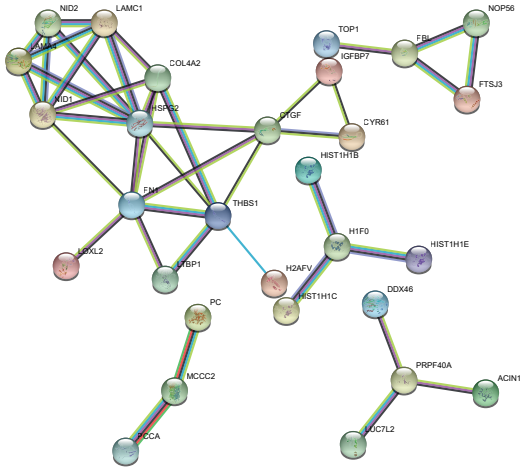

B

Enriched clustered						
CDC2	CAD	PRSS23	NT5E	PRKDC	RPS2	CTSB
RPS24	SLC25A3	FADS2	RPS3	S100A12	CD59	SURF4
SPTBN1	UBAP2L	LMNA	STOM	PFKP	FLOT1	HSP90B1
RPL17	**CD44**	APOB	RPL10	LMNB2	FLNB	PPIA
NUP214	FUS	HSPB1	GRN	AHNAK	ATP6V1B2	MYO1B
IGHV1-3	RPL38	GNAI2	PML	SQSTM1	VCAM1	ARPC3
HSPA1B	SRSF1	RPLP1	MCM7	SPTAN1	ACTA1	EEF2
APOC3	DAZAP1	KRT18	MYH10	DYNC1H1	TPM4	ACTR2
TSPO	MYO1C	MYL1	IQGAP1	CTTN	DHCR7	FBLIM1
DERL1	SNAP23	ANXA6	NES	LBR	CAPRIN1	CCT7
RAN	IGF2BP3	MGP	MMP14	MVP	PSMD3	TUBB6
NAP1L1	SYNM	VIM	ALDH18A1	LTBP1	GLB1	LUZP1
FLOT2	ARPC1B	CTSA	SEC13	PLEC	RPS21	ACTR3
LMNB1	ARPC2	RALA				
Enriched unclustered						
LAMA4	PRPF40A	HIST1H1E	FBL	MMRN2	CYR61	HIST1H1C
RRBP1	KHDRBS3	LAMC1	CTGF	MCCC2	H2AFV	FTSJ3
DDX46	FN1	TOP1	HSPG2	CALML5	TRIM21	COL4A2
PTBP1	PCCA	PC	ACACA	LUC7L2	TINAGL1	ACIN1
VNN2	H1F0	NID1	NID2	LOXL2	NOP56	IGFBP7
COL12A1	THBS1	HIST1H1B				

Supplemental Figure 1. (A) String network analysis of proteins enriched in unclustered condition. **(B)** All significantly enriched proteins in either clustered condition.

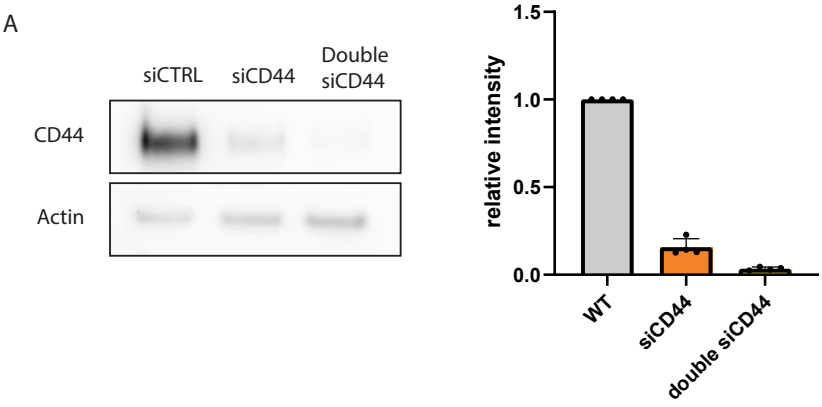

Supplemental Figure 2. (A) WB showing CD44 and Actin as a loading control in HUVEC treated with non-sense siRNA or siRNA against CD44. Double siCD44 transduction was used to generate a more robust knockdown for FRAP experiments. Quantification performed using ImageJ, intensity normalized to siCTRL and corrected for loading by actin.

CHAPTER 4

The endothelial diapedesis synapse regulates transcellular migration of human T lymphocytes in a CX3CL1- and SNAP23-dependent manner

Rouven Schoppmeyer[1,2,3]
Abraham C.I. van Steen[1,2]
Lanette Kempers[1,2]
Anne L. Timmerman[1,2]
Martijn A. Nolte[2,4]
Pleun Hombrink[2,5,6]
Jaap D. van Buul[1,2,3,7,*]

[1]Molecular Cell Biology Lab, Department of Molecular Hematology, Sanquin Research, Plesmanlaan 125, 1066CX Amsterdam, the Netherlands

[2]Landsteiner Laboratory, Amsterdam UMC, University of Amsterdam, Amsterdam, the Netherlands

[3]Leeuwenhoek Centre for Advanced Microscopy (LCAM), Section Molecular Cytology at Swammerdam Institute for Life Sciences (SILS) at University of Amsterdam, Amsterdam, the Netherlands

[4]Research Facility, Sanquin Research, Amsterdam, the Netherlands

[5]Department of Hematopoiesis, Sanquin Research, Amsterdam, the Netherlands

[6]Present address: Department of Translational Immunology, Hubrecht Organoid Technology, Utrecht, the Netherlands

[7]Lead contact

[*]Correspondence: j.vanbuul@sanquin.nl

Cell Reports 38.3 (2022): 110243

SUMMARY

Understanding how cytotoxic T lymphocytes (CTLs) efficiently leave the circulation to target cancer cells or contribute to inflammation is of high medical interest. Here, we demonstrate that human central memory CTLs cross the endothelium in a predominantly paracellular fashion, whereas effector and effector memory CTLs cross the endothelium preferably in a transcellular fashion. We find that effector CTLs show a round morphology upon adhesion and induce a synapse-like interaction with the endothelium where ICAM-1 is distributed at the periphery. Moreover, the interaction of ICAM-1:β2integrin and endothelial-derived CX3CL1:CX3CR1 enables transcellular migration. Mechanistically, we find that ICAM-1 clustering recruits the SNARE-family protein SNAP23, as well as syntaxin-3 and -4, for the local release of endothelial-derived chemokines like CXCL1/8/10. In line, silencing of endothelial SNAP23 drives CTLs across the endothelium in a paracellular fashion. In conclusion, our data suggest that CTLs trigger local chemokine release from the endothelium through ICAM-1-driven signals driving transcellular migration.

Graphical abstract

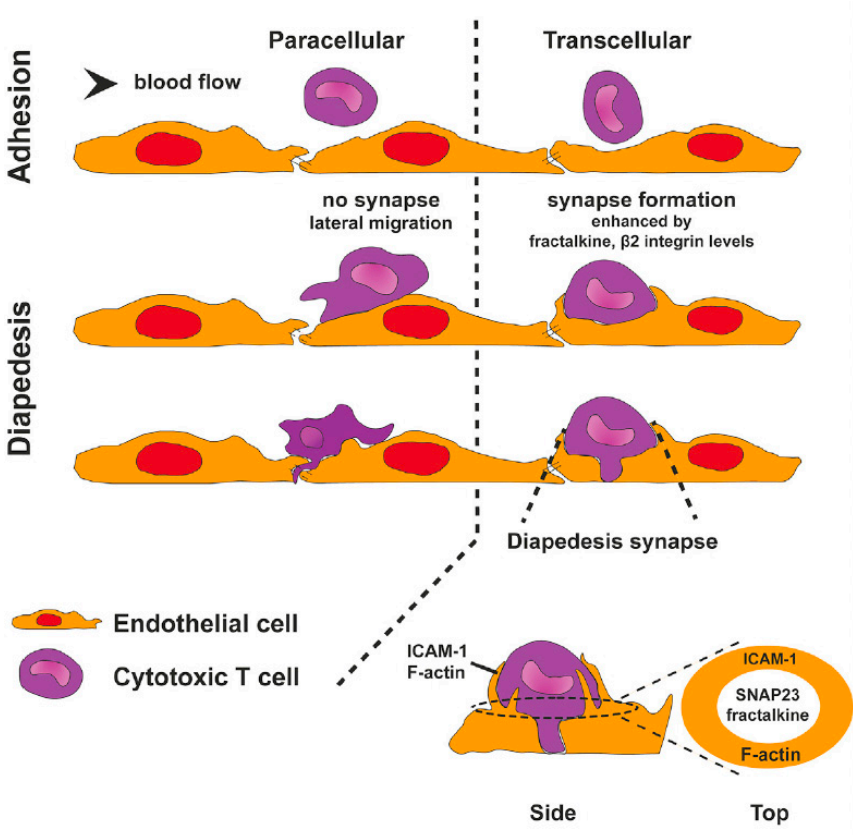

INTRODUCTION

Leukocytes efficiently cross the vasculature to enter underlying tissues by migrating through the endothelial cell lining (Anderson and Anderson, 1976). This process, called transendothelial migration (TEM), involves a cascade of events (Vestweber, 2015) that (i) catches cells from the bloodstream, (ii) activates them to facilitate adhesion, and (iii) finally leads to TEM either at cell junctions, known as the paracellular route, or through the endothelial cell body, known as the transcellular route. Currently, it is accepted that both routes can occur for T cells and other leukocyte subsets and may depend on factors like organ-specific vascular beds and inflammation (Marchesi, 1961; Feng et al., 1998; Kvietys and Sandig, 2001; Yang et al., 2005; Carman et al., 2007; Mamdouh et al., 2009; Rademakers et al., 2020). So far, transcellular diapedesis has been attributed to high ICAM-1 expression levels on endothelial cells (Yang et al., 2005; Gorina et al., 2014; Abadier et al., 2015). In recent studies on infiltration of neuronal tissue, for $CD4^+$ and $CD8^+$ T cells that cross inflamed brain endothelial cells, $CD8^+$ T cells showed a strong preference for transcellular diapedesis (Abadier et al., 2015; Rudolph et al., 2016). So far, transcellular diapedesis has been attributed to high ICAM-1 expression levels on endothelial cells (Yang et al., 2005; Gorina et al., 2014; Abadier et al., 2015), but further mechanistic details of how this route is regulated are still elusive.

$CD8^+$ cytotoxic T lymphocytes (CTLs) represent an essential anti-tumor and anti-viral response of the immune system, but they are also involved in various autoimmune diseases. After activation, naive T cells proliferate into effector cells, which are short lived but efficient at eliminating target cells. Additionally, some generated CTLs will develop into memory cells that are long lived and roam either peripheral tissues (effector memory [EM]) or lymphoid tissues (central memory [CM]) (Sallusto et al., 1999). According to the classical model, tissue-selective entry is mediated by the expression profile of chemokines presented by the endothelium to adhering leukocytes that in turn express specific sets of chemokine receptors, depending on the subset (Olson and Ley, 2002; Hughes and Nibbs, 2018). Adhering leukocytes will be selectively activated by chemokines fitting their receptor profile prior to crossing the endothelium. The different tissue preferences of T cell subsets (Janossy et al., 1989) thus rely on the different chemokine receptor profiles (Schaerli and Moser, 2005). Chemokines themselves can be produced and presented by endothelial cells (Middleton et al., 2002a; Speyer and Ward, 2011) but also derive from the underlying tissue (Middleton et al., 2002b) or infiltrating immune cells (Girbl et al., 2018). Surface deposition via intracellular transport mechanisms has been described for CXCL8, where the endothelium presents CXCL8 on microvilli-like structures on the apical surface (Middleton et al., 1997). This was also found for the surface deposition of endothelial-derived CCL5 and CXCL10 (Whittall et al., 2013). Shulman et al. showed that the extravasation of T cells is mediated by intra-endothelial vesicle stores

rather than extracellular chemokine depots (Shulman et al., 2011). Our group recently showed that inflamed endothelial cells induce myosin-10- and Cdc42-dependent filopodia, specific membrane structures at the luminal surface of the endothelium that are thought to be important for the transition of leukocytes from rolling to the adherent phase (Kroon et al., 2018). During the adhesion step, the endothelium can induce apical cup structures, also known as docking structures or transmigratory cups, in order to guide leukocyte TEM and prevent local leakage (Barreiro et al., 2002; Carman and Springer, 2004; van Buul et al., 2007; Heemskerk et al., 2016). These structures have been found around many different types of leukocytes, including T cells. However, how these structures are involved in T cell TEM has not yet been clearly defined.

Here, we present evidence that effector and effector memory CTL, more efficiently than central memory, cross-inflamed endothelial monolayers in a transcellular manner. They do so by making use of ICAM-1 clustering and endothelial-derived chemokines. Endothelial CX3CL1 enhances the firm adhesion, generating ICAM-1 clustering at the outer circle of the CTL:EC interaction. ICAM-1 clustering recruits the vesicle transport protein SNAP23 and to a lower degree syntaxin-3 and -4, resulting in the local release of the endothelial-derived chemokines CXCL1, -8, and -10. Together, this drives transcellular migration of CTLs. If one of these parameters is not in place, CTLs leave the initial site of adhesion and cross the endothelial monolayer in a paracellular manner. Our work shows how different CTL subsets use different routes of transmigration. Targeting such specific routes can be utilized in future therapy development.

RESULTS

To determine if CTLs cross the inflamed endothelium in a transcellular or paracellular manner, we monitored the migration route using a microscopy-based flow chamber containing cultured human primary human umbilical vein endothelial cells. We found that CTLs crossed the endothelium in both a transcellular and a paracellular manner (Figure 1A), in line with previous research (Martinelli et al., 2014). When we used real-time imaging to monitor CTL TEM events, we found that CTL transcellular events were preceded by a depolarized phenotype, meaning that CTL either rounded up just prior to diapedesis or remained unpolarized after adhesion until transcellular transmigration and do not involve apical migration (Figures 1B and 1C). For paracellular events, CTLs remained polarized during the full process of TEM (Figures 1D and 1E). Note, that CTLs do not show rolling on the endothelium but after contact remain stationary and transmigrate either at the spot through the endothelial cell body (transcellular) or at the nearest junction (paracellular) that they reach by apical migration.

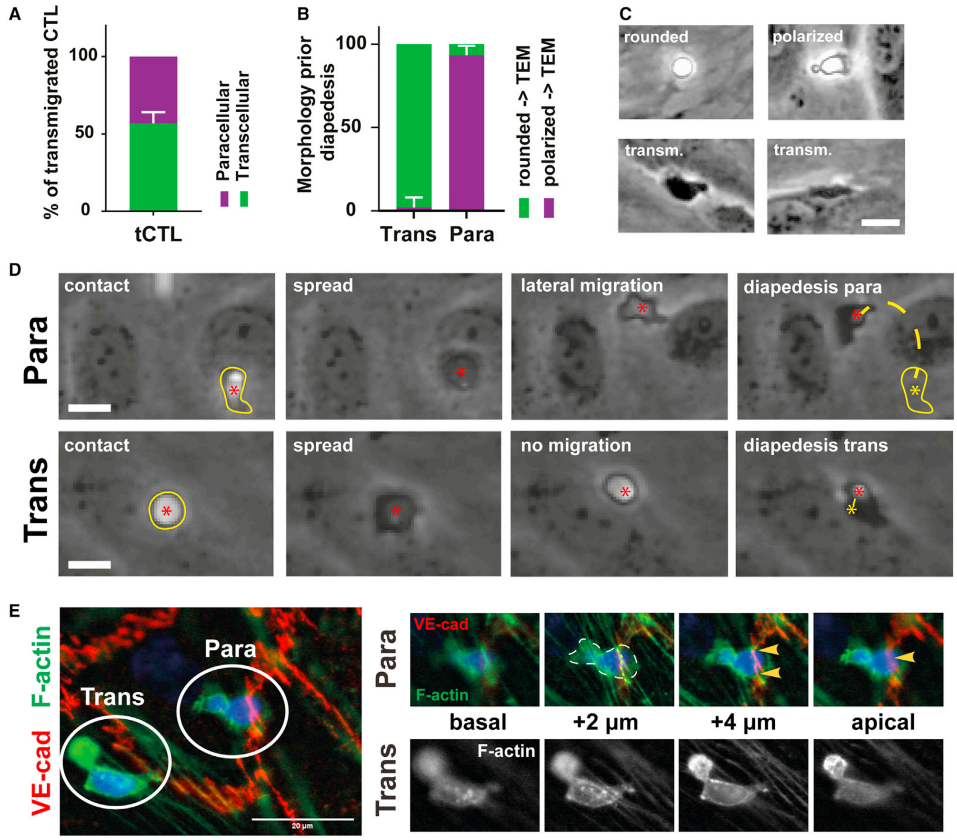

Figure 1. Transcellular diapedesis of CTLs involves no apical migration or lateral polarization of CTLs and is preceded by a rounded CTL morphology

(A) CTLs were flown over TNFα-activated (20 h) HUVECs. Route of transmigration was determined as being paracellular (transmigration including crossing a junction with previous lateral polarization phenotype) or transcellular (completed transmigration without polarization prior to diapedesis and without crossing a junction). (B) CTL morphology before transmigration was analyzed. Transcellular events are preceded by a rounded morphology of CTLs; this can be with or without former spreading phenotype immediately upon adhesion to EC. (C) common morphologies of CTLs on TNFα-stimulated HUVECs are shown. "Rounded" cells show no visible polarization phenotype directly after adhesion, and this morphology precedes transcellular events. Rounded morphology usually resembles an inactive state of CTL. The CTL labeled "polarized" shows the classical CTL migration morphology resembling a Y shape. The bottom pictures provide examples of transmigrated CTLs that show a polarized morphology and migration under the endothelium. (D) Shown are examples from bright-field images of total CTLs flown over TNFα-stimulated HUVECs. Top row shows a paracellular event from adhesion to polarization and lateral migration prior to diapedesis. CTL adhering to luminal side of the endothelium is marked with red asterisk. Bottom row shows a T cell adhering (red asterisk) followed by local cell spreading and adapting a rounded morphology before transcellular diapedesis without lateral migration or taking a polarized phenotype. Transcellular diapedesis than finishes from the horizontal rounded state of the cell. No lateral migration is involved. Yellow stars mark positions of CTL underneath the endothelium. (E) Sorted effector CTLs could settle on TNFα-activated HUVECs for 1 min, followed by staining for VE-cadherin and F-actin. The image shows two CTLs undergoing diapedesis, one transcellular and one paracellular. (transm., transmigrated; VE-cad, VE-cadherin; tCTL, total CTL, human CD8+ T cell isolate from PBMC; trans, transcellular; para, paracellular; TEM, transendothelial migration). Experiments were performed in triplicate, and 4–6 CTL donors were analyzed per condition in total. Scale bars (C and D), 10 µm; (E), 20 µm.

Previous reports recognized that inflamed endothelium induces a membrane structure around adherent T cells, also known as docking structures or transmigratory cups (Barreiro et al., 2002; Carman and Springer, 2004; Sage et al., 2012). By transfecting endothelial cells with a membrane marker, CAAX-mScarlet, we found that, during the initiation of transcellular migration events, CTLs were partly surrounded by an endothelial membrane structure (Figure 2A; Videos S1 and S2), resembling the previously described docking structures (Barreiro et al., 2002; Carman and Springer, 2004; van Buul et al., 2007). Strikingly, we observed these cups for transcellular but not for paracellular CTL transmigration events (Figure 2B). A hallmark of immune synapse (IS) formation, i.e., the interaction between an antigen-presenting cell and a T cell, is the absence of F-actin at the center of the synapse (Mace and Orange, 2014; Sanchez et al., 2019). We observed a similar distribution of F-actin at the initial CTL-endothelium interaction: when CTLs were firmly adhered to the endothelium, we found a clear F-actin ring at the periphery but an absence of F-actin at the center of the synapse (Figure 2C), similar to the immunological synapse (Springer and Dustin, 2012). Another similarity is that we found that for transcellular migration events ICAM-1-rich filopodia were rapidly recruited to CTLs (Figure 2D). Interestingly, ICAM-1 recruitment was observed at the periphery of the contact areas between the CTL and the endothelium and was exceptionally low at the center of the cell-cell contact area (Figure 2D; Video S3). This is also in agreement with the IS, where ICAM-1 and the associated LFA-1 are also located at the cell's periphery.

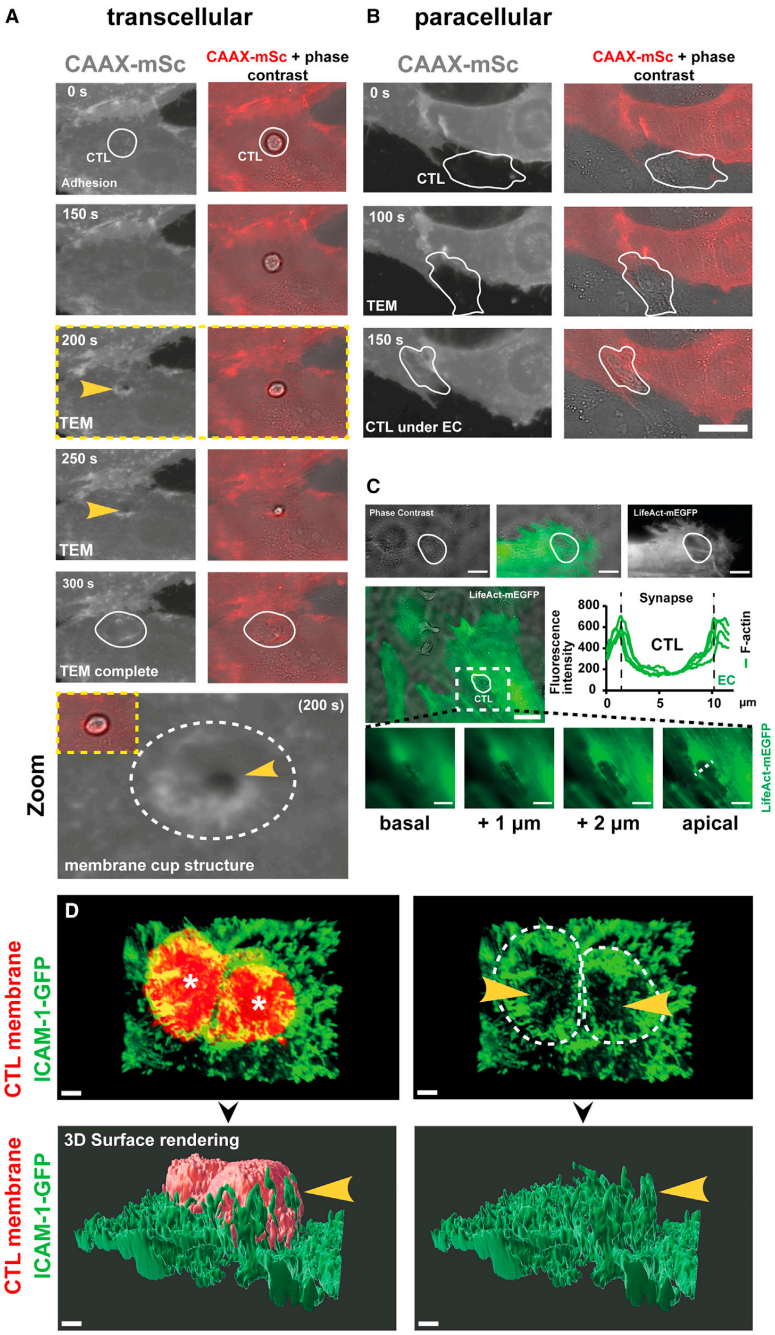

Figure 2. CTL transcellular events involve the formation of a diapedesis synapse and include ICAM-1 clustering at the periphery and ICAM-1 and actin clearance at the synapse

(A and B) HUVECs were transduced with CAAX-mScarlet and 3–5 days after transduction seeded in µ-channels for 24 h followed by 20 h of TNFα stimulation. Total CTLs were flown over CAAX-mScarlet-transduced 20-h TNFα-stimulated HUVECs. Images were recorded at 50-s intervals. Shown are a transcellular (A) and a paracellular event (B). Note the engulfing membrane cup visible during transcellular diapedesis

events (A), which is shown enlarged in the bottom image. The bottom image in (A) is a zoom of the membrane cup structure from the 200-s time point in the series above, with the white dotted circle highlighting the membrane cup and the yellow arrow pointing at the transmigration pore. See Video S1 for more detail. Image series were acquired with Zeiss Axiovert fluorescent wide-field microscope using a 63× objective. (C) HUVECs were transfected with LifeAct-mEGFP and treated for 20 h with TNFα before the flow assay. Underneath adhering non-horizontally polarized CTL endothelial actin clears at the contact site. (D) Endothelial ICAM-1-rich filopodia capture adhering CTLs (see also Video S2). CTL membranes were labeled using DiD (red fluorescent membrane label) and were allowed to settle for 1 min on 20-h TNFα-activated pLV_ICAM-1-GFP-transduced HUVECs grown in an 8-well µ-dish. The samples were washed with PBS (containing Ca2+ and Mg2+) and fixed using 4% formaldehyde solution at RT for 10 min. Images were captured using a Zeiss Airy Scan confocal microscope. Surface rendering was prepared using Imaris (Bitplane). Asterisks in (D) mark individual T cells (red fluorescent membrane label DiD). White circles (A–D) indicate CTL cell outline; yellow arrows (A) indicate diapedesis synapse membrane cup. In (D, top right) yellow arrows mark ICAM-1-cleared area at the synaptic interface and in (D, bottom images) ICAM-1 filopodia. CAAX-mSc, CAAX-mScarlet; TEM, transendothelial migration). Experiments were performed in triplicate, and at least three CTL donors were analyzed. (Scale bars in A–C, 10 µm; in D, = 2 µm).

If, as often proposed, ICAM-1-mediated adhesion is the regulating factor of the route of transmigration, T cell subsets should show similar behavior if β2-integrin expression levels are comparable, which they are considered to be for CTL subsets (Bertoni et al., 2018). Yet, our flow cytometry analysis of total CTLs after recovery culture showed that CD18 expression was highest for effector (Eff), whereas effector memory (EM) and central memory (CM) showed no significant differences in CD18 expression (Figures S3D and S4B). CD18 was lowest on naive CTLs (Figures S3D and S4B). To study the capacity of the different CTL subsets to cross the endothelium, we specifically sorted classical CTL subsets, i.e., naive, central memory, effector, and effector memory T cells, via fluorescence-activated cell sorting. Except for naive CTLs, all subsets efficiently adhered to and migrated across the endothelium, with effector CTLs showing the highest efficiency (Figure 3A). Interestingly, we found that effector CTLs showed high levels of transcellular diapedesis, whereas central memory CTLs favored the paracellular pathway (Figure 3B). For the route of transmigration analysis, we only considered non-distant transmigrated CTLs. Effector memory CTLs did not prefer either route (Figure 3B). However, the different CTL subsets did not show increased lateral migration prior to diapedesis, which we define as a CTL that transmigrates after passing at least two different endothelial junctions from their initial adhesion point (i.e., distant diapedesis; Figure 3C). The differences in subset transmigration route choice, after 20 h of TNFα, indicate that ICAM-1, although critical to initiation of the whole transmigration cascade, is not the only determinant factor of transcellular diapedesis. Our data show that effector/effector memory CTLs cross the endothelium preferably in a transcellular manner, whereas central memory use mostly the paracellular route. CM show no increased levels of extended lateral migration or distant diapedesis (Figure 3C). Thus, transcellular diapedesis is not solely dependent on differences in ICAM-1 adhesion of the subsets. We continued by using total $CD8^+$ populations for the experiments. CTL subset composition analysis after recovery by flow cytometry showed that almost ~50% was quantified as naive T cells, ~25% defined as central memory, and ~15% and ~10% as effector memory and effector T cells, respectively (Figure S1A). We previously

reported that long-term stimulation of the endothelium with TNFα increased the expression levels of adhesion molecules such as ICAM-1 (Rijssel et al., 2013). The data revealed that CTLs crossed endothelial cells that had been treated for 20 h with TNFα more efficiently than those that crossed 4-h-treated endothelium (Figure 3D). Interestingly, 4 h of TNFα treatment resulted in more paracellular migration of CTLs, whereas 20 h of TNFα treatment resulted in more transcellular events (Figure 3E). These data correlate well with previous reports showing that increased ICAM-1 levels promote transcellular migration (Yang et al., 2005; Millán et al., 2006). Also, CTLs showed more distant transmigration events after 4 h of TNFα treatment compared with the 20-h treatment (Figure 3F). Blocking ICAM-1 directly on endothelial cells or its counterpart β2-integrin on CTLs significantly reduced the number of CTLs that crossed the endothelium (Figure 3G; for controls see Figures S2A–S2C). Strikingly, we also found that blocking these adhesion molecules drastically shifted the transmigration route of CTLs from transcellular to paracellular (Figure 3H), in conjunction with increased levels of distant diapedesis events (Figure 3I). From these data, we conclude that ICAM-1/β2-integrin-mediated adhesion enables transcellular migration by facilitating adhesion and arrest of adhering CTLs, but CTL subset transmigration parameters imply that ICAM-1 does not constitute the only determinant of transcellular migration. Next, we pointed our attention at chemokines, as CTL subsets are defined by their different chemokine receptor profiles (Olson and Ley, 2002; Schaerli and Moser, 2005; Hughes and Nibbs, 2018).

Endothelial cells use chemokines to selectively recruit specific leukocytes (Schaerli and Moser, 2005; Vestweber, 2015). It has been reported that chemokines presented by the endothelium drive CTL transmigration under flow (Contento et al., 2008; Shulman et al., 2011; Sage et al., 2012). We determined the endothelial cell chemokine profile by measuring chemokines in the supernatant of the endothelium, using an antibody array, at 20 h (high transcellular frequency) and 4 h (low transcellular frequency) of TNFα stimulation and an unstimulated control without TNFα stimulation. We found that endothelial cells constitutively secreted CXCL8, CXCL1, and CCL14 under non-inflammatory basal conditions (Table 1; Figure S1B). TNFα treatment for 4 h increased the release of CXCL8 and CXCL1. In addition, we found low-level release of chemokines CCL2, CCL20, and CXCL10 (Table 1). Over a period of 20 h of TNFα stimulation, we found a general increase of the levels of these chemokines. Moreover, we found additional chemokines to be released into the supernatant over the course of 20 h of stimulation time: CX3CL1, CXCL7, CXCL5, CCL7, and CCL5 (Table 1). Thus, endothelial cells release a different profile of chemokines, depending on the inflammation time including chemotactic stimulants for CTLs like CXCL10, CX3CL1, and CCL20 at 20 h of TNFα stimulation. Using pertussis toxin (1 µg mL^{-1} for 2 h on CTLs) to block, among others, chemokine activation by G_{α} inhibition, completely abolishes transmigration (Figure S3A). CTLs adhere but retain a round, non-migratory phenotype (Figure S3B). A low percentage of adhering CTLs treated with pertussis toxin showed lateral migration but no transmigration.

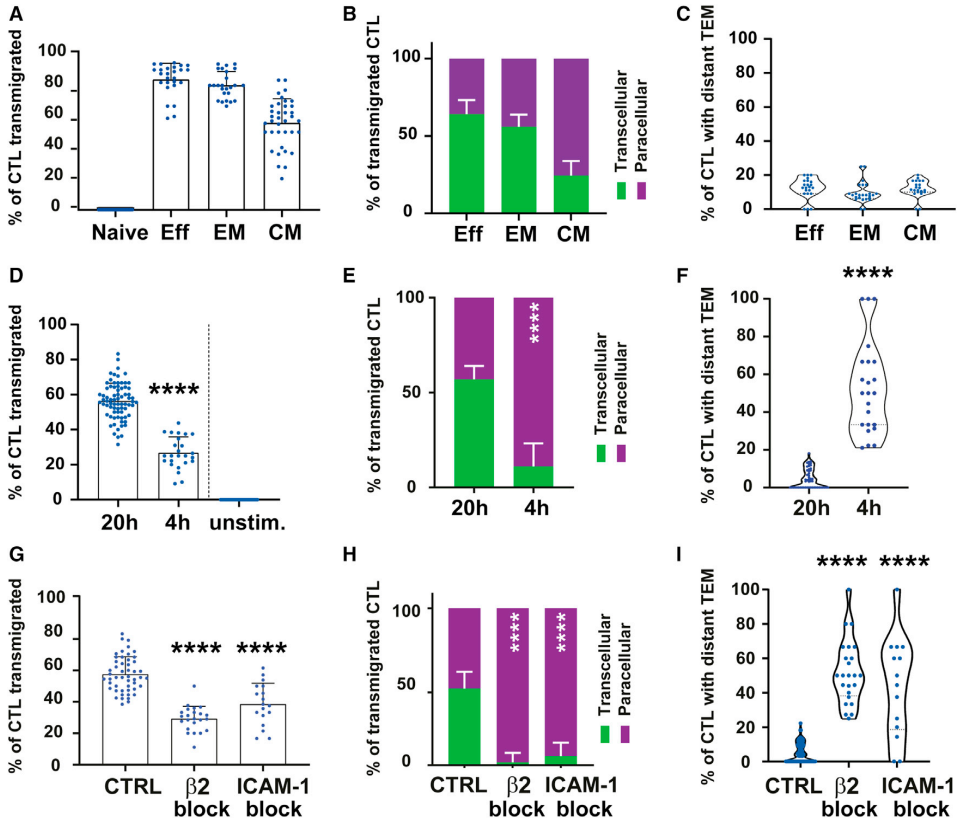

Figure 3. Transcellular migration is most prominent for effector and EM CTLs and favored by high ICAM-1 and chemokine levels, initiating local arrest of CTLs

(A) Classical CTL subsets (naive, effector [Eff], effector memory [EM], and central memory [CM]) were separated by fluorescence-activated cell sorting (FACS) from fresh human blood-derived PBMC (further described in STAR Methods) were perfused over TNFα-activated (20 h) HUVECs. All except naive CTLs show transmigration. (B) Analyzing the route of transmigration of the classical CTL subsets showed that effector (Eff) and effector memory (EM) show more events of transcellular transmigration compared to central memory (CM) that prefer the paracellular route. (C) Individual transmigrated CTLs were marked, and their diapedesis location was compared with their point of adhesion. If a CTL migrated past at least 2 different junctions from their point of adhesion from flow and transmigrated afterward, it was labeled as a distant transmigration event (distant TEM). (D–F) CTL isolations as well as sorted classical subsets show low percentages of transmigrating CTLs showing this behavior. HUVECs were grown in μ-channels and stimulated for 20 h or 4 h using TNFα. CTLs were perfused over the activated HUVECs at physiological flow. Transmigration percentage of adherent cells (D), route of transmigration (E), and percentage of distant TEM CTL s (F) was analyzed. For the shorter TNFα stimulation time of 4 h, CTLs show less efficient TEM, significantly more paracellular transmigration, and significantly more distant TEM CTLs. HUVECs were grown in μ-channels and activated for 20 h with TNFα (G–I). CTLs were perfused over the activated HUVECs at physiological flow. HUVECs were incubated with 10 μg mL−1 of blocking antibody for 30 min before the flow experiments. For blocking β2-integrins (β2) on CTLs, CTLs were incubated with 10 μg mL−1 for 30 min prior to flow experiments. Notably both β2 and ICAM-1 blocking results in decreased TEM efficiency (G), but also shifted CTLs route of TEM to paracellular (H) and resulted in more distant TEM events (I). Flow experiments using sorted subsets were performed in 4 separate preparations of HUVECs and using 8 different CTL donors. Flow experiments using total CTLs were performed in triplicate using 4–6 CTL donors. Data are mean ± SD; **** $p < 0.0001$.

In our analysis, we found soluble CX3CL1 to be released into the supernatant by the endothelial cells during 20-h TNFα treatment (Table 1). Its cognate receptor, CX3CR1, is specifically expressed on effector and effector memory CTLs (Gerlach et al., 2016a) and is lacking on central memory T cells (Conroy et al., 2018). Using flow cytometry analysis, we can confirm, that in CTL post recovery culture, most effector, and effector memory CTLs were CX3CR1^{+}, and CM and naive showed no expression of CX3CR1 (Figures S3E and S3F). As particularly effector T cells showed high levels of transcellular migration, we investigated whether CX3CL1 participates in mediating transcellular migration. Interestingly, blocking experiments using anti-CX3CL1 antibodies on 20-h TNFα-treated endothelial cells did not result in an inhibition of TEM of CTLs (Figure 4A). However, we did find a dramatic shift in the route of transmigration of CTLs from transcellular to paracellular migration (Figure 4B). Moreover, we found that CTLs showed more distant diapedesis when CX3CL1 was blocked and preferred paracellular migration (Figure 4C). Additional immunofluorescent staining identified the presence of CX3CL1 evenly distributed on the surface of TNFα-treated endothelium (Figure 4D). We hypothesized that CX3CL1 is recruited upon ICAM-1 clustering and increased at the center of the synapse to trigger transmigration of CTLs, which in turn would initiate transcellular migration. To test this, we generated fluorescent-intensity profile plots of areas of adhering CTLs and found that ICAM-1 intensity was increased at the periphery of the endothelial:CTL synapse, whereas CX3CL1 was evenly distributed and did not show any enrichment compared with the endothelial surface areas outside of the synapse (Figure 4E). From these results, we conclude that endothelial CX3CL1 drives transcellular migration of CTLs by inducing ICAM-1-initiated firm local adhesion.

Table 1. HUVEC cumulative chemokine secretion profile after different time points of TNFα stimulation

Unstimulated	4h TNFα stimulation	20h TNFα stimulatio
CXCL8	CXCL8	CXCL8
CCL14	CCL14	CCL14
CXCL1	CXCL1	CXCL1
	CCL2	CCL20
	CCL20	CXCL10
	CXCL10	CCL5
		CCL7
		CXCL5
		CXCL7
		CX3CL1

HUVEC monolayers were subjected to 10 ng mL^{-1} TNFα for 4 h or 20 h, and the supernatant was collected from individual samples after those time points had been reached. Unstimulated control samples were also taken after 20 h parallel to 20 h of TNFα stimulation. After clearing by centrifugation, the supernatant was directly applied to a chemokine array analysis. For unstimulated samples, HUVECs were treated as for 20-h TNFα stimulation without TNFα in the medium. See supplements for relative expression levels. Without TNFα activation, CCL14, midkine, and IL-8 (CXCL8) and CXCL1 can be detected. After 4 h of stimulation, CCL2, CCL20, and CXCL10 can be additionally detected in the supernatant. After 20 h, CCL5, CCL7, CXCL5, CXCL7, and CX3CL1 can also be found in the supernatant. Note that 4-h and 20-h profiles are cumulative. For bead clustering assays, the profile is more limited due to several washing steps after the indicated stimulation time. Chemokine arrays were performed at least 2 times for each condition. Semi-quantitive data are presented in Figure S1B.

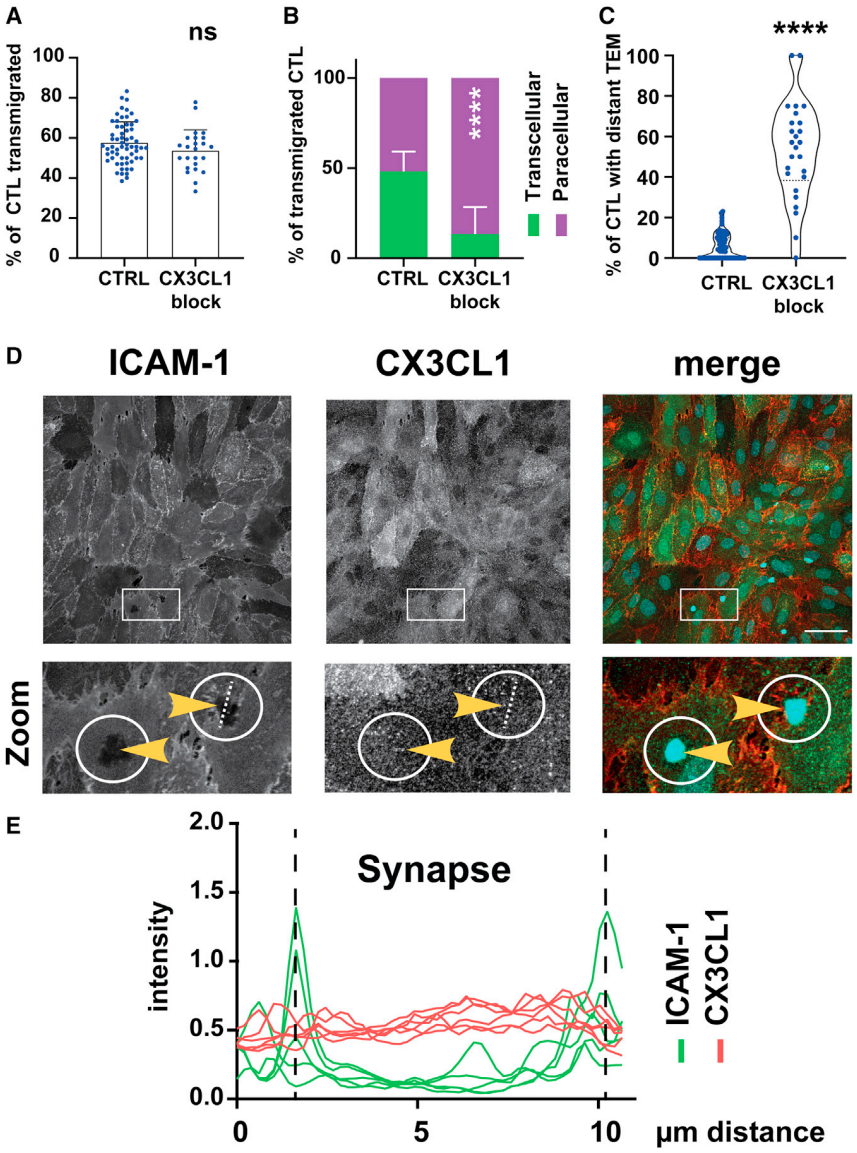

Figure 4. Endothelial CX3CL1 induces firm adhesion of CTLs to enhance transcellular diapedesis
(A–C) HUVECs were grown in µ-channels and activated with 10 ng mL–1 for 20 h using TNFα. CTLs were flown over the activated HUVECs at physiological flow. HUVECs were incubated with 10 µg mL^{-1} of blocking antibody for 60 min before the flow experiments. Blocking CX3CL1 using antibodies did not decrease transmigration efficiency (A) but resulted in a shift to more paracellular diapedesis events (B) and more distantly transmigrating CTL (C) (data are of CTL from 6 donors). Data are mean ± SD; **** $p < 0.0001$. (D) HUVECs were cultured as described before and stimulated for 20 h with TNFα. Isolated CTLs (3 donors were analyzed) were added to the HUVECs, allowed to settle for 1–2 min, and immediately fixed with PFA. This was followed by immunolabeling of ICAM-1 and CX3CL1. Nuclei were labeled with Hoechst 33342 to identify CTLs. (E) The synapses shown in (D) were analyzed using Fiji/ImageJ by determining intensity profiles along lines crossing the synapse from side to side. Yellow arrows highlight CTL nuclei. White circles highlight adherent CTLs. White rectangles indicate zoom-in area shown underneath. Dotted white line indicates an example line of measurement for plot profiles. Scale bar, 50 µm.

CTL transmigration was shown to depend on release of intracellular vesicle-stored chemokines (Shulman et al., 2011). It was recently reported that SNAP23 is a key component of the endothelial SNARE machinery that mediates endothelial exocytosis (Zhu et al., 2015); therefore, we tested whether ICAM-1 clustering physically recruited SNAP23. Using α-ICAM-1 antibody-coated beads, we mimicked the adhesion of the CTLs to ICAM-1, resulting in local clustering of ICAM-1 (Schimmel et al., 2018). As control, α-ICAM-1 antibody-coated beads were added to the cell lysate of HUVECs, enabling them to precipitate ICAM-1 but making it impossible for the beads to induce ICAM-1 clustering. Indeed, we found SNAP23 to be strongly recruited to ICAM-1 in clustered but not non-clustered conditions (Figure 5A). Interestingly, we additionally found syntaxin-3 and -4 to be recruited to ICAM-1 upon clustering, whereas VAMP-8 was not (Figure 5A). VAMP-3 appeared to bind to ICAM-1 under both conditions. Filamin B was used as a positive control, known to associate with ICAM-1 upon clustering (Kanters et al., 2008; van Rijssel et al., 2012). In line with these biochemical data, we found SNAP23 distribution to be increased at sites of T cell-endothelium synapse formation (Figure 5B). Additionally, we generated intensity profile plots indicating that SNAP23 is not excluded from the synapse area as is ICAM-1 or actin (Figure 5C). These data indicate that ICAM-1 clustering results in a strong recruitment of the secretory machinery to ICAM-1 clusters, potentially triggering the release of submembrane vesicle-stored chemokines (Shulman et al., 2011).

To study if active chemokine release from the endothelium is involved in control of CTL diapedesis and the route chosen, we used brefeldin A, a known blocker of vesicle trafficking, including transport out of the endoplasmic reticulum-Golgi system (Helms and Rothman, 1992; Rabouille, 2017). Endothelial cells were treated with brefeldin A for only 30 min prior to the flow experiments to reduce potential side effects. The results showed a reduction in the number of transmigrating CTLs (Figure 6A). Endothelial monolayer integrity was not affected under the conditions used. Interestingly, we found that, for CTLs that did cross the endothelium, the route of transmigration was shifted from transcellular to paracellular (Figure 6B). In line with this, we found more T cells moving away from their initial point of adhesion migrating extended distances (Figure 6C). Shulman and colleagues showed that CTLs are triggered to transmigrate through stimulation by intra-endothelial chemokines stored in vesicles rather than endothelial-surface-presented chemokines (Shulman et al., 2011). Therefore, we mimicked adhering CTLs by using α-ICAM-1-coated beads and measured the levels of chemokines in the supernatant after clustering. Addition of anti-ICAM-1 antibody-coated beads to TNFα-stimulated endothelial cells resulted in increased levels of CXCL1, CXCL8, and CXCL10 in the supernatant (Figure 6D), whereas CCL20 levels were unchanged. For SNAP23 knockdown endothelium, this ICAM-1 clustering-triggered release was specifically reduced for CXCL10. These results led us to the hypothesis that ICAM-1 clustering results in SNAP23-dependent release of vesicle-stored chemokines. We expected a general decrease of baseline chemokine secretion levels, as SNAP23 is the main-expressed SNARE in HUVECs. And indeed, knockdown of SNAP23 resulted in

a significant reduction of secreted CXCL1, -8, and -10 and CCL20 compared with control (Figure 6E). To confirm that CTL diapedesis was mediated by SNAP23-mediated release of chemokines, we silenced SNAP23 using siRNA (Figure S1C) and found that SNAP23 depletion significantly reduced the TEM efficiency of CTLs (Figure 6F). Also, and in line with the brefeldin A data, we found that depletion of SNAP23 shifted the transmigration route from transcellular to paracellular (Figure 6G) and resulted in more distantly transmigrating CTLs (Figure 6H).

Together, these data showed that chemokines drive different subsets of CTLs to cross the endothelium in a transcellular or paracellular manner in a two-phased model. First, global exposure of one chemokine on the endothelium, i.e., CX3CL1, activates a specific CTL subset to strongly adhere to the endothelium in an ICAM-1-dependent manner. Next, T cell-induced ICAM-1 clustering triggers the local release of specific chemokines to initiate transcellular migration.

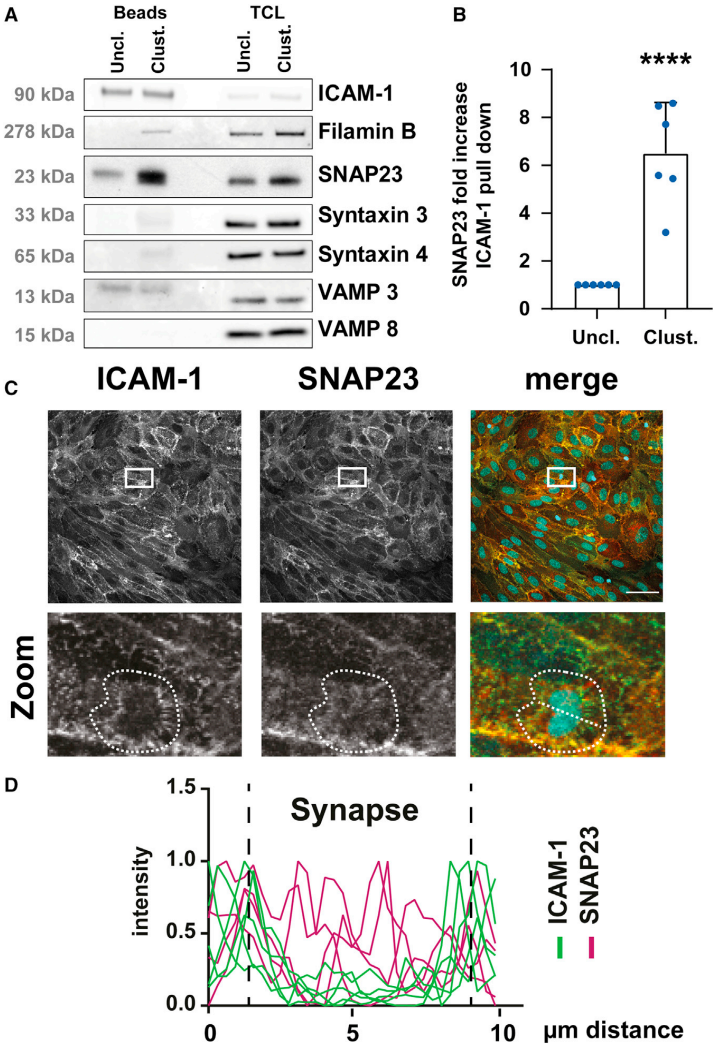

Figure 5. ICAM-1 clustering on endothelial cells recruits the endothelial secretory machinery to clustered ICAM-1

(A) To induce clustering, antibody-coated Dynabeads were added to 20-h (10 ng mL^{-1}) TNFα-stimulated HUVECs. For "unclustered" conditions, beads were added to cell lysate 30 min after lysis. For the "clustered" conditions α-ICAM-1-coated beads were added to live 20-h TNFα-activated HUVECs, and cell lysis was performed after 30 min. TCL, total cell lysate. For TCL unclustered and TCL clustered, the remaining lysate after magnetic bead clearing was applied as input control. The resulting protein samples (magnetic bead pull-down and total cell lysate input controls) were analyzed by western blotting for the presence of proteins of the endothelial secretory machinery (SNAP23, VAMP3/8, syntaxin-3/4). (B) Quantification of 6 experiments as seen in (A) are shown. Data are mean ± SD; **** $p < 0.0001$. (C) HUVECs were cultured as described and stimulated for 20 h with TNFα. Isolated CTLs were added to the HUVECs, allowed to settle for 1 min, and immediately fixed with PFA. This was followed by immunolabeling of ICAM-1 and SNAP23. Nuclei were labeled with Hoechst 33342 to identify CTLs. (D) The synapses shown in (C) were analyzed using Fiji/ImageJ by determining intensity profiles along lines crossing the synapse from side to side. Yellow circles highlight adherent CTLs. White dotted circles outline the diapedesis synapse. White rectangles indicate zoom-in area shown underneath. Dotted white line indicates an example line of measurement for plot profiles. (unclu., unclustered, beads added to cell lysate; clust., clustered, beads added to live cells). The pull-down was performed 6 times with individual experimental preparations. Scale bar, 50 µm.

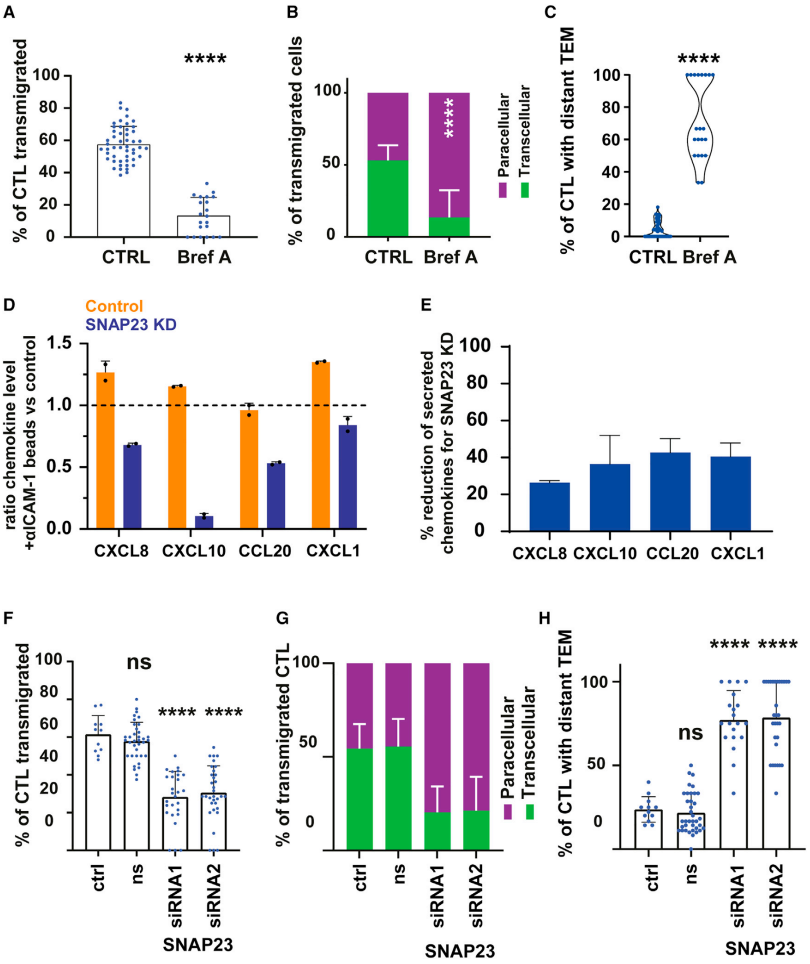

Figure 6. Transcellular diapedesis relies on active chemokine secretion via ICAM-1 clustering-initiated SNAP23-mediated synaptic release of CXCL1/8/10

(A–C) HUVECs were grown in µ-channels and activated for 20 h (10 ng mL−1) using TNFα. CTLs were flown over the activated HUVECs at physiological flow. Thirty minutes prior to the flow experiments, HUVECs were treated with 1 µg mL−1 brefeldin A (data of CTL from 4 donors). The described treatment has a strong impact on transmigration efficiency of CTLs (A); the CTLs that do transmigrate mainly use the paracellular route (B) and show high levels of distant diapedesis (C). (D and E) HUVEC were transfected with SNAP23 siRNA and control siRNA using electroporation and cultured on fibronectin-coated culture dishes for 48 h. This was followed by a 24-h TNFα stimulation, after which the medium was changed 3 times to reduce residual chemokines. Identically treated samples received full medium or full medium containing anti-ICAM-1-coated beads. After 30 min, the supernatant was harvested and cleared by centrifugation (14,000 rpm, 15 min) and frozen at −80°C until analysis. (D) SNAP23 knockdown reduces ICAM-1 clustering-induced chemokine release of CXCL1/8/10. In control conditions, ICAM-1 clustering induces CXCL1/8/10 to be secreted at higher levels than without clustering. (E) sShown are the relative changes in supernatant chemokine levels (continuous secretion) in SNAP23-knocked-down (KD) HUVECs compared with control cells. HUVECs were transfected with siRNA against SNAP23 and using a non-silencing control. (F–H). An untreated sample (not transfected) was used as control next to non-silencing for each donor. After electroporation (3 separate preparations), the cells were plated in µ-channels (seeding density 80%) and cultured for 48 h followed by a 20-h TNFα stimulation. CTLs were flown and CTL behavior when contacting HUVECs was analyzed (CTL of 6 donors). (F–H) (F) SNAP23 KD HUVECs support less efficient transmigration (G) affect the route of transmigration of CTL, which was shifted to more paracellular events, and (H) cause T cells to transmigrate more distantly. Data are mean ± SD; **** $p < 0.0001$.

DISCUSSION

Although many details have been studied of how T cells leave the circulation, it is still not clear how different T cell subsets cross the endothelium and whether or why they would cross certain endothelia in a transcellular or paracellular manner (Carman and Martinelli, 2015). Leukocyte subsets show remarkably different phenotypes when crossing the endothelial cell monolayers. Upon adhesion to the endothelium, neutrophils spread out and start crawling over the endothelial cell surface (Schimmel et al., 2018), whereas CTLs can be rather stationary for several minutes, followed by transcellular migration (this study). If CTLs do not cross transcellularly, the phenotype changes to the neutrophilic spreading type and they start crawling, followed by paracellular migration. It is noteworthy that naive T cells, although capable of transmigrating into non-lymphoid tissue (Lewis et al., 2008), showed hardly any adhesion to inflamed endothelium, and the ones that did remained rounded and inactive without transmigration or lateral migration. This might be due to the fact that endothelial cells do not express CCR7-targeting chemokines, and rolling of naive cells is low on inflamed endothelium due to low selectin binding (Tinoco et al., 2017). And although naive cells express β2-integrin, expression is very low compared with effector, effector memory, and central memory CTLs (this study; Nolz et al., 2011).

The interaction of CTLs with endothelial ICAM-1 initiates the formation of endothelial cup structures (Carman and Springer, 2004; Barreiro et al., 2008). Our data suggest that a specific interaction hub, initiated by ICAM-1, was created to support efficient migration of effector and effector memory T cells in a transcellular manner. Indeed, effector and effector memory T cells prominently induced a typical synapse: a tight endothelial membrane structure that surrounds the adherent CTL upon initial contact with the endothelium, comparable with the previously identified docking structures or transmigratory cups (Carman and Springer, 2004; Barreiro et al., 2008).

We also found that both effector and effector memory CTLs show high levels of transcellular diapedesis across inflamed endothelial monolayers compared with those of central memory. As ICAM-1 has been recognized as being a requirement for transcellular diapedesis (Yang et al., 2005; Millán et al., 2006), we tested how blocking this interaction would affect the behavior of adhering CTLs. And indeed, blocking of ICAM-1 (EC) or its counterpart β2-integrin/CD18 (CTL) shifted the general transmigration route from trans-to paracellular, but transmigration efficiency was also highly reduced, and adherent CTLs that did adhere migrated long distances on the endothelial surface from their original points of adhesion before undergoing paracellular migration. Also, many leukocytes use ICAM-1 for adhesion, and increasing the expression of ICAM-1 actually triggers immune cells to cross the endothelium in a transcellular manner, indicating that ICAM-1 is clearly an important player in determining which transmigration route to take (Yang et al., 2005; Carman et al.,

2007). Central memory CTLs show low transcellular events, whereas effector and effector memory CTLs show higher levels. In line with this, effector CTLs express higher levels of β2-integrin/CD18 compared with effector memory and central memory. Yet, we found that CM behave differently immediately after contacting the endothelial cells: CM CTLs showed lateral polarization moving away from their initial point of adhesion. In line with this, CM CTLs also showed stronger random migration even when provided with continuous stimulation via CD3 (Mayya et al., 2018). We concluded that other factors than β2-integrin/ICAM-1 interactions participate to these observed differences, so there should be additional triggers or enhancing factors for CTLs to migrate via the transcellular route. Only having adhesion factors present was not enough to support CTL transcellular transmigration.

We turned our attention to chemotactic activation of adhering CTLs. Blocking chemotactic activation on CTLs using pertussis toxin completely blocked transmigration and drastically reduced CTL polarization and migration (i.e., apical migration, local transcellular diapedesis, and local and distant paracellular diapedesis). Most CTLs, however, remained unpolarized (rounded) without any movement or change in morphology. From this, we concluded that chemotactic stimulation from deposited and/or actively secreted chemokines is essential for CTL transmigration. To further dissect the involved process, we applied short-term blocking of vesicle fusion, to not affect surface deposition of chemokines during inflammatory stimulation, which shifted the migration route from transcellular to paracellular. We went on to analyze which chemokines are produced and presented by endothelial cells upon inflammation that could mediate the observed behavior of CTL subsets. We found that, apart from secreting effector and memory CTLs targeting chemokines like CXCL10 and CCL20, endothelial cells also expressed CX3CL1 on the surface, which was also shed by the endothelium during long-term inflammation and could be detected at low levels in the supernatant (20 h of TNFα stimulation). Blocking CX3CL1 resulted in a shift from transcellular to paracellular migration events. Interestingly, when we studied the distribution of CX3CL1, we found that CX3CL1 was evenly distributed over the apical surface of the endothelial monolayer. From this, we conclude that CXC3L1 arrests CTLs immediately upon contact (Fong et al., 1998), as blocking CX3CL1 interaction did not affect transmigration efficiency or adhesion numbers but instead caused adhering CTLs to migrate away from their initial contact point and show distant paracellular migration events.

Additionally, we found that ICAM-1 clustering triggered the SNAP23-dependent release of endothelial-derived chemokines, including CXCL10, that can enhance transcellular diapedesis of CTLs. Interestingly, the CXCL10 receptor CXCR3 is expressed by effector, effector memory, and central memory CTLs (Groom and Luster, 2011; Maurice et al., 2019), while the CX3CL1 receptor CX3CR1 is highly expressed by effector and effector memory CTLs (Gerlach et al., 2016b). On the basis of these data, we suggest that effector CTLs perform transcellular migration by first becoming activated through endothelial-

bound CX3CL1 to strongly adhere to the endothelium surface, followed by inducing ICAM-1 clustering. ICAM-1 clustering allows the local SNAP23-mediated release of, among others, CXCL10, activating effector CTLs to induce transmigration, resulting in a transcellular migration mode.

Although we believe that this mechanism of transcellular migration of CTLs may occur systemically, it is important to note that endothelial cell behavior and phenotype can differ from one bed to another depending on the organ context (Aird, 2007a; 2007b). As we noted that the CTL-EC interaction shows similarities to the immunological synapse, including the formation of EC membrane protrusions, and many different names have been given to these endothelial membrane protrusions (e.g., docking structures, transmigratory cups, apical cup structures, actin-rich contact areas), we propose to introduce the term "diapedesis synapse." for the interaction of the CTLs with the endothelium, as this interaction includes the interplay among adhesion molecules, chemokines, and chemokine receptors and has therefore strong similarities to the immunological synapse.

In conclusion, we propose that CTLs make use of a sequential chemokine activation model that orchestrates the transcellular passage of CTLs across the endothelium.

Limitations of the study

In this study, we analyzed the transmigration behavior of human cytotoxic T cells by using human umbilical vein endothelial cells (HUVECs) as endothelial model. Our study indicates how important endothelial cells are for the control of tissue entry, specifically via their chemokine secretion profile, which can change over time of inflammation. Although many fundamental studies on transmigration have been performed using HUVECs as endothelial model, endothelial cells from different vascular beds can differ in their chemokine profile, reactivity to inflammation, degree of adhesion molecule expression, and other factors. In addition, we used a simplified 2D flow assay to monitor transmigration that lacks the influence of the *in vivo* tissue environment. These experimental setups are limitations to the current study.

STAR★METHODS

Experimental model and subject details

Endothelial cell model

Human umbilical vein endothelial cells (HUVEC), from pooled donors, were used as human endothelial model system. HUVEC were bought frozen and stored in liquid nitrogen. After thawing (at p3) the cells were cultured for one week to recover and used the week after thawing. HUVEC were split twice after thawing.

Cytotoxic T cells

CD8+ T cells were magnetically isolated from fresh human blood derived PBMC. The blood was provided by anonymous, voluntary, adult male and female donors at Sanquin Blood Supply, Amsterdam, The Netherlands via the Sanquin Buisjesdonor system.

REAGENT or RESOURCE	SOURCE	IDENTIFIER
Antibodies		
Monoclonal mouse anti-human VE-cadherin, IF	BD Pharmigen	Cat#555661; RRID: AB_396015
Polyclonal rabbit anti-human SNAP23, purified, WB	Synaptic Systems	Cat#111203
Polyclonal rabbit antiserum, anti-human SNAP23, IF	Synaptic Systems	Cat#111202
Monoclonal mouse anti-human CX3CL1, blocking	RnD Systems	Cat#MAB3652
Polyclonal rabbit anti-human CX3CL1, IF	Fisher Scientific	Cat#50-137-14
Monoclonal mouse anti-human β-actin, purified, WB	Merck	Cat# MABT825
Monoclonal mouse anti-human Filamin A, WB	Serotec	Cat#MCA464S
Monoclonal mouse anti-human CD54 (ICAM-1), IF	Biorad Laboratories	Cat#MCA1615ST
Monoclonal mouse anti-humanCD54 (ICAM-1), blocking	eBioscience	Cat#14-0549-82
Monoclonal mouse anti-human CD54 (ICAM-1), biotinylated, bead pull down	RnD Systems	Cat#BBA9
Rabbit polyclonal anti-human CD54 (ICAM-1), WB	Santa Cruz	Cat#SC-7891
Monoclonal mouse anti-human CD18 (β2 integrin), blocking	Merck Millipore	Cat#217660
Polyclonal mouse anti-human Syntaxin-4, WB	BD Bioscience	Cat#610439; RRID: AB_397814
Polyclonal rabbit anti-human Syntaxin-3, purified, WB	Synaptic Systems	Cat#110033
Polyclonal rabbit anti-human VAMP3, purified, WB	Synaptic Systems	Cat#104203
Polyclonal rabbit anti-human VAMP8, purified, WB	Synaptic Systems	Cat#104303
Mouse Isotype control IgG1	Thermo Fisher Scientific	Cat#02-6100
Mouse Isotype control IgG2a	BD Bioscience	Cat#554126
Monoclonal mouse anti-human TCRγδ, PE-Cy7, FC	BD	Cat#333141
Monoclonal mouse anti-human CD8, APC, FC	BD Bioscience	Cat#561952
Monoclonal mouse anti-human CD45RA, BV785	Biolgegend	Cat#304139; RRID: AB_2561369
Monoclonal mouse anti-human CD45RA, FITC, FC	BD Bioscience	Cat#561882; RRID: AB_395879
Monoclonal mouse anti-human CD27, AF488, FC	Sanquin Pelicluster	Cat#M1764
Monoclonal mouse anti-human CD27, BV650, FC	Biolegend	Cat#302827; RRID: AB_11124941
Monoclonal mouse anti-human CD16, PE, FC	BD Pharma	Cat#555407; RRID: AB_395807
Monoclonal mouse anti-human CD56, PE, FC	BD Pharma	Cat#555516; RRID: AB_395906
Monoclonal mouse anti-human CD4, PE, FC	eBioscience	Cat#12-0047-42; RRID: AB_1518750
Monoclonal mouse anti-human CX3CR1, PEDazzle594, FC	Biolegend	Cat#341623; RRID: AB_2687151
Monoclonal mouse anti-human CD18, AF488, FC	BD Bioscience	Cat#561687; RRID: AB_2129268
Goat anti-Mouse IgG (H+L) Cross-Adsorbed Secondary Antibody, Alexa Fluor 488, IF	Thermo Fisher Scientific	Cat#A-11001; RRID: AB_2534069

REAGENT or RESOURCE	SOURCE	IDENTIFIER
Goat anti-Mouse IgG (H+L) Cross-Adsorbed Secondary Antibody, Alexa Fluor 568, IF	Thermo Fisher Scientific	Cat#A-11004; RRID: AB_2534072
Goat anti-Mouse IgG (H+L) Cross-Adsorbed Secondary Antibody, Alexa Fluor 633, IF	Thermo Fisher Scientific	Cat#A-21050; RRID: AB_2535718
Goat Anti-Mouse Immunoglobulins/HRP (affinity isolated), WB	Dako	Cat#P0447
Swine Anti-Rabbit Immunoglobulins/HRP (affinity isolated), WB	Dako	Cat#P0399
Biological samples		
Fresh blood, in heparin tubes, from voluntary healthy donors	Sanquin Blood Supply, Amsterdam, NL	N/A
Buffy coats, from the transfusion service	Sanquin Blood Supply, Amsterdam, NL	N/A
Chemicals, peptides, and recombinant proteins		
Brefeldin A, BioXtra, for molecular biology	Sigma Aldrich	Cat#B6542
Recombinant human tumor necrosis factor α, TNF-α	Peprotech	Cat#300-01A; Accession Number: P01375
Pertussis toxin from *Bordetella pertussis*	Merck, formerly from Sigma Aldrich	Cat#P7208
Phalloidin Alexa Fluor 488	Thermo Fisher Scientific	Cat# A12379
Vybrant™ DiD Cell-Labeling Solution	Thermo Fisher Scientific	Cat#V22887
HOECHST 33342	Thermo Fisher Scientific	Cat#H1399
Critical commercial assays		
Proteome profiler human chemokine kit	Biotechne, RnD Systems	Cat#ARY017
Experimental models: Cell lines		
HUVEC, human umbilical vein endothelial cells, pooled	Lonza, Bornem, Beligum	Cat#C2519A
Oligonucleotides		
Human SNAP23, (NM_003825, NM_130798), siRNA1	Qiagen	GeneGlobeID: SI00056448
Human SNAP23, (NM_003825, NM_130798), siRNA2	Qiagen	GeneGlobeID: SI00056455
Negative Control siRNA, human	Qiagen	GeneGlobeID: 1022076
Recombinant DNA		
pmEGFP-N1-Lifeact	Jaap van Buul, Sanquin, Amsterdam, NL	N/A
pLV-mScarlet_CAAX	Jaap van Buul, Sanquin, Amsterdam, NL	N/A
pLV_ICAM-1_GFP	Bram van Steen, Sanquin, Amsterdam, NL	N/A
Software and algorithms		
Fiji/ImageJ, ImageJ v1.53	(Schindelin et al., 2012)	https://doi.org/10.1038/nmeth.2019
Graphpad Prism 9.1.0 (221)	Graphpad Software, LLC	https://www.graphpad.com/scientific-software/prism/
FlowJo v10.8	BD	https://www.flowjo.com/solutions/flowjo
Imaris 9.7.2	Bitplane	https://imaris.oxinst.com/
Other		
Ficoll-Paque PLUS, density gradient media	GE Healthcare	Cat#17144003
$CD8^+$ T cell isolation kit	Miltenyi Biotech	Cat#130-045-201
EGM-2 medium	Promocell	Cat#C-22011
EGM-2 supplement kit	Promocell	Cat#C-39216
Leukosep tubes, cell sorting	Greiner BioOne	Cat#227290
RPMI1640, Glutamax	Thermo Fisher Scientific	Cat#61870036

REAGENT or RESOURCE	SOURCE	IDENTIFIER
Penicillin-Streptomycin (10,000 U/mL)	Thermo Fisher Scientific	Cat#15140122
Fetal bovine serum	Bodinco	N/A
Fibronectin solution	Sanquin Reagents	N/A
Trypsin-EDTA (0.5%), no phenol red	Thermo Fisher Scientific	Cat#15400054
µ slides VI (0.4)	Ibidi	Cat#80606
µ-slide 8 well	Ibidi	Cat#80826
Human serum albumin, Albuman 200 g/L	Sanquin Reagents	N/A
Phosphate bufferd saline (PBS)	Frisenius Kabi	Cat#8717973380153
Table-top pump (flow channel assays)	Prosense BV	Cat#NE-1010
iBlot Transfer Stack, nitrocellulose, mini	Thermo Fisher Scientific	Cat#IB301002
PageRuler, prestained protein ladder	Thermo Fisher Scientific	Cat#26617
Trypsin Neutralizer Solution	Thermo Fisher Scientific	Cat#R002100
IMDM medium	Lonza	Cat#12-722F
Sodium pyruvate, cell culture	Thermo Fisher Scientific	Cat# 11360070
L-glutamine, cell culture	Thermo Fisher Scientific	Cat# 25030081
TransIT-L1 lentiviral packaging plasmid kit	Mirus	Cat#MIR2360
Lenti-X concentrator	Takara Bio	Cat#631231
3-µm polystyrene beads	Polysciences	Cat#17145-5
Streptavidin-coated Dynabeads	Invitrogen	Cat#11205D
Protease inhibitor cocktail	Merck	Cat#P8340
Neon transfection system 100 µL kit	Thermo Fisher Scientific	Cat#MPK10096
Prolong Diamond Antifade, mounting medium	Thermo Fisher Scientific	Cat#P36961
Plastipak Syringe 60 mL Luer Lock	BD	Cat#309653
Amersham Protran 0.2 µm NC	GE	Cat#10600001
Skim milk powder	Elk, Campina	N/A
Criterion™ Cell/Plate Blotter System	Biorad	Cat#1656024
XCell SureLock MiniCell electrophoresis system	Thermo Fisher Scientific	Cat#EI0001

METHOD DETAILS

HUVEC cell culture (subculture, and TNFα activation) and CTL recovery culture

Endothelial cells were cultured under sterile conditions according to the specifications of the provider in an incubator at 37°C and 5% CO_2. HUVEC were grown in EGM-2 (PromoCell) containing the endothelial cell growth supplement and 1% Penicillin/Streptomycin. CTL were recovered in RPMI containing 10% FCS and 1% Pen/Strep in an incubator at 37°C and 5% CO_2. For continuous culture HUVEC were grown on fibronectin (Sanquin Reagents) coated plastic culture dishes (TPP). For trypsinization endothelial cells were washed with warmed (37°C) PBS and incubated with Trypsin*EDTA (1 mL per 100 mm dish) until detachment. The reaction was stopped using the same amount of trypsin neutralizing solution as trypsin solution, followed by centrifugation at 100 g for 5 min to change to full medium. HUVEC pool used in the experiments of this study was 1052 (Lonza). HUVEC were stimulated with TNFα (10 ng mL^{-1}) in EGM-2 for indicated times. If not stated otherwise stimulation was done overnight (20 h).

Cell treatments

Brefeldin A (in DMSO) was stored at – 20°C at 10 mg mL^{-1} and used at a working concentration of 1 µg mL^{-1} for 30 min in EMG-2. Pertussis toxin (in H_2O with 1% BSA) was stored at 4°C at 100 µg mL^{-1} and used at a working dilution of 1 µg mL^{-1} in RPMI1640 full medium. Antibodies used in flow assay blocking experiments (Cat#14-0549-82, Cat#217660, Cat#MAB3652, Cat#02-6100, Cat#554126) were used at 10 µg mL^{-1} in EGM-2 (EC treatment) or RPMI (CTL treatment) full medium for 30 min prior to injection of CTL into the flow system followed by a washing step at 100 g for 10 min for CTL. For fluorescent membrane labeling, CTL were stained in HEPES buffer (20 mM HEPES,132 mM NaCl, 6 mM KCL, 1 mM $CaCl_2$, 1 mM $MgSO_4$, 1.2 mM K_2HPO_4, 1 g L^{-1} D-glucose, and 0.5% (w/v) human serum albumin) using 1:6000 diluted Vybrant DiD (Thermo Fisher) for 20 min at 37° in an Eppendorf tube. This was followed by a washing step (250 g, 5 min) and resuspension in medium.

Table. Bead pulldown assay and Western blot

Cat#	Specificity	Application	Conjugate	Concentration/Dilution
BBA9	ICAM-1	Bead coating	Biotin	300 ug per mL beads
111 203	SNAP23	WB	–	1 µg/mL
MCA464S	Filamin A	WB	–	1:1000
SC-7891	ICAM-1	WB	–	0.2 µg/mL
P0447	GαM-HRP	WB	HRP	133 ng/mL
P0399	SwαRb-HRP	WB	HRP	40 ng/mL
610439	Sntx-4	WB	–	0.25 µg/mL
110033	Sntx-3	WB	–	2 µg/mL
104203	VAMP-3	WB	–	1 µg/mL
104303	VAMP-8	WB	–	2 µg/mL

Table. Antibodies for cell sorting

Cat#	Conjugate	Specificity	Dilution	Clone
L10119	APC-Cy7	Live/Dead	1:1000	–
333141	PE-Cy7	TCR γδ	1:50	11F2
561952	APC	CD8	1:50	RPA-T8
304139	BV785	CD45RA	1:500	HI100
M1764	AF488	CD27	1:100	CLB-CD27/1, 9F4
555407	PE	CD16	1:100	3G8
555516	PE	CD56	1:100	B159
12-0047-42	PE	CD4	1:100	RPA-T4/SK3

Table. Antibodies for CTL phenotyping

Cat #	Conjugate	Specificity	Dilution	Clone
L10119	APC-Cy7	Live/Dead	1:1000	–
561952	APC	CD8	1:50	RPA-T8
304139	BV785	CD45RA	1:500	HI100
302828	BV650	CD27	1:100	O323
341624	PEDazzle594	CX3CR1	1:100	2A9-1
561687	AF488	CD18	1:100	AB_2129268

Virus production

pLV_CAAX-mScarlet and pLV_ICAM-1_GFP was packaged into lentiviral particles in HEK293 T cells cultured in IMDM (supplemented with 10% FCS, 2 mM L-glutamine, 100 U/mL Penicillin, 100 µg/mL Streptomycin, 1 mM Sodiumpyruvate) by means of third generation lentiviral packaging plasmids using TransIT®-L1. Lentivirus-containing supernatant was harvested on day 2 and 3 after transfection and concentrated using Lenti-X Concentrator according to the manufacturer's instructions. HUVEC were transduced using lentiviruses with pLV_CAAX-mScarlet or pLV_ICAM-1-GFP and used 3–5 days after transduction.

Coating of polystyrene beads with α-ICAM-1 antibodies

For live cell experiments 3-µm polystyrene beads (Polysciences) were coated with mouse monoclonal antibody anti-ICAM-1 (clone: BBIG-I1, Cat#BBA9). For pull-out experiments, 40 µL 2.8-µm magnetic streptavidin-coated Dynabeads (Cat: 11205D, Invitrogen) per condition were used. The beads were washed using a washing buffer (PBS, 2 mM EDTA, 0.1% BSA) before coated with 1.6 µg biotinylated mouse mAb anti-ICAM-1 (clone BBIG-I1, Cat#BBA9) for 45 min at 4° under continuous mixing. After antibody coating the beads were washed three times using washing buffer with aid of a table-top magnet before being resuspended in 250 µL medium. Antibody coated beads were used within 1 day after preparation.

ICAM-1 pull-out

To induce clustering, the antibody-coated dynabeads were added to TNFα-stimulated confluent HUVEC monolayers in a 10-cm dish containing 3 mL medium and incubated for 30 min at 37°C and under 5% CO_2. Cells were washed with 4° PBS containing 1 mM $CaCl_2$ and 0.5 mM $MgCl_2$, lysed for 5 min on ice with RIPA buffer (50 mM Tris-HCl pH 7.4, 100 mM NaCl, 10 mM $MgCl_2$, 1% NP40, 0.1% SDS and 1% sodium deoxycholate) and incubated for 1 h at 4°C under continuous mixing. Beads were isolated using a magnetic holder, washed twice with RIPA buffer, three times with NP40 buffer (50 mM Tris-HCl pH 7.4, 100 mM NaCl, 10 mM $MgCl_2$, 1% NP40) and resuspended in SDS sample buffer. For 'non-clustered' conditions, beads were added to the culture dish after cell lysis, washed as described above and resuspended in SDS sample buffer. Protein levels were analysed by western blotting. Quantified signals were normalized to the unclustered condition.

Western blot analysis of ICAM-1 bead pull-out

The resulting protein samples (magnetic bead pulldown and total cell lysate input controls) were analyzed by Western blotting. Samples were separated using NUPAGE 10-well 1.0 mm Bis Tris 4–12% precast gels in a XCell SureLock MiniCell electrophoresis system at 200 V for 50 min using NuPAGE MES buffer. As molecular weight marker a pre-stained protein ladder was used (Thermo Fisher). Blotting was performed using the PowerPac system (BioRad) and 0.2 µm nitrocellulose blotting membrane (Amersham) at 100 V for 75 min. The

membrane was carefully removed and immediately placed into 50 mL TBST-T containing 10% skim milk powder (Elk, Campina) and blocked for 1 h at RT. Afterwards transferred proteins were labelled by incubating the membrane for 2 h at RT with antibodies targeting proteins of the endothelial secretory machinery (SNAP23, VAMP3/8, Syntaxin-3/4) and ICAM-1 (see the table "Bead pulldown assay and Western blot" for dilutions and antibodies used; filamin A serves as positive pull-down control). Unbound antibody was removed by three 10 min washing steps using TBS-T and incubation with horseradish peroxidase (HRP)-labelled antibodies (Dako) for 1 h followed by another three 10 min washing steps using TBS-T. The membrane was transferred to a metal tray and incubated with 1 mL of enhanced chemiluminescence (ECL; West Dura, Thermo Fisher Scientific) reagent by mixing reagent A and B in equal amounts and directly applying the solution to the membrane. Detection of the chemiluminescent signal was done using the ImageQuant 800 (Amersham). For quantification, integrated intensity was calculated from the mean value and area using Image J.

Protein isolation for Western blot

For Western blot HUVEC were grown in fibronectin coated 24 well plates (TTP) under the same conditions as the cells from the same siRNA transfection in µ-channels or µ-slides and subjected to the same TNFα activation time. 3 × 10^4 HUVEC were seeded per well after electroporation. For SNAP23 KD HUVEC were grown for 48 h before TNFα stimulation to achieve sufficient knock down. This was followed by a 20 h TNFα stimulation. At the start of the experiments the cells were 1) washed in ice cooled PBS for 1 min after which 2) 80 µL of RIPA buffer (50 mM Tris-HCl pH 7.4, 100 mM NaCl, 10 mM $MgCl_2$, 1% NP40, 0.1% SDS and 1% deoxycholic acid + protease inhibitor cocktail 1:100) were added to each well followed by shaking at 4°C for 15 min. The lysis buffer was collected into ice cooled Eppendorf tubes and sonicated for 3 × for 30 s in ice water with 30 s breaks between sonication using a table-top sonication bath. The samples were cleared by centrifugation at 14,000 rpm for 15 min at 4°C in an Eppendorf centrifuge. The supernatant was harvested and either used for Western analysis directly or frozen at −80°C until use.

Western blot of siRNA knock-down efficiency

12.5 µL of protein isolate was mixed 1:1 with 2× sample buffer and 25 µL were separated using NUPAGE 10-well 1.0 mm Bis Tris 4–12% precast gels in a XCell SureLock MiniCell electrophoresis system at 200 V for 30 min using NuPAGE MES buffer. As molecular weight marker a pre-stained protein ladder was used (Thermo Fisher). The gel was removed from its cast and rinsed with deionized water. Blotting was performed using the iBlot system (Thermo Fisher) and mini nitrocellulose transfer stacks according to the manufacturer's instructions. After transfer using program 3, the membrane was carefully removed and immediately placed into 50 mL TBST-T containing 10% skim milk powder (Elk, Campina) and blocked for 1 h at 4°C. Afterwards transferred proteins were labelled by incubating the

membrane for 1 h with antibodies targeting SNAP23 (Synaptic Systems, Cat#111203) and β-actin (Merck, Cat#MABT825) for 1 h at RT followed by three 10 min washing steps using TBS-T and incubation with HRP-conjugated secondary antibodies for 30 min followed by another three 10 min washing steps using TBST-T. The membrane was transferred to a plastic sheet and incubated with 1 mL of ECL reagent by mixing reagent A and B in equal amounts and directly applying the solution to the membrane to be covered in the plastic sheet. After 1 min excess ECL solution was removed with tissues and the membrane was exposed to X-ray films (SuperRX-N, Fujifilm, Cat # 47410-19289) for 10 to 30 s after which the X-ray film was developed.

Transfection of HUVEC cells with plasmid DNA and siRNA

HUVEC were grown in fibronectin coated culture dishes to 70% confluency at p3. After trypsin harvest cells were washed once with PBS and transfected using the Neon electroporation system (Thermo Fisher) using buffer R according to the manufacturer's instructions, with 100 µL gold pipette tips and 2 µg of plasmid or 200 nM siRNA with 0.5 × 10^6 cells in 100 µL buffer R. Neon electroporation settings: 1350 V, 30 ms, 1 pulse. The 100 µL of cell suspension was added to 150 µL warm full EGM-2 and 40 µL were added to fibronectin coated µ-channels (VI 0.4, Ibidi GmbH). The cells were allowed to adhere for 20 to 30 min and the channels were filled with 110 µL of warm EGM-2. After 24 h (plasmid) or 48 h (siRNA) HUVEC were activated with 10 ng mL^{-1} TNFα by aspirating the reservoirs and adding 120 µL of TNFα containing EGM-2.

Flow channel preparation

µ-channels VI 0.4 (Ibidi) were coated with 30 µL fibronectin (Sanquin Reagents) for 1 h at RT followed by a washing step with PBS. Afterwards trypsinized HUVEC, resuspended in EMG-2 (1×10^6 cells mL^{-1}), were added at 30.000 cells per channel (30 µL medium) and allowed to adhere for 20 to 30 min assured by visual inspection under a microscope. The chambers were then filled up with EGM-2 medium (120 µL) which was exchanged twice a day by aspirating and replacing with 120 µL fresh warmed EGM-2. For stimulation 120 µL of 10 ng mL^{-1} TNFα was added to each channel and fresh medium was added when the stimulation time point was reached, and the experiments were started.

Live imaging transmigration under flow

TNFα treated HUVEC were flown with HEPES buffer (20 mM HEPES, 132 mM NaCl, 6 mM KCL, 1 mM $CaCl_2$, 1 mM $MgSO_4$, 1.2 mM K_2HPO_4, 1 g L^{-1} D-glucose, and 0.5% (w/v) human serum albumin). HEPES flow buffer was prepared fresh for every experiment, filtered, warmed to 37°C and used on the same day. A flow rate of 0.5 mL min^{-1}, corresponding to ~0.8 dyne cm^{-2}, was set on a table-top pump (Prosense) with a BD 60 mL Syringe Luer-Lock tip (Becton, Dickinson, and Company). Endothelial cells were exposed to flow for 10 min prior

to injection of 1 mL containing CTL at 1 × 10^6 mL^{-1} in RPMI 10% FCS 1% Pen/Strep. Imaging of live cells was performed using a Zeiss Axiovert 200 Widefield microscope with a HXP lighting unit and incubation (37°C and 5% CO_2). For each channel multiple random positions were recorded and analyzed.

Imaging of CTL synapse

To image the ICAM-1 synapse in detail, HUVEC overexpressing ICAM-1-GFP grown in a fibronectin coated µ-Slide 8-well slides (Ibidi GmbH) were treated with TNF-α (10 ng mL^{-1}) for 18 h 2*10^5 DiD labelled CTL were added to the HUVEC and allowed to attach for 2 min at 37° 5% CO2. The HUVEC were then washed using PBS (including 1 mM $CaCl_2$ and 0.5 mM $MgCl_2$) to remove unattached CTL. Afterwards the cells were fixed using 4% PFA for 10 min at 37° and 5% CO_2. The sample was then washed 3 x with PBS to completely remove PFA and imaged using the LSM980 AiryScan 2 (Zeiss) in Airyscan SuperResolution (SR) modus with a 63× objective. All recommended settings were used for optimal SR processing (1.7 x zoom and 0.17 µm z-step size) which was performed at standard strength. Image analysis was performed in Imaris. Raw data was displayed using the MIP 3D mode and surfaces were created using the surface module in a semiautomatic fashion.

PBMC and CTL isolation for *in vitro* experiments

PBMC were obtained from fresh blood provided by healthy anonymous donors at Sanquin, Amsterdam, The Netherlands. Blood was diluted 1:2 (1:4 for buffy coats) with isolation buffer (PBS +0.5% FCS) and up to 35 mL layered over 15 mL of Ficoll Paque Plus. This was followed by a centrifugation step at 400 g for 40 min at RT without breaks or acceleration. Then the lymphocyte ring was harvested and transferred into a fresh tube to be filled (to 50 mL) using isolation buffer. After three centrifugation steps (1) 350 g for 10 min, (2) 200 g for 10 min, (3) 200 g for 10 min, cells were counted and used for magnetic bead isolation. $CD8^+$ were isolated from fresh PBMC isolate using the CD8 T cell isolation kit (Cat # 130-096-495, Miltenyi Biotech) and LS columns (Cat # 130-042-401, Miltenyi Biotech) according to the manufacturer's instructions. Isolated CTL were placed in an incubator overnight in RPMI 1640 medium with 10% FCS and 1% Pen/Strep at a density of 2 × 10^6 mL^{-1}.

Fluorescent activated cell sorting of CTL subsets

Leukosep tubes were filled with 16 mL Ficoll paque and centrifuged at 1000 g for 30 s. Blood was diluted 1:4 using isolation buffer (PBS +0.5% FCS) and the diluted blood was carefully applied (35 mL) to a Leukosep tube and centrifuged at 1000 g for 20 min at RT. Afterwards PBMC were harvested and washed using cold isolation buffer adding up to 50 mL in a conical tube followed by centrifugation at 350 g for 10 min. This step was repeated twice but using 200 g for 10 min each whilst decanting the previous supernatant and resuspending the cells in 50 mL isolation buffer prior to every centrifugation step. From the resulting PBMC population $CD8^+$ cells were isolated using magnetic labeling ($CD8^+$ isolation kit,

Milteny Biotech). Buffy coats were obtained from Sanquin, Plesmanlaan, Amsterdam. The isolated $CD8^+$ T cells were stained in PBS (+0.5% FBS). The PE/PE-Cy7 channel was used as a dump to exclude remaining NK and CD4 and TCR-δγ T cells. Isolated T cells were selected in the FCS/SSC scatter plot and further gated as alive (Live/Dead negative), $CD3^+$, $CD8^+$, TCR $\gamma\delta^-$, $CD16^-$, $CD56^-$ and $CD4^-$. CTL subsets of the gated cells were identified by CD45RA and CD27 expression. Naïve: $CD27^+$ $CD45RA^+$; effector: $CD45RA^+$ $CD27^-$; effector memory: $CD45RA^-$ CD27-; central memory: $CD45RA^-$ $CD27^+$ (gating example see Figures S4A and S4B). Sorted cells were placed in an incubator overnight in RPMI 1640 with 10% FBS and 1% Pen/Strep at 1×10^6 mL^{-1}. Sorting was performed on a BD Aria III cell sorter.

Flow cytometry analysis of CTL after overnight culture

CTL were isolated and cultured as described above (PBMC and CTL isolation for *in vitro* experiments). After overnight recovery CTL were harvested by centrifugation at 125 g for 10 min and resuspended at 10×10^6 cells mL^{-1} in PBS (+0.5% FCS) and kept on ice. Antibody solutions were prepared in brilliant stain buffer (BD Bioscience, 563794) at the dilutions indicated under materials with thorough mixing. The antibody solutions were added to 96-well V-bottom plates (50 µL per well) and 50 µL of CTL suspension (10×10^6 mL^{-1}) was added and mixed by pipetting up and down several times. Staining was performed for 30 min followed by two washing steps with 200 µL of PBS (+0.5% FCS) and centrifugation at 200 g for 10 min. Afterwards the cells were resuspended in 250 µL of PBS (+0.5% FCS) and added to polystyrene FACS tubes for loading onto the flow cytometer. For compensation single stained controls for each fluorophore were prepared and treated exactly like full stained samples. Compensation was calculated using the BD FACS DIVA integrated automatic compensation algorithm. Cytometers were calibrated daily, and performance is checked by the central facility staff. CTL were stained using Live/DEAD NIR, CD8-APC, CD45RA-BV785/FITC, $CD27^-$BV650/PE-CF594, combined with either CX3CR1-PEDazzle594 or CD18-AF488. T cells were selected using forward and side scatter and cells were gated as alive and $CD8^+$. Subsets were identified as described above: Naïve: $CD27^+$ $CD45RA^+$; effector: $CD45RA^+$ $CD27^-$; effector memory: $CD45RA^-$ $CD27^-$; central memory: $CD45RA^-$ $CD27^+$. The identified subsets were analyzed for expression of CXCR3, CX3CR1 and CD18. Analysis was performed using FlowJo (v10.8).

Image analysis

Recorded image series were analyzed using Fiji is just ImageJ using the latest available updates (Schindelin, J.; Arganda-Carreras, I. & Frise, E. et al. (2012), "Fiji: an open-source platform for biological-image analysis", Nature methods 9(7): 676–682, PMID 22743772, https://doi.org/10.1038/nmeth.2019). For transmigration efficiency all adherent CTL were counted, as well as all transmigration events. TEM efficiency is given as percentage of adherent cells that transmigrate. For the route of transmigration CTL adhering from flow were determined visually from image series as either transcellular or paracellular. Only local

transmigration events (diapedesis occurs at the HUVEC where adherent T cell initially adhere to from flow) were used for assessment and data are presented as percentage of each route of all TEM events. For distant TEM all transmigrating CTL in a series were counted and marked and the number of transmigrated CTL that performed diapedesis at a location that required to cross at least two different endothelial junctions were categorized as distantly transmigrating. For this individual transmigrated CTL are traced back manually to their point of adhesion and crossed junctions are counted. If a cell passes more than two junctions before transmigrating it is counted as distant transmigration event. Distantly transmigrating CTL are given as percentage of all transmigrated CTL within an image series. For each experimental flow assay condition between 10 and 15 image series were recorded in parallel from the same flow channel. All series recorded were analyzed if possible (route of transmigration was not analyzed when no transmigration occurred e.g., pertussis toxin).

Chemical fixation of cells for immunofluorescence labelling

Cells were washed once using warm (37°C) PBS (including 1 mM $CaCl_2$ and 0.5 mM $MgCl_2$), to be fixed using 4% PFA solution at RT for 10 min. This was followed by two washing step using PBS (no additives) and cells were either stained immediately or stored for short periods in PBS at 4°C.

Immunofluorescence staining of cells for microscopy

All steps are performed at RT. If required permeabilization was performed for 10 min using 0.5% Triton X100 in PBS prior to blocking. Fixed cells were blocked using PBS containing 1% bovine serum albumin and 5% fetal bovine serum for 20 min on a rocking platform. Without washing steps continue by applying the primary antibody (in PBS-T: PBS containing 0.05% Tween20) solution for 1 h on a rocking platform. Afterwards wash samples with PBS-T three times for 5 min. The secondary antibody solution (also containing HOECHST 33342) was applied in PBS-T for 30–60 min on a rocking platform protected from light. Afterwards samples were washed 3 x with PBS-T, 2 x with PBS and 1 x with ddH_2O. Excess water was carefully removed using a tissue. The samples were than mounted using Prolong Diamond and cured overnight in the dark at RT before imaging.

Chemokine analysis

HUVEC were grown on fibronectin coated dishes (µ-slide 8 well, plastic bottom) and stimulated using TNFα (10 ng mL^{-1}) or left unstimulated. After the stimulation time α-ICAM-1 coated beads (about 5 beads per cell) were added (30 min) after which the supernatant (300 µL) was collected and centrifuged at 14,000 g for 10 min to remove cell debris and or beads. The whole 300 µL were used for the assay. The chemokine profile was analyzed using the Proteome profiler human chemokine kit and was used according to the manufacturer's instructions. Membranes were developed using X-ray film (SuperRX-N, Fujifilm, Cat # 47410-19289) with an exposure time of around 10–20 s.

Fluorescence microscopy

Fluorescent images were acquired using either a Zeiss LSM980 with Airyscan2 module, a Leica SP8 confocal microscope or an Axiovert 200 fluorescence widefield microscope. Live imaging was performed on an Axiovert 200 fluorescence widefield microscope.

Quantification and statistical analysis

Data analysis and plotting was done using Graphpad Prism 9.1.0 (221), Graphpad Software LLC. Shown significance indicators are derived from t-Tests or ANOVA analyses comparing to controls. ns = not significant or p >= 0.05. * = p <= 0.05. ** = p <= 0.01. *** = p <= 0.001. **** = p <= 0.0001.

Acknowledgments

This work was supported by LSBR grant #1649 and #1820 (A.C.I.v.S. and L.K.), and ZonMW NWO Vici grant #91819632 (R.S. and J.D.v.B.).

Author contributions

R.S.: conceptualization, methodology, investigation, data analysis, visualization, writing original draft and revisions; A.C.I.v.S.: investigation, data analysis, visualization; L.K.: investigation, data analysis, visualization; A.L.T.: investigation, data analysis, visualization; M.A.N.: supervision, writing - review & editing; P.H.: investigation, writing - review & editing; J.D.v.B.: conceptualization, methodology, supervision, funding acquisition, project administration, writing original draft and revisions.

Declaration of interests

The authors declare no competing interests.

REFERENCES

Abadier, M., Haghayegh Jahromi, N., Cardoso Alves, L., Boscacci, R., Vestweber, D., Barnum, S., Deutsch, U., Engelhardt, B., and Lyck, R. (2015). Cell surface levels of endothelial ICAM-1 influence the transcellular or paracellular T-cell diapedesis across the blood-brain barrier. Eur. J. Immunol. 45, 1043– 1058.

Aird, W.C. (2007a). Phenotypic heterogeneity of the endothelium: I. Structure, function, and mechanisms. Circ. Res. 100, 158–173.

Aird, W.C. (2007b). Phenotypic heterogeneity of the endothelium: II. Representative vascular beds. Circ. Res. 100, 174–190.

Anderson, A.O., and Anderson, N.D. (1976). Lymphocyte emigration from high endothelial venules in rat lymph nodes. Immunology 31, 731–748.

Barreiro, O., Yanez-Mo, M., Serrador, J.M., Montoya, M.C., Vicente-Manzanares, M., Tejedor, R., Furthmayr, H., and Sanchez-Madrid, F. (2002). Dynamic interaction of VCAM-1 and ICAM-1 with moesin and ezrin in a novel endothelial docking structure for adherent leukocytes. J. Cell Biol. 157, 1233–1245.

Barreiro, O., Zamai, M., Ya´ n˜ ez-Mo´, M., Tejera, E., Lo´ pez-Romero, P., Monk, P.N., Gratton, E., Caiolfa, V.R., and Sa´ nchez-Madrid, F. (2008). Endothelial adhesion receptors are recruited to adherent leukocytes by inclusion in pre- formed tetraspanin nanoplatforms. J. Cell Biol. 183, 527–542.

Bertoni, A., Alabiso, O., Galetto, A.S., and Baldanzi, G. (2018). Integrins in T cell physiology. Int. J. Mol. Sci. 19, 485.

van Buul, J.D., Allingham, M.J., Samson, T., Meller, J., Boulter, E., Garcı´a- Mata, R., and Burridge, K. (2007). RhoG regulates endothelial apical cup as- sembly downstream from ICAM1 engagement and is involved in leukocyte trans-endothelial migration. J. Cell Biol. 178, 1279–1293.

Carman, C.V., and Martinelli, R. (2015). T lymphocyte–endothelial interactions: emerging understanding of trafficking and antigen-specific immunity. Front. Immunol. 6, 603.

Carman, C.V., and Springer, T.A. (2004). A transmigratory cup in leukocyte dia- pedesis both through individual vascular endothelial cells and between them. J. Cell Biol. 167, 377–388.

Carman, C.V., Sage, P.T., Sciuto, T.E., de la Fuente, M.A., Geha, R.S., Ochs, H.D., Dvorak, H.F., Dvorak, A.M., and Springer, T.A. (2007). Transcellular dia- pedesis is initiated by invasive podosomes. Immunity 26, 784–797.

Conroy, M.J., Maher, S.G., Melo, A.M., Doyle, S.L., Foley, E., Reynolds, J.V., Long, A., and Lysaght, J. (2018). Identifying a novel role for fractalkine (CX3CL1) in memory CD8+ T cell accumulation in the omentum of obesity- associated cancer patients. Front. Immunol. 9, 1867.

Contento, R.L., Molon, B., Boularan, C., Pozzan, T., Manes, S., Marullo, S., and Viola, A. (2008). CXCR4-CCR5: a couple modulating T cell functions. Proc. Natl. Acad. Sci. U S A 105, 10101–10106.

Feng, D., Nagy, J.A., Pyne, K., Dvorak, H.F., and Dvorak, A.M. (1998). Neutro- phils emigrate from venules by a transendothelial cell pathway in response to FMLP. J. Exp. Med. 187, 903–915.

Fong, A.M., Robinson, L.A., Steeber, D.A., Tedder, T.F., Yoshie, O., Imai, T., and Patel, D.D. (1998). Fractalkine and CX3CR1 mediate a novel mechanism of leukocyte capture, firm adhesion, and activation under physiologic flow. J. Exp. Med. 188, 1413–1419.

Gerlach, C., Moseman, E.A., Loughhead, S.M., Alvarez, D., Zwijnenburg, A.J., Waanders, L., Garg, R., de la Torre,

J.C., and von Andrian, U.H. (2016a). The chemokine receptor CX3CR1 defines three antigen-experienced CD8 T cell subsets with distinct roles in immune surveillance and homeostasis. Immunity 45, 1270–1284.

Gerlach, C., Moseman, E.A., Loughhead, S.M., Alvarez, D., Zwijnenburg, A.J., Waanders, L., Garg, R., de la Torre, J.C., and von Andrian, U.H. (2016b). The chemokine receptor CX3CR1 defines three antigen-experienced CD8 T cell subsets with distinct roles in immune surveillance and homeostasis. Immunity 45, 1270–1284.

Girbl, T., Lenn, T., Perez, L., Rolas, L., Barkaway, A., Thiriot, A., Del Fresno, C., Lynam, E., Hub, E., Thelen, M., et al. (2018). Distinct compartmentalization of the chemokines CXCL1 and CXCL2 and the atypical receptor ACKR1 deter- mine discrete stages of neutrophil diapedesis. Immunity 49, 1062–1076.e6.

Gorina, R., Lyck, R., Vestweber, D., and Engelhardt, B. (2014). b2 integrin- mediated crawling on endothelial ICAM-1 and ICAM-2 is a prerequisite for transcellular neutrophil diapedesis across the inflamed blood-brain barrier. J. Immunol. 192, 324–337.

Groom, J.R., and Luster, A.D. (2011). CXCR3 in T cell function. Exp. Cell Res.317, 620–631.

Heemskerk, N., Schimmel, L., Oort, C., van Rijssel, J., Yin, T., Ma, B., van Unen, J., Pitter, B., Huveneers, S., Goedhart, J., et al. (2016). F-actin-rich con- tractile endothelial pores prevent vascular leakage during leukocyte diape- desis through local RhoA signalling. Nat. Commun. 7, 10493.

Helms, J.B., and Rothman, J.E. (1992). Inhibition by brefeldin a of a golgi mem- brane enzyme that catalyses exchange of guanine nucleotide bound to ARF. Nature 360, 352–354.

Hughes, C.E., and Nibbs, R.J.B. (2018). A guide to chemokines and their re- ceptors. FEBS J. 285, 2944–2971.

Janossy, G., Bofill, M., Rowe, D., Muir, J., and Beverley, P.C. (1989). The tissue distribution of T lymphocytes expressing different CD45 polypeptides. Immu- nology 66, 517–525.

Kanters, E., van Rijssel, J., Hensbergen, P.J., Hondius, D., Mul, F.P.J., Deelder, A.M., Sonnenberg, A., van Buul, J.D., and Hordijk, P.L. (2008). Filamin B mediates ICAM-1-driven leukocyte transendothelial migration. J. Biol. Chem. 283, 31830–31839.

Kroon, J., Schaefer, A., van Rijssel, J., Hoogenboezem, M., van Alphen, F., Hordijk, P., Stroes, E.S.G., Stro¨ mblad, S., van Rheenen, J., and van Buul,

J.D. (2018). Inflammation-sensitive myosin-X functionally supports leukocyte extravasation by cdc42-mediated ICAM-1-rich endothelial filopodia formation. J. Immunol. 200, 1790–1801.

Kvietys, P.R., and Sandig, M. (2001). Neutrophil diapedesis: paracellular or transcellular? Physiology 16, 15–19.

Lewis, M., Tarlton, J.F., and Cose, S. (2008). Memory versus naive T-cell migration. Immunol. Cell Biol. 86, 226–231.

Mace, E.M., and Orange, J.S. (2014). Lytic immune synapse function requires filamentous actin deconstruction by coronin 1A. Proc. Natl. Acad. Sci. U S A 111, 6708–6713.

Mamdouh, Z., Mikhailov, A., and Muller, W.A. (2009). Transcellular migration of leukocytes is mediated by the endothelial lateral border recycling compart- ment. J. Exp. Med. 206, 2795–2808.

Marchesi, V.T. (1961). The site of leucocyte emigration during inflammation. Q. J. Exp. Physiol. Cogn. Med. Sci. 46, 115–118.

Martinelli, R., Zeiger, A.S., Whitfield, M., Sciuto, T.E., Dvorak, A., Van Vliet, K.J., Greenwood, J., and Carman, C.V. (2014). Probing the biomechanical contribution of the endothelium to lymphocyte migration: diapedesis by the path of least resistance. J. Cell. Sci. 127, 3720–3734.

Maurice, N.J., McElrath, M.J., Andersen-Nissen, E., Frahm, N., and Prlic, M. (2019). CXCR3 enables recruitment

and site-specific bystander activation of memory CD8 + T cells. Nat. Commun. 10, 4987.

Mayya, V., Judokusumo, E., Abu Shah, E., Peel, C.G., Neiswanger, W., Depoil, D., Blair, D.A., Wiggins, C.H., Kam, L.C., and Dustin, M.L. (2018). Durable in- teractions of T cells with T cell receptor stimuli in the absence of a stable immu- nological synapse. Cell Rep. 22, 340–349.

Middleton, J., Neil, S., Wintle, J., Clark-Lewis, I., Moore, H., Lam, C., Auer, M., Hub, E., and Rot, A. (1997). Transcytosis and surface presentation of IL-8 by venular endothelial cells. Cell. 91, 385–395.

Middleton, J., Patterson, A.M., Gardner, L., Schmutz, C., and Ashton, B.A. (2002a). Leukocyte extravasation: chemokine transport and presentation by the endothelium. Blood 100, 3853–3860.

Middleton, J., Patterson, A.M., Gardner, L., Schmutz, C., and Ashton, B.A. (2002b). Leukocyte extravasation: chemokine transport and presentation by the endothelium. Blood 100, 3853–3860.

Milla´ n, J., Hewlett, L., Glyn, M., Toomre, D., Clark, P., and Ridley, A.J. (2006). Lymphocyte transcellular migration occurs through recruitment of endothelial ICAM-1 to caveola- and F-actin-rich domains. Nat. Cell Biol. 8, 113–123.

Nolz, J.C., Starbeck-Miller, G.R., and Harty, J.T. (2011). Naive, effector and memory CD8 T-cell trafficking: parallels and distinctions. Immunotherapy. 3, 1223–1233.

Olson, T.S., and Ley, K. (2002). Chemokines and chemokine receptors in leukocyte trafficking. Am. J. Physiol. Regul. Integr. Comp. Physiol. 283, R7–R28.

Rabouille, C. (2017). Pathways of unconventional protein secretion. Trends Cell Biol. 27, 230–240.

Rademakers, T., Goedhart, M., Hoogenboezem, M., Garcı´a Ponce, A., van Rijssel, J., Samus, M., Schnoor, M., Butz, S., Huveneers, S., Vestweber, D., et al. (2020). Hematopoietic stem and progenitor cells use podosomes to transcellularly cross the bone marrow endothelium. Haematologica 105. https://doi.org/10.3324/haematol.2018.196329.

Rijssel, J.V., Timmerman, I., Alphen, F.P.J.V., Hoogenboezem, M., Korchyn- skyi, O., Geerts, D., Geissler, J., Reedquist, K.A., Niessen, H.W.M., and Buul, J.D.V. (2013). The Rho-GEF Trio regulates a novel pro-inflammatory pathway through the transcription factor Ets2. Biol. Open 2, 569–579.

van Rijssel, J., Kroon, J., Hoogenboezem, M., van Alphen, F.P.J., de Jong, R.J., Kostadinova, E., Geerts, D., Hordijk, P.L., and van Buul, J.D. (2012). The Rho-guanine nucleotide exchange factor Trio controls leukocyte transen- dothelial migration by promoting docking structure formation. Mol. Biol. Cell 23, 2831–2844.

Rudolph, H., Klopstein, A., Gruber, I., Blatti, C., Lyck, R., and Engelhardt, B. (2016). Postarrest stalling rather than crawling favors CD8(+) over CD4(+) T- cell migration across the blood-brain barrier under flow in vitro. Eur. J. Immu- nol. 46, 2187–2203.

Sage, P.T., Varghese, L.M., Martinelli, R., Sciuto, T.E., Kamei, M., Dvorak, A.M., Springer, T.A., Sharpe, A.H., and Carman, C.V. (2012). Antigen recogni- tion is facilitated by invadosome-like protrusions formed by memory/effector T cells. J. Immunol. 188, 3686–3699.

Sallusto, F., Lenig, D., Fo¨ rster, R., Lipp, M., and Lanzavecchia, A. (1999). Two subsets of memory T lymphocytes with distinct homing potentials and effector functions. Nature. 401, 708–712.

Sanchez, E., Liu, X., and Huse, M. (2019). Actin clearance promotes polarized dynein accumulation at the immunological synapse. PLoS One 14, e0210377.

Schaerli, P., and Moser, B. (2005). Chemokines: control of primary and mem- ory T-cell traffic. Immunol. Res.

31, 57–74.

Schimmel, L., van der Stoel, M., Rianna, C., van Stalborch, A.-M., de Ligt, A., Hoogenboezem, M., Tol, S., van Rijssel, J., Szulcek, R., Bogaard, H.J., et al. (2018). Stiffness-induced endothelial DLC-1 expression forces leukocyte spreading through stabilization of the ICAM-1 adhesome. Cell Rep. 24, 3115–3124.

Schindelin, J., Arganda-Carreras, I., Frise, E., Kaynig, V., Longair, M., Pietzsch, T., Preibisch, S., Rueden, C., Saalfeld, S., Schmid, B., et al. (2012). Fiji: an open-source platform for biological-image analysis. Nat. Methods. 28, 676–682.

Shulman, Z., Cohen, S.J., Roediger, B., Kalchenko, V., Jain, R., Grabovsky, V., Klein, E., Shinder, V., Stoler-Barak, L., Feigelson, S.W., et al. (2011). Transen- dothelial migration of lymphocytes mediated by intraendothelial vesicle stores rather than by extracellular chemokine depots. Nat. Immunol. 13, 67–76.

Speyer, C.L., and Ward, P.A. (2011). Role of endothelial chemokines and their receptors during inflammation. J. Invest. Surg. 24, 18–27.

Springer, T.A., and Dustin, M.L. (2012). Integrin inside-out signaling and the immunological synapse. Curr. Opin. Cell Biol. 24, 107–115.

Tinoco, R., Otero, D.C., Takahashi, A., and Bradley, L.M. (2017). PSGL-1: a new player in the immune checkpoint landscape. Trends Immunol. 38, 323–335.

Vestweber, D. (2015). How leukocytes cross the vascular endothelium. Nat. Rev. Immunol. 15, 692–704.

Whittall, C., Kehoe, O., King, S., Rot, A., Patterson, A., and Middleton, J. (2013). A chemokine self-presentation mechanism involving formation of endothelial surface microstructures. J. Immunol. 190, 1725–1736.

Yang, L., Froio, R.M., Sciuto, T.E., Dvorak, A.M., Alon, R., and Luscinskas,F.W. (2005). ICAM-1 regulates neutrophil adhesion and transcellular migration of TNF-alpha-activated vascular endothelium under flow. Blood. 106, 584–592.

Zhu, Q., Yamakuchi, M., and Lowenstein, C.J. (2015). SNAP23 regulates endo- thelial exocytosis of von Willebrand factor. PLoS One 10, e0118737.

SUPPLEMENTAL FILES

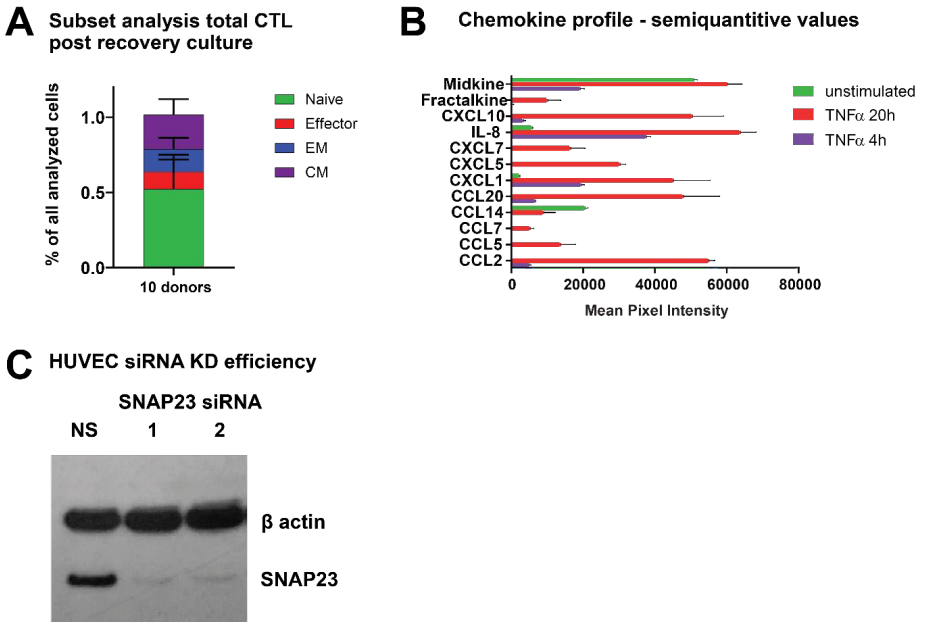

Supplemental Figure 1. Total CTL subset composition analysis by flow cytometry (A recovered CTL prepared as for all experiments were analyzed), semi-quantitative chemokine array data (B, see table 1) and SNAP23 siRNA knock down efficiency in HUVEC (C, related to figure 6). (A) Subset composition of CTL population used in experiments after overnight recovery in RPMI. CTL were isolated from PBMC derived from whole blood and magnetically separated. For recovery CTL were placed in an incubator overnight in RPMI +10% FCS +1% Pens/Strep. About half the population on average is made up of naive CTL. Eff and EM make about a quarter of the total population and half of the transmigration capable population. The same antibody panel that was used for sorting was used to identify classical CTL subsets in CTL populations after overnight recovery in an incubator. CTL from recovery were antibody labelled to identify CTL subsets via LIVE/DEAD, CD8, CD45RA, CD27, CD16 and CD56. (B) Supernatant of HUVEC monolayers stimulated for the indicated amount of time using 10 ng mL-1 TNFα was analyzed for chemokine presence using an antibody array as described in table 1. (C) Western blot of representative knock down of SNAP23 using siRNA transfected via electroporation into HUVEC. Protein samples were harvested at the time of starting the flow assays as described in methods. KD was confirmed by Western blot for all experiments analyzed and presented here.

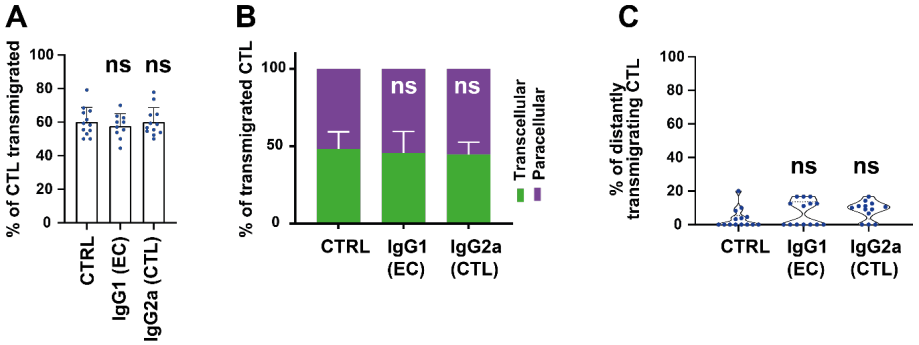

Supplemental Figure 2. Blocking antibody isotype controls do not affect CTL transmigration parameters (related to figure 3 and 4 antibody blocking experiments)
HUVEC were grown in µ-channels and activated 20 h (10 ng mL^{-1}) using TNFα. CTL were flown over the activated HUVEC at physiological flow. Prior to the flow experiments HUVEC (mouse IgG1) or CTL (mouse IgG2a) were incubated with the corresponding antibodies for 30 min at 10 µg mL^{-1} in EGM-2 (EC) or RPMI (CTL). Neither of the isotype control antibodies affected CTL transmigration parameters. (**A**) Transmigration efficiency was unaffected, as well as the frequency of the routes of transmigration (**B**) and the frequency of distant diapedesis events (**C**).

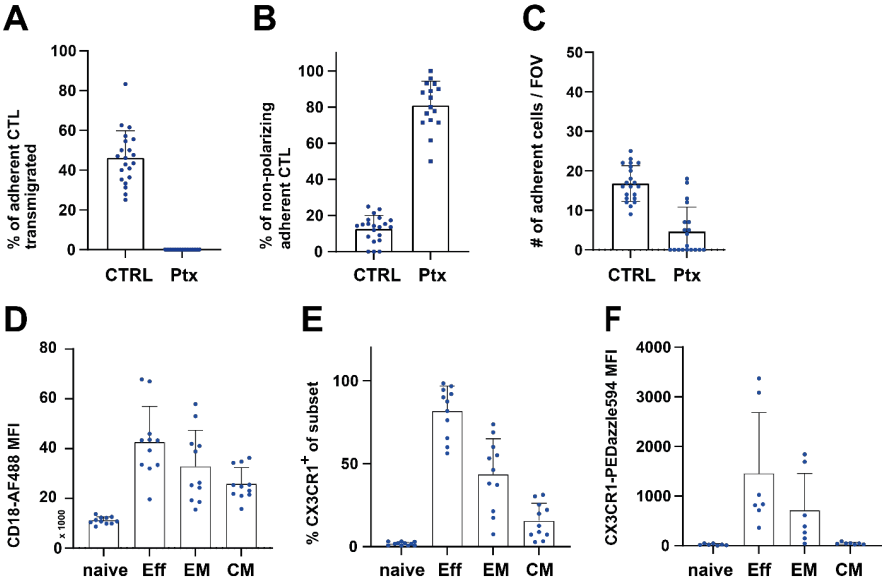

Supplemental Figure 3 - CTL transmigration and chemotactic activation (related to Figure 3+6 and table 1, CTL receive chemotactic activation upon endothelial contact which is required for polarization, apical migration and transmigration) (**A+B**) CTL were isolated from fresh blood and recovered overnight. HUVEC were grown in µ- slides for 48h followed by 20 h TNFα stimulation. 2h before injection into the flow system CTL were treated with 1 µg mL^{-1} pertussis toxin. Transmigration parameters were analyzed from live image series. After pertussis treatment CTL showed no transmigration (**A**) and hardly any polarization or migration (**B**) after contacting the HUVEC monolayer. (**C+D+E**) CTL were isolated from fresh blood and recovered overnight, harvested and surface stained for flow cytometry analysis. CD8+ and alive cells were gated into subset by CD45RA and CD27 expression (naïve: CD45RA$^+$ CD27$^+$, CM: CD45RA$^-$ CD27$^+$, EM: CD45RA$^-$ CD27$^-$, effector: CD45RA$^+$ CD27$^-$). For CD18 all cells in all subsets were positive. (C) shows the median fluorescence intensity of the CD18-AF488 signal for each subset. The percentage of CX3CR1 positive cells within each subset is shown in (**D**) and the MFI of CX3CR1-PEDazzle594 for each subset is shown in (**E**).

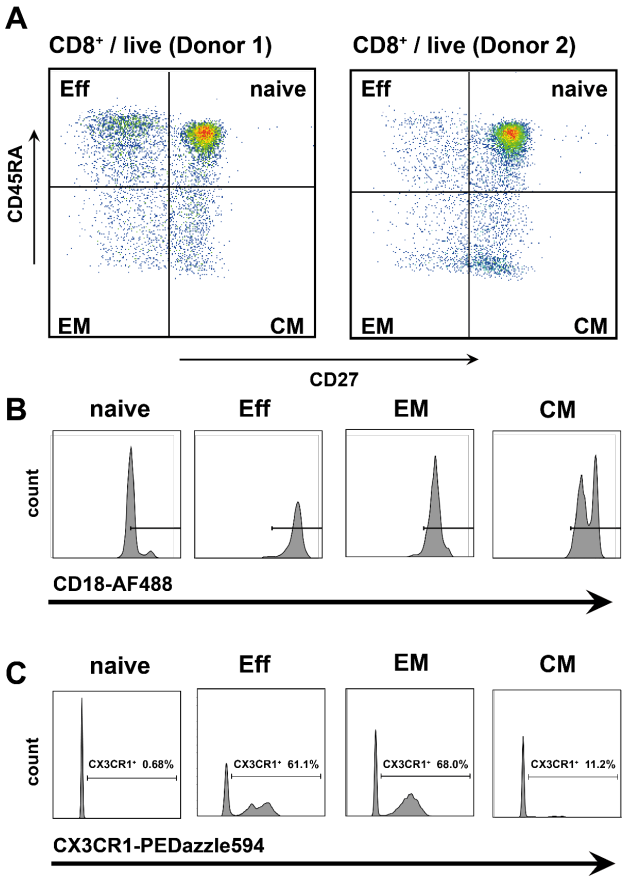

Supplemental Figure 4. CD18 and CX3CR1 expression of recovered total CTL (related to figure 3 and 4, CTL subsets expressing fractalkine receptor and high β2 integrin levels (effector and EM CTL) show higher levels of transcellular diapedesis)

(**A**) CTL were isolated from fresh blood and recovered overnight, harvested and surface stained for flow cytometry analysis. $CD8^+$ and alive cells were gated into subset by CD45RA and CD27 expression (naïve: $CD45RA^+$ $CD27^+$, CM: $CD45RA^-$ $CD27^+$, EM: $CD45RA^-$ $CD27^-$, effector: $CD45RA^+$ $CD27^-$). Two exemplary donors are shown. (**B**) shows an example of the expression of CD18 on the gated subsets from one exemplary donor. (**C**) shows the expression of CX3CR1 for the subsets of the same donor as in (**B**).

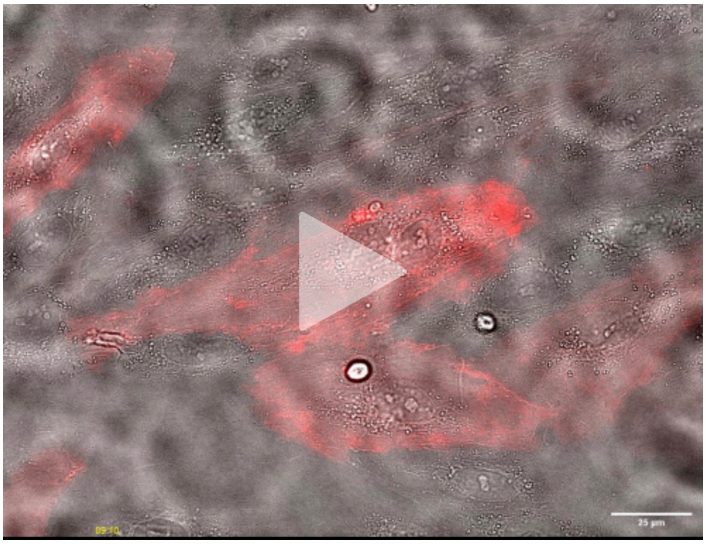

Video 1. Transcellular migration of a human CTL on CAAX_mScarlet expressing TNFα activated HUVEC (CAAX_mScarlet and phase contrast overlay). Related to figure 2.

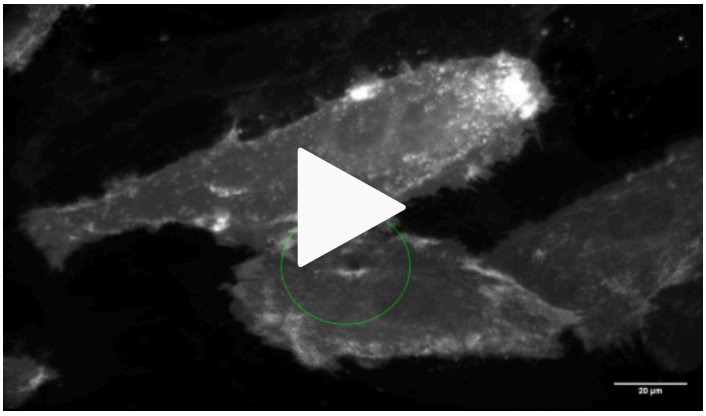

Video 2. Transcellular migration of a human CTL on CAAX_mScarlet expressing TNFα activated HUVEC (CAAX_mScarlet only). Related to figure 2.

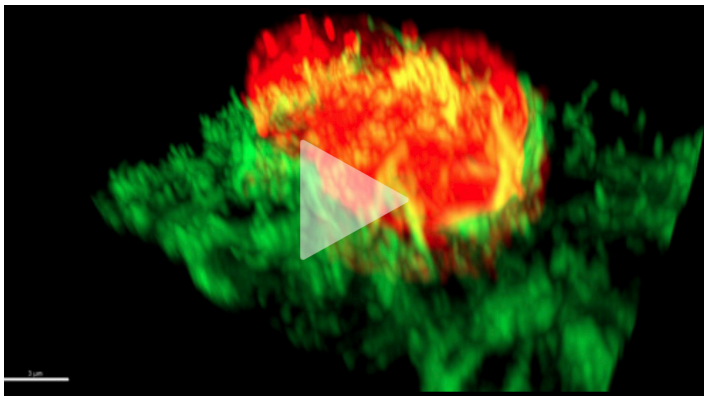

Video 3. The diapedesis synapse of adhered CTL visualized with ICAM-1_GFP and red membrane labeling of CTL membranes. Related to figure 2

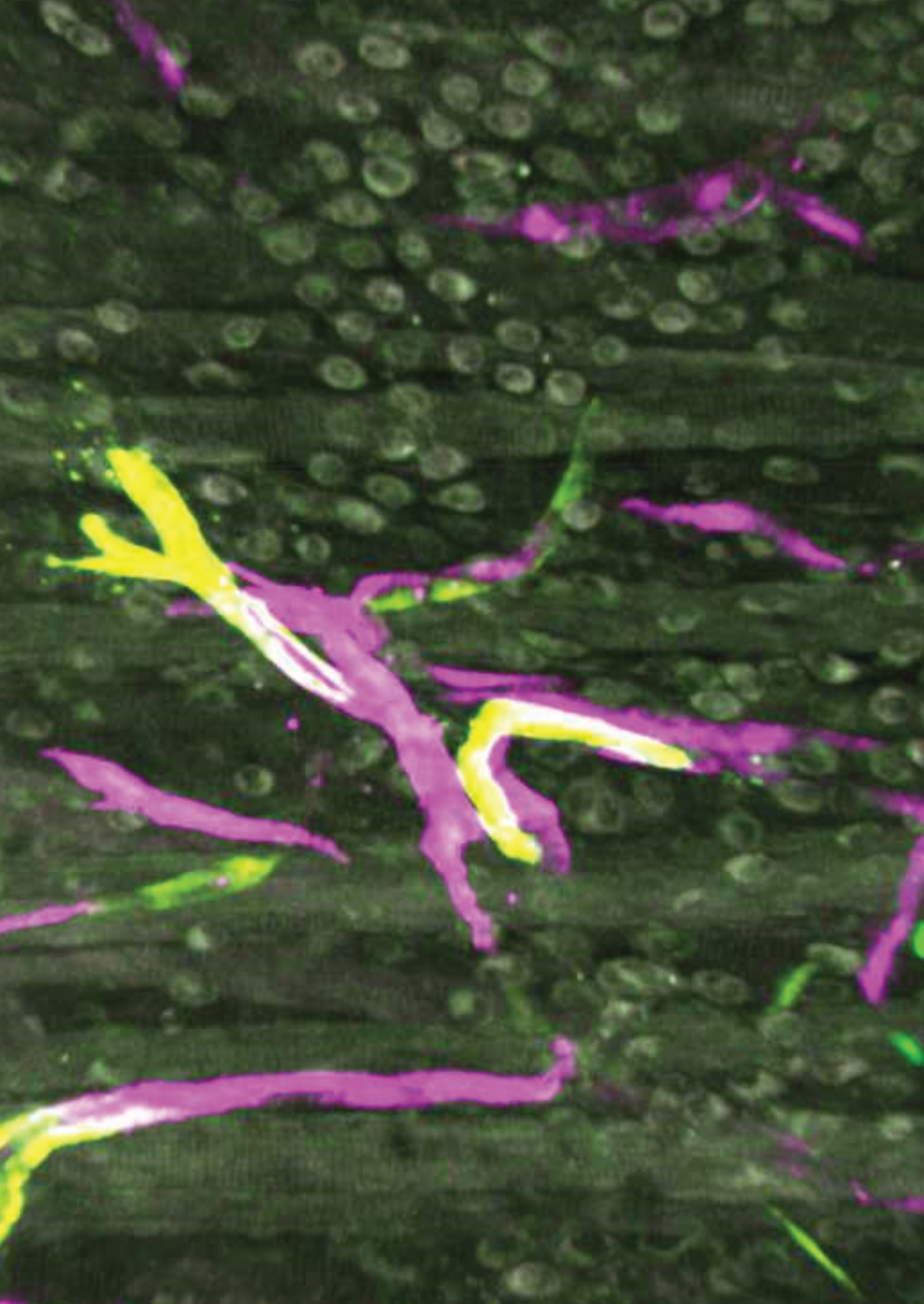

CHAPTER 5

Overlapping membrane at endothelial junctions form tunnels during neutrophil transmigration

Abraham C.I. van Steen[1]
Werner J. van der Meer[1,2]
Lanette Kempers[1]
Eike Mahlandt[2]
Janine J.G. Arts[1]
Rianne M. Schoon[1]
Amber Driessen[1]
Jos van Rijssel[1]
Janine Arts[1,2]
Mark Hoogenboezem[4]
Yosif Manavski[3]
Reinier A. Boon[3]
Max Grönloh[1,2]
Joachim Goedhart[2]
Martijn A. Nolte[4]
Jaap D. van Buul[1,,2,*]

[1]Molecular Cell Biology Lab at Dept. Molecular Hematology, Sanquin Research, and Landsteiner Laboratory, Amsterdam, the Netherlands;

[2]Leeuwenhoek Centre for Advanced Microscopy (LCAM), section Molecular Cytology at Swammerdam Institute for Life Sciences (SILS) at the University of Amsterdam, Amsterdam, the Netherlands.

[3]the Institute for Cardiovascular Regeneration, Center of Molecular Medicine, Goethe University, Frankfurt, Germany; [4]Core facility at Dept. Molecular Hematology, Sanquin Research and Landsteiner Laboratory, Amsterdam, the Netherlands.

ABSTRACT

Upon inflammation, leukocytes extravasate from the bloodstream through the endothelial cells that line the vessel wall into the underlying inflamed tissue. Leukocytes can cross the endothelium in a paracellular or transcellular manner. When using the paracellular route, junctional proteins must move out of the way to allow leukocytes to cross. It is believed that endothelial cells transiently must let go of each other and rapidly reseal after passage. When carefully examining endothelial cell junctions, endothelial cells form overlapping membrane regions spanning a greater surface than VE-cadherin on the junction and are rich in PECAM-1.

Interestingly, these endothelial membrane overlaps are preferred by leukocytes to cross the endothelium. Detailed 3D Analysis of leukocyte transmigration in real-time using lattice light-sheet microscopy revealed that the overlapping endothelial cells provide a tunnel for transmigrating leukocytes. Once penetrating the endothelium, leukocytes use the underlying endothelial overlap as a slide to migrate under the adjacent endothelial cell. Using an endothelial-specific Confetti knock-in animal model, we show that overlapping membranes are found in different vascular beds. Overlaps are regulated by flow and actin polymerization but, although marked by PECAM-1, do not require PECAM-1 to form. Our work shows that endothelial cells do not dissociate from each other upon passage of leukocytes but rather form membrane tunnels to allow leukocytes to penetrate through the endothelial monolayer. This discovery opens new insights into the multistep paradigm of leukocyte transendothelial migration.

Keywords

Transendothelial Migration, Actin, Membrane, Inflammation

INTRODUCTION

Our immune system protects our body from infection with bacteria, viruses, and parasites, by rapidly detecting, containing, and eliminating the invading pathogens. To fully reach the site of infection, immune cells need to leave the circulation and penetrate the vessel wall by a process known as leukocyte transendothelial migration. This process is believed to occur in multiple steps: leukocytes in the bloodstream are tethered by endothelial selectins from the inflamed vessel wall, lined with endothelial cells. Next, leukocytes start adhering to the endothelium, which induces rolling, followed by firm adhesion and a subsequent crawling phase. Finally, they can cross the endothelial monolayer in two ways, either through the endothelial cell-to-cell junctions, called the paracellular route, or through the endothelial cell body, called the transcellular route (Wittchen, 2009). It was Eugene Butcher who was the first to propose three or more steps of the leukocyte extravasation model to specificity and diversity (Butcher, 1991). This work was further fine-tuned by Timothy Springer, who introduced "traffic signals" and the multistep paradigm for the TEM model (Springer, 1994). Since then, many more studies have added mechanistic and molecular details to this model, but the basics of this model are still standing. One of these dogmas is the final step: the actual paracellular penetration of the leukocytes through the endothelial monolayer. This pathway is preferred by leukocytes that characterize the innate immune system: neutrophils and monocytes. About 90% of these leukocytes cross the inflamed endothelium through the junctions (Vestweber, 2012, 2015; Woodfin et al., 2011). However, there are exceptions, as in some tissues, the transcellular pathway can also enable leukocytes from the innate immune system to cross when the paracellular pathway is blocked (Schulte et al., 2011).

Leukocyte paracellular migration can be promoted by blocking one of the major constituents of the adherens junctions: VE-cadherin. Using antibodies that interfere with the homotypic interactions of VE-cadherin molecules showed not only an increase in permeability but also an increase in leukocyte extravasation *in vitro* as well as *in vivo* (Buul et al., 2002; Corada et al., 1999, 2002; Gotsch et al., 1997). Vice versa, when locking the endothelial cell-cell junctions, by introducing a VE-cadherin-alpha-catenin chimera construct that stabilizes the cell-cell contacts, leukocyte extravasation is inhibited, albeit not in all vascular beds (Rademakers et al., 2020; Schulte et al., 2011).

In general, it is believed that when leukocytes use the paracellular route, the two or three adjacent endothelial cells that form the junction transiently dissociate from each other to allow the leukocyte to cross and rapidly after crossing close the gap (Alon & van Buul, 2017; Schimmel et al., 2016; Vestweber, 2015). Several previous structural studies focusing on the architecture of the vessel wall using transmission or scanning electron microscopy revealed that the endothelial cells that line the inner layer of blood vessels do not just connect, like a sheet of epithelial cells, but in fact, partially overlap (Baluk et al., 1998; Hirata et al., 1995; Thurston et al., 1996). The membrane from one cell seems to protrude underneath the neighboring endothelial cell, as has also recently been reviewed (Claesson-Welsh et al., 2021).

When studying such architectural structures, it is hard to imagine how leukocytes manage to go through and locally disrupt endothelial cell-to-cell contacts without harming the vascular integrity. In this study, we sought to investigate the correlation between endothelial overlap and transendothelial migration and found that overlapping junctions are sites where the leukocytes prefer to extravasate. To properly study this in real-time in 3 dimensions at a high-resolution level with low phototoxicity, we used lattice light-sheet microscopy. We found that leukocytes prefer overlapping endothelial membranes to cross by squeezing themselves through, forming a so-called “transmigration tunnel”. Detailed Analysis revealed that leukocytes use the membrane of the endothelial cell underneath the adjacent one to slide under, and the adjacent membranes are not disconnected from each other during the leukocyte passage.

A deeper understanding of cellular overlap and its role in the transendothelial migration of leukocytes will ultimately contribute to developing therapeutical applications.

RESULTS

Endothelial cells overlap when forming a monolayer

When carefully analyzing endothelial cell-to-cell contacts using atomic force microscopy and transmission electron microscopy, we found that endothelial membranes partially overlap at junction regions (Figure 1A, B). These data are in line with other studies (Claesson-Welsh et al., 2021). To characterize and quantify the endothelial membrane overlap, the two adjacent endothelial cells need to be clearly distinguishable. Therefore, we mixed two populations of endothelial cells that were transduced with either the membrane anchoring protein CAAX-mNeonGreen fluorescent protein or the CAAX-mScarlet (Figure 1C). Alternatively, we used CAAX-mTurquoise2 and CAAX-YFP. Z-stacks were acquired using confocal microscopy to ensure the entire overlap was imaged. For quantification, images were processed by thresholding the maximum Z-projection of each color channel (Figure 1D), allowing us to quantify the length, width, and area of the endothelial membrane overlap (Figure 1E). We found an average overlap width of 5.4 µm in a range between 0.5-18 µm (Figure 1F)

We additionally used a vessel-on-a-chip model to mimic human physiology more closely and investigate the overlapping endothelial membranes in more physiological models (van Steen et al., 2021). We found the presence of similar endothelial membrane overlaps (Figure 2A) with a width of 5.6 µm (Figure 2B). We used endothelial-specific tamoxifen-inducible confetti mice to show that overlapping endothelial membranes are also found in vivo. The Rosa26 cassette contains multiple lox sites, which lead to the expression of 1 out of 4 possible fluorescent proteins after Cre recombination. Rosa26-confetti mice were bred with mice expressing Cre^{ERT2} (tamoxifen-inducible Cre-recombinase) under the regulation of the Cdh5 (vascular endothelial cadherin) promoter ($Confetti^{fl/wt}$ Cdh5-Cre^{ERT2}) to induce endothelium-specific, tamoxifen-inducible conditional recombinase expression resulting in

the exclusive labeling of ECs (Figure 2C) (Manavski et al., 2018). Male mice, 6 weeks of age, were injected with tamoxifen to induce Cre-recombination, and organs were collected 14 days later to ensure mosaic labeling of endothelial cells. During clonal expansion, daughter cells inherit the floxed cassette from their parent. Therefore, tamoxifen recombination was performed in 6 weeks old mice. The heterogeneous induction of the different fluorescent markers allowed us to study the endothelial membrane overlap between two adjacent endothelial cells in the vasculature. Analysis of the vessels in the lung, liver, and spleen showed that in all these organs, overlapping endothelial membranes can be found (Figure 2D). Magnification of the junctional regions of these vessels clearly showed overlapping membrane sections of YFP-expressing endothelial cells with RFP-expressing endothelial cells, indicating that membranes of adjacent endothelial cells also overlap *in vivo*.

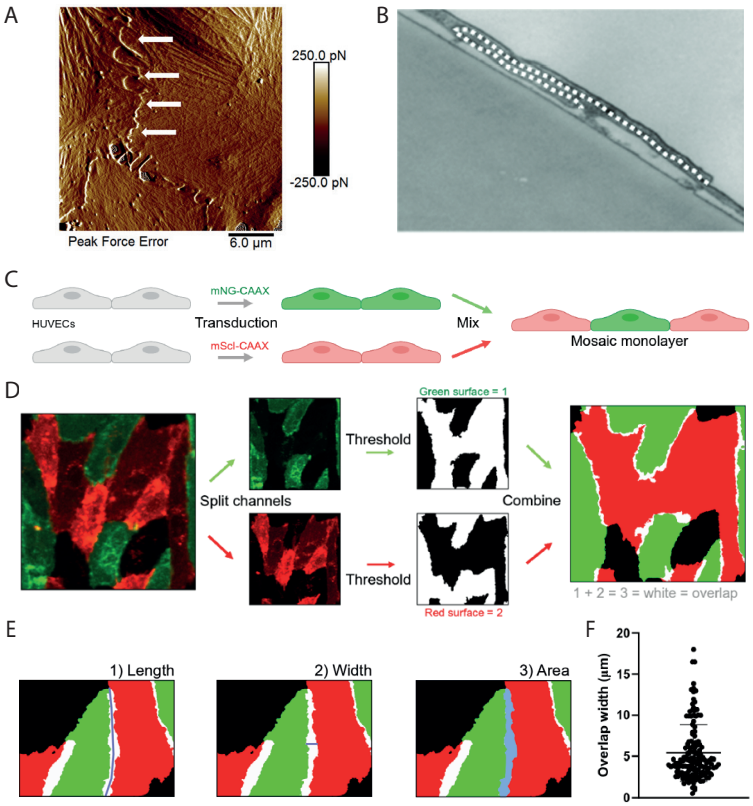

Figure 1. *Overlap analysis using mosaic CAAX expression*. **A.** Live atomic force microscopy peak force error image of HUVEC monolayer, arrows indicate overlapping membranes. **B.** Transmission electon microscopy image of overlapping membranes in HUVEC monolayer, dashed line indicates overlapping membranes. **C.** Mosaic monolayers were obtained by mixing two pools of HUVECs that were transduced with CAAX fluorescently labeled with either one of the colors combinations mNeonGreen/mScarlet or YFP/mTurquoise2. D. Maximum projections of confocal Z-stacks were split into separate channels that were set threshold and cleaned up. The resulting binary images were assigned different values, after which images were summed to reveal overlapping surfaces. **E.** Examples of overlap aspects that can be quantified in blue: 1) length, 2) width, and 3) area. **F.** Mean overlap width of CAAX expressing HUVECs is 5.4µm. n=142 junctions, 4 independent experiments.

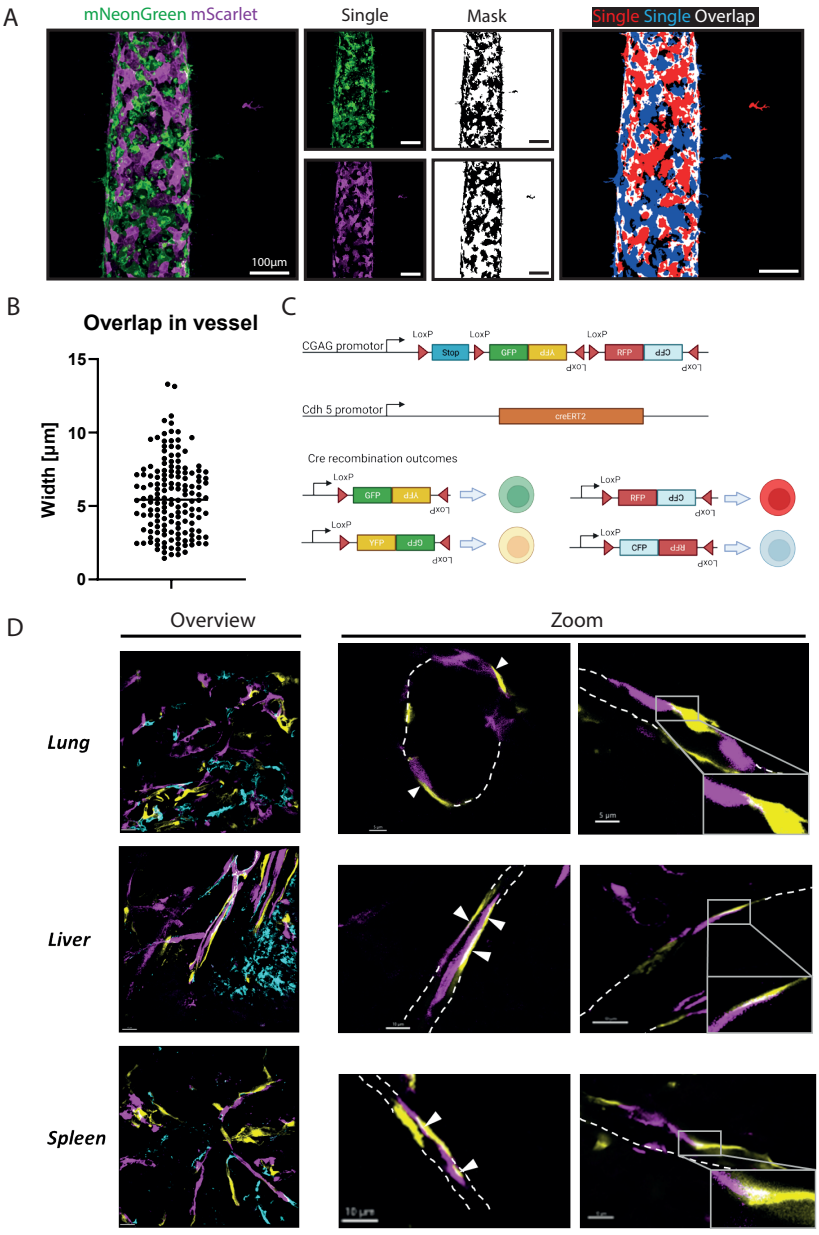

Figure 2. Overlapping membranes in bloodvessel-on-a-chip and in vivo.
A. Bloodvessel-on-a-chip generated with HUVEC in a collagen-1 hydrogel seeded with HUVEC transduced with either CAAX-mNeonGreen or CAAX-mScarlet. **B.** Mean width of overlap in bloodvessel-on-a-chip is 5.8 µm. n=153 junctions, 3 independent experiments. **C.** Schematic of the Cdh5-CreERT2 transgene and Rosa26-Confetti reporter cassette. Tamoxifen induced recombination leads to expression of one of the fluorescent proteins in endothelial cells: cyan fluorescent protein (CFP), green fluorescent protein (GFP), yellow fluorescent protein (YFP), and red fluorescent protein (RFP). **D.** Confocal images of Confetti$^{fl/wt}$ Cdh5-Cre^{ERT2} mouse lung, liver, and spleen 2 weeks after tamoxifen induction. Overview images are generated with maximum projection Z-projection. Zoom images show single confocal planes, white color indicates overlapping membranes.

To study the effect on junctions and overlap morphology, we quantitatively analyzed overlap using the thresholding method on mosaic CAAX-expression and qualitatively investigated the junctions using a fluorescently-labeled anti-VE-cadherin antibody. Studying overlap dynamics in time revealed that the mean overlap area remained relatively stable (Figure 3A). To investigate the role of the actin cytoskeleton in junction maintenance and endothelial membrane overlap formation, we used small-molecule inhibitors that target different cytoskeletal regulators. Cytochalasin B inhibits F-actin formation, CK-666 binds to ARP2/3 and inhibits nucleation, and Y27632 inhibits Rho-kinase activity. These inhibitors were administered to CAAX-expressing mosaic HUVEC monolayers and recorded in real-time using confocal microscopy. The inhibitor studies showed the importance of actin polymerization, as blocking polymerization or Arp2/3 complex activation resulted in reduced overlap ratios in time (Figure 3B-E). Interestingly, blocking Rho-kinase also resulted in a drop in the overlap region (Figure 3B,3F). These results showed that both myosin-mediated actin contractility and regulation of actin turnover are both necessary for endothelial membrane overlap. Next, we investigated the molecular make-up of the overlapping membrane regions. Therefore, we measured the percentage of overlapping cell area that was positive for F-actin and found 87% of the overlapping area positive for F-actin (Figure 3G). Next, we investigated the distribution of the junctional proteins PECAM-1, JAM-A, and VE-cadherin and found that PECAM-1 covered overlapping areas for 73%, whereas VE-cadherin covered the overlap for only 22% and JAM-A for 16% (Figure 3G, H). Since PECAM-1 is present in most of the overlapping regions, we made a knockdown of PECAM-1 using siRNA, which reduced PECAM-1 expression by 77% (Supplemental Figure 1) and measured overlap width (Figure 3I). Knockdown of PECAM-1 did not change the width of the membrane overlap.

To investigate whether the blood flow through a vessel may influence endothelial overlap, we cultured confluent CAAX-expressing mosaic HUVEC monolayers in a flow channel for 24 hours under laminar flow. Cell alignment was quantified as described in experimental procedures. Results indicated that 88% of cells align to the direction of flow, with the long junctional cell sides in parallel to the direction of the flow direction (Supplemental Figure 2A, B) in accordance with previous work (Heemskerk et al., 2016).

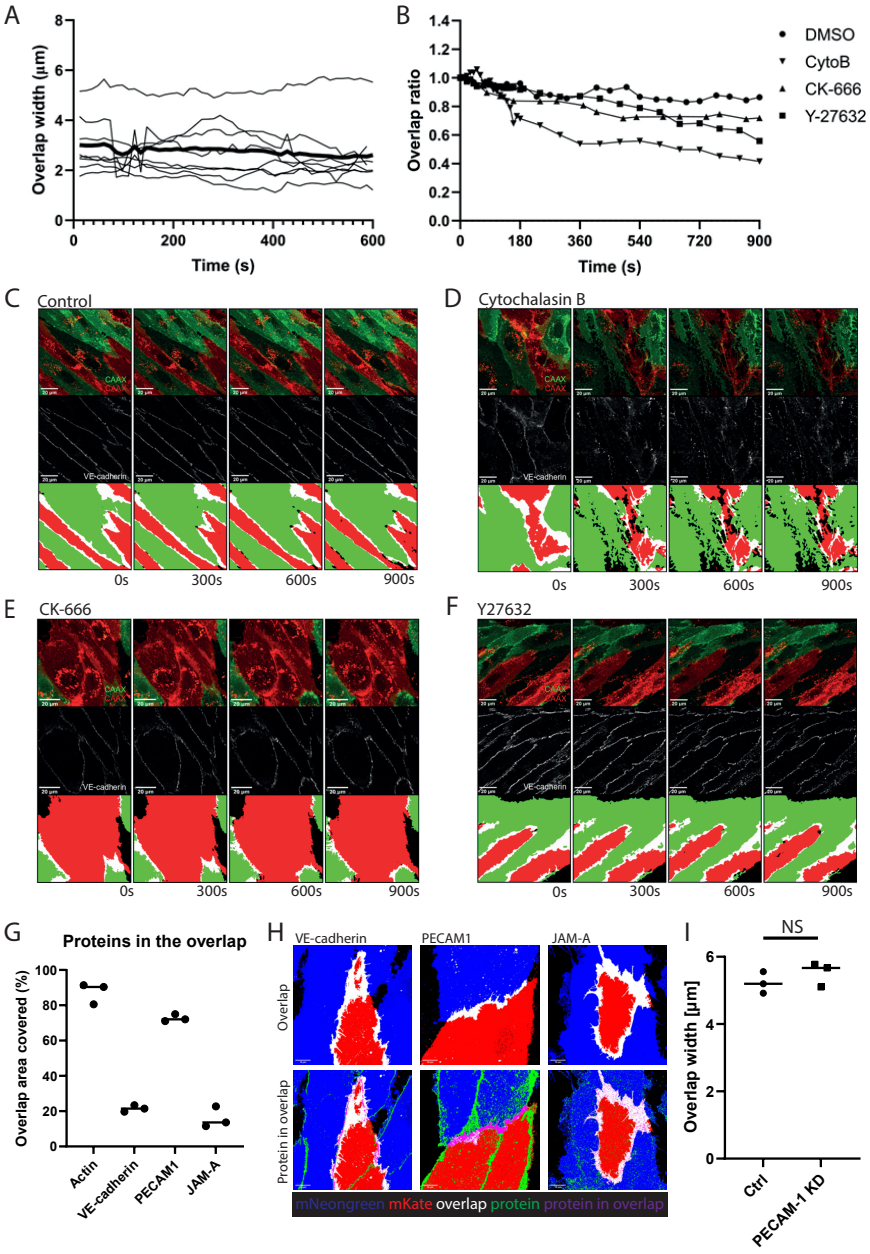

Figure 3. Junction overlap is dynamic and depends on the cytoskeleton: actin polymerization, branching and turnover all contribute.
A. Overlap width of individual junctions and their average (thick line) indicates a dynamic monolayer in which total overlap is maintained through the dynamics of individual junctions. n=9: 3 junctions per time series in 3 separate experiments. **B.** Overlap of TNF-/alpha- inflamed HUVEC monolayers is decreases upon treatment with all inhibitors, the greatest effect exerted by cytochalasin B. Overlap calculated as a ratio relative to t0 pre-treatment. n>5 junctions in 1 time series. **C-F.** Live confluent TNF-α-inflamed HUVEC monolayers were treated with DMSO (**C**), cytochalasin B (**D**), CK-666 (**E**), or Y27632 (**F**) at t0. Representative stills from time-series of maximum confocal Z-projections, 5 minutes apart. Upper panels: red/green CAAX. Middle panels: α-VE-

cadherin-AF647. Lower panels: thresholded and masked versions of upper panel images showing red/green CAAX and their overlapping surface in white. **G.** Area of overlap positive for VE-Cadherin, PECAM-1, or actin determined by masking overlapping areas and measuring positive immunostaining for respective proteins. Data representative of 3 individual experiments. **H.** Immunostaining for junctional proteins VE-cadherin, PECAM1 and JAM-A in overlapping membrane junctions. Top shows overlapping membranes with CAAX-mNeongreen masked as blue, MEM-mKate as red, overlapping membrane as white. Bottom shows junctional proteins in green and in overlapping membrane as magenta. **I.** Membrane overlap width in cells transduced with non-sense siRNA or siRNA against PECAM-1 is not changed.

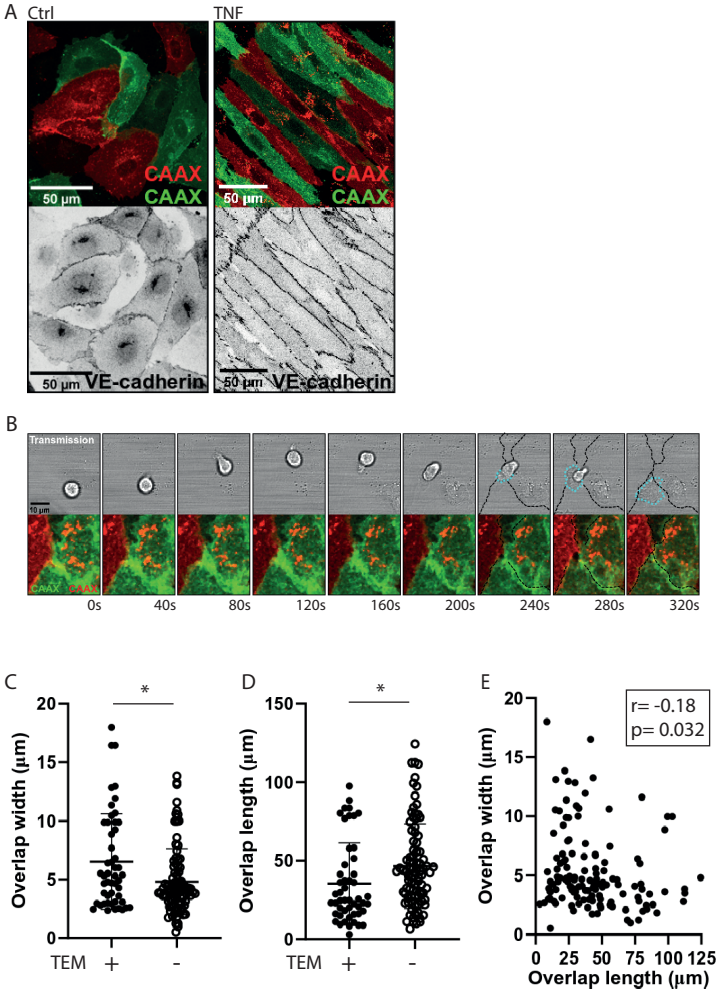

Figure 4. Transmigrating leukocytes prefer shorter, wider junctions.
A. Representative confocal image of uninflamed (left) and elongated HUVEC phenotype upon TNF-α-induced inflammation (right). Upper panels: maximum confocal Z-projections red and green CAAX. Lower panels: maximum Z-projections of αVE-cadherin-AF647, inverted image look-up table. **B.** Confocal microscopy images of a transmigrating leukocyte through the mosaic HUVEC monolayer grown in a specialized flow channel. Upper panels: transmission images of one confocal Z-slice. Lower panels: overlay of maximum projections of confocal Z-stacks of mScarlet- and mNeonGreen-CAAX. Stills from time series, 40s apart. **C.** Overlap width of µm of TEM event (+, n=50) is significantly greater than non-event junctions (-, n=92) (Mann Whitney, p=0.0242). **D.** Overlap length of µm of TEM event(+, n=50) is significantly smaller than non-event junctions (-, n=92) (Mann Whitney, p=0.0.0037). **E.** Overlap length and width correlate negatively. Pearson r=-0.18 (p=0.0324). Data from C-E from 6 independent experiments.

We hypothesized that during inflammation, these endothelial membrane overlaps might support paracellular transmigration. We observed that stimulation of HUVECs with TNF-α results in an elongated cell phenotype where two opposite sides are markedly shorter than the other two (Figure 4A), as is an established inflammatory phenotype (Marcos-Ramiro et al., 2014). To investigate the relation between endothelial membrane overlap characteristics and leukocyte paracellular transendothelial migration, we performed flow experiments on confluent CAAX mosaic-expressing endothelial monolayers stimulated with the pro-inflammatory cytokine TNF-α. These cells were grown to confluency in specialized channels that allowed laminar flow and in which neutrophils can be introduced and monitored in real-time to migrate through the endothelium (Figure 4B). We analyzed the time series of neutrophils transmigrating via the paracellular route and quantified overlap length and width in the field of view. Then, we distinguished between junctions facilitating a transmigration event and non-event junctions. Remarkably, our data indicated that the overlap width of junctions that facilitate transmigration was significantly greater than the width of junctions where no neutrophil transmigrated (Figure 4C). Moreover, our results indicated that junctions that support transendothelial migration (TEM) events are significantly shorter than non-TEM event junctions within the same monolayer (Figure 4D). Interestingly, endothelial membrane overlap junction width and length were slightly yet significantly inversely correlated (Figure 4E), indicating that the shorter sides of elongated inflamed HUVECs tend to overlap more. Together, our findings suggest that leukocyte transmigration is related to the inflammatory HUVEC phenotype, displaying a preference for specific junctions where the short sides of ECs meet and overlap.

Previous studies have suggested the existence of transmigratory hotspots at tricellular corners (Burns et al., 2000; Hyun et al., 2019). We observed that often, more than two adjacent endothelial cells form a TEM-event junction: tri- or even quadro-cellular corners were observed (Figure 5A-C). Interestingly, 60% of PMNs transmigrate through junctions where more than two cells meet (Figure 5D). These findings confirm previous reports that leukocytes prefer multicellular junctions for transmigration. The differences in width and length between TEM event- and non-TEM event junctions and the preference for multicellular junctions led us to investigate whether neutrophils prefer the nearest junction they encounter upon adhesion. To investigate this, we measured the distance that one neutrophil traveled from the time it first adhered to the monolayer until it was completely underneath the endothelial cells. (Figure 5E). Our results show neutrophils traveled an average distance of 18 µm (Figure 5F).

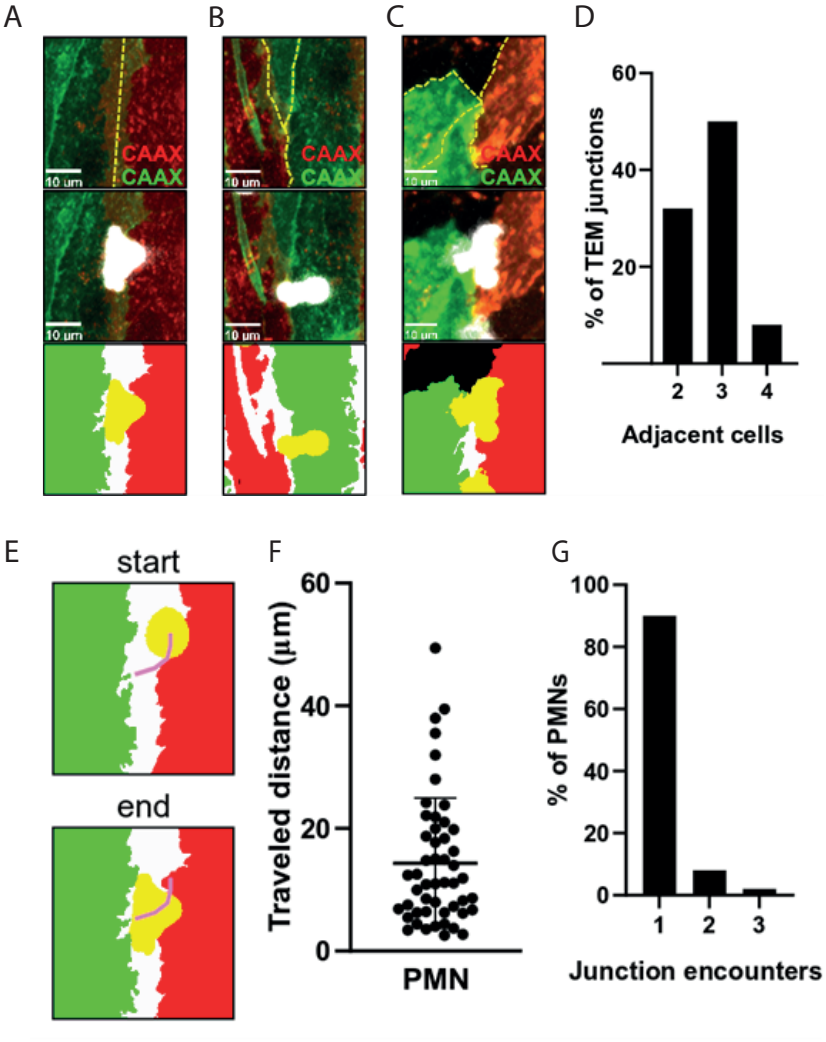

Figure 5. Transmigrating leukocytes prefer junctions where more than two cells meet.
A. Representative examples of a TEM event through a bicellular (**A**), tricellular (**B**), or quadro-cellular (**C**) junction. Upper panels: maximum Z projection of confocal images pre-event with red/green CAAX, junctions depicted with a yellow dashed line. Middle panels: maximum confocal Z-projection of red/green CAAX and DiD-stained PMN. Lower panels: thresholded and masked versions of middle panel images with overlapping EC surface in white, PMN in yellow. **D.** Frequency distribution of the number of cells that form an event junction (n=50). Tri- or quadricellular junctions make up 60% of TEM events. **E.** Method of travel distance quantification of PMNs from first monolayer contact (upper panel, start) until completed transmigration (lower panel, end) (n=50). Thresholded and masked maximum Z projection of confocal images: red and green CAAX, white overlap, yellow PMN. The purple line indicates the traveled path. **F.** Travel distance of PMNs between first adherence to the monolayer until completed transmigration, mean=14.3µm. **G.** 90% of PMNs transmigrate through the first junction they encounter (n=50). Data from **D,F,G** from 6 independent experiments.

To investigate in more detail whether leukocytes cross the endothelial monolayer at the nearest junction they encounter upon adhesion, we quantified the number of junctions a neutrophil crossed before diapedesis. 90% of neutrophils transmigrated through the first junction they encountered; only 8% transmigrated through the second junction and a mere 2% through the third junction (Figure 5G). Combined with the distances leukocytes travel on the endothelium, these findings suggest that leukocytes adhere anywhere on the endothelium and travel to specific PECAM-1-rich junctions for transmigration.

To understand how neutrophils make their way through overlapping endothelial membranes, detailed imaging in 3 dimensions in real-time is required. As the average diapedesis time of neutrophils is within 1-2 minutes, this requires ultrafast recording with low phototoxicity. Therefore, we used lattice light sheet imaging to map how neutrophils breach the endothelial overlaps. Using endothelial cells that express either GFP- or Scarlet-CAAX membrane markers, we found that neutrophils squeezed themselves through the endothelial layers (Figure 6A). We observed that the overlapping membrane region is opened up by the neutrophil, squeezing itself in between the overlapping membranes, thereby forming a “transmigration tunnel” (Figure 6B). During the diapedesis step, the overlapping membranes tightly adhere to the transmigrating neutrophil, closing the tunnel as soon as the neutrophil leaves the junction (Figure 6C, D). This shows that the PECAM-1 rich overlapping membrane forms a tight seal around transmigrating neutrophils.

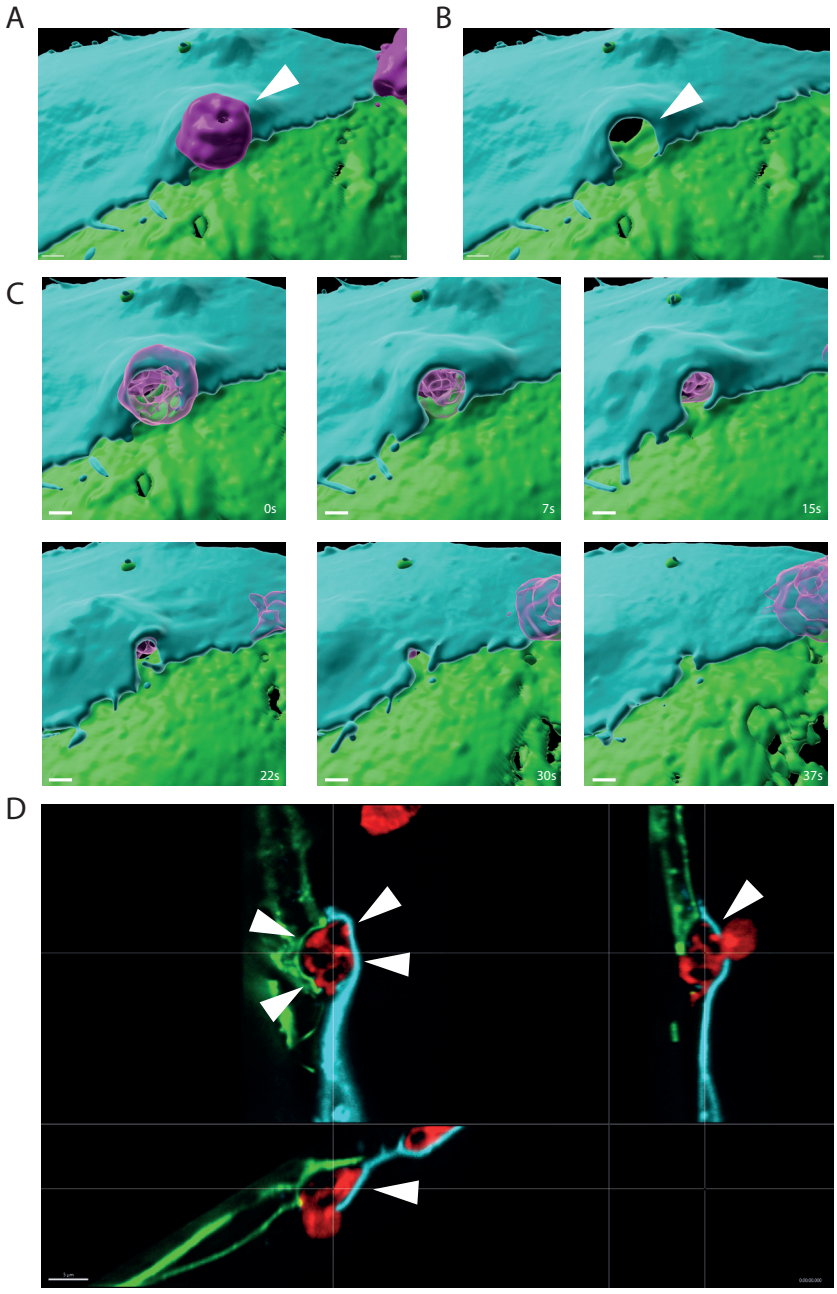

Figure 6. Overlapping membranes form transmigration tunnel around extravasating neutrophil.
A-D. High spatiotemporal resolution lattice lightsheet microscopy of TNF-activated HUVEC monolayer expressing either CAAX-mNeonGreen or mScarlet and DiD labeled primary neutrophils. **A.** Volume rendering of transmigrating neutrophil indicated with white arrow. **B.** Rendering of tunnel formed by overlapping membrane junction indicated with white arrow. **C.** Timeseries of neutrophil squeezing through the endothelial overlapping membranes, forming a tight-fitting tunnel in the process. **D.** Orthogonal view of neutrophil at T=0, arrows indicate one HUVEC on top of the neutrophil and the other below the neutrophil.

DISCUSSION

Leukocytes extravasating in a paracellular manner squeeze through endothelial cell-cell junctions without fluid leaking into underlying tissues (Heemskerk et al., 2016). Although it was previously noted that endothelial cells overlap at junctions, the characteristics and how leukocytes manage to cross these overlapping membranes remain incompletely understood. The current study characterizes the overlap between endothelial cells and during transendothelial migration of leukocytes. We found that overlap length and width relate to the elongated inflammatory endothelial cell phenotype, with shorter junctions tending to overlap more. Leukocytes display a preference for such shorter junctions, which feature a relatively high PECAM-1 expression in contrast to longer and more linear adherens junctions; notably, these shorter overlapping junctions depend on the flow and an active actin cytoskeleton, and they are also more apparent when the endothelium is activated by TNFα. Moreover, overlapping endothelial membranes form a “tunnel” for leukocytes to migrate through. Our work presents novel insight into PECAM-1-rich overlapping junctions, which leukocytes actively select for transendothelial migration.

We hypothesized that the direction of endothelial membrane overlaps is correlated with the flow direction for hydrodynamic reasons as well as to shield transmigrating leukocytes from the forces of the flow potentially. This scenario would imply that neutrophils transmigrate against the direction of flow in an upstream manner, as has also been reported previously (Anderson et al., 2019; Valignat et al., 2013). Moreover, as shorter and wider junctions are perpendicular to the flow, we hypothesized that the alignment in combination with the increased overlap width at these junctions was preferred by neutrophils to transmigrate.

Our results suggest PECAM-1 as a molecular marker for overlap as it co-localizes with the endothelial membrane overlaps, in contrast to the more conventional junction marker VE-cadherin, which displays a much narrower distribution pattern. Previous studies support the localization of PECAM-1 at overlapping junctions as this protein is subject to ’diffusion trapping’: PECAM-1 molecules diffuse freely through the cell membrane until they interact in a homophilic manner between cells, leading to retention at junctions on the entire surface of overlapping cells (Sun et al., 2000).

Whether a leukocyte migrates using the paracellular or transcellular route is suggested to depend on the relative tightness of the endothelial junctions and the ability of the leukocyte to breach them (Carman & Springer, 2004). It is speculated that the leukocytes take the ‘path of least resistance’ when crossing the endothelium(Martinelli et al., 2014). VE-cadherin phosphorylation status is reported to regulate stable adherens junctions to protect against vascular leakage during leukocyte extravasation or permeability-inducing factors such as VEGF or histamine (Wessel et al., 2014). Moreover, VE-cadherin can endure considerable myosin-mediated tension (Conway et al., 2013). Interestingly, previous studies report that PECAM-1 deletion strengthens endothelial cell-junctional integrity (Liao et al., 2018). Hence, PECAM-1-rich junctions might benefit transmigration by decreasing the force

needed to separate cells for crossing leukocytes. Indeed, we observed that leukocytes prefer transmigrating through wider junctions, which would offer more surface for PECAM-1 presentation. Furthermore, a maximized contact surface between endothelial cells and leukocytes is suggested to prevent vascular leakage during transendothelial migration (Vestweber, 2015), which offers another argument for the preference of leukocytes to cross wider junctions. Overlapping PECAM-1 rich membranes are also found in the lymphatic capillary vasculature (Baluk et al., 2007). Junctions between lymphatic endothelial cells do not form continuous junctions but specialized junctions with a button phenotype, small buttons made up of VE-cadherin and tight junction-associated proteins such as occludin, claudin-5, and ZO-1 (Baluk et al., 2007; Yao et al., 2012). The membrane regions between the button junctions are enriched in PECAM-1 and LYVE-1 creating a barrier that is more permeable than continuous junctions (Jackson, 2019; Zhang et al., 2020). Our data could hint at a shift in endothelial junction morphology upon inflammation towards a phenotype where shorter, wider overlapping membranes are less tightly closed, allowing for easier leukocyte passage while maintaining barrier function.

The cytoskeleton is an important regulator of cell shape and motility and was previously indicated to play an essential part in maintaining vascular integrity during transmigration. We observed loss of overlap upon inhibition of ROCK. ROCK inhibition is known to induce membrane blebbing via its action on actomyosin (Riento & Ridley, 2003). Although we observed “wobbly” junctions due to loss of tension, inhibition of ROCK did not induce membrane blebbing. Additionally, increased actin contractility through thrombin stimulation is recognized to decrease barrier integrity (van Nieuw Amerongen et al., 1998). However, local tension during diapedesis was found at F-actin-rich contractile pores that limited leakage during diapedesis (Heemskerk et al., 2016). Considering our results, showing the dependence of the endothelial membrane overlaps on actin regulation, we reasoned that the overlaps play a role in forming such pores and are essential for efficient transmigration.

The relatively long distances a leukocyte travels before transmigrating may indicate that the leukocyte does not transmigrate at the nearest cell border after adhesion but actively crawls over the endothelium to seek a favorable junction. The question remains whether the endothelium guides the leukocytes toward these junctions or leukocytes navigate their rolling. Our results indicate a relatively high travel distance of neutrophils from first contact to the endothelial monolayer to their site of transmigration. Previously, it was reported that neutrophils crawl over the endothelium for approximately 12 µm before crossing the endothelium (Phillipson et al., 2006), in line with our findings. Monocytes have been described to patrol non-inflamed microvessels for distances up to 200 µm, dependent on LFA- 1 but not Mac-1, the latter being only required for patrolling under inflammatory conditions (Auffray et al., 2007). Considering this, the relatively long travel path we observed may therefore be attributed to both LFA-1 and Mac-1.

ICAM-1-clustering and ICAM-1-rich filopodia have been identified to surround adherent leukocytes upon inflammation and form a so-called docking structure or transmigratory cup

(Barreiro et al., 2002; Carman & Springer, 2004; Kroon et al., 2018; Schaefer et al., 2014; Schimmel et al., 2018; van Buul et al., 2007). We recently showed that junctional membrane protrusions could guide leukocyte diapedesis (Arts et al., 2021). Clearly, these endothelial membranes play a regulatory role in assisting the leukocytes on their way through. Furthermore, we observed that multiple neutrophils tend to transmigrate in a row at the same spot, which has also been noticed before (Hashimoto et al., 2011). These authors argue that neutrophils follow each other because transmigration leads to altered junctions that show increased PECAM-1 and decreased VE-cadherin expression, resulting in that spot becoming more favorable for subsequent neutrophils for transmigration. This is in accordance with our observation that leukocytes transmigrate through PECAM-1-rich junctions. We found that profound PECAM-1 expression at junction regions is favored by the leukocytes, as can be explained by diffusion trapping of PECAM-1 at overlaps and the notion that PECAM-1-rich junctions are less stable. Together, junctions that exhibit transmigration-favorable characteristics, such as PECAM-1 and membrane protrusions, might be subject to a feedback mechanism that reinforces this phenotype upon initial diapedesis for subsequent leukocytes.

In conclusion, this study presents how endothelial membrane overlap is regulated and present not only *in vitro* experiments, but also in various organs *in vivo*. Moreover, we show how leukocytes prefer these overlaps for extravasation, during which they create a membrane-based tunnel marked by PECAM-1.

Acknowledgement

This work was supported by LSBR grant # 1649 (A.C.I.v.S.), LSBR grant # 1820 (L.K.), and ZonMW NWO Vici grant #91819632 (J.D.v.B., W.J.v.d.M).

MATERIALS AND METHODS

Mouse lines

Mice carrying the Rosa26-Confetti transgene were bred with Cdh5-CreERT2 mice to induce endothelial-specific, tamoxifen-inducible conditional Cre-recombinase expression in endothelial cells resulting in the exclusive labeling of endothelial cells with the heterogeneous labeling of the confetti construct. These confetti$^{fl/wt}$ -Cdh5-CreERT2 mice were injected for five consecutive days with tamoxifen (2mg/mouse) to induce sufficient recombination of the rosetta construct for imaging purposes. To preserve fluorophore function and avoid the collapse of bloodvessels, mice were perfused with PLP-fixation buffer before sacrifice by cervical dislocation. Mice were put into deep anesthesia using hexafluorane, and the thorax was opened, after which a cut to the left ventricle was made. 10 ML PLP fixation buffer was then slowly injected into the left ventricle, replacing the blood. After this procedure, the mouse was sacrificed by cervical dislocation, and organs were harvested.

Mouse tissue preparation and staining

Liver, lung, and spleen were further fixated overnight using 4% PFA in PBS, washed with P-buffer, and stored in 30% sucrose overnight. The organs were then put into cryo molds filled with Tissue-TEK, frozen, and stored at -80. Afterward, coupes were sliced and mounted for imaging using Prolong antifade Glass. Imaging was performed on a Leica SP8, and image analysis was performed using Imaris.

Cell culture and transduction

Pooled human umbilical vein endothelial cells (HUVECs; Lonza, P1052, #C2519A) were cultured at 37°C with 5% CO2 in enriched Endothelial Growth Medium (EGM2; #C-22211, Promocell) supplemented with 2% endothelial growth factor mix (#C-39216, Promocell), 100 U/mL penicillin, and 100 µg/mL streptomycin (#15140122, Gibco). Cells were cultured on fibronectin (FN; CLB) coated surfaces until at most passage 8. For fluorescence microscopy, cells were transduced (1:500) with lentiviral constructs to express CAAX tagged with fluorescent protein mScarlet, YFP, mNeonGreen, or mTurquoise2, and selected with 100µg/mL puromycin in EGM2. Cells were allowed to form a confluent mosaic monolayer after mixing transduced cells 1:1 in the combinations mScarlet/mNeongreen- and YFP/mTurqoise2-CAAX to enable overlap quantification as described later. To mimic inflammation, confluent cells received 10ng/mL human TNF-α (Peprotech, #300-01A) in EGM2 O/N and fresh EGM2 with TNF-α 4 hours prior to imaging.

Sample fixation

For antibody stainings, mosaic monolayers of two-color-CAAX-transduced HUVECs were cultured at FN-coated 12mm diameter glass imaging coverslips. Cells were fixed with 4% final concentration paraformaldehyde in phosphate buffered saline ++ (PBS, Fresenius Kabi, #M090001/02) with 1µg/mL CaCl2 and .5µg/mL MgCl2 for 10 minutes at 37°C and treated with antibodies and/or dyes (as specified). Coverslips were secured on imaging slides using Mowiol mounting medium (Sigma-Aldrich).

Cytoskeleton manipulation during live imaging

Confluent mosaic monolayers of two-color-CAAX-transduced HUVECs were cultured at FN-coated 8-well µ-slides (#80826, Ibidi). F-actin modulating compounds were added in warm EGM2 to live cells during imaging at 37°C with 5% CO2 to a final concentration of 1µM Cytochalasin B (Sigma-Aldrich, #C26762), 10µM Y-27632 (Calbiochem, #688000), 100µM CK-666 (Sigma-Aldrich, #SML006), or 10mM DMSO (Sigma-Aldrich). Afterward, cells were fixed with PFA as described above, and endothelial cell overlap was quantified using ImageJ/FIJI as described below.

Neutrophil isolation

Polymorphonuclear neutrophils were isolated from whole peripheral blood from healthy

donors. Blood was diluted (1:1) in RT PBS with 1:10 TNC, transferred onto 1.076g/mL Percoll separation medium at RT, and separated by centrifuging at RT for 20 minutes at 800G with start and brake at setting 3. The supernatant was removed to leave only Percoll containing the CD14+ neutrophils and the erythrocyte layer below. Erythrocytes were lysed in ice-cold buffer (water for injection with 155mM NH_4Cl, 10mM $KHCO_3$, 0.1mM EDTA (all Sigma-Aldrich)) on ice for 5-15 minutes until the suspension either cleared or became dark red. Neutrophils were pelleted at 4°C for 5 minutes at 450G with start and brake at setting 9. The supernatant was removed, and the remaining erythrocytes were lysed again with an ice-cold buffer for 5 minutes on ice. Neutrophils were pelleted and supernatant discarded, after which neutrophils were rewashed with 4°C PBS and pelleted. Neutrophils were then resuspended in HEPES+ buffer (20mM HEPES, 132mM NaCl, 6mM KCl, 1mM $MgSO_4$, 1.2mM K_2HPO_4, pH7.4, 1mM $CaCl_2$, 5mM D-glucose (all Sigma-Aldrich) and 0.4% human serum albumin (Sanquin Reagents)).

Flow-induced neutrophil transendothelial migration

Confluent mosaic monolayers of two-color-CAAX-transduced HUVECs were cultured at FN-coated 6-channel µ-slides VI 0.4 #80666, Ibidi). Cells received 10ng/mL human TNFα in EGM2 O/N to mimic inflammation before flow experiments. During microscopy at 37°C and 5% CO_2, channels were connected to a pump system providing a laminar flow of 0.8dyne/cm2 of 37°C HEPES+ medium. Every channel received 2 million freshly isolated neutrophils resuspended in HEPES+ medium that were activated by incubation at 37°C for 15-30 minutes. Neutrophils were visualized using 1:2000 DiD dye that incubated with the neutrophils during activation. Transmigration was captured for 10 minutes after neutrophil injection to the flow system by acquiring repeated Z-stacks with step size never exceeding 1µm. Fluorescence was detected with the Zeiss LSM980 AiryScan2 machine (ZEISS) with ZEN software, using the 25x water-immersion NA.8 objective at 2.5x zoom and 8x multiplex imaging settings. Endothelial cell junction overlap was quantified using ImageJ/FIJI as described, classifying junctions based on the presence or absence of a neutrophil transmigration event.

Antibodies

Antibodies were used on fixed cells (see above) that were permeabilized, if necessary, 0.1% TritonX for 5-10 minutes. Cells were blocked by PBS with 2% bovine serum albumin (SERVA, #11920) and incubated with primary and secondary antibodies (Table 1), washing coverslips with PBS++ between antibody steps.

Imaging

Live cells were imaged at 37°C and 5% CO_2. Overlap was visualized by acquiring Z-stack images using fluorescence microscopy, with Z-step size never exceeding 1µm. On the Leica SP8 machine with LAS X software (Leica Microsystems BV), images were acquired at 1024*1024 resolution using the 40x NA1.4 oil-immersion objective, and fluorescence

was detected using PMT and HyD detectors with suitable gain and AOBS filter settings. On the Zeiss LSM980 AiryScan2 machine (ZEISS) with ZEN software, the 40x NA1.4 oil-immersion objective was used for imaging near-superresolution at 1.5x Nyquist sampling. On both microscopes, excitation lasers were 405nm for Hoechst and Alexa405, 442nm for mTurqoise2, 488nm for mNeonGreen, 514nm for YFP, 561nm for mScarlet, 633nm for DiD, 633 nm and 671nm for respective Alexas.

Confocal overlap analysis

Maximum projections of Z-stacks were obtained using ImageJ/FIJI to quantify overlap. Before thresholding, the noise was reduced using the despeckle tool and the 2D median filter with a radius of 2.0 pixels. Fluorescent vesicles, an artifact of HUVEC transduction with fluorescent proteins, were removed using the particle analysis tool or by hand. Endothelial cell overlap width, length, and area were quantified using ImageJ/FIJI measure tool, taking into account the image scale.

Quantification of cell alignment

EC alignment was quantified by measuring the angle of a line drawn between the two most opposite points of the cell compared with the direction of the flow. If the angle was <45°, the cell was quantified as aligned. If the angle was >45° compared with the direction of the flow, cells were quantified as not aligned.

Quantification of travel distance

PMN travel distances were quantified between the first adhesion of the PMN on the monolayer and completed diapedesis. The travel start point was considered the PMN center of gravity upon adhesion. Then, the PMN center of mass was followed as it traveled the endothelium. The endpoint was considered the outer end of the overlap at the transmigration location.

Statistical analysis

Data was plotted and analyzed using Graphpad Prism software.

REFERENCES

Alon, R., & van Buul, J. D. (2017). Leukocyte Breaching of Endothelial Barriers: The Actin Link. *Trends in Immunology*, *38*(8), 606–615. https://doi.org/10.1016/J.IT.2017.05.002

Anderson, N. R., Buffone, A., & Hammer, D. A. (2019). T lymphocytes migrate upstream after completing the leukocyte adhesion cascade. *Cell Adhesion and Migration*, *13*(1), 164–169. https://doi.org/10.1080/19336918.2019.1587269/SUPPL_FILE/KCAM_A_1587269_SM8866.ZIP

Arts, J. J. G., Mahlandt, E. K., Grönloh, M. L. B., Schimmel, L., Noordstra, I., Gordon, E., van Steen, A. C. I., Tol, S., Walzog, B., van Rijssel, J., Nolte, M. A., Postma, M., Khuon, S., Heddleston, J. M., Wait, E., Chew, T. L., Winter, M., Montanez, E., Goedhart, J., & van Buul, J. D. (2021). Endothelial junctional membrane protrusions serve as hotspots for neutrophil transmigration. *ELife*, *10*. https://doi.org/10.7554/ELIFE.66074

Auffray, C., Fogg, D., Garfa, M., Elain, G., Join-Lambert, O., Kayal, S., Sarnacki, S., Cumano, A., Lauvau, G., & Geissmann, F. (2007). Monitoring of blood vessels and tissues by a population of monocytes with patrolling behavior. *Science (New York, N.Y.)*, *317*(5838), 666–670. https://doi.org/10.1126/SCIENCE.1142883

Baluk, P., Bolton, P., Hirata, A., Thurston, G., & McDonald, D. M. (1998). Endothelial gaps and adherent leukocytes in allergen-induced early- and late-phase plasma leakage in rat airways. *The American Journal of Pathology*, *152*(6), 1463. /pmc/articles/PMC1858452/?report=abstract

Baluk, P., Fuxe, J., Hashizume, H., Romano, T., Lashnits, E., Butz, S., Vestweber, D., Corada, M., Molendini, C., Dejana, E., & McDonald, D. M. (2007). Functionally specialized junctions between endothelial cells of lymphatic vessels. *Journal of Experimental Medicine*, *204*(10), 2349–2362. https://doi.org/10.1084/JEM.20062596/VIDEO-1

Barreiro, O., Yáñez-Mó, M., Serrador, J. M., Montoya, M. C., Vicente-Manzanares, M., Tejedor, R., Furthmayr, H., & Sánchez-Madrid, F. (2002). Dynamic interaction of VCAM-1 and ICAM-1 with moesin and ezrin in a novel endothelial docking structure for adherent leukocytes. *The Journal of Cell Biology*, *157*(7), 1233–1245. https://doi.org/10.1083/JCB.200112126

Burns, A. R., Bowden, R. A., MacDonell, S. D., Walker, D. C., Odebunmi, T. O., Donnachie, E. M., Simon, S. I., Entman, M. L., & Smith, C. W. (2000). Analysis of tight junctions during neutrophil transendothelial migration. *Journal of Cell Science*, *113 (Pt 1)*(1), 45–57. https://doi.org/10.1242/JCS.113.1.45

Butcher, E. C. (1991). Leukocyte-endothelial cell recognition: Three (or more) steps to specificity and diversity. *Cell*, *67*(6), 1033–1036. https://doi.org/10.1016/0092-8674(91)90279-8

Buul, J. D. van, Voermans, C., Berg, V. van den, Anthony, E. C., Mul, F. P. J., Wetering, S. van, Schoot, C. E. van der, & Hordijk, P. L. (2002). Migration of Human Hematopoietic Progenitor Cells Across Bone Marrow Endothelium Is Regulated by Vascular Endothelial Cadherin. *The Journal of Immunology*, *168*(2), 588–596. https://doi.org/10.4049/JIMMUNOL.168.2.588

Carman, C. v., & Springer, T. A. (2004). A transmigratory cup in leukocyte diapedesis both through individual vascular endothelial cells and between them. *The Journal of Cell Biology*, *167*(2), 377–388. https://doi.org/10.1083/JCB.200404129

Claesson-Welsh, L., Dejana, E., & McDonald, D. M. (2021). Permeability of the Endothelial Barrier: Identifying and Reconciling Controversies. *Trends in Molecular Medicine*, *27*(4), 314–331. https://doi.org/10.1016/J.MOLMED.2020.11.006

Conway, D. E., Breckenridge, M. T., Hinde, E., Gratton, E., Chen, C. S., & Schwartz, M. A. (2013). Fluid shear stress on endothelial cells modulates mechanical tension across VE-cadherin and PECAM-1. *Current Biology : CB*, *23*(11), 1024. https://doi.org/10.1016/J.CUB.2013.04.049

Corada, M., Mariotti, M., Thurston, G., Smith, K., Kunkel, R., Brockhaus, M., Lampugnani, M. G., Martin-Padura, I., Stoppacciaro, A., Ruco, L., Mcdonald, D. M., Ward, P. A., & Dejana, E. (1999). Vascular endothelial-cadherin is an important determinant of microvascular integrity in vivo. *Proceedings of the National Academy of Sciences of the United States of America*, *96*(17), 9815–9820. https://doi.org/10.1073/PNAS.96.17.9815/ASSET/2B1256A9-EA24-467D-9D04-69E4C81B6828/ASSETS/GRAPHIC/PQ1794391010.JPEG

Corada, M., Zanetta, L., Orsenigo, F., Breviario, F., Lampugnani, M. G., Bernasconi, S., Liao, F., Hicklin, D. J., Bohlen, P., & Dejana, E. (2002). A monoclonal antibody to vascular endothelial–cadherin inhibits tumor angiogenesis without side effects on endothelial permeability. *Blood*, *100*(3), 905–911. https://doi.org/10.1182/BLOOD.V100.3.905

Gotsch, U., Borges, E., Bosse, R., Böggemeyer, E., Simon, M., Mossmann, H., & Vestweber, D. (1997). VE-cadherin antibody accelerates neutrophil recruitment in vivo. *Journal of Cell Science*, *110 (Pt 5)*(5), 583–588. https://doi.org/10.1242/JCS.110.5.583

Hashimoto, K., Kataoka, N., Nakamura, E., Hagihara, K., Hatano, M., Okamoto, T., Kanouchi, H., Minatogawa, Y., Mohri, S., Tsujioka, K., & Kajiya, F. (2011). Monocyte trans-endothelial migration augments subsequent transmigratory activity with increased PECAM-1 and decreased VE-cadherin at endothelial junctions. *International Journal of Cardiology*, *149*(2), 232–239. https://doi.org/10.1016/J.IJCARD.2010.12.018

Heemskerk, N., Schimmel, L., Oort, C., van Rijssel, J., Yin, T., Ma, B., van Unen, J., Pitter, B., Huveneers, S., Goedhart, J., Wu, Y., Montanez, E., Woodfin, A., & van Buul, J. D. (2016). F-actin-rich contractile endothelial pores prevent vascular leakage during leukocyte diapedesis through local RhoA signalling. *Nature Communications*, *7*. https://doi.org/10.1038/NCOMMS10493

Hirata, A., Baluk, P., Fujiwara, T., & McDonald, D. M. (1995). Location of focal silver staining at endothelial gaps in inflamed venules examined by scanning electron microscopy. *Https://Doi.Org/10.1152/Ajplung.1995.269.3.L403*, *269*(3 13-3). https://doi.org/10.1152/AJPLUNG.1995.269.3.L403

Hyun, Y. M., Choe, Y. H., Park, S. A., & Kim, M. (2019). LFA-1 (CD11a/CD18) and Mac-1 (CD11b/CD18) distinctly regulate neutrophil extravasation through hotspots I and II. *Experimental & Molecular Medicine 2019 51:4*, *51*(4), 1–13. https://doi.org/10.1038/s12276-019-0227-1

Jackson, D. G. (2019). Leucocyte trafficking via the lymphatic vasculature-mechanisms and consequences. *Frontiers in Immunology*, *10*(MAR), 471. https://doi.org/10.3389/FIMMU.2019.00471/BIBTEX

Kroon, J., Schaefer, A., van Rijssel, J., Hoogenboezem, M., van Alphen, F., Hordijk, P., Stroes, E. S. G., Strömblad, S., van Rheenen, J., & van Buul, J. D. (2018). Inflammation-Sensitive Myosin-X Functionally Supports Leukocyte Extravasation by Cdc42-Mediated ICAM-1-Rich Endothelial Filopodia Formation. *Journal of Immunology (Baltimore, Md. : 1950)*, *200*(5), 1790–1801. https://doi.org/10.4049/JIMMUNOL.1700702

Liao, D., Mei, H., Hu, Y., Newman, D. K., & Newman, P. J. (2018). CRISPR-mediated deletion of the PECAM-1 cytoplasmic domain increases receptor lateral mobility and strengthens endothelial cell junctional integrity. *Life Sciences*, *193*, 186–193. https://doi.org/10.1016/J.LFS.2017.11.002

Manavski, Y., Lucas, T., Glaser, S. F., Dorsheimer, L., Günther, S., Braun, T., Rieger, M. A., Zeiher, A. M., Boon, R. A., & Dimmeler, S. (2018). Clonal Expansion of Endothelial Cells Contributes to Ischemia-Induced

Neovascularization. *Circulation Research*, *122*(5), 670–677. https://doi.org/10.1161/CIRCRESAHA.117.312310

Marcos-Ramiro, B., García-Weber, D., & Millán, J. (2014). TNF-induced endothelial barrier disruption: beyond actin and Rho. *Thrombosis and Haemostasis*, *112*(6), 1088–1102. https://doi.org/10.1160/TH14-04-0299

Martinelli, R., Zeiger, A. S., Whitfield, M., Sciuto, T. E., Dvorak, A., van Vliet, K. J., Greenwood, J., & Carman, C. v. (2014). Probing the biomechanical contribution of the endothelium to lymphocyte migration: Diapedesis by the path of least resistance. *Journal of Cell Science*, *127*(17), 3720–3734. https://doi.org/10.1242/JCS.148619/VIDEO-7

Phillipson, M., Heit, B., Colarusso, P., Liu, L., Ballantyne, C. M., & Kubes, P. (2006). Intraluminal crawling of neutrophils to emigration sites: a molecularly distinct process from adhesion in the recruitment cascade. *The Journal of Experimental Medicine*, *203*(12), 2569–2575. https://doi.org/10.1084/JEM.20060925

Rademakers, T., Goedhart, M., Hoogenboezem, M., Ponce, A. G., van Rijssel, J., Samus, M., Schnoor, M., Butz, S., Huveneers, S., Vestweber, D., Nolte, M. A., Voermans, C., & van Buul, J. D. (2020). Hematopoietic stem and progenitor cells use podosomes to transcellularly cross the bone marrow endothelium. *Haematologica*, *105*(12), 2746–2756. https://doi.org/10.3324/HAEMATOL.2018.196329

Riento, K., & Ridley, A. J. (2003). ROCKs: multifunctional kinases in cell behaviour. *Nature Reviews Molecular Cell Biology 2003 4:6*, *4*(6), 446–456. https://doi.org/10.1038/nrm1128

Schaefer, A., Riet, J. te, Ritz, K., Hoogenboezem, M., Anthony, E. C., Mul, F. P. J., de Vries, C. J., Daemen, M. J., Figdor, C. G., van Buul, J. D., & Hordijk, P. L. (2014). Actin-binding proteins differentially regulate endothelial cell stiffness, ICAM-1 function and neutrophil transmigration. *Journal of Cell Science*, *127*(20), 4470–4482. https://doi.org/10.1242/JCS.154708/VIDEO-4

Schimmel, L., Heemskerk, N., & van Buul, J. D. (2016). Leukocyte transendothelial migration: A local affair. *Http://Dx.Doi.Org/10.1080/21541248.2016.1197872*, *8*(1), 1–15. https://doi.org/10.1080/21541248.2016.1197872

Schimmel, L., van der Stoel, M., Rianna, C., van Stalborch, A. M., de Ligt, A., Hoogenboezem, M., Tol, S., van Rijssel, J., Szulcek, R., Bogaard, H. J., Hofmann, P., Boon, R., Radmacher, M., de Waard, V., Huveneers, S., & van Buul, J. D. (2018). Stiffness-Induced Endothelial DLC-1 Expression Forces Leukocyte Spreading through Stabilization of the ICAM-1 Adhesome. *Cell Reports*, *24*(12), 3115–3124. https://doi.org/10.1016/J.CELREP.2018.08.045

Schulte, D., Küppers, V., Dartsch, N., Broermann, A., Li, H., Zarbock, A., Kamenyeva, O., Kiefer, F., Khandoga, A., Massberg, S., & Vestweber, D. (2011). Stabilizing the VE-cadherin–catenin complex blocks leukocyte extravasation and vascular permeability. *The EMBO Journal*, *30*(20), 4157–4170. https://doi.org/10.1038/EMBOJ.2011.304

Springer, T. A. (1994). Traffic signals for lymphocyte recirculation and leukocyte emigration: the multistep paradigm. *Cell*, *76*(2), 301–314. https://doi.org/10.1016/0092-8674(94)90337-9

Sun, J., Paddock, C., Shubert, J., Zhang, H. B., Amin, K., Newman, P. J., & Albelda, S. M. (2000). Contributions of the extracellular and cytoplasmic domains of platelet-endothelial cell adhesion molecule-1 (PECAM-1/CD31) in regulating cell-cell localization. *Journal of Cell Science*, *113 (Pt 8)*(8), 1459–1469. https://doi.org/10.1242/JCS.113.8.1459

Thurston, G., Baluk, P., Hirata, A., & McDonald, D. M. (1996). Permeability-related changes revealed at endothelial cell borders in inflamed venules by lectin binding. *Https://Doi.Org/10.1152/Ajpheart.1996.271.6.H2547*,

271(6 40-6). https://doi.org/10.1152/AJPHEART.1996.271.6.H2547

Valignat, M. P., Theodoly, O., Gucciardi, A., Hogg, N., & Lellouch, A. C. (2013). T Lymphocytes Orient against the Direction of Fluid Flow during LFA-1-Mediated Migration. *Biophysical Journal*, *104*(2), 322. https://doi.org/10.1016/J.BPJ.2012.12.007

van Buul, J. D., Allingham, M. J., Samson, T., Meller, J., Boulter, E., García-Mata, R., & Burridge, K. (2007). RhoG regulates endothelial apical cup assembly downstream from ICAM1 engagement and is involved in leukocyte trans-endothelial migration. *The Journal of Cell Biology*, *178*(7), 1279. https://doi.org/10.1083/JCB.200612053

van Nieuw Amerongen, G. P., Draijer, R., Vermeer, M. A., & van Hinsbergh, V. W. M. (1998). Transient and Prolonged Increase in Endothelial Permeability Induced by Histamine and Thrombin. *Circulation Research*, *83*(11), 1115–1123. https://doi.org/10.1161/01.RES.83.11.1115

van Steen, A. C. I., Kempers, L., Schoppmeyer, R., Blokker, M., Beebe, D. J., Nolte, M. A., & van Buul, J. D. (2021). Transendothelial migration induces differential migration dynamics of leukocytes in tissue matrix. *Journal of Cell Science*, *134*(21). https://doi.org/10.1242/JCS.258690

Vestweber, D. (2012). Relevance of endothelial junctions in leukocyte extravasation and vascular permeability. *Annals of the New York Academy of Sciences*, *1257*(1), 184–192. https://doi.org/10.1111/J.1749-6632.2012.06558.X

Vestweber, D. (2015). How leukocytes cross the vascular endothelium. *Nature Reviews. Immunology*, *15*(11), 692–704. https://doi.org/10.1038/NRI3908

Wessel, F., Winderlich, M., Holm, M., Frye, M., Rivera-Galdos, R., Vockel, M., Linnepe, R., Ipe, U., Stadtmann, A., Zarbock, A., Nottebaum, A. F., & Vestweber, D. (2014). Leukocyte extravasation and vascular permeability are each controlled in vivo by different tyrosine residues of VE-cadherin. *Nature Immunology*, *15*(3), 223–230. https://doi.org/10.1038/NI.2824

Wittchen, E. S. (2009). Endothelial signaling in paracellular and transcellular leukocyte transmigration. *Frontiers in Bioscience (Landmark Edition)*, *14*(7), 2522–2545. https://doi.org/10.2741/3395

Woodfin, A., Voisin, M. B., Beyrau, M., Colom, B., Caille, D., Diapouli, F. M., Nash, G. B., Chavakis, T., Albelda, S. M., Rainger, G. E., Meda, P., Imhof, B. A., & Nourshargh, S. (2011). The junctional adhesion molecule JAM-C regulates polarized transendothelial migration of neutrophils in vivo. *Nature Immunology 2011 12:8*, *12*(8), 761–769. https://doi.org/10.1038/ni.2062

Yao, L. C., Baluk, P., Srinivasan, R. S., Oliver, G., & McDonald, D. M. (2012). Plasticity of Button-Like Junctions in the Endothelium of Airway Lymphatics in Development and Inflammation. *The American Journal of Pathology*, *180*(6), 2561. https://doi.org/10.1016/J.AJPATH.2012.02.019

Zhang, F., Zarkada, G., Yi, S., & Eichmann, A. (2020). Lymphatic Endothelial Cell Junctions: Molecular Regulation in Physiology and Diseases. *Frontiers in Physiology*, *11*, 509. https://doi.org/10.3389/FPHYS.2020.00509

SUPPLEMENTAL MATERIAL

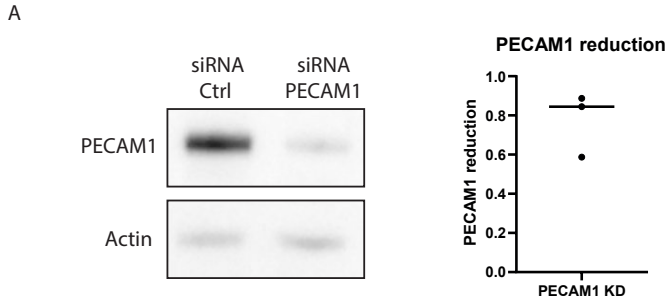

Supplemental Figure 1. (A) WB of PECAM-1 and Actin in HUVEC transduced with either non-sense control siRNA or anti-PECAM1 siRNA. Quantification of 3 individual experiments, PECAM-1 levels corrected for loading with Actin intensity.

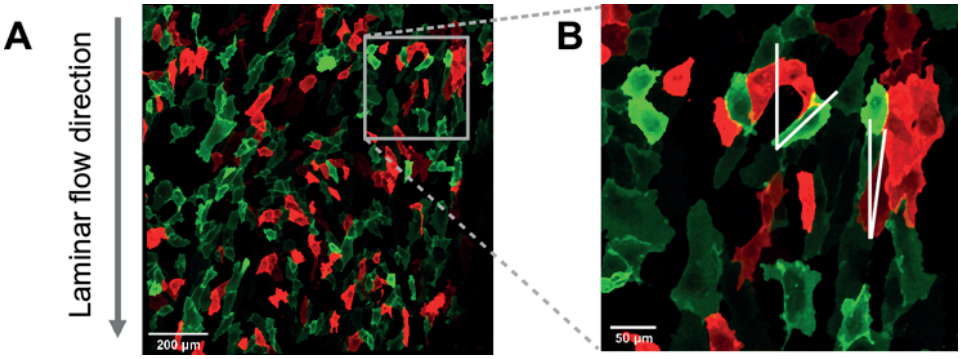

Supplemental Figure 2. Endothelial cells align to the flow direction.
A. Maximum Z-projection of confocal microscopy images of the mosaic HUVEC monolayer expressing mTurquoise- and sYFP-tagged CAAX (red and green look-up table in image) that were cultured under laminar flow (downward direction in the image) for 24 hours. Cells align in the flow direction. **B.** Quantification of cell alignment by measuring the angle between a line drawn between the two most opposite points of a cell and a line parallel to the flow direction (white lines). Cells positioned in <45° angles to the flow were counted as aligned, as the right example cell.

Volume 134 (21) November 2021

Journal of Cell Science

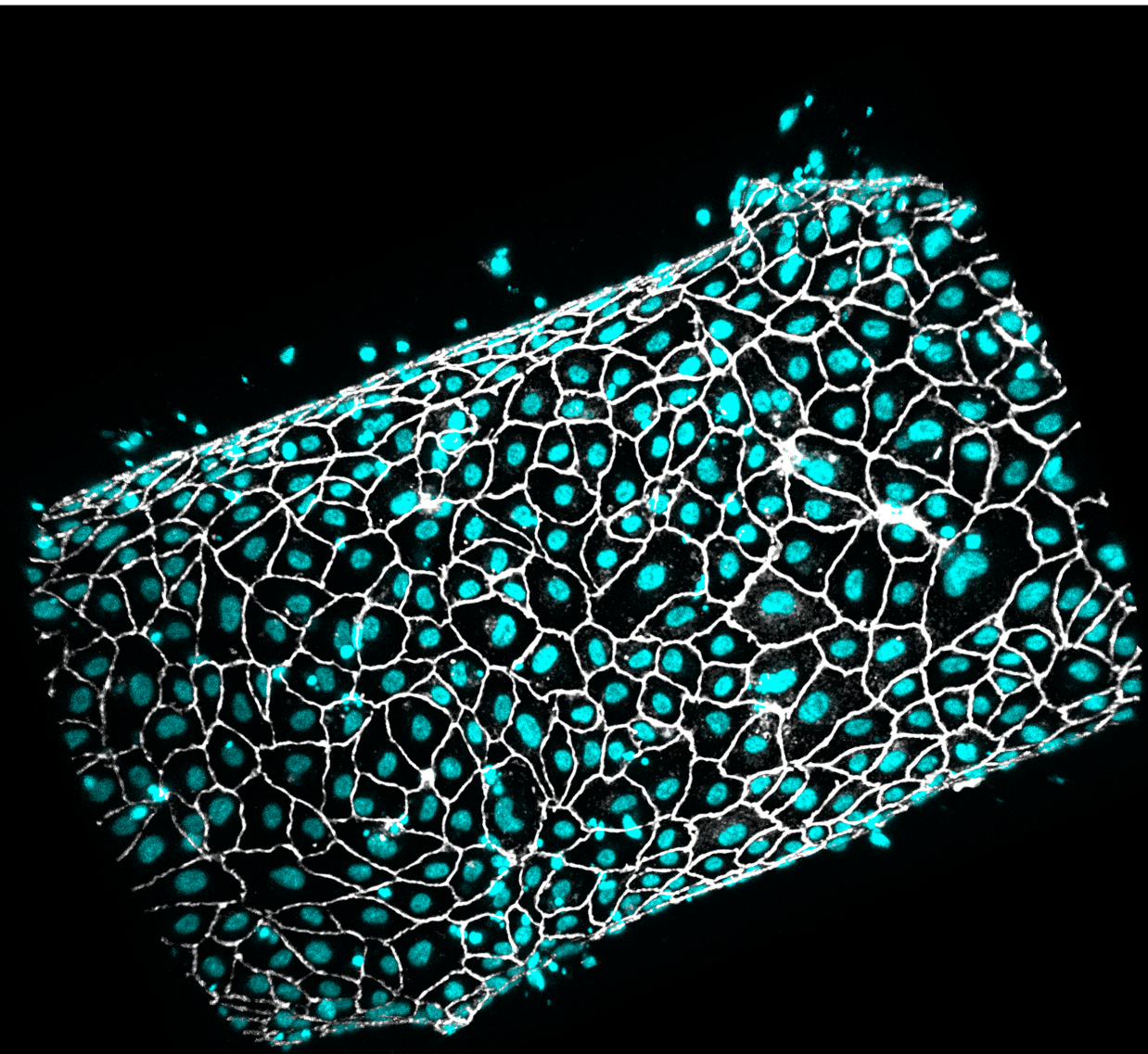

The Company of Biologists

CHAPTER 6

Transendothelial migration induces differential migration dynamics of leukocytes in tissue matrix

Abraham C.I. van Steen[1,*]
Lanette Kempers[1,*]
Rouven Schoppmeyer[1,2]
Max Blokker[3]
David J. Beebe[4]
Martijn A. Nolte[1]
Jaap D. van Buul[1,2,‡]

[1]Department of Molecular Hematology, Sanquin Research, Plesmanlaan 125, 1066 CX Amsterdam, The Netherlands.

[2]Leeuwenhoek Centre for Advanced Microscopy (LCAM), Section of Molecular Cytology, Swammerdam Institute for Life Sciences (SILS), University of Amsterdam, Science Park 904, 1098 XH Amsterdam, The Netherlands.

[3]Department of Physics, Vrije Universiteit Amsterdam, De Boelelaan 1081, 1081 HV Amsterdam, The Netherlands.

[4]Department of Biomedical Engineering, Department of Pathology and Laboratory Medicine, Carbone Cancer Center, University of Wisconsin -Madison, 1111 Highland Drive, Madison, WI 53705, USA.

**These authors contributed equally to this work*

‡Author for correspondence

Journal of cell science 134.21 (2021): jcs258690

ABSTRACT

Leukocyte extravasation into inflamed tissue is a complex process that is difficult to capture as a whole *in vitro*. We employed a blood-vessel-on-a-chip model in which human endothelial cells were cultured in a tube-like lumen in a collagen-1 matrix. The vessels are leak tight, creating a barrier for molecules and leukocytes. Addition of inflammatory cytokine TNF-α (also known as TNF) caused vasoconstriction, actin remodelling and upregulation of ICAM-1. Introducing leukocytes into the vessels allowed real-time visualization of all different steps of the leukocyte transmigration cascade, including migration into the extracellular matrix. Individual cell tracking over time distinguished striking differences in migratory behaviour between T-cells and neutrophils. Neutrophils cross the endothelial layer more efficiently than T-cells, but, upon entering the matrix, neutrophils display high speed but low persistence, whereas T-cells migrate with low speed and rather linear migration. In conclusion, 3D imaging in real time of leukocyte extravasation in a vessel-on-a-chip enables detailed qualitative and quantitative analysis of different stages of the full leukocyte extravasation process in a single assay.

INTRODUCTION

Leukocyte transendothelial migration (TEM) forms the basis of immune surveillance and pathogen clearance, and hence plays a pivotal role in many (patho)physiological processes. This process is highly regulated and strongly differs between the various leukocyte subsets and tissues involved. Leukocyte extravasation mainly occurs in postcapillary venules, where adherens junctions allow for transient opening of the barrier to allow leukocytes to pass.

Importantly, most venules only allow leukocyte TEM when the surrounding tissue is inflamed, thereby locally exposed to pro-inflammatory cytokines. One of those is tumour necrosis factor-α (TNF-α; also known as TNF), which is produced by a variety of cells under inflammatory conditions (Heller and Krönke, 1994). Once leukocytes have crossed the endothelial barrier, they continue migrating into the underlying matrix to fight the invading pathogens (Woodfin et al., 2010). Tissue penetration is an important aspect of the extravasation process as this determines whether a pathogen will be successfully cleared or not (Yamada and Sixt, 2019). It is therefore essential to understand how immune cells migrate through the extracellular matrix once they have crossed the endothelium. To date, the full extravasation process, including intraluminal rolling, crawling, diapedesis and extracellular 3D matrix migration, can only be studied using *in vivo* models as no proper *in vitro* models are available. As *in vivo* models have their limitations, it would be more than desirable to have an *in vitro* system that allows study of the full process in real time.

Research regarding the TEM process on a cellular level is mainly done using 2D *in vitro* models, generally based on endothelial cell monolayers cultured on flat stiff surfaces, such as coverslips (Muller and Luscinskas, 2008). Substrate stiffness has been shown to affect cell–cell and cell–matrix interactions of endothelial cells, as well as leukocyte–endothelial cell interactions and, subsequently, TEM (Huynh et al., 2011; Stroka and Aranda-Espinoza, 2011). Another limitation is that leukocytes encounter this stiff impermeable surface after traversing the endothelial barrier, making it impossible to study leukocyte detachment from the vessel and entry into the tissue. Three-dimensional systems, such as transwell assays and Boyden chamber assays, allow leukocytes to advance beyond the endothelial cell monolayer; however, these systems are unsuitable for microscopy-based imaging and are also based on stiff substrates (Muller and Luscinskas, 2008). To achieve the next step in TEM research, a more intricate model is required that allows imaging of the entire process from the luminal side of the endothelium into a physiological matrix substrate.

Organ-on-a-chip (OOAC) models use microfluidics-based approaches to create biomimetic systems emulating physiological organ function. Blood vessels are well suited for OOAC development, as their structure is relatively simple compared to entire organs (Virumbrales-Muñoz et al., 2020). Knowledge on vascularization of *in vitro* systems obtained from blood-vessel-on-a-chip (BVOAC) models could also be applied to organoids to overcome their current size and function limitations. BVOAC systems typically consist of a tubular endothelial cell monolayer generated in a stiff glass or plastic substrate (Farahat et

al., 2012; Zervantonakis et al., 2012; Zheng et al., 2012) or hydrogel (Wong et al., 2012; Kim et al., 2016; Sobrino et al., 2016). A perfusable and hydrogel-based BVOAC system overcomes the aberrations associated with stiff substrates and, in addition, allows leukocytes to extravasate into the matrix surrounding the vessel.

A system that meets these requirements is the LumeNext system, which is also highly suited for imaging analysis (Jiménez-Torres et al., 2016). Apart from building a 3D blood vessel in a physiological matrix, this device allowed us to track the subsequent migration of primary human neutrophils as well as T-cells beyond the diapedesis stage into the matrix in real time using confocal microscopy. We discovered that neutrophils and T-lymphocytes use markedly different migration modes to enter the tissue. Moreover, by applying a chemotactic gradient of complement component 5a (C5a) into the hydrogel matrix, we found that C5a did not increase the number of neutrophils that crossed the endothelium, but rather promoted migration towards C5a by adjusting the directionality of cell migration, while reducing migration speed. These findings demonstrate that the combination of cutting-edge BVOAC systems with advanced microscopy offers valuable new insights into how different leukocyte subsets respond to chemokines and cross the vascular barrier and enter the tissue.

RESULTS

Characterization of endothelium-lined blood vessels

To study leukocyte TEM in a reproducible BVOAC device and monitor this in real time, we used the LumeNext device (Fig. 1A) (Jiménez-Torres et al., 2016). Human endothelial cells were seeded in the lumen inside a collagen-1 matrix using a head-over-head incubator, allowing the formation of a 3D vessel (Fig. 1B). Staining of VE-cadherin, F-actin and nuclei showed the formation of a confluent endothelial monolayer (Fig. 1C), as well as a vascular lumen (Fig. 1D). Detailed imaging showed a confluent endothelial monolayer with linear junctions, marked by VE-cadherin and F-actin, representative of a functional barrier (Fig. 1E) (Ando et al., 2013).

As the barrier function of endothelial monolayers is an essential function of blood vessels, we measured the barrier function in the BVOAC model by perfusing the lumen with fluorescently labelled 70 kDa dextran, of a comparable size to albumin, an abundant plasma protein. In a non-vascularized lumen (i.e. no endothelial lining), dextran rapidly diffused into the matrix, whereas in endothelialized lumen, dextran was contained for more than 20 min without leakage. Addition of thrombin, a well-known vascular permeability factor (Van Nieuw Amerongen et al., 1998) to the lumen temporally induced endothelial permeability that recovered over time (Fig. 1F,G). This shows that the vessels are functionally lined with endothelial cells and provide a proper barrier function.

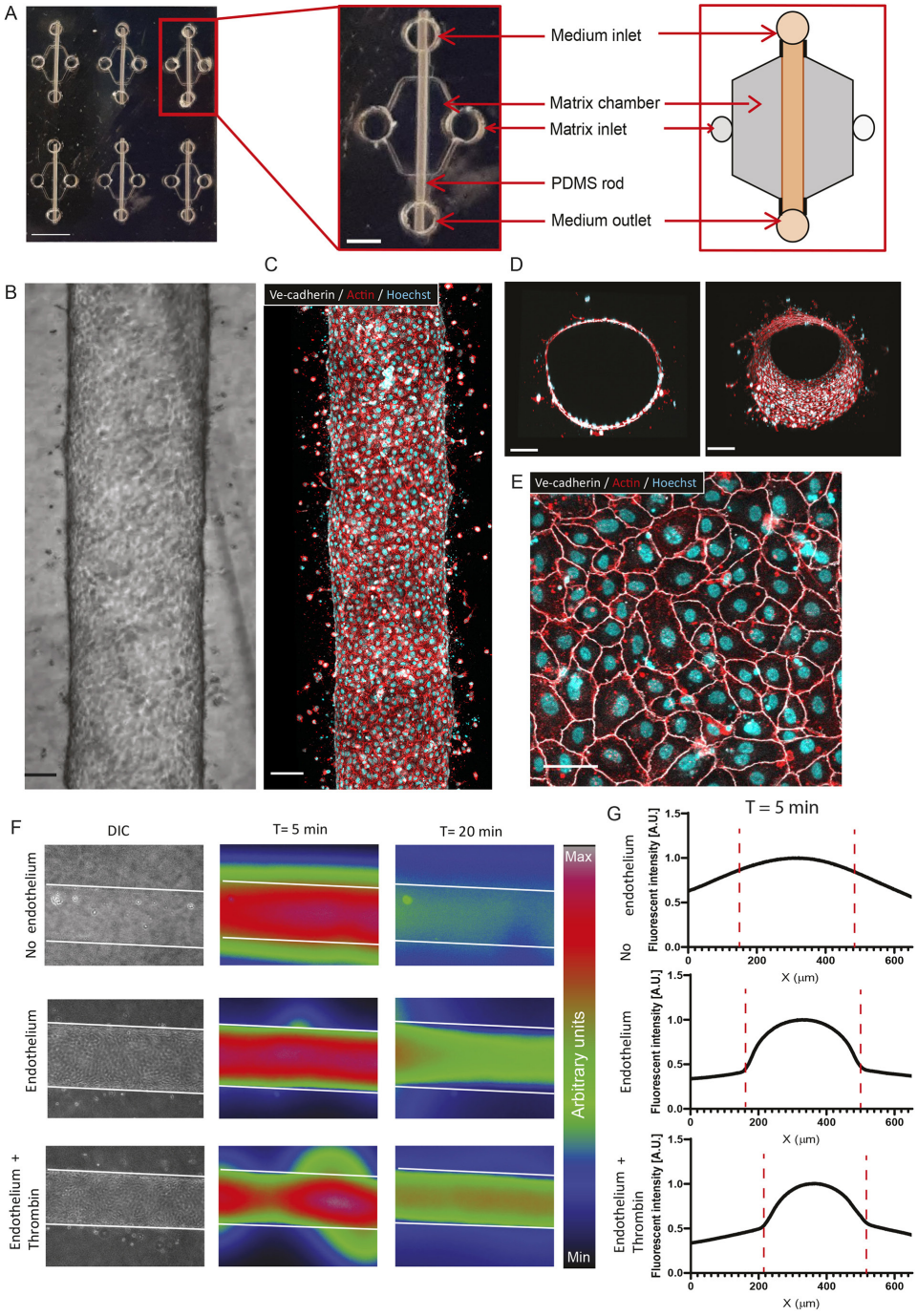

Figure 1. Making and characterization of the blood-vessel-on-a-chip (BVOAC).
(A) Overview of the device: six chambers to make a BVOAC (left), zoom-in on one BVOAC (middle) and schematic overview of one vessel place (right). PDMS, polydimethylsiloxane. (B–D) Differential interference contrast (DIC) (B) and confocal (C) image of a lumen lined with endothelial cells, and orthogonal view showing the open lumen of the BVOAC (D, left) and the Imaris surface rendering (D, right). (E) Zoom-in on the BVOAC

in D, showing the endothelial monolayer. (F,G) Representative images of leakage of 70 kDa dextran in the BVOAC (F) and quantification of the leakage 5 min after injection (G). Quantification was done by measuring the average fluorescent intensity over the y-axis of the image, which is then normalized to the maximum signal measured. The red dashed lines represent the vessel outlines. A.U., arbitrary units. Scale bars: 3 mm (A, left), 1 mm (A, right), 100 µm (B–D), 50 µm (E).

BVOAC under inflammatory conditions

Upon inflammation, the endothelium upregulates crucial adhesion molecules and chemokines required for leukocyte extravasation. Therefore, we incubated the vessels overnight with the inflammatory mediator TNF-α to activate the endothelial cells (Fig. 2A,B). Interestingly, TNF-α did not alter the number of endothelial cells in the BVOAC (Fig. 2C) but did lead to a smaller vessel diameter 24 h after addition of TNF-α (Fig. 2D). TNF-α treatment resulted in the induction of actin stress fibres through the cell body and the upregulation of ICAM-1 (Fig. 2E). In untreated cells, F-actin was predominantly present at the cell junctions, where they colocalized with VE-cadherin. In TNF-α-treated cells, cytosolic actin stress fibres are observed in addition to junctional actin stress fibres (Fig. 2F). In addition, the endothelial cells produced a layer of collagen IV around the vessel, making up a basement membrane (Fig. 2G). In the orthogonal view, it can be observed that the collagen IV is present at the basolateral side of the endothelium (Fig. 2H). The reduced vessel size, upregulation of ICAM-1, increased stress fibre formation and presence of collagen IV around the vessel illustrate that the endothelial cells were in an inflamed state after TNF-α treatment.

3D analysis of leukocyte transmigration in vessels

Next, we investigated TEM of neutrophils in the BVOAC model. Neutrophils were injected into uninflamed and inflamed vessels and incubated for 2.5 h. The devices were then washed to remove non-adherent neutrophils, fixed and imaged using confocal microscopy. We found that neutrophils not only crossed the endothelial monolayer but also continued migration into the underlying collagen matrix (Fig. 3A). Imaris software was used to generate a 3D rendering of the BVOAC, which revealed that neutrophils mostly transmigrated to the bottom of the vessel (Fig. 3B) due to gravity. When allowing transmigration during continuous turning of the device, thereby reducing the effect of local gravity, we found that neutrophils left the vessels at all sides (Fig. S1). This rendering was adapted for analysis by manually creating a surface at the position of the vessel (Fig. 3C) and creating spots at the centre of mass for neutrophils (Fig. 3D), based on automatic detection and manual curation. Following this analysis step, we were able to calculate the distance between the surface and the individual spots, which were then colour coded, with warm colours representing longest distance from the endothelium into the matrix (Fig. 3D). This analysis allowed us to distinguish between the different steps of TEM, namely adhesion, diapedesis and penetration into the ECM (Fig. 3F). To demonstrate the three different steps of the TEM cascade, we imaged in more detail the wall of the vessel and were able to observe the full TEM process, i.e. rolling, adhesion and diapedesis (Fig. 3G; Movies 1 and 2).

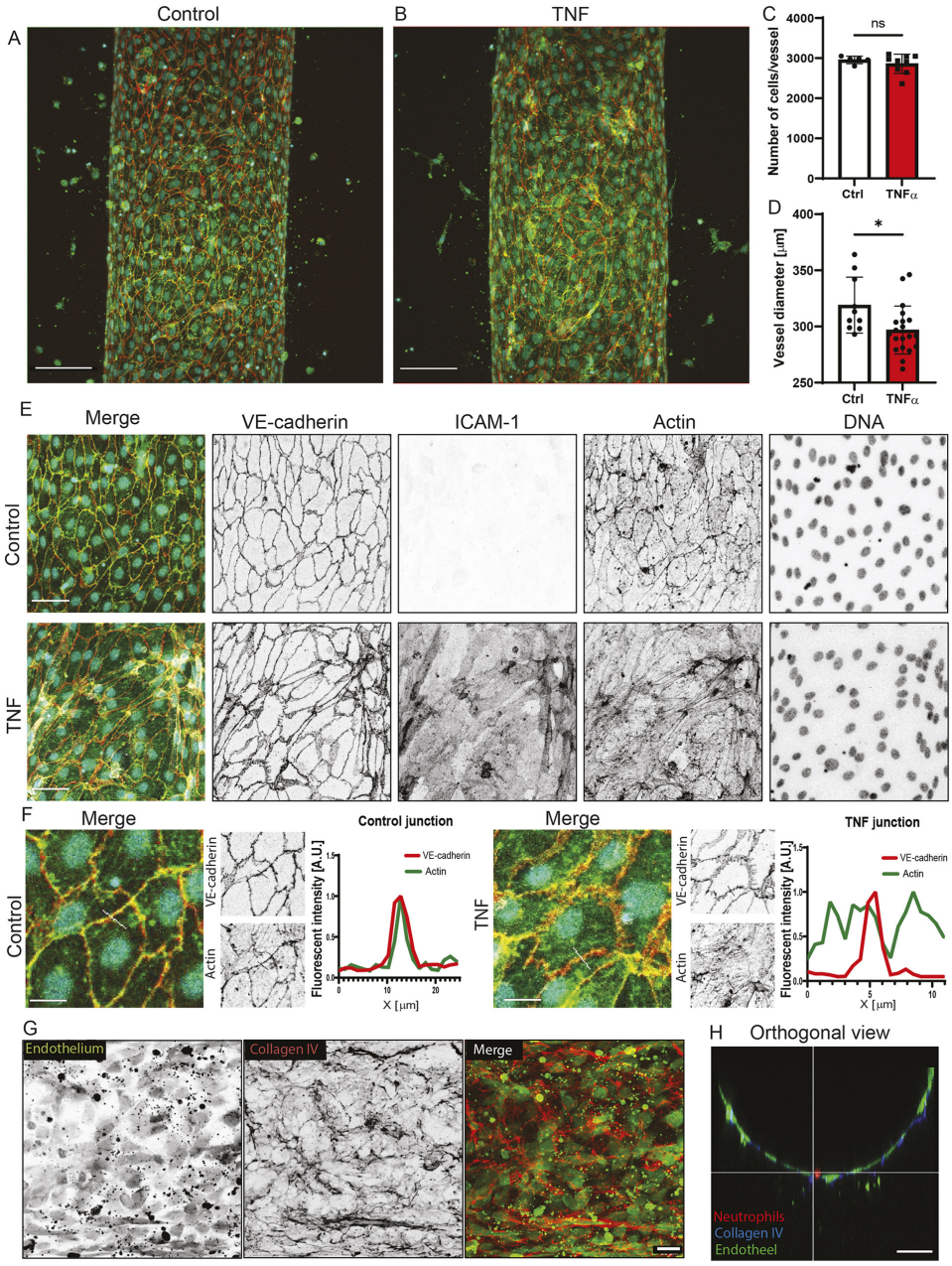

Figure 2. TNF-α in the vessel induces inflammation.
(A,B) Overview of a control (A) or TNF-α-treated vessel (B). (C,D) Quantification of the number of cells (C) and vessel diameter (D) in TNF-α-treated vessels compared to control vessels. ns, not significant; *P<0.05 (Student's t-test). (E,F) Representative images of control and inflamed endothelial cells (E) and junctions with line plots showing the localization of VE-cadherin and actin in these junctions (F). (G) Representative images of the presence of collagen IV around the vessels. (H) Orthogonal view of a vessel with collagen IV staining around. Scale bars: 100 µm (A,B), 50 µm (E,H), 25 µm (F,G). Data quantified from five control and nine TNF-α-treated BVOACs for the number of endothelial cells per BVOAC. Diameter measurements were taken on 10 control and 20 TNF-α-treated BVOACs. Staining and line plots were performed on three BVOACs per condition.

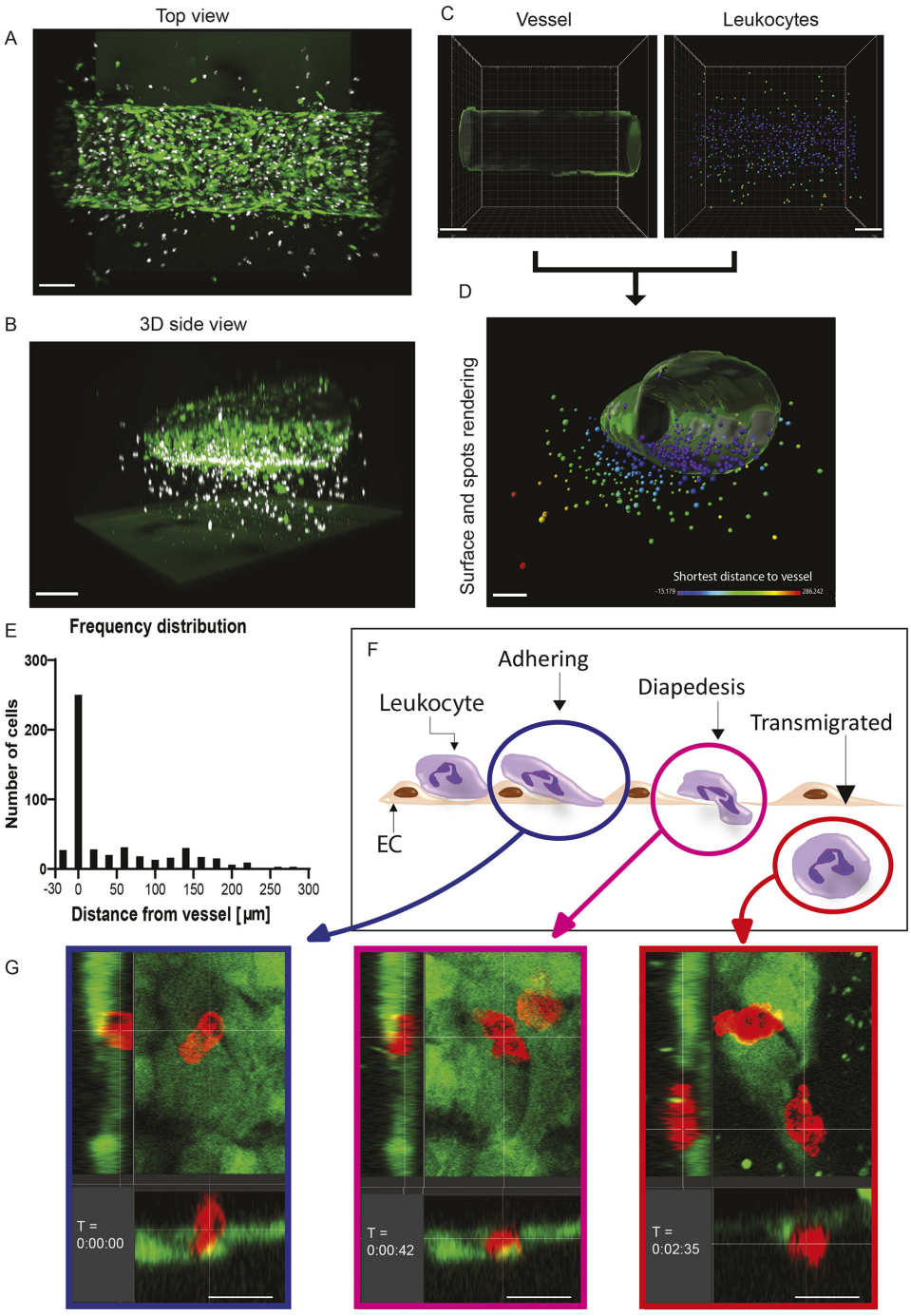

Figure 3. Vessel and leukocyte analysis in Imaris.
(A,B) Microscopy image depicting a BVOAC (green) with neutrophils (white) from top (A) and side view (B). (C) Surface of the BVOAC (left) and the leukocytes (right). (D) Overview of the BVOAC surface with colour-coded spots based on the distance from the surface, allowing calculations and analysis. (E) Distribution of the distance between the leukocytes and the vessel displayed in D. (F) Schematic overview of the different

transmigration steps: adhering to the endothelial cells on the inside of the lumen (blue circle), diapedeses (pink circle) and transmigrated cells (red circle). EC, endothelial cell. (G) Orthogonal view of stills taken from detailed high-speed imaging of neutrophil transendothelial migration (TEM) in the vessel over time. Scale bars: 150 µm (B,C), 100 µm (A,D), 15 µm (G).

In Movie 2, neutrophils transmigrate at the same spot, shortly after each other, indicating the possible presence of a transmigration hotspot (Grönloh et al., 2021). Quantification showed that the distance neutrophils travelled from the vessels into the matrix ranged from −18 µm (in the lumen) to 286 µm into the matrix (Fig. 3E). Neutrophils with a distance of ≤8 µm from the vessel were still adhering to the endothelium. From these data, we conclude that this new analysis tool can track individual neutrophils at all stages of TEM, comparable with *in vivo* analysis.

BVOAC allows chemokinesis-mediated TEM into the tissue

To quantify the number of neutrophils that left the vessel lumen and entered the matrix, we used a 3D rendering and tracking approach to study chemokine-induced neutrophil TEM under inflammatory conditions. This 3D rendering allowed us to observe a difference in number of transmigration events that was not detectable using a 2D analysis (Fig. 4A,B). Using this approach, we accurately discriminated between adherent and transmigrated neutrophils (Fig. 4A), revealing a strong increase in both leukocyte TEM states in TNF-α-stimulated vessels compared to control vessels (Fig. 4C). Interestingly, neutrophils that crossed TNF-α-stimulated endothelium migrated further away from the vessel than neutrophils that crossed untreated endothelium, indicating that the inflamed endothelium may stimulate neutrophil migration (Fig. 4D).

To test whether neutrophils respond to a chemotactic gradient, we injected C5a, a chemoattractant, into one of the matrix inlets (see schematic in Fig. 4E). Addition of C5a did not alter the number of neutrophils that crossed inflamed endothelium (Fig. 4H) but changed the migration direction of neutrophils towards C5a significantly (Fig. 4F,G,I). Interestingly, whereas the migration distance that neutrophils travelled was not different between the two sides under control conditions (Fig. 4J, left), in the presence of C5a on one side the migration distance towards this side was significantly increased (Fig. 4J, right). In summary, these data demonstrate that luminal application of TNF-α in this BVOAC model strongly enhances neutrophil extravasation and entry into the surrounding matrix, which can be directionally steered by applying a chemotactic gradient inside the matrix.

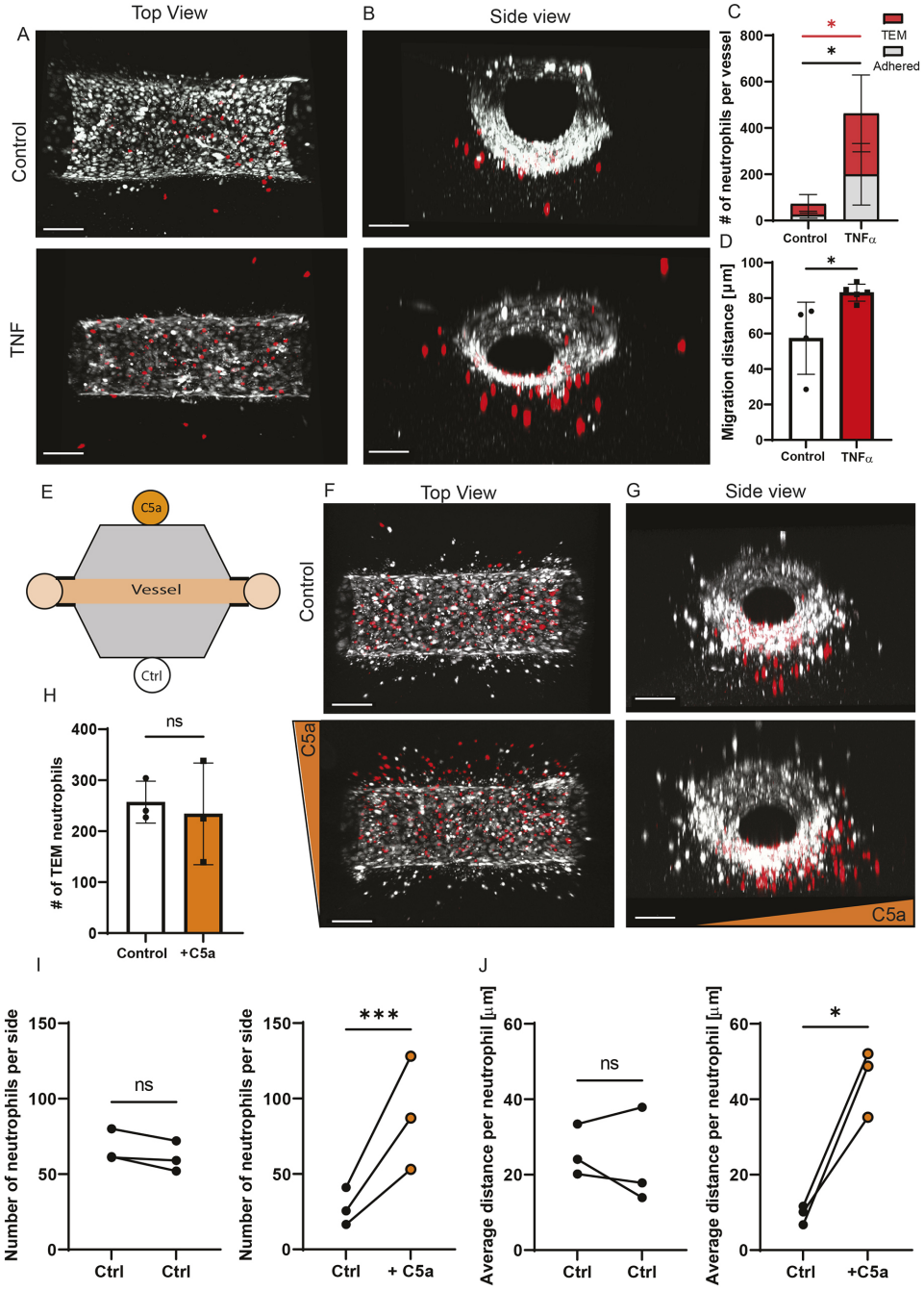

Figure 4. Neutrophil transmigration in a 3D environment.
(A,B) Representative top view (A) and side view (B) images of neutrophil transmigration in control and TNF-α-treated BVOAC. (C,D) Quantification of the number of neutrophils per field of view (C) and average transmigration distance after exiting the BVOAC (D). (E) Diagram of the experiment with one-sided addition of C5a. (F,G) Representative top view (F) and side view (G) images of neutrophil transmigration in TNF-α-treated BVOAC with C5a or PBS on one side. (H–J) Quantification of the total number of transmigrated neutrophils per

field of view (H), number of neutrophils per side of PBS (I, left)- and C5a (I, right)-treated BVOAC, and average migration distance between left and right of PBS (J, left)- or C5a (J, right)-treated BVOAC. Scale bars: 150 µm. Data quantified from four BVOACs per condition for neutrophil TEM and three BVOACs per condition for C5a TEM. ns, not significant; *P<0.05, ***P<0.001 [unpaired t-test (C,D), paired t-test (I,J)].

T-cell transmigration through a human umbilical vein endothelial cell (HUVEC)-lined vessel and neutrophil transmigration in pancreatic and lung microvascular vessels

To examine the versatility of this system and determine whether this system is also suitable for analysing T-cell TEM, we injected purified T-cells into the lumen of both inflamed and control vessels. After 2.5 h, vessels were flushed, fixed and imaged (Fig. 5A,B). We found that the number of adhered and transmigrated T-cells was five times increased in inflamed vessels compared to control conditions (Fig. 5C). In addition, T-cells migrated further into the underlying matrix when the vessels were inflamed (Fig. 5D), in line with the finding that neutrophils also extended their migration track when crossing inflamed endothelium. However, whereas neutrophils travelled from the vessel into the matrix for on average 83 µm, T-cells only travelled on average 44 µm, indicating that the intrinsic migration speed of neutrophils through the 3D matrix is 89% higher than that of T-cells.

In addition to using different leukocyte subsets, we analysed whether different endothelial cells may be used to generate the vessel. For this, we used human microvascular endothelial cells from the lungs and pancreas. Both cell types formed a nice vessel (Fig. 5E,F). Next, neutrophils were added to the vessels of both endothelial cell types, similar to previous experiments. Neutrophils transmigrated across both endothelial cell types and migrated into the matrix (Fig. 5G). Although the total number of cells in the field of view did not differ between lung and pancreas vessels (138 and 158, respectively), transmigration percentage was increased in the lung vessels (78% and 41%, respectively). The distance travelled by neutrophils from the vessel into the matrix was similar in both cell types (Fig. 5H). These data indicate that the BVOAC device is very versatile, both for different leukocyte and endothelial cell types, and can be adjusted to the research question that needs to be answered.

Live-cell imaging reveals differences in leukocyte migration

We next investigated the source of the difference in migration distance between T-cells and neutrophils. Although 3D confocal imaging analysis offers a more accurate detection of transmigration events compared to 2D widefield imaging, it does not allow us to distinguish between actual migration speed and relative track distance over time. Using high-speed imaging, we generated *z*-stacks of 200 µm with a time interval of 10 s, giving us sufficient spatiotemporal resolution for semi-automatic tracking of individual leukocytes through the collagen matrix in time. Automatic tracking was performed on all leukocytes in the field of view, after which tracks were filtered to exclude neutrophils exiting or entering the field of view. For analysis requiring complete leukocyte tracks, such as displacement or total track length, we selected ten tracks per experiment, which were manually checked to ensure quality of the data.

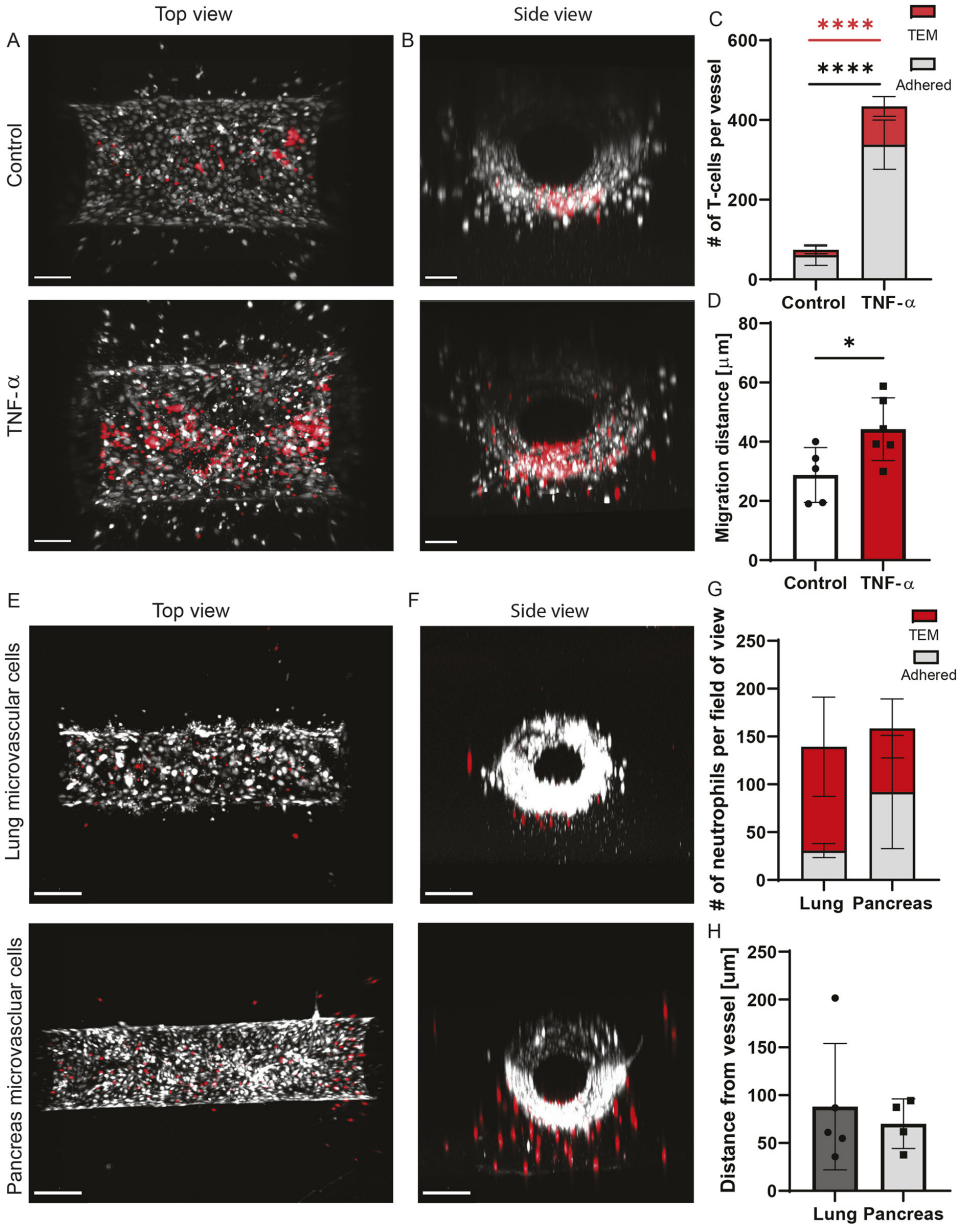

Figure 5. T-cell transmigration in a 3D-environment.
(A,B) Representative top view (A) and side view (B) images of T-cell transmigration in control and TNF-α-treated BVOAC. (C,D) Quantification of the number of transmigrated cells (C) and cumulative transmigration distance (D). (E,F) Representative top view (E) and side view (F) images of neutrophil transmigration in vessels lined with lung or pancreatic endothelial cells. (G,H) Quantification of the number of adhered and transmigrated cells (G) and migration distance of the transmigrated cells (H). Scale bars: 50 μm. Data quantified from four (pancreas), five (control, lung vessels) and six (TNF-α-treated) vessels per condition. *P<0.05, ****P<0.0001 (unpaired t-test).

Using this approach, we were able to track migrating neutrophils or T-cells in time in 3D (Fig. 6A,B; Movies 3 and 4). We found that the migration speed of T-cells inside the matrix after crossing the inflamed endothelium is significantly slower on average than that of neutrophils (Fig. 6C; 0.10±0.03 µm/s and 0.20±0.02 µm/s, respectively). Based on these measurements, neutrophil migration speed is 100% higher than that of T-cells, which is different from the 89% larger migration distance observed in the end-point experiment. To assess whether the speed of both leukocyte subsets was consistent over time from the initial start until the end of the recordings, we compared the initial and final migration speed, and found that both neutrophils and T-cells maintain a constant speed over time (Fig. 6D,E).

Next, we analysed the linearity of the migration tracks, which is defined as the ratio of the displacement over the total distance travelled by that cell (Boissonnas et al., 2007). This ratio has a maximum of 1, which occurs when the cells travelled in a straight line from the start position to the end position. We found that T-cells migrate in a more linear manner than neutrophils (Fig. 6F; 0.25±0.07 and 0.10±0.02, respectively). Accordingly, the total distance travelled within the same timeframe was higher for neutrophils than for T-cells (Fig. 6G; 948 µm versus 400 µm, respectively). These results indicated that neutrophils exerted a more intrinsic exploratory behaviour than T-cells in our system. Therefore, we conclude that neutrophils migrate faster but wander around more through the collagen, whereas T-cells migrate slower, but in a more directed fashion.

C5a gradient increases neutrophil speed in the first half hour

We examined to what extent the exploratory behaviour of neutrophils can be regulated by a chemotactic gradient such as C5a. Three-dimensional live imaging of neutrophil migration in the presence of a C5a gradient showed that most neutrophils migrated towards the chemoattractant (Fig. 7A,B; Movie 5), confirming our previous results. Interestingly, when analysing the direction of migration over time, we observed that the C5a-driven migration pattern occurred predominantly in the first 15 min of the experiment. After this time point, C5a-driven migration directionality was strongly diminished and neutrophil migration directionality appeared to be random, as if no chemoattractant was present (Fig. 7C,D). We also calculated the speed of the neutrophils that were exposed to C5a and found that, over the course of the experiment, the speed was reduced (Fig. 7E). We found that the migration linearity was significantly increased in the presence of C5a compared to the control condition (Fig. 7F; 0.17±0.04 versus 0.10±0.02, respectively). The decreased migration speed and increased directionality together led to a total migration distance that was not changed in the presence of C5a compared to control (Fig. 7G). These data indicate that the chemotactic gradient in the matrix disappeared in time, with the consequence that neutrophils change their migratory behaviour from a linear to a random migration pattern.

In conclusion, this BVOAC device enables us to accurately visualize and analyse TEM of primary human leukocytes in 3D over time, which can be modulated by applying a chemoattractant gradient. As such, this novel platform holds great promise for future studies

unravelling the complex cellular and molecular mechanisms that underlie leukocyte TEM.

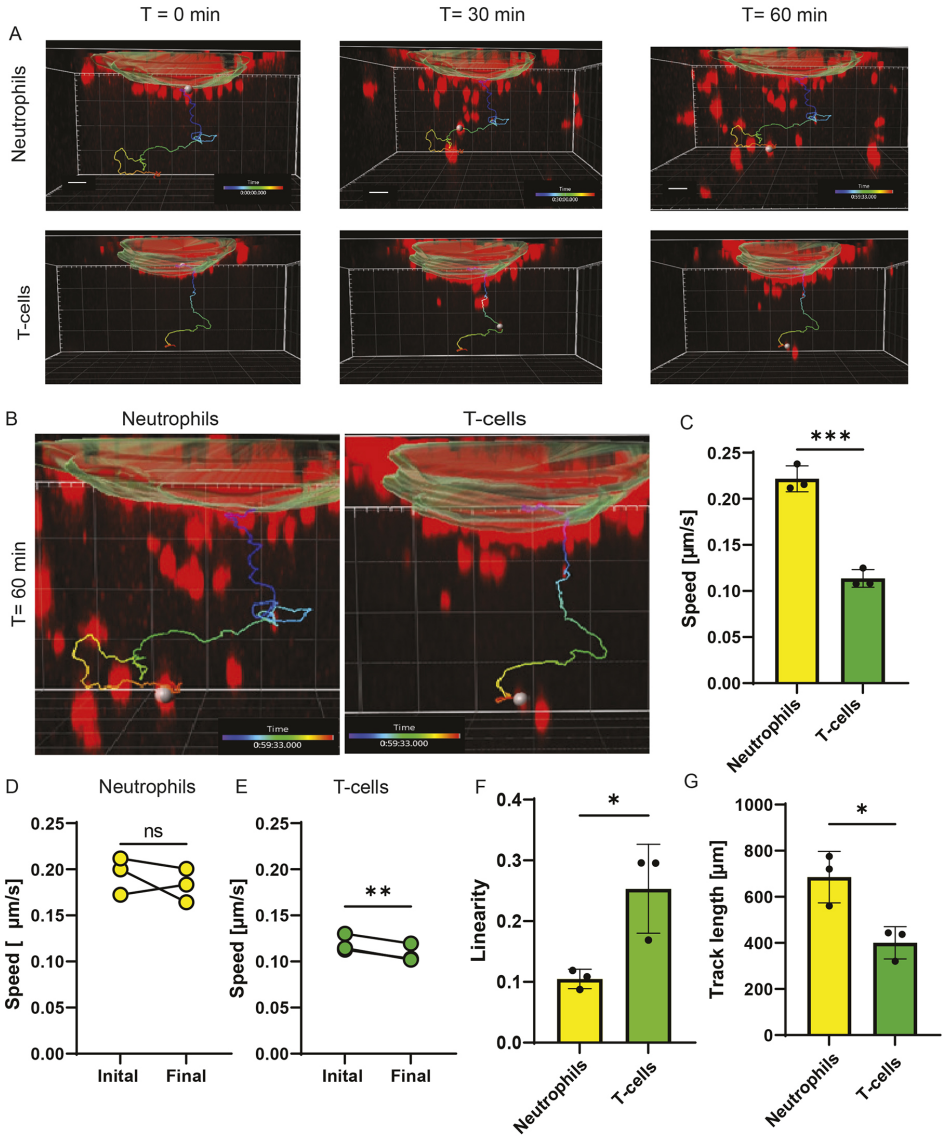

Fig. 6. Live transmigration of neutrophils and T-cells.
(A) Stills from a video in which neutrophils (top row) and T-cells (bottom row) migrate out of the BVOAC. Per condition, one track representing the general migration manner of that leukocyte is highlighted. (B) Zoom-in on the track at t=60 of both neutrophils (left) and T-cells (right). (C–G) Quantification of the average track speed (C), initial and final migration speed of neutrophils (D) and T-cells (E), linearity (F) and track length (G) for both neutrophils and T-cells. Scale bars: 50 µm. Data quantified from ten cells per BVOAC and three BVOACs per condition. ns, not significant; *P<0.05,
**P<0.01, ***P<0.001 (unpaired t-test).

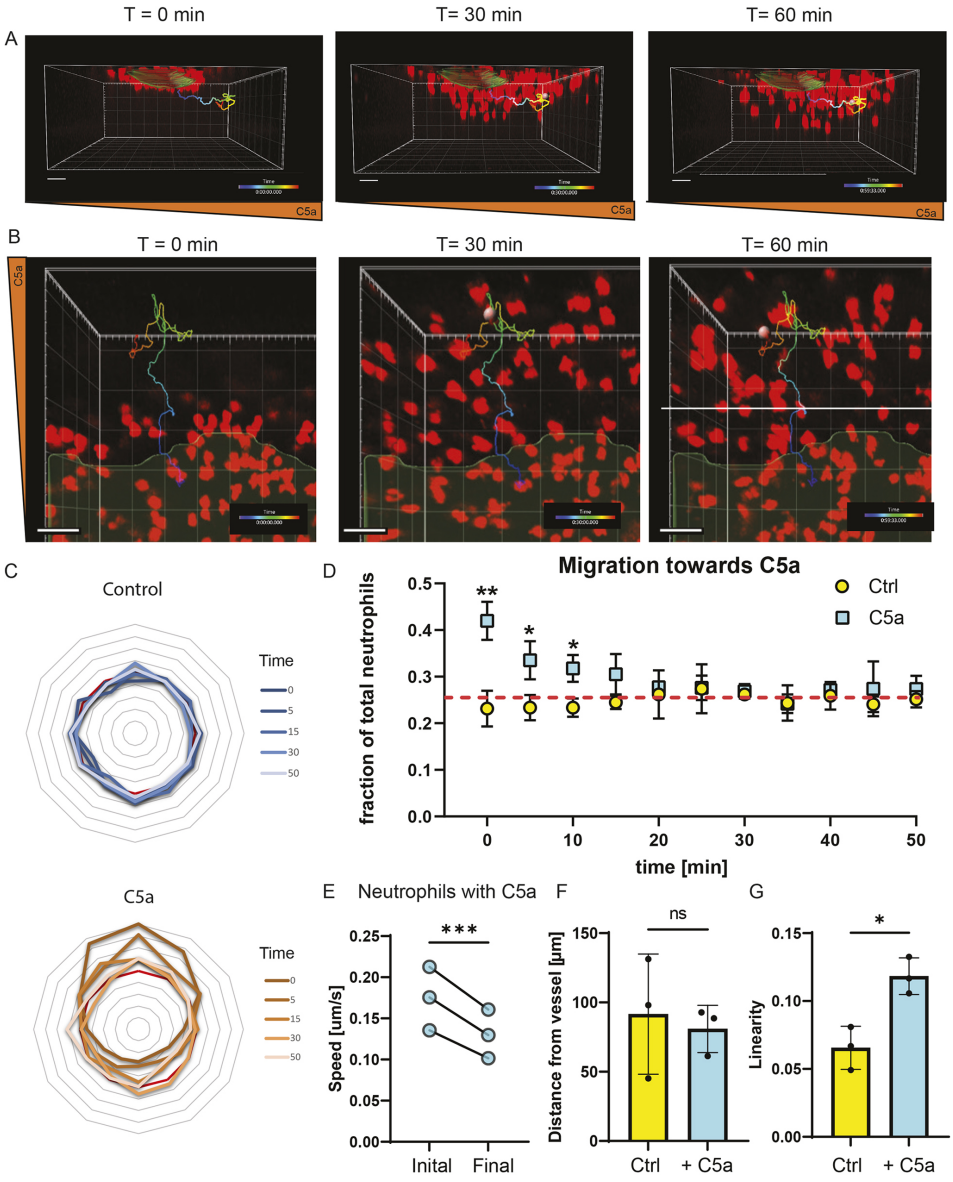

Fig. 7. Live transmigration of neutrophils andmigration dynamics with C5a.
(**A,B**) Stills from a movie showing the migration of neutrophils towards one side from side (**A**) and top (**B**) view. (**C**) The wind rose plots show the distribution of leukocyte migration directions at distinct times as shown in the keys. Each concentric axis indicates 1.7% of the total number of neutrophil movements at the indicated time. (**D**) Quantification of the direction of neutrophils in the control and C5a condition over time. The red dashed line represents the situation in which leukocyte migration in every direction is equal, and directionality is not observed. (**E–G**) Quantification of the initial and final speed of neutrophils in the presence of C5a (**E**), end-point distance from the vessel (**F**), and the ratio between the endpoint distance from the vessel and the total length travelled, also called linearity (**G**). Scale bars: 50 µm. Data quantified from ten cells per BVOAC and three BVOACs per condition. ns, not significant; *P<0.05, **P<0.01, ***P<0.001 [unpaired t-test (**D,F,G**); paired t-test (**E**)].

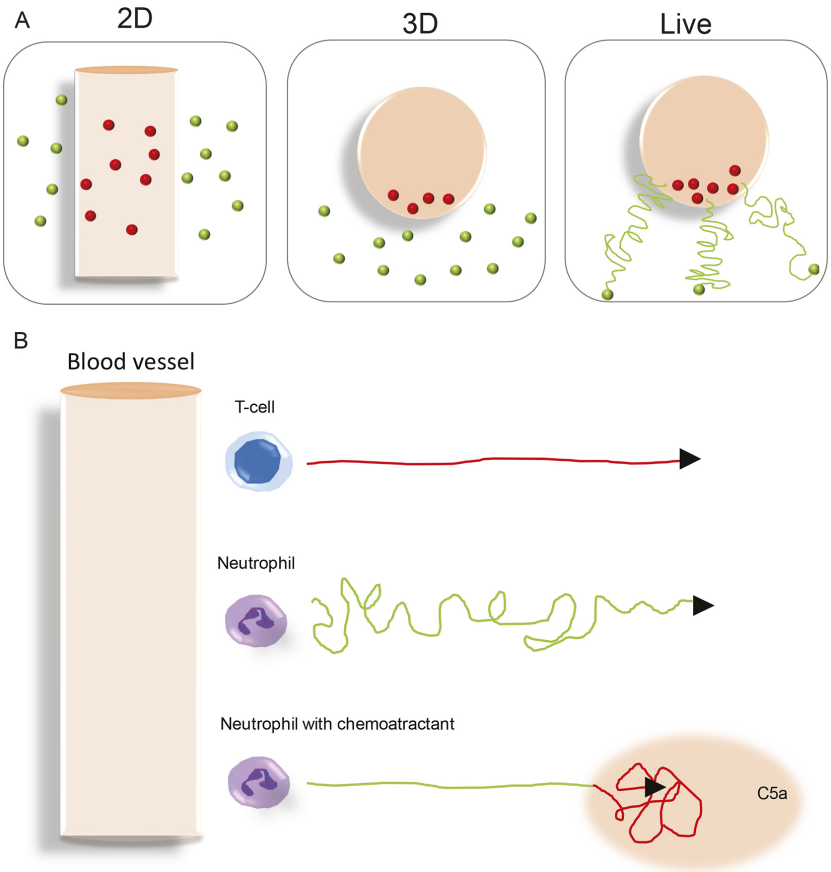

Fig. 8. Different imaging methods to study different aspects of leukocyte (trans)migration.
(**A**) Schematic representation of the similar experiment imaged in 2D, 3D or live 3D and with leukocytes perceived to be outside of the vessel indicated as green dots. 2D imaging underestimates the number of extravasated leukocytes because cells underneath the vessel are indistinguishable from cells inside the BVOAC. 3D live imaging allows the tracking of cells over time and therefore analysis of migration dynamics, which is not possible based on 3D endpoint imaging. (**B**) Migration dynamics of different leukocytes in a 3D matrix. T-cells migrate slower and more linearly, whereas neutrophils travel faster while wandering around. When adding a chemoattractant to neutrophils, they initially migrate at a similar speed compared to control, but much more linearly. Over time, however, they lose speed and directionality. Red, slower migration; green, faster migration.

DISCUSSION

Leukocyte extravasation through the vessel wall is mostly studied using classical *in vitro* 2D models that allow for analysis of the molecular details of this process. However, in these models, endothelial cells are typically cultured on artificial stiff substrates, which alters endothelial behaviour and responses. Moreover, these models preclude analysis of the final part of the leukocyte extravasation, penetration of the surrounding matrix. Thus, there

is an urgent need for a proper *in vitro* model that mimics the *in vivo* conditions and allow the study of molecular details of this process. We demonstrate that a hydrogel-based BVOAC model perfectly meets these demands and allow study of the full extravasation process at the single-cell level in 3D over time.

In the human body, inflammation typically leads to vasoconstriction by contracting smooth muscle cells around the vessel wall (Pleiner et al., 2003; Lim and Park, 2014). Leukocyte extravasation mostly occurs in inflamed post-capillary venules, where the blood vessels only consist of a single layer of endothelial cells (Baluk et al., 1998). Because inflammatory mediators such as TNF-α induce strong F-actin stress fibres, they are expected to induce cellular tension and potential contraction on an endothelial monolayer (Wójciak-Stothard et al., 1998). In 2D monolayers, TNF-α stimulation leads to the formation of intracellular gaps, an observation that is supported by an increase in permeability. However, using the BVOAC model, we confirmed that TNF-α increased the number of F-actin stress fibres, and the vessel lumen diameter was reduced, instead of a loss of contact between individual endothelial cells and the formation of intracellular gaps. In addition, in the human body, vessels are surrounded by a collagen IV layer (Yurchenco, 2011; Xu and Shi, 2014). In our system, this collagen IV layer was also present, mimicking *in vivo*-like conditions. This indicated that the BVOAC much better represents the physiological situation than any 2D cell culture model used to study inflammation-related events.

In addition, when culturing endothelial cells on glass or plastics, F-actin stress fibres are prominently present through the cell body, even without inflammatory stimuli. In human arteries, these fibres are also prominently present; however, in veins and post-capillary venules, such fibres are lacking (Van Geemen et al., 2014). Under control conditions, the BVOAC model represents the *in vivo* non-inflamed condition, as we observed no endothelial F-actin stress fibres. Only upon stimulation with TNF-α do stress fibres appear in the cell body. Therefore, we conclude that our *in vitro*-generated vessels accurately represent both resting and inflamed states of blood vessels *in vivo*, and thus are a major improvement compared to conventional inflammatory 2D models.

Another point where the BVOAC system shows its potential as a model is importance of real-time analysis of migrating leukocytes in 3D. When comparing end-point measurements with real-time TEM data, we found that our analysis of fixed samples leads to a large underestimation of the migration distance, particularly for leukocytes such as neutrophils that exhibit a strong exploratory behaviour. A schematic representation illustrating the various measurement methods and the difference they report for identical events is displayed in Fig. 8A. Based on end-point measurement, we observed that neutrophils migrated further away from the vessel than T-cells in the same timeframe, indicating higher migration speed for neutrophils. Using live imaging, we found that the effect is even larger than expected due to their exploratory behaviour through the matrix. Live imaging also allowed us to discriminate between migration behaviour of the neutrophil away from, but also back towards, the vessel. This type of migration behaviour would otherwise not be observed.

T-lymphocyte migration is characterized by the stop-and-go manner they display to survey the environment, which makes speed measurements challenging (Dupré et al., 2015; Jerison and Quake, 2020). Sadjadi and colleagues investigated the migration speed of T-cells in different collagen concentrations (Sadjadi et al., 2020). They tested 2, 4 and 5 mg/ml. In our system, we used ~2.5 mg/ml and measured a speed of 6 µm/min, comparable with the speed observed by Sadjadi et al. in 2 mg/ml collagen. This is supported by the study of Niggemann et al., who found a migration speed of 7 µm/min in a collagen concentration of 1.67 mg/ml (Niggemann et al., 1997). *In vivo*, higher migration speeds are observed (10–15 µm/min), but this depends on activation status and differs between organs (Miller et al., 2002). Neutrophil migration speed measured in our system is 12 µm/min. A recent study by Wolf et al. measured speed of neutrophils in 3.3 mg/ml and 8 mg/ml collagen gels and observed migration speeds of 5–10 µm/min (Wolf et al., 2018). Considering that the collagen concentration in our study is slightly lower, the speeds found in our experiments support the speeds mentioned in the literature for both T-cells and neutrophils.

The hydrogel-based BVOAC system allows us to study the full TEM process in real time in great detail, not hampered by the limitations of classical TEM models. However, there is an important parameter of TEM lacking in this system, which is flow. The importance of flow for endothelial cell function has been shown extensively and is known to affect TEM (Kitayama et al., 2000; Conway et al., 2017; Polacheck et al., 2017). The addition of flow to our BVOAC model would be the next important step, allowing us to investigate the full TEM multistep process from rolling and adhesion, to transmigration and penetration of the collagen matrix in one assay.

Using the BVOAC, we found that neutrophils migrate twice as fast as T-cells, and that both cell types showed increased migration distance in 3D when first crossing an inflamed endothelial lining. This finding highlights the benefits and opportunities of a BVOAC model over 2D models. Moreover, neutrophils migrate in a random fashion whereas T-cells have a much more directed migration pattern. Under a chemotactic gradient, neutrophil migration adopts more T-cell-like directionality for a limited amount of time, before reverting to the exploratory migration pattern. Schematic representations of the various migration dynamics are shown in Fig. 8B. Because of the real-time imaging possibility, we found that neutrophils can also migrate back to the vessel once they have entered the matrix. Others have reported on this phenomenon, called reverse transmigration, as well, using *in vivo* animal models (Woodfin et al., 2011; Colom et al., 2015). The BVOAC model now opens new opportunities to study reverse transmigration at the molecular level. This remarkable migration behaviour can also be found when neutrophils do not sense the chemotactic gradient anymore, indicating that the endothelial vessel wall might, in fact, attract neutrophils back once the final destination in the tissue has been reached and gradients are cleared. This type of migration is typical for resolving inflammation and was studied using *in vivo* models (Peiseler and Kubes, 2018; Bogoslowski et al., 2020). In this situation, the BVOAC model may offer new opportunities to study this migration behaviour as well.

In conclusion, TEM experiments with the BVOAC platform enable the exploration of many parameters previously unobtainable. The level of imaging and analysis determines which aspects of the leukocyte extravasation can be observed. Our comparison between 2D, 3D and live 3D imaging of leukocyte TEM dynamics demonstrates that it is imperative to image and analyse TEM experiments in 3D over time for an accurate interpretation of the events in this system. This hydrogel-based BVOAC model now facilitates studying the full process of human leukocyte extravasation under inflammatory conditions *in vitro* and thereby identifying the underlying cellular characteristics and molecular requirements.

MATERIALS AND METHODS

Cell culture and seeding

Pooled HUVECs (Lonza, P1052, C2519A) were cultured at 37°C with 5% CO_2 on fibronectin-coated culture flasks in endothelial cell growth medium 2 (EGM-2; Promocell, C22011) supplemented with supplement mix (Promocell, C39216). HUVECs were passaged at 60–70% confluency and used for experiments between passage 3 and 7. Pulmonary (Pelobiotech, PB-CH-147-4011) and lung (Lonza, CC-2527) microvascular cells were cultured at 37°C with 5% CO_2 on fibronectin-coated culture flasks in SupplementPack Endothelial Cell GM2 (Sigma-Aldrich), containing 0.01 ml/ml L-glutamine (G3202), 0.02 ml/ml fetal calf serum (FCS; C-37320), 5 ng/ml human epidermal growth factor (C-30224), 0.2 µg/ml hydrocortisone (C-31063), 0.5 ng/ml vascular endothelial growth factor 165 (C-3260), 10 ng/ml human basic fibroblast growth factor (C-30321), 20 ng/ml insulin-like growth factor (R3; C-31700), 1 µg/ml ascorbic acid (C-31750). The cells were passaged at 60–70% confluency and used for experiments between passage 5 and 8.

Collagen gel preparations

All following steps were carried out on ice to halt polymerization of the collagen. Then, 50 µl of 10× PBS (Gibco, 70011-044) was added carefully on top of 250 µl bovine collagen type-1 (10 mg/ml FibriCol, Advanced BioMatrix, 5133) and mixed. When the solution was sufficiently mixed, 48.6 µl of 0.1 M NaOH was added, and the mixture was put on ice for 10 min. pH was checked before mixing 1:1 with cell culture medium, bringing the final collagen concentration to 2.5 mg/ml.

3D vessel production

The LumeNext devices were obtained from the Beebe laboratory (University of Wisconsin School of Medicine and Public Health, WI, USA; see https://mmbwisc.squarespace.com/). The hollow chambers were coated with 1% polyethylenimine (Polysciences, 23966) and incubated for 10 min at room temperature (RT). Sequentially, chambers were coated with 0.1% glutaraldehyde (Merck, 104239) and washed 5× with water for injection (WFI; Gibco,

A12873-01). Chambers were air-dried before addition of collagen. Collagen was prepared according to the protocol above. Collagen (5 µl) was added to the chambers and allowed to polymerize for 30 min. Each chamber is ~2 mm^3 in total. PBS-drenched cotton balls were added to the device to prevent drying of the collagen. When polymerization of collagen was confirmed, rods were removed and medium was added to the lumen. HUVECs were dissociated using trypsin/EDTA (Sigma-Aldrich, T4049), neutralized 1:1 with trypsin-neutralizing solution (Lonza, CC-5002), spun down and concentrated to 15×10^6 cells/ml in EGM-2. Five microlitres of cell suspension were added per vessel, and the devices were placed in a head-over-head rotator for 2 h at 1 RPM at 37°C with 5% CO_2 for seeding. Medium was replaced twice daily, and vessels were allowed to mature for 2 days before use.

Neutrophil and T-cell isolation

Polymorphonuclear neutrophils were isolated from whole blood derived from healthy donors who signed an informed consent under the rules and legislation in place within the Netherlands and maintained by the Sanquin Medical Ethical Committee. Heparinized whole blood was diluted (1:1) with 10% (v/v) trisodium citrate diluted in PBS. Diluted whole blood was pipetted carefully on 12.5 ml Percoll (RT) 1.076 g/ml. Tubes were centrifuged (Rotanta 96R) at 450 ***g***, slow start, low brake for 20 min. Plasma and the peripheral blood mononuclear cell (PBMC) ring fraction were removed. Erythrocytes were lysed in an ice-cold isotonic lysis buffer (155 mM NH_4Cl, 10 mM $KHCO_3$, 0.1 mM EDTA, pH 7.4 in WFI) for 10 min. Neutrophils were pelleted at 450 ***g*** for 5 min at 4°C, resuspended in lysis buffer and incubated for 5 min on ice. Neutrophils were centrifuged again at 450 ***g*** for 5 min at 4°C, washed once with PBS, centrifuged again at 450 ***g*** for 5 min at 4°C and resuspended in HEPES medium [20 mM HEPES, 132 mM NaCl, 6 mM KCl, 1 mM $CaCl_2$, 1 mM $MgSO_4$, 1.2 mM K_2HPO_4, 5 mM glucose (Sigma-Aldrich) and 0.4% (w/v) human serum albumin (Sanquin Reagents), pH 7.4] and kept at room temperature for no longer than 4 h until use. This isolation method typically yields >95% purity.

Cytotoxic T lymphocytes (CTLs) were isolated from density-gradient isolated PBMCs by use of magnetic separation. Whole blood was diluted 1:1 with balanced salt solution at RT and layered onto Ficoll Paque PLUS (GE Healthcare, GE17-1440-02) followed by centrifugation at 400 ***g*** for 30 min. From here on, cells and buffers were kept at 4°C. The PBMC ring fraction was harvested and washed three times using isolation buffer (PBS+0.5% FCS). CTLs were isolated negatively using a Miltenyi CD8 T-cell isolation kit (Miltenyi, 130-096-495) with LS columns (Miltenyi, 130-042-401) and a QuadroMACS, according to the manufacturer's instructions. Afterwards, CTLs were harvested and resuspended in RPMI 1640 (Thermo Fisher Scientific, 61870010) containing 10% FBS and kept at 37°C in 5% CO_2 overnight until use. T-cell purity is typically >95–98% $CD8^+$ T cells.

Immunofluorescence staining

The vessel lumen was washed three times with PBS++ (PBS with 1 mM $CaCl_2$, 0.5 mM

$MgCl_2$) and fixed with 4% paraformaldehyde (PFA; Merck, 30525-89-4) at 37°C for 15 min. Afterwards, vessels were incubated with directly conjugated antibodies in PBST (PBS with 0.2% bovine serum albumin and 0.1% Tween) overnight at 4°C. After staining, vessels were washed three times with PBS and kept at 4°C before imaging. The following antibodies and stains were used according to manufacturers' protocols: mouse anti-hVE-cadherin/CD144 Alexa Fluor 647 conjugated (55-7H1; BD, 561567; 1:200), phalloidin Alexa Fluor 488 conjugated (Molecular Probes, A12379; 1:500), Hoechst 33342 (Molecular Probes, H-1399; 1:50,000), mouse anti-hICAM-1 Alexa Fluor 546 conjugated (15.2; Santa Cruz Biotechnology, sc-107AF546; 1:200) and anti-collagen IV (Abcam, ab6586; 1:100).

FITC-dextran leakage assay

Six microlitres of 70 kDa FITC-dextran in EGM-2 (5 mg/ml; Merck, 46945) were added to each vessel. Thrombin (1 U/ml, Merck, T1063) was added to the dextran and injected at the same time. The device was placed under a widefield microscope, and, every 10 s, an image was captured. Images were analysed in Fiji (ImageJ, version 1.52). Fluorescent intensity was measured over the cross-section of the vessel at six time points throughout the movie.

TEM assay

Endothelial cells were stained with CellTracker™ Green CMFDA Dye (1 µM; Molecular Probes, C7025), according to the manufacturer's protocol, before seeding. TNF-α (10 ng/ml; Peprotech, 300-01A) was added overnight inside the vessel. Leukocytes were stained with Vybrant™ DiD Cell-Labelling Solution (1 µM; Molecular Probes) for 15 min at 37°C, pelleted at 450 ***g*** for 5 min, washed, pelleted again and resuspended in medium, before 2 µl of 16×10^6 neutrophils or T-cells per ml was added per vessel. For live imaging, migration was imaged for 60 min; for end-point conditions, neutrophils were allowed to migrate for 2.5 h at 37°C. Vessels were flushed with PBS++ and fixed for 15 min with 4% PFA. Vessels were stored in PBS at 4°C until imaging.

Imaging and analysis

Brightfield images were acquired on an Axio Observer Microscope (ZEISS) using Zen 2 blue edition using a 10× air objective (ZEISS, 420341-9911, Plan-Neofluor 10×/0.3 Ph1). Fluorescent staining of the vessels was imaged using a SP8 confocal microscope (Leica) with a 25× long working distance water objective (Leica, 15506375, HC FLUOTAR L 25×/0.95 NA). Control and inflamed vessels were imaged using identical settings. TEM experiments (both live and fixed) were imaged on an LSM980 Airyscan2 (ZEISS) with a 10× air objective (ZEISS, 420640-9900-000, Objective Plan-Apochromat 10×/0.45 NA). Laser power was kept to a minimum to limit phototoxicity during live imaging. The transmigration assays and the 3D rendering and orthogonal views were analysed with Imaris Bitplane software (version 9.5/9.6), while the leakage data, zoom-in on the cell junctions and collagen IV staining were analysed with Fiji (ImageJ, version 1.52).

3D analysis in Imaris

To analyse the distance from the neutrophils to the surface of the vessel, the spot function was applied to automatically detect fluorescently labelled neutrophils, and a surface rendering of the vessel was generated from the XYZ-fluorescent label. The vessel surface was created manually by tracing the outline of the vessel; the software then rendered a cylindrical shape corresponding to the immunofluorescent signal. Possible holes were automatically filled by the software. The spot function was applied automatically with the same parameters for all experiments, but checked manually afterwards to ensure that detection was correct. When both the vessel surface and spots were created, data such as number of neutrophils and distance to the vessels could be extracted from the Imaris spot function and further analysed in Excel.

Statistics

Statistics were performed in GraphPad Prism 9 (version 9.0.1). Data were checked for normality via the Anderson–Darling test. If normally distributed, a (paired) Student's *t*-test was used to test for statistical significance.

FOOTNOTES

Author contributions

Conceptualization: A.C.I.v.S., L.K., M.A.N., J.D.v.B.; Methodology: A.C.I.v.S., L.K., D.J.B.; Software: M.B.; Validation: A.C.I.v.S., L.K.; Formal analysis: A.C.I.v.S., L.K., R.S., M.B.; Investigation: A.C.I.v.S., L.K.; Resources: A.C.I.v.S., L.K. D.J.B.; Data curation: A.C.I.v.S., L.K., R.S.; Writing – original draft: A.C.I.v.S., L.K., M.A.N., J.D.v.B.; Writing – review & editing: A.C.I.v.S., L.K., R.S., M.B., M.A.N., J.D.v.B.; Visualization: A.C.I.v.S., L.K.; Supervision: M.A.N., J.D.v.B.

Funding

This work was supported by grants from the Landsteiner Foundation for Blood Transfusion Research [1649 to A.C.I.v.S.; 1820 to L.K.], the National Institutes of Health [R01AI134749, R33CA225281 and P30CA014520 to D.J.B.] and ZonMW [NWO Vici grant 91819632 to J.D.v.B.]. Deposited in PMC for release after 12 months.

Competing interests

D.J.B. holds equity in Bellbrook Labs LLC, Tasso Inc., Salus Discovery LLC, Lynx Biosciences Inc., Stacks to the Future LLC, Turba LLC, Flambeau Diagnostics LLC and Onexio Biosystems LLC. D.J.B. is also a consultant for Abbott Laboratories.

REFERENCES

Ando, K., Fukuhara, S., Moriya, T., Obara, Y., Nakahata, N. and Mochizuki, N. (2013). Rap1 potentiates endothelial cell junctions by spatially controlling myosin I activity and actin organization. *J. Cell Biol*. 202, 901-916. doi:10.1083/jcb.201301115

Baluk, P., Bolton, P., Hirata, A., Thurston, G. and McDonald, D. M. (1998). Endothelial gaps and adherent leukocytes in allergen-induced early- and late-phase plasma leakage in rat airways. *Am. J. Pathol*. 152, 1463-1476.

Bogoslowski, A., Wijeyesinghe, S., Lee, W.-Y., Chen, C.-S., Alanani, S., Jenne, C., Steeber, D. A., Scheiermann, C., Butcher, E. C., Masopust, D. et al. (2020). Neutrophils recirculate through lymph nodes to survey tissues for pathogens. *J. Immunol*. 204, ji2000022. doi:10.4049/jimmunol.2000022

Boissonnas, A., Fetler, L., Zeelenberg, I. S., Hugues, S. and Amigorena, S. (2007). In vivo imaging of cytotoxic T cell infiltration and elimination of a solid tumor. *J. Exp. Med*. 204, 345-356. doi:10.1084/jem.20061890

Colom, B., Bodkin, J. V., Beyrau, M., Woodfin, A., Ody, C., Rourke, C., Chavakis, T., Brohi, K., Imhof, B. A. and Nourshargh, S. (2015). Leukotriene B4-neutrophil elastase axis drives neutrophil reverse transendothelial cell migration in vivo. *Immunity* 42, 1075-1086. doi:10.1016/j.immuni.2015.05.010

Conway, D. E., Coon, B. G., Budatha, M., Arsenovic, P. T., Orsenigo, F., Wessel, F., Zhang, J., Zhuang, Z., Dejana, E., Vestweber, D. et al. (2017). VE-cadherin phosphorylation regulates endothelial fluid shear stress responses through the polarity protein LGN. *Curr. Biol*. 27, 2219-2225.e5. doi:10.1016/j.cub. 2017.06.020

Dupré, L., Houmadi, R., Tang, C. and Rey-Barroso, J. (2015). T lymphocyte migration: an action movie starring the actin and associated actors. *Front. Immunol*. 6, 586. doi:10.3389/fimmu.2015.00586

Farahat, W. A., Wood, L. B., Zervantonakis, I. K., Schor, A., Ong, S., Neal, D., Kamm, R. D. and Asada, H. H. (2012). Ensemble analysis of angiogenic growth in three-dimensional microfluidic cell cultures. *PLoS ONE 7*, e37333. doi:10.1371/journal.pone.0037333

Grönloh, M. L. B., Arts, J. J. G. and Van Buul, J. D. (2021). Neutrophil transendothelial migration hotspots – mechanisms and implications. *J. Cell Sci*. 134, jcs255653. doi:10.1242/jcs.255653

Heller, R. A. and Krönke, M. (1994). Tumor necrosis factor receptor-mediated signaling pathways. *J. Cell Biol*. 126, 5-9. doi:10.1083/jcb.126.1.5

Huynh, J., Nishimura, N., Rana, K., Peloquin, J. M., Califano, J. P., Montague, C. R., King, M. R., Schaffer, C. B. and Reinhart-King, C. A. (2011). Age-related intimal stiffening enhances endothelial permeability and leukocyte transmigration. *Sci. Transl. Med*. 3, 112ra122. doi:10.1126/scitranslmed.3002761

Jerison, E. R. and Quake, S. R. (2020). Heterogeneous T cell motility behaviors emerge from a coupling between speed and turning in vivo. *eLife* 9, 1-26. doi:10.7554/eLife.53933

Jiménez-Torres, J. A., Peery, S. L., Sung, K. E. and Beebe, D. J. (2016). LumeNEXT: a practical method to pattern luminal structures in ECM gels. *Adv. Healthcare Mater*. 5, 198-204. doi:10.1002/adhm.201500608

Kim, S., Chung, M., Ahn, J., Lee, S. and Jeon, N. L. (2016). Interstitial flow regulates the angiogenic response and phenotype of endothelial cells in a 3D culture model. *Lab. Chip* 16, 4189-4199. doi:10.1039/C6LC00910G

Kitayama, J., Hidemura, A., Saito, H. and Nagawa, H. (2000). Shear stress affects migration behavior of polymorphonuclear cells arrested on endothelium. *Cell. Immunol*. 203, 39-46. doi:10.1006/cimm.2000.1671

Lim, S. and Park, S. (2014). Role of vascular smooth muscle cell in the inflammation of atherosclerosis. *BMB*

Reports 47, 1-7. doi:10.5483/BMBRep.2014.47.1.285

Miller, M. J. (2002). Two-photon imaging of lymphocyte motility and antigen response in intact lymph node. *Science* 296, 1869-1873. doi:10.1126/science.1070051

Muller, W. A. and Luscinskas, F. W. (2008). Chapter 9 assays of transendothelial migration in vitro. *Methods Enzymol*. 443, 155-176. doi:10.1016/S0076-6879(08)02009-0

Niggemann, B., Maaser, K., Lü, H., Kroczek, R., Zänker, K. S. and Friedl, P. (1997). Locomotory phenotypes of human tumor cell lines and T lymphocytes in a three-dimensional collagen lattice. *Cancer Lett*. 118, 173-180. doi:10.1016/S0304-3835(97)00328-5

Peiseler, M. and Kubes, P. (2018). Macrophages play an essential role in trauma-induced sterile inflammation and tissue repair. *Eur. J. Trauma and Emerg. Surg*. 44, 335-349. doi:10.1007/s00068-018-0956-1

Pleiner, J., Mittermayer, F., Schaller, G., Marsik, C., Macallister, R. J. and Wolzt, M. (2003). Inflammation-induced vasoconstrictor hyporeactivity is caused by oxidative stress. *J. Am. Coll. Cardiol*. 42, 1656-1662. doi:10.1016/j.jacc.2003.06.002

Polacheck, W. J., Kutys, M. L., Yang, J., Eyckmans, J., Wu, Y., Vasavada, H., Hirschi, K. K. and Chen, C. S. (2017). A non-canonical Notch complex regulates adherens junctions and vascular barrier function. *Nature* 552, 258-262. doi:10.1038/nature24998

Sadjadi, Z., Zhao, R., Hoth, M., Qu, B. and Rieger, H. (2020). Migration of cytotoxic T lymphocytes in 3D collagen matrices. *Biophys. J.* 119, 2141-2152. doi:10.1016/j.bpj.2020.10.020

Sobrino, A., Phan, D. T. T., Datta, R., Wang, X., Hachey, S. J., Romero-López, M., Gratton, E., Lee, A.P., Gratton, E., Lee, A. P., George, S. C. and Hughes, C. C. W. (2016). 3D microtumors *in vitro* supported by perfused vascular networks. Sci. Rep. 6, 1-11. doi:10.1038/srep31589

Stroka, K. M. and Aranda-Espinoza, H. (2011). Endothelial cell substrate stiffness influences neutrophil transmigration via myosin light chain kinase-dependent cell contraction. *Blood* 118, 1632-1640. doi:10.1182/blood-2010-11-321125

Van Geemen, D., Smeets, M. W. J., Van Stalborch, A.-M. D., Woerdeman, L. A. E., Daemen, M. J. A. P., Hordijk, P. L. and Huveneers, S. (2014). F-actin-anchored focal adhesions distinguish endothelial phenotypes of human arteries and veins. *Arterioscler. Thromb. Vasc. Biol*. 34, 2059-2067. doi:10.1161/ATVBAHA.114.304180

Van Nieuw Amerongen, G. P., Draijer, R., Vermeer, M. A. and Van Hinsbergh, V.W.M. (1998). Transient and prolonged increase in endothelial permeability induced by histamine and thrombin: role of protein kinases, calcium, and RhoA. *Circ. Res*. 83, 1115-1123. doi:10.1161/01.RES.83.11.1115

Virumbrales-Munõz, M., Ayuso, J. M., Gong, M. M., Humayun, M., Livingston, M. K., Lugo-Cintrón, K. M., Mcminn, P., Álvarez-Garcí,Y. R. and Beebe, D. J. (2020). Microfluidic lumen-based systems for advancing tubular organ modeling. *Chem. Soc. Rev*. 49, 6402-6442. doi:10.1039/D0CS00705F

WójciakStothard, B., Entwistle, A., Garg, R. and Ridley, A. J. (1998). Regulation of TNF-α-induced reorganization of the actin cytoskeleton and cell-cell junctions by Rho, Rac, and Cdc42 in human endothelial cells. *J. Cell. Physiol*. 176, 150-165. doi:10.1002/(SICI)1097-4652(199807)176:1<150::AID-JCP17>3.0.CO;2-B

Wolf, K., Textor, J., Hustin, L. S. P., Wolf, K., Koenderman, L. and Vrisekoop, N. (2018). Immature neutrophils released in acute inflammation exhibit efficient migration despite incomplete segmentation of the nucleus. *J. Immunol*. 202, 207-217. doi:10.4049/jimmunol.1801255

Wong, K. H. K., Chan, J. M., Kamm, R. D. and Tien, J. (2012). Microfluidic models of vascular functions. *Annu.*

Rev. Biomed. Eng. 14, 205-230. doi:10.1146/annurev-bioeng-071811-150052

Woodfin, A., Voisin, M. B. and Nourshargh, S. (2010). Recent developments and complexities in neutrophil transmigration. *Curr. Opin Hematol*. 17, 9-17. doi:10.1097/MOH.0b013e3283333930

Woodfin, A., Voisin, M.-B., Beyrau, M., Colom, B., Caille, D., Diapouli, F.-M., Nash, G. B., Chavakis, T., Albelda, S. M., Rainger, G. E. et al. (2011). The junctional adhesion molecule JAM-C regulates polarized transendothelial migration of neutrophils *in vivo*. *Nat. Immunol*. 12, 761-769. doi:10.1038/ni.2062

Xu, J. and Shi, G.-P. (2014). Vascular wall extracellular matrix proteins and vascular diseases. *Biochim. Biophys. Acta* 1842, 2106-2119. doi:10.1016/j.bbadis.2014.07.008

Yamada, K. M. and Sixt, M. (2019). Mechanisms of 3D cell migration. *Nat. Rev. Mol. Cell Biol*. 20, 738-752. doi:10.1038/s41580-019-0172-9

Yurchenco, P. D. (2011). Basement membranes: cell scaffoldings and signaling platforms. Cold Spring *Harbor Perspect. Biol*. 3, 1-27. doi:10.1101/cshperspect.a004911

Zervantonakis, I. K., Hughes-Alford, S. K., Charest, J. L., Condeelis, J. S., Gertler, F. B. and Kamm, R. D. (2012). Three-dimensional microfluidic model for tumor cell intravasation and endothelial barrier function. *Proc. Natl. Acad. Sci*. USA 109, 13515-13520. doi:10.1073/pnas.1210182109

Zheng, Y., Chen, J., Craven, M., Choi, N. W., Totorica, S., Diaz-Santana, A., Kermani, P., Hempstead, B., Fischbach-Teschl, C., Lopez, J. A. et al. (2012). In vitro microvessels for the study of angiogenesis and thrombosis. *Proc. Natl. Acad. Sci. USA* 109, 9342-9347. doi:10.1073/pnas.1201240109

SUPPLEMENTAL FILES

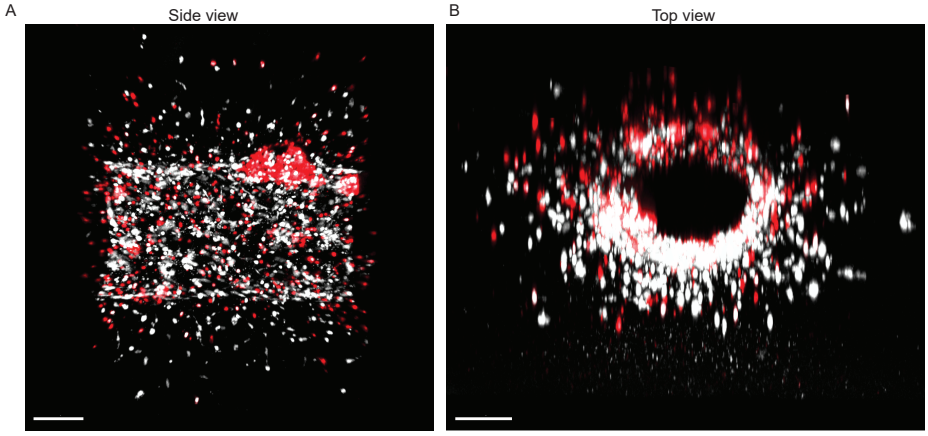

Fig. S1. Neutrophil transmigration during continuous turning.
Representative top view (**A**) and side view (**B**) image of neutrophil transmigration in TNF-α treated BVOAC that was placed in a head-over-head during the 2 hour transmigration period. Scalebar = 150 µm.

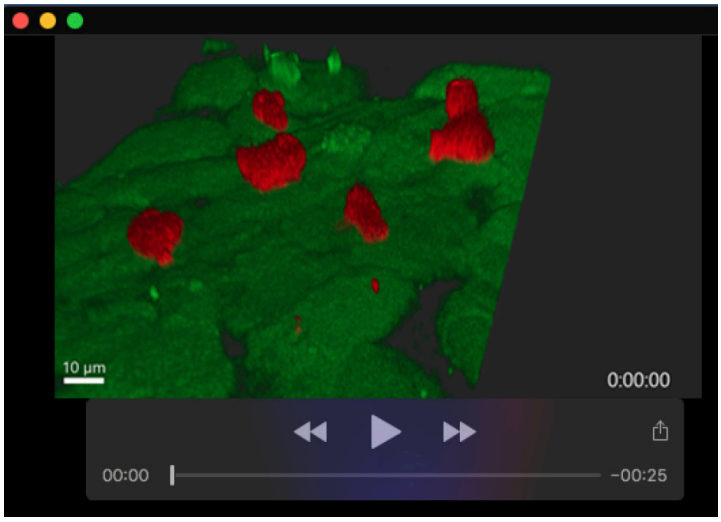

Movie 1. Neutrophil transmigration through the endothelial wall of the BVOAC in high resolution over time.
The video is a blended projection of 3D imaging over time of neutrophils extravasating from the lumen of the BVOAC, through the vessel wall and into the collagen matrix surrounding the vessel. The video rotates the scene to give an overview of the red neutrophils in the lumen of the vessel on top of the green endothelial cell layer. Green blobs inside the lumen are detached and rounded up HUVEC. At 10 seconds into the video the experiment starts playing and 2 red neutrophils start poking through the vessel wall after which the time is paused and the scene is rotated to show the outside of the endothelial layer with the neutrophils poking through. The scene then changes back to inside the lumen and resumes playing at 18 seconds showing the neutrophils both crossing the barrier layer until finally they have completely crossed the endothelium and are seen migrating at the basolateral side of the endothelium. Time elapsed in the experiment is shown in the bottom right corner of the video and the adaptive scale bar is shown in the bottom left of the video.

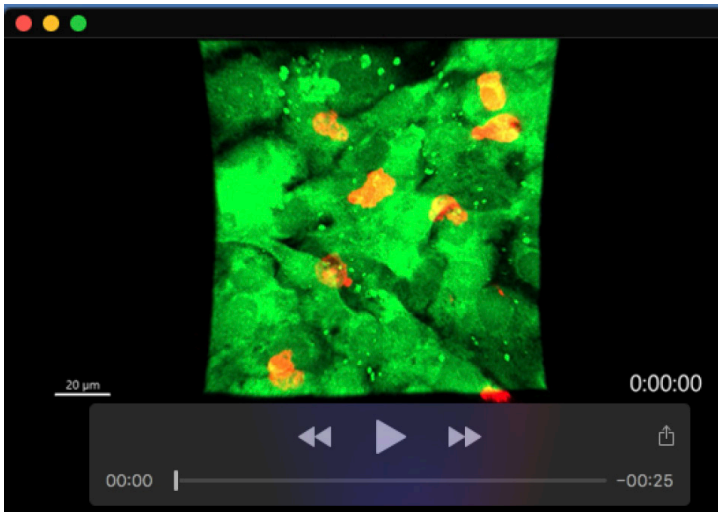

Movie 2. Data of experiment shown in supplemental video 1 with rendered surfaces to further reveal details of the TEM event.
The video shows the raw data in a MIP projection and rotates the scene 360 degrees first before zooming in on the location where 2 neutrophils sequentially migrate at the same junction. The rendered volumes are projected on top of the MIP projection of the data at 9 seconds into the video, to clarify outlines of the EC and the 2 neutrophils focussed in this rendering. The video then plays the experiment over time until 17 seconds where the neutrophil is poking through the endothelial layer. The video stops the time and rotates to show the leading edge of the neutrophil in the matrix outside of the endothelial barrier. The video afterwards resumes displaying the experiment over time. Time elapsed in the experiment is shown in the bottom right corner of the video and the adaptive scale bar is shown in the bottom left of the video.

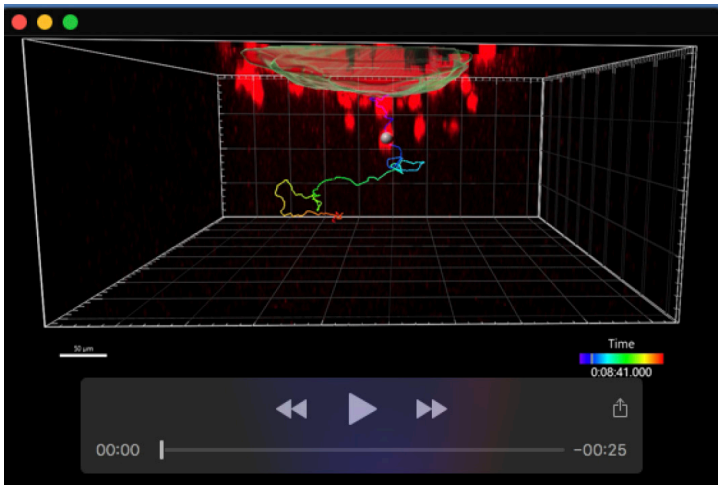

Movie 3. Neutrophils migrating out of the BVOAC lumen into the collagen matrix imaged in 3D over one hour displayed from a side view.
This experiment shows the raw data of red labelled neutrophils migrating out of the CellTracker green stained HUVEC vessel rendered in transparent green. HUVEC were treated overnight with TNF-α to induce inflammation. To capture as many neutrophils as possible the bottom part of the vessel and a large part of the collagen matrix were imaged. To illustrate the path travelled by a single neutrophil, the track is shown in a colour coded line which represents the time passed in the experiment. Scale bar for size is shown in the left bottom corner of the video and time including colour legend is shown in the bottom right of the video.

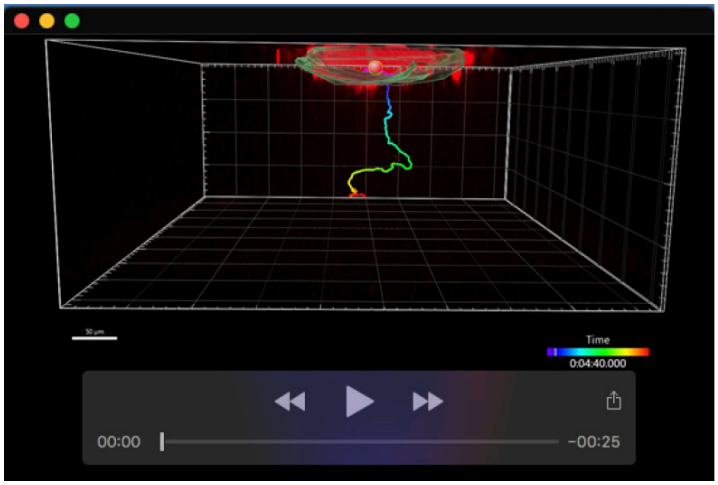

Movie 4. T-cells migrating out of the BVOAC lumen into the collagen matrix imaged in 3D over one hour displayed from a side view.
This experiment shows the raw data of red labelled T-cells migrating out of the CellTracker green stained HUVEC vessel rendered in transparent green. HUVEC were treated overnight with TNF-α to induce inflammation. To capture as many events as possible the bottom part of the vessel and a large part of the collagen matrix were imaged. To illustrate the path travelled by a single T-cell the track is shown in a colour coded line which represents the time passed in the experiment. Scale bar for size is shown in the left bottom corner of the video and time including colour legend is shown in the bottom right of the video.

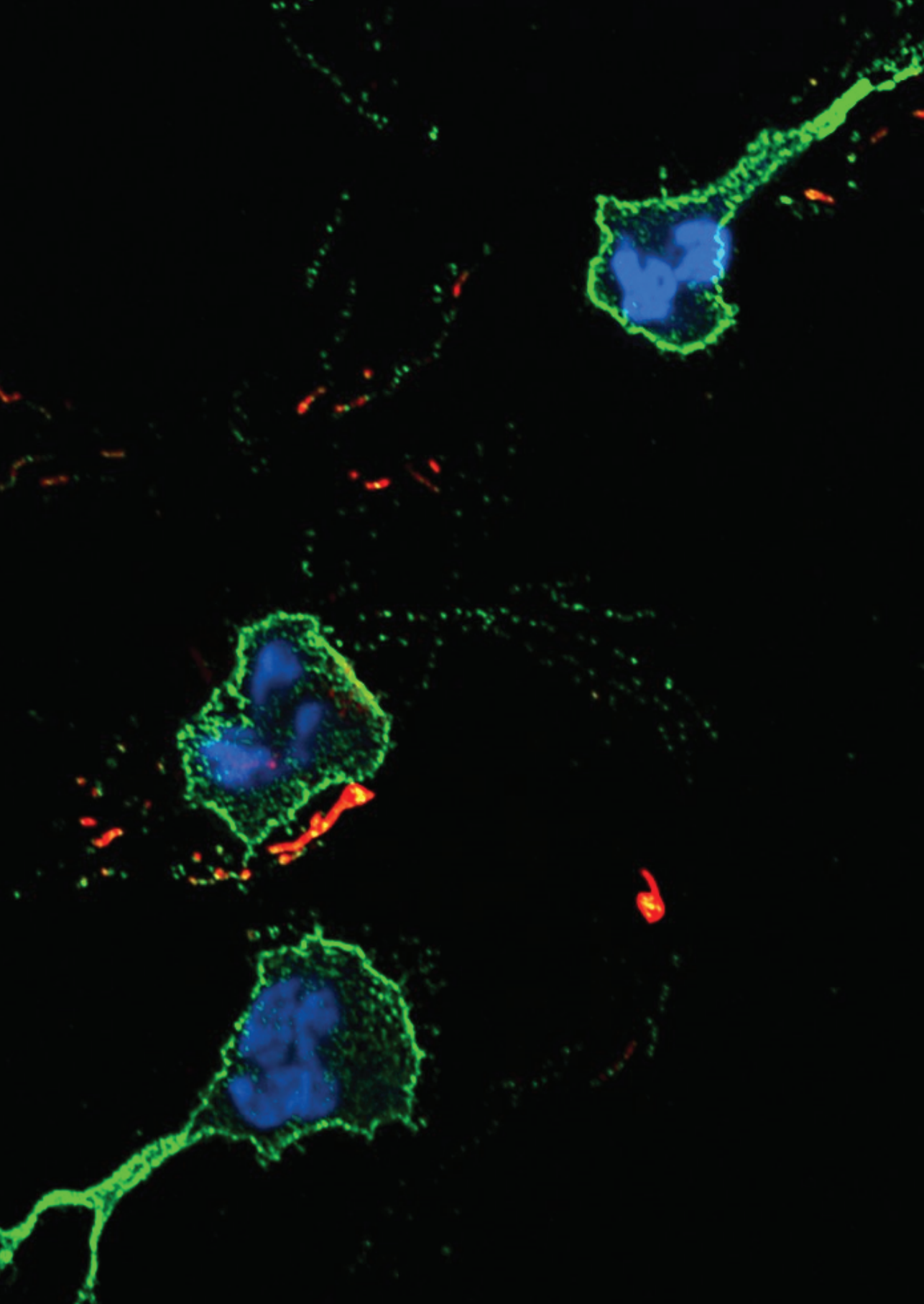

CHAPTER 7

Defective Neutrophil Transendothelial Migration and Lateral Motility in ARPC1B Deficiency Under Flow Conditions

Abraham C.I. van Steen [1†]
Lanette Kempers [1†]
Evelien G. G. Sprenkeler [2,3*†]
Jaap D. van Buul [1,4*‡]
Taco W. Kuijpers [2,3‡]

[1] *Molecular Cell Biology Laboratory, Department of Molecular and Cellular Haemostasis, Sanquin Research, Amsterdam University Medical Center (AUMC), Amsterdam, Netherlands*

[2] *Department of Blood Cell Research, Sanquin Research, AUMC, University of Amsterdam, Amsterdam, Netherlands*

[3] *Department of Pediatric Immunology, Rheumatology and Infectious Diseases, Emma Children's Hospital, AUMC, University of Amsterdam, Amsterdam, Netherlands*

[4] *Leeuwenhoek Centre for Advanced Microscopy, Section Molecular Cytology, Swammerdam Institute for Life Sciences, University of Amsterdam, Amsterdam, Netherlands*

Frontiers in immunology 12 (2021): 678030

ABSTRACT

The actin-related protein (ARP) 2/3 complex, essential for organizing and nucleating branched actin filaments, is required for several cellular immune processes, including cell migration and granule exocytosis. Recently, genetic defects in ARPC1B, a subunit of this complex, were reported. Mutations in *ARPC1B* result in defective ARP2/3-dependent actin filament branching, leading to a combined immunodeficiency with severe inflammation. *In vitro*, neutrophils of these patients showed defects in actin polymerization and chemotaxis, whereas adhesion was not altered under static conditions. Here we show that under physiological flow conditions human ARPC1B-deficient neutrophils were able to transmigrate through TNF-α-pre-activated endothelial cells with a decreased efficiency and, once transmigrated, showed definite impairment in subendothelial crawling. Furthermore, severe locomotion and migration defects were observed in a 3D collagen matrix and a perfusable vessel-on-a-chip model. These data illustrate that neutrophils employ ARP2/3-independent steps of adhesion strengthening for transmigration but rely on ARP2/3-dependent modes of migration in a more complex multidimensional environment.

INTRODUCTION

Neutrophils are the most abundant type of leukocytes in the human circulation and important effector cells in the innate immune system. They are the first cells recruited to sites of infection or inflammation, where they extravasate through the blood vessel into the tissue. This process, also known as transendothelial migration (TEM), can be divided into several steps, namely tethering, selectin-mediated rolling and slow rolling, selectin-mediated and chemokine-mediated integrin activation resulting in arrest, adhesion strengthening, spreading, intravascular crawling, and transmigration (either paracellular or transcellular) (1). Once neutrophils cross the endothelial cell layer they encounter a second barrier, the vascular basement membrane (BM). This BM provides structural support for endothelial cells and is composed of a network of multiple extracellular matrix (ECM) proteins, including laminins and collagen type IV (2). After crossing these layers, neutrophils continue to migrate and enter the tissue to reach and fight infection.

By studying rare primary immunodeficiencies (PIDs), essential proteins in the different steps of TEM have been identified. Well-known PIDs resulting in defective TEM are leukocyte adhesion deficiencies (LADs), where patients have mutations in genes involved in leukocyte integrin signaling (LAD-I and LAD-III), resulting in an adhesion defect. In LAD-II, defective fucosylation of selectin ligands results in the inability of neutrophils to bind to endothelial selectins (E- and P-selectins), resulting in a rolling defect (3).

In 2017, a novel PID involving infections, bleeding episodes, allergy and auto-inflammation was identified caused by mutations in the *ARPC1B* gene (4). ARPC1B is one of 7 subunits of the actin-related protein (ARP) 2/3 complex, which is required for the formation of branched actin networks as it nucleates a daughter filament to the side of a pre-existing actin filament (5). These branched actin filaments are of vital importance for the formation of lamellipodia at the leading edge of migrating cells. Analysis of patient-derived neutrophils showed a defect in actin polymerization, resulting in a severe chemotaxis defect through 3-µm pore-size filters (4). Here we investigated ARPC1B-deficient neutrophil migration in more depth by using TEM flow and 3D vessel-on-a-chip models allowing us to monitor the full process of neutrophil migration from the vessel lumen into the tissue environment.

MATERIALS AND METHODS

Isolation of Human Primary Cells From Patient and Controls

Heparinized venous blood was drawn from healthy controls and an ARPC1B-deficient patient after informed consent had been obtained. A detailed description of the patient's history has been reported previously (4). Neutrophils were isolated as previously described (6). Subsequently, neutrophils ($5x10^6$/mL) were fluorescently labelled with Vybrant™ DiD Cell-Labeling Solution (dilution 1:1,000; Invitrogen, Carlsbad, CA, USA) or calcein-AM (33.3

ng/mL; Molecular Probes, Eugene, OR, USA) for 20 minutes at 37°C, washed twice in PBS, and resuspended to a concentration of $1x10^6$/mL in HEPES medium (containing 132 mM of NaCl, 20 mM of HEPES, 6.0 mM of KCl, 1.0 mM of $MgSO_4$, 1.0 mM of $CaCl_2$, 1.2 mM of potassium phosphate, 5.5 mM of glucose, and 0.5% (wt/vol) human serum albumin, pH 7.4). Labelling of neutrophils did not influence their TEM capacity as compared to unlabeled cells (data not shown).

All experiments involving human blood samples were conducted in accordance to the Declaration of Helsinki. The study was approved by the local ethical committees of the Amsterdam University Medical Center and Sanquin Blood Supply, Amsterdam, The Netherlands.

SDS-PAGE and Western Blot Analysis

Total cell lysates were prepared from freshly purified neutrophils. Samples were separated by SDS polyacrylamide gel electrophoresis and transferred onto a nitrocellulose membrane. Individual proteins were detected with antibodies against ARPC1B (rabbit polyclonal, Sigma-Aldrich, St Louis, MO, USA) and actin (mouse monoclonal, Sigma-Aldrich).

Secondary antibodies were donkey anti-mouse-IgG IRDye 800CW or donkey-anti–rabbit-IgG IRDye 680LT (LI-COR Biosciences, Lincoln, NB, USA). Visualization of bound antibodies was performed on an Odyssey Infrared Imaging system (LI-COR Biosciences).

Neutrophil Adhesion (Static Condition)

Neutrophils ($5x10^6$/mL) were labeled with calcein-AM (1 µM; Molecular Probes, Eugene, OR, USA) for 30 minutes at 37°C, washed twice in PBS, and resuspended to a concentration of $2x10^6$/mL in HEPES medium. Neutrophil adhesion was determined on an uncoated 96-well MaxiSorp plate (Nunc, Wiesbaden, Germany) in response to numerous stimuli as described previously (4).

Flow Cytometry

Flow cytometry was performed to assess the expression of various neutrophil surface markers. Fluorescein isothiocyanate (FITC)-, allophycocyanin (APC), phycoerythrin (PE), Brilliant Violet 510 (BV510)-, or Alexa Fluor 647 (AF647)-labelled monoclonal antibodies and isotype controls were used according to the instructions of the manufacturer. Antibodies were CD18-FITC (mouse IgG1 clone MEM48, Diaclone, Besançon cedex, France), CD11a-FITC (mouse IgG2a, Sanquin reagents, Amsterdam, The Netherlands), CD11b-FITC (mouse IgM clone CLB-mon-gran/1, B2, Sanquin reagents), CD11c-FITC (mouse IgG1 clone BU15, Bio-Rad, Kidlington, UK) CD66b-FITC (mouse IgG1 clone CLB-B13.9, Sanquin reagents), L-selectin-APC (mouse IgG clone DREG-56, BD Pharmingen, San Diego, CA, USA), CD177-FITC (mouse IgG1 clone MEM-166, Bio-Rad), FPR1-FITC (mouse IgG2a clone 350418, R&D Systems, Minneapolis, MN, USA), TNFRI-PE (mouse IgG1 clone 16803, R&D Sytems), TNFRII-APC (mouse IgG2A clone 22235, R&D Sytems), TLR4-APC (mouse IgG2A clone HTA125,

Invitrogen), ICAM-1-AF647 (mouse IgG1 clone 15.2, Bio-Rad), PECAM-1-BV510 (mouse IgG1 clone WM59, BD Biosciences, San Jose, CA, USA), JAM-A (mouse IgG1 clone WK9, Thermo Fisher Scientific, Waltham, MA, USA).

Samples were analyzed on a FACSCanto-II flow cytometer using FACS-Diva software (BD Biosciences). Neutrophils were gated based on their forward- and side scatter. Per sample, 10,000 gated events were collected. Data were analyzed with FACS-Diva software.

Endothelial Cell Culture

Pooled human umbilical vein endothelial cells (HUVEC P1052; Lonza, Basel, Switzerland, cat C2519A) were cultured at 37°C with 5% CO_2 in fibronectin-coated 10 cm tissue culture plastic petri dishes in Endothelial cell growth medium (EGM-2; PromoCell, Heidelberg, Germany, cat C22011) supplemented with supplementMix (Promocell, cat C39216). The HUVECs were passaged at 60-70% confluency and used for experiments at passage 3-4.

Transendothelial Migration Under Physiological Flow Conditions

Neutrophil transendothelial migration under flow conditions was assessed as described previously (7), with the exception of labeling of endothelial junctional VE-cadherin and PECAM-1. Neutrophils were flowed over the endothelium for a total of 45 minutes. To induce inflammation, HUVECs were stimulated with 10 ng/mL tumor necrosis factor-alpha (TNF-α; Peprotech, London, United Kingdom) overnight for 16 hours. Neutrophil migration was analyzed using IMARIS Bitplane software (Version 9.5/9.6). Tracking was done using assisted automatic tracking of the neutrophils using manual parameters to classify superendothelial and subendothelial neutrophils. Speed is calculated as the scalar equivalent of the object velocity. We used the track speed mean = average velocity of the spots over time according to the IMARIS reference manual 9.2.0. TEM time was analyzed using Fiji (ImageJ, version 1.52).

Collagen Gel Preparation

All following steps were carried out on ice to halt polymerization of the collagen. 50 µl of 10x PBS (Gibco, Thermo Fisher Scientific, cat 70011-044) was added to of 400 µl of bovine collagen type-1 (10 mg/mL FibriCol; Advanced BioMatrix, San Diego, CA, USA, cat 5133) and gently mixed. Subsequently, pH was set to 7.4 using 48.6 µl of 0.1M NaOH and checked. The collagen was then diluted 1:1 with medium to achieve a final collagen concentration of 4 mg/mL for vessel-on-a chip or 3D collagen experiments.

Migration in 3D Collagen Matrix

The 8 mg/mL neutralized collagen was mixed 1:1 with HEPES medium containing $8*10^6$ neutrophils and complement component 5a (C5a; 10 nM; Sino Biological, Wayne, PA, USA). An 8 µl drop of this mixture was placed in the middle of a well of an µ-Slide 8 Well (Ibidi, Gräfelfing, Germany, cat 80826) and flattened with a coverslip, creating a ±10 µm 3D matrix. The device was placed at 37°C for 30 minutes to allow collagen polymerization before adding

250 µL HEPES medium supplemented with 10 nM C5a (37°C). Neutrophil migration was then assessed using an LSM980 Airyscan2 (ZEISS, Oberkochen, Germany) using a 10x air objective (ZEISS, 420640-9900-000, Objective Plan-Apochromat 10x/0.45). Every 5 seconds an image was taken for 50 minutes in total. For integrin blocking experiments, neutrophils were pre-incubated with 10 µg/mL anti-CD11b monoclonal antibody (mAb) clone 44a and 10 µg/mL anti-CD18 mAb clone IB4 for 20 minutes. These antibodies were isolated from the supernatant of hybridoma clones obtained from the American Type Culture Collection (Rockville, MD, USA). Neutrophil migration through the collagen matrix was analyzed in IMARIS Bitplane software (Version 9.5/9.6). The tracking was performed automatically using the autoregressive motion algorithm and checked manually for accuracy. Speed is calculated as the scalar equivalent of the object velocity. We used the track speed mean = average velocity of the spots over time according to the IMARIS reference manual 9.2.0.

Perfusable Vessel-on-a-Chip

The vessels-on-a chip were made using the devices developed by the lab of Beebe, as previously described (8). Minor alterations to the protocol were made. Briefly, the devices were coated with 1% PEI (Polysciences Inc., Warrington, PA, USA, #23966) and incubated for 10 minutes at room temperature (RT). Sequentially chambers were coated with 0.1% glutaraldehyde (Merck, Darmstadt, Germany, #104239), washed 5x with water for injection (WFI; Gibco, #A12873-01) and air-dried. Collagen-1 was prepared according to the protocol above. 10 µl Collagen-1 was added to each chamber and polymerized for 30 minutes at 37°C, 5% CO_2. PBS-drenched cotton balls were added to the device to control humidity of the device. Rods were removed using tweezers and EGM-2 was added to the lumen. HUVECs were washed twice with PBS, trypsinized for 5 minutes, treated with trypsin neutralizing solution (TNS; Lonza, cat CC-5002) and centrifuged for 5 minutes at 200xg. HUVECs were then stained using CellTracker™ Green CMFDA Dye (1 µM; Molecular Probes, cat C7025) according to manufactures protocol, washed twice with PBS and pelleted. HUVECs were then resuspended to a concentration of $15*10^6$ cells/mL. 5µl of cell suspension was added to each lumen and placed in head-over-head at 37°C, 5% CO_2 for 2 hours at 1 RPM. Vessels were matured for 2 days with medium replacement twice daily.

Neutrophil Transendothelial Migration and Migration Through Collagen Matrix

To induce inflammation, the vessels were stimulated overnight with 10 ng/mL TNF-α. Before the experiment, excess medium was removed and 2 µl of HEPES medium containing $8*10^6$ DiD labelled neutrophils were added to each vessel. Vessels were incubated for 2.5 hours, washed twice and fixed for 15 minutes using 4% paraformaldehyde. Devices were then imaged using an LSM980 Airyscan2 (ZEISS) using a 10x air objective (ZEISS, 420640-9900-000, Objective Plan-Apochromat 10x/0.45). Analysis was done using IMARIS Bitplane software (Version 9.5/9.6).

Statistical Analysis

Experimental data were plotted and analyzed by GraphPad Prism V9.0.0 (GraphPad Software, San Diego, CA, USA). Results are shown as mean ± standard deviation. Normality was tested using the Shapiro-Wilk test. The paired or unpaired Student *t* test was used to test statistical significance (* = $p<0.05$; ** = $p<0.01$; *** = $p<0.001$; ns = non-significant).

RESULTS

ARPC1B-Deficient Neutrophils Display Impaired Subendothelial Motility Upon Transendothelial Migration

We investigated the capacity of neutrophils to transmigrate through an endothelial monolayer under physiological flow conditions. HUVECs were grown on fibronectin, and stimulated with tumor necrosis factor-alpha (TNF-α) which leads to the upregulation of cell adhesion molecules such as ICAM-1 and VCAM-1, as well as the production of important chemoattractants for neutrophils like platelet-activating factor and interleukin-8 (9, 10). Inflamed endothelial cells also release and remodel ECM proteins, including different types of laminins, collagen-I and fibronectin (11).

Lack of ARPC1B expression in patient neutrophils was confirmed by Western blotting, which showed the complete absence of ARPC1B protein while actin levels were normal (Supplementary Figure 1A). Control and ARPC1B-deficient neutrophils were differently fluorescently labeled and simultaneously perfused over the inflamed endothelium. Control neutrophils rolled over the endothelium, whereupon they firmly adhered and transmigrated (Figure 1A and Supplementary Video 1). Patient neutrophils rolled and adhered on the endothelium in a similar fashion as control cells (Figure 1B), but once arrested, they hardly crawled away from their initial arrest site. Under normal inflammatory conditions, neutrophils crawl on endothelium in order to find suitable sites to transmigrate, mostly at endothelial junctions (12). The observed lack of crawling indicated that patient neutrophils crossed the endothelium at non-optimal locations. Furthermore, ARPC1B-deficient neutrophils remained mostly round-shaped and unable to polarize, which coincided with a significantly decrease in TEM speed as well as a reduced number of neutrophils that successfully crossed the endothelium (Figures 1C, D). Both control and ARPC1B-deficient neutrophils transmigrated solely *via* the paracellular pathway (Supplementary Figure 1B). The adherence of ARPC1B-deficient neutrophils to the endothelial monolayer under flow conditions is remarkable but well in accordance with our observations that ARPC1B-deficient neutrophils show normal expression of adhesion and signaling receptors, including CD11a (integrin αL chain), CD11b (integrin αM chain), CD18 (integrin β2 chain), L-selectin, PECAM-1 and ICAM-1, as well as adherence under static conditions in response to a range of stimuli (Supplementary Figure 1C, D).

Once transmigrated, control neutrophils were actively migrating away from the initial TEM site underneath the endothelium. However, ARPC1B-deficient neutrophils that did

cross the endothelium showed a prominent decrease in subendothelial motility (Figure 1E). Moreover, they failed to migrate away from their initial TEM site, in contrast to control neutrophils (Figures 1F, G). These results indicate that ARPC1B-deficient neutrophils have a minor defect in actual TEM, but a more pronounced defect in their ability to migrate underneath the endothelium.

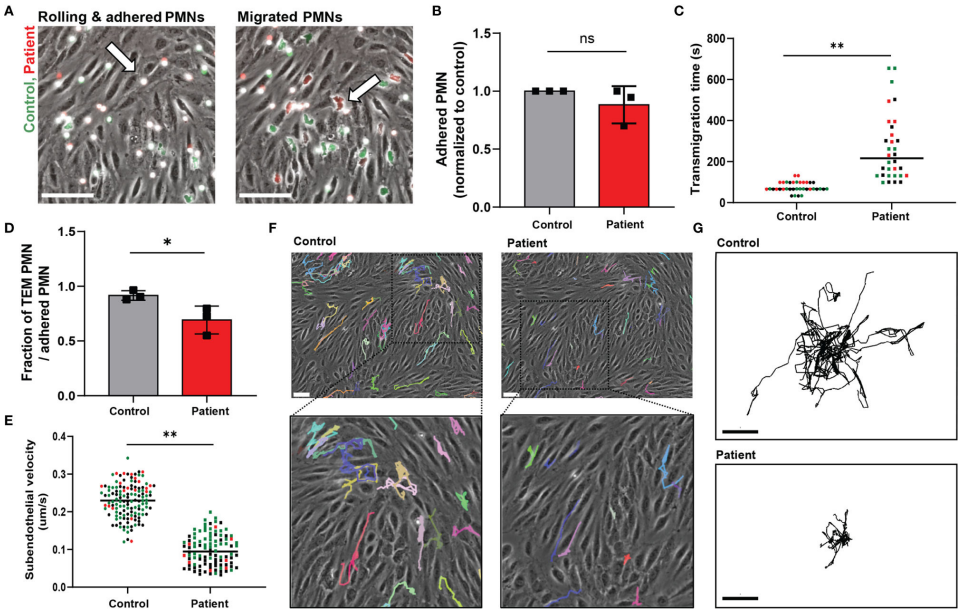

Figure 1. ARPC1B-deficient neutrophils display impaired subendothelial motility upon transendothelial migration.

(A) Neutrophil TEM through TNF-α inflamed HUVECs was investigated upon physiological flow conditions. Neutrophils (green = control; red = patient) rolled over the endothelium, whereupon they firmly adhered (left panel) and transmigrated (right panel). Neutrophils are circular above the endothelium (left panel, arrow) and become polarized (right panel, arrow) under the endothelium. Representative stills are displayed, see also Supplementary Video 1. Scale bar = 100 µm. (B) The number of firmly adhered ARPC1B-deficient neutrophils was quantified and normalized to control neutrophils (mean ± SD, n = 3). (C) Average time of neutrophils to complete transendothelial migration, starting from firm adherence. Individual cells are depicted. Colors (black, green and red) are corresponding to independent experiments. (D) Transendothelial migratory events were quantified and normalized to the number of firmly adhered neutrophils (mean ± SD, n = 3). (E–G) Subendothelial motility of transmigrated neutrophils, with (E) average velocity of neutrophils (n = 3, individual cells are depicted, colors are corresponding to independent experiments) and cell track analysis of subendothelial neutrophils with (F) representative cell trajectories of control and ARPC1B-deficient neutrophils as indicated lasting for 45 minutes (scale bar = 70 µm) and (G) showing trajectory plots displayed with their origins brought to a common point. Scale bar = 50 µm. Results are representative of 3 independent experiments. The Student t test was used to test statistical significance (*$p < 0.05$; **$p < 0.01$; ns, non-significant).

Neutrophil Infiltration Into 3D Tissue Matrices Is Defective in ARPC1B Deficiency

The dimensions change for a neutrophil as soon as they enter the area underneath the endothelium, i.e. from a luminal 2D to an ECM 3D setting. It has been previously observed that several types of leukocytes, including granulocytes, are able to efficiently migrate in 3D matrices in an integrin-independent manner (13). We investigated neutrophil motility and migration in an artificial 3D gel of bovine collagen-I and visualized chemokinesis of neutrophils upon activation with the chemoattractant C5a. First, we confirmed the integrin-independency of (control) neutrophils for 3D migration in collagen by usage of blocking monoclonal antibodies directed against the common integrin β2 chain (clone IB4, CD18) or the αM chain (clone 44a, CD11b). Indeed, we did not observe an effect from integrin blockage on 3D migration in collagen I (Supplementary Figure 2A), indicating that this mode of migration is independent of the main integrins of neutrophils. Next, we investigated the requirement of ARPC1B in neutrophil migration in the collagen-I 3D gel by visualizing chemokinesis of differently fluorescently labeled control and ARPC1B-deficient neutrophils upon activation with C5a (Supplementary Video 2 and Figure 2A) and TNF-α stimulation (Supplementary Figure 2B). Both C5a and TNF-α induced migration of control neutrophils in the collagen matrix. Quantification of migration paths upon C5a stimulation revealed that control neutrophils migrated successfully into the collagen matrix with average speeds of 0.085 um/s up to 0.31 um/s. However, ARPC1B-deficient neutrophils were practically non-motile (Figure 2B).

To study both processes, i.e. TEM and 3D matrix migration of neutrophils in one assay, we used a vessel-on-a-chip model (see *Methods*). Neutrophils were injected in the vessel, whereupon they were allowed to adhere and migrate for 2.5 hours before the vessels were washed and fixed. As the vessels were subsequently washed and fixed, non-adherent neutrophils were lost. Of note, no flow was applied on the vessel. Using the 3D vessel-on-a-chip model, we found that the number of ARPC1B-deficient neutrophils retrieved in the vessel was significantly lower than control neutrophils (Supplementary Videos 3, 4 and Figures 2C, D). Most ARPC1B-deficient neutrophils were found at the intraluminal site firmly adhered to the endothelium, as multiple washing steps did not remove them (Figure 2E). Around 45% of the retrieved control neutrophils transmigrated successfully, while only 15% of ARPC1B-deficient neutrophils completed their transendothelial migration route (Figure 2F). Neutrophils that did penetrate the matrix were found in closer proximity to the vessel compared to control neutrophils. ARPC1B-deficient neutrophils migrated on average 5 µm into the matrix, while this was almost 30 µm for control neutrophils (Figure 2G).

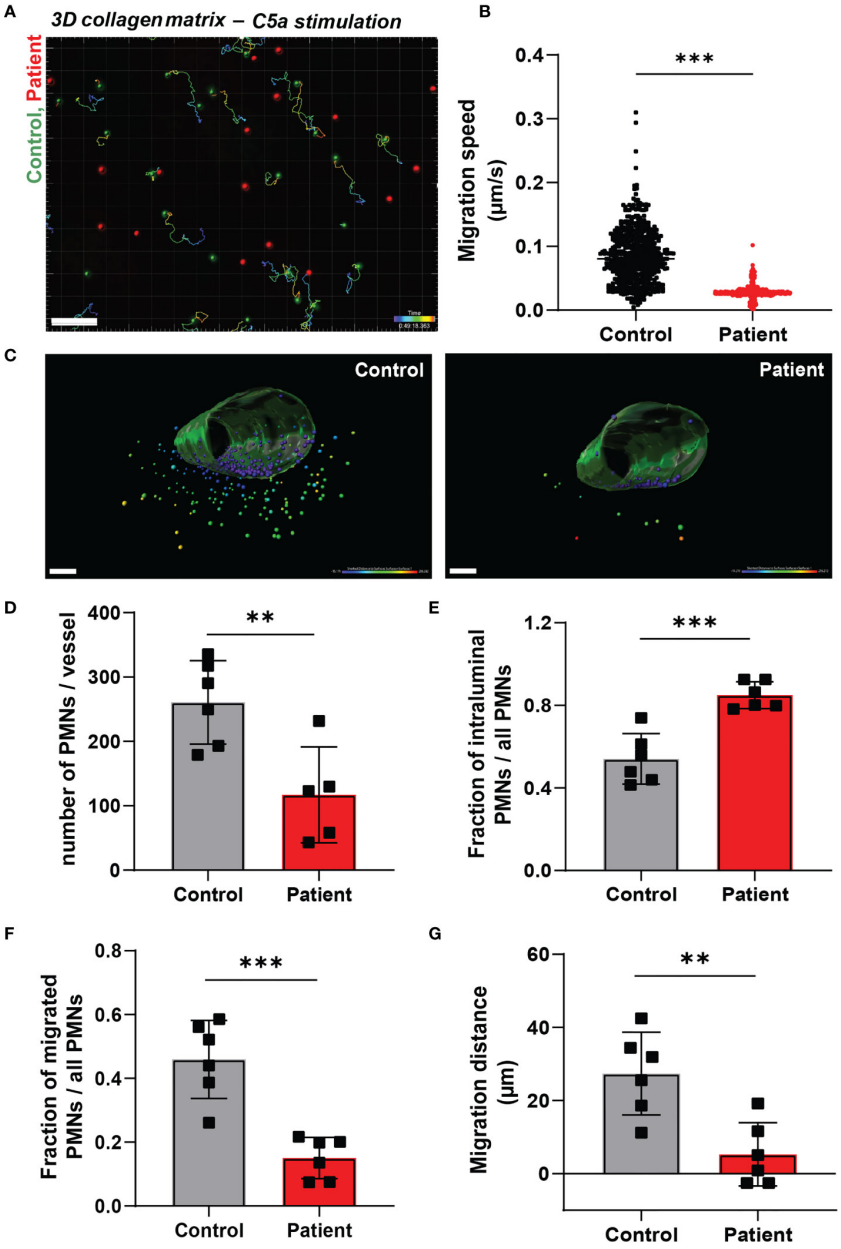

Figure 2. Neutrophil infiltration into 3D tissue matrices is defective in ARPC1B deficiency.
(A) Motility tracks of neutrophils (green = control; red = patient) in a collagen-I 3D matrix upon C5a stimulation, see also Supplementary Video 2. Only control neutrophils show motility tracks as ARPC1B-deficient neutrophils were found to be non-motile. Scale bar = 100 µm. Heat bar = time in minutes. Results are representative of 3 independent experiments. (B) Migration speed of neutrophils in collagen matrix (cells of 3 experiments pooled). (C) Representative images of neutrophil TEM in a perfusable vessel-on-a-chip, see also Supplementary Videos 3, 4. Scale bar = 100 µm. Heat bar = distance starting from vessel surface. Results are representative of 6 vessels, 2 fields of view per vessel were analyzed. (D–F) Quantification of neutrophil TEM using vessel-on-a-chip model, with (D) number of neutrophils retrieved in the vessel, (E) number of intraluminal neutrophils (normalized to total number of neutrophils), (F) number of neutrophils infiltrated into subendothelial collagen matrix (normalized to

total number of neutrophils), (G) and average migration distance of neutrophils into the vessel. Mean ± SD, results are representative of 6 vessels, 2 fields of view per vessel were analyzed. The Student t test was used to test statistical significance (**p < 0.01; ***p < 0.001; ns, non-significant).

DISCUSSION

Overall, our results indicate that the ARP2/3 complex is particularly important for motility in a 3D environment subsequent to the endothelial cell layer itself. Yet, the initial steps of rolling and adhesion strengthening under flow conditions seems independent of ARPC1B, allowing transendothelial migration. Of interest, the number of ARPC1B-deficient neutrophils retrieved in the vessel was significantly lower than control neutrophils, though input was equal (Figure 2D). This indicates that these patient neutrophils were not firmly adhered to the endothelial cells and lost during washing. This might be explained by the fact that no physiological flow was applied to the vessel-on-a-chip system. Flow forces have been shown to induce forces between adhering cells and substrates that leads to integrin activation and adhesion strengthening (14, 15). This flow-enhanced integrin activity may explain the difference observed between firm adhesion under flow conditions and the static vessel-on-a-chip environment. Alternatively, it might also be that neutrophils which fail to transmigrate over a longer period of incubation in the vessel-on-a-chip approach (2.5 hours) are more prone to detach from the endothelium again compared to the shorter incubations under flow conditions (45 minutes) or static adhesion on plastic (30 minutes). The process of adhesion is energy-demanding and neutrophils which fail to transmigrate might be prone to detach from the endothelium again, perhaps as a result of being deprived from their energy reserves.

Recent attention was raised to the issue of leukocytes employing alternative migration mechanisms depending on 2- or 3 dimensionality (16). The impaired TEM observed when using the vessel-on-a-chip model may thus indicate that ARPC1B is of more importance for migration in 3D environments. Indeed, when neutrophils are flowed over inflamed endothelium, they migrate in a 2D-manner, while under the endothelium they are in a ‘confined’ 3D environment and clearly lack such capacity to move around. This implicates that ARPC1B-deficient neutrophils are able to extravasate, but cannot penetrate through the BM into the tissue. Interestingly, 69% of patients with APRC1B deficiency suffer from cutaneous vasculitis (17). Previous investigations showed that ARPC1B-deficient neutrophils release their azurophilic granules prematurely *in vitro* (4), both of which may contribute to the vascular damage as observed in these patients.

After neutrophils have crossed the endothelium, and before entering the tissue, there is a second layer of cells to cross: the pericytes (18). We were not able to include the role for pericytes in the current study as our vessel-on-a-chip has its limitations and does not allow culturing a second cell layer. However, this would be a future challenge.

Our results emphasize the importance of ARPC1B for neutrophil migration, thereby explaining

the severe susceptibly of these rare patients to bacterial infections, while neutrophil killing mechanisms have been found to be intact (4).

DATA AVAILABILITY STATEMENT

The raw data supporting the conclusions of this article will be made available by the authors, without undue reservation.

ETHICS STATEMENT

The studies involving human participants were reviewed and approved by the local ethical committees of the Amsterdam University Medical Center and Sanquin Blood Supply, Amsterdam, The Netherlands. Written informed consent to participate in this study was provided by the participants' legal guardian/next of kin.

AUTHOR CONTRIBUTIONS

ES wrote the manuscript. all authors designed the experiments. LK, AS, and ES performed experiments. LK and AS analyzed the data. All authors contributed to the article and approved the submitted version.

FUNDING

ES and TK are supported by the European Union's Horizon 2020 research and innovation programme under Grant Agreement No 668303 and TK is supported by the E-Rare ZonMW grant #90030376506. AS is supported by LSBR grant #1649. LK is supported by LSBR grant #1820 JB is supported by ZonMW NWO Vici grant # 91819632.

CONFLICT OF INTEREST

The authors declare that the research was conducted in the absence of any commercial or financial relationships that could be construed as a potential conflict of interest.

ACKNOWLEDGMENTS

We are most grateful to the patient and parents for their collaboration.

REFERENCES

1. Ley K, Laudanna C, Cybulsky MI, Nourshargh S. Getting to the Site of Inflammation: The Leukocyte Adhesion Cascade Updated. Nat Rev Immunol (2007) 7(9):678–89. doi: 10.1038/nri2156
2. Wang S, Voisin MB, Larbi KY, Dangerfield J, Scheiermann C, Tran M, et al. Venular Basement Membranes Contain Specific Matrix Protein Low Expression Regions That Act as Exit Points for Emigrating Neutrophils. J Exp Med (2006) 203(6):1519–32. doi: 10.1084/jem.20051210
3. Etzioni A. Defects in the Leukocyte Adhesion Cascade. Clin Rev Allergy Immunol (2010) 38(1):54–60. doi: 10.1007/s12016-009-8132-3
4. Kuijpers TW, Tool ATJ, van der Bijl I, de Boer M, van Houdt M, de Cuyper IM, et al. Combined Immunodeficiency With Severe Inflammation and Allergy Caused by ARPC1B Deficiency. J Allergy Clin Immunol (2017) 140 (1):273–7 e10. doi: 10.1016/j.jaci.2016.09.061
5. Mullins RD, Heuser JA, Pollard TD. The Interaction of Arp2/3 Complex With Actin: Nucleation, High Affinity Pointed End Capping, and Formation of Branching Networks of Filaments. Proc Natl Acad Sci USA (1998) 95 (11):6181–6. doi: 10.1073/pnas.95.11.6181
6. Sprenkeler EGG, Henriet SSV, Tool ATJ, Kreft IC, van der Bijl I, Aarts CEM, et al. MKL1 Deficiency Results in a Severe Neutrophil Motility Defect Due to Impaired Actin Polymerization. Blood (2020) 135(24):2171–81. doi: 10.1182/ blood.2019002633
7. Kroon J, Daniel AE, Hoogenboezem M, van Buul JD. Real-Time Imaging of Endothelial Cell-Cell Junctions During Neutrophil Transmigration Under Physiological Flow. J Vis Exp (2014) 90):e51766. doi: 10.3791/51766
8. Jimenez-Torres JA, Peery SL, Sung KE, Beebe DJ. LumeNEXT: A Practical Method to Pattern Luminal Structures in ECM Gels. Adv Healthc Mater (2016) 5(2):198–204. doi: 10.1002/adhm.201500608
9. Yang L, Froio RM, Sciuto TE, Dvorak AM, Alon R, Luscinskas FW. ICAM-1 Regulates Neutrophil Adhesion and Transcellular Migration of TNF-Alpha- Activated Vascular Endothelium Under Flow. Blood (2005) 106(2):584–92. doi: 10.1182/blood-2004-12-4942
10. Kuijpers TW, Hakkert BC, Hart MH, Roos D. Neutrophil Migration Across Monolayers of Cytokine-Prestimulated Endothelial Cells: A Role for Platelet- Activating Factor and IL-8. J Cell Biol (1992) 117(3):565–72. doi: 10.1083/ jcb.117.3.565
11. Davis GE, Senger DR. Endothelial Extracellular Matrix: Biosynthesis, Remodeling, and Functions During Vascular Morphogenesis and Neovessel Stabilization. Circ Res (2005) 97(11):1093–107. doi: 10.1161/01.RES. 0000191547.64391.e3
12. Schenkel AR, Mamdouh Z, Muller WA. Locomotion of Monocytes on Endothelium Is a Critical Step During Extravasation. Nat Immunol (2004) 5 (4):393–400. doi: 10.1038/ni1051
13. Lammermann T, Bader BL, Monkley SJ, Worbs T, Wedlich-Soldner R, Hirsch K, et al. Rapid Leukocyte Migration by Integrin-Independent Flowing and Squeezing. Nature (2008) 453(7191):51–5. doi: 10.1038/nature06887
14. Polacheck WJ, German AE, Mammoto A, Ingber DE, Kamm RD. Mechanotransduction of Fluid Stresses Governs 3D Cell Migration. Proc Natl Acad Sci USA (2014) 111(7):2447–52. doi: 10.1073/pnas.1316848111
15. Sun Z, Costell M, Fassler R. Integrin Activation by Talin, Kindlin and Mechanical Forces. Nat Cell Biol

(2019) 21(1):25–31. doi: 10.1038/s41556- 018-0234-9

16. Kameritsch P, Renkawitz J. Principles of Leukocyte Migration Strategies. Trends Cell Biol (2020) 30(10):818–32. doi: 10.1016/j.tcb.2020.06.007

17. Volpi S, Cicalese MP, Tuijnenburg P, Tool ATJ, Cuadrado E, Abu-Halaweh M, et al. A Combined Immunodeficiency With Severe Infections, Inflammation, and Allergy Caused by ARPC1B Deficiency. J Allergy Clin Immunol (2019) 143(6):2296–9. doi: 10.1016/j.jaci.2019.02.003

18. Proebstl D, Voisin MB, Woodfin A, Whiteford J, D'Acquisto F, Jones GE, et al. Pericytes Support Neutrophil Subendothelial Cell Crawling and Breaching of Venular Walls In Vivo. J Exp Med (2012) 209(6):1219–34. doi: 10.1084/ jem.20111622

SUPPLEMENTARY MATERIAL

The Supplementary Material for this article can be found online at: https://www.frontiersin.org/articles/10.3389/fimmu.2021.678030/full#supplementary-material

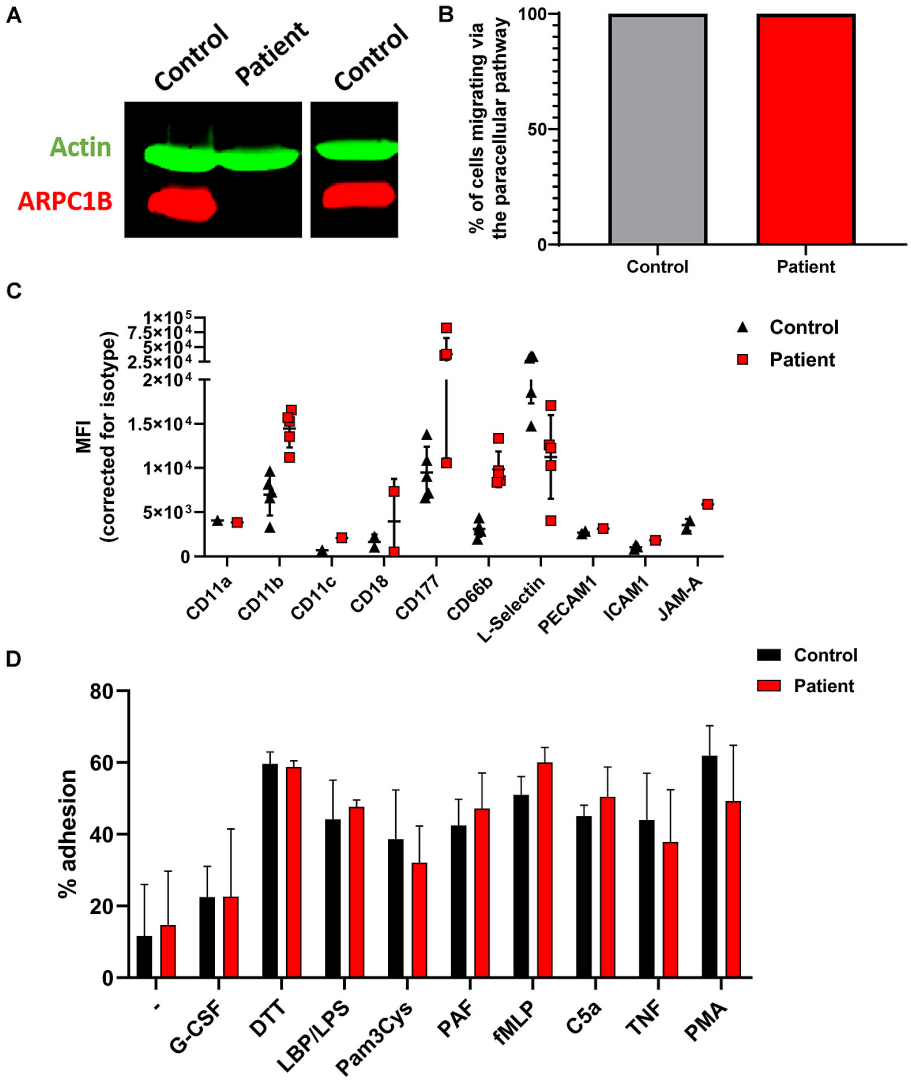

Supplementary Figure 1.
(A) Absence of ARPC1B protein and normal actin levels in patient neutrophils was found by Western blot. (B) Quantification of neutrophil migration via paracellular mode of control- and ARPC1B-deficient neutrophils. (C) Expression of adhesion and surface molecules on the neutrophil membrane was assessed by flow cytometry. Neutrophils are gated based on forward/side scatter. Mean fluorescence intensity (MFI) is corrected for the isotype control (mean ± SD, n = 1 – 5). (D) Adhesion of neutrophils to plastic (static condition) as percentage of total input upon stimulation with the indicated stimuli (mean + SD, n = 2 - 3).

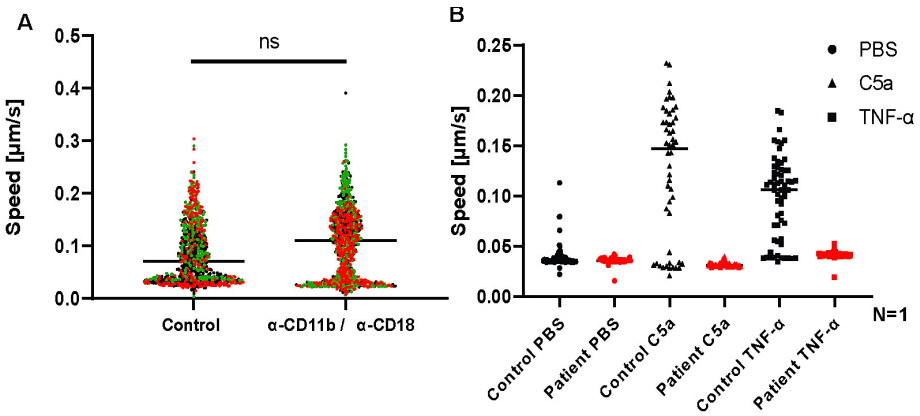

Supplementary Figure 2.
(A) Migration speed of neutrophils in collagen matrix in response to C5a with or without blockage of integrin b2 chain (clone IB4, CD18) and the aM chain (clone 44a, CD11b). Individual cells are depicted. Colors (black, green and red) are corresponding to independent experiments. (B) Migration speed of control- and ARPC1B-deficient neutrophils in collagen matrix in response to PBS (negative control), C5a or TNF-a. Individual cells are depicted, n = 1.

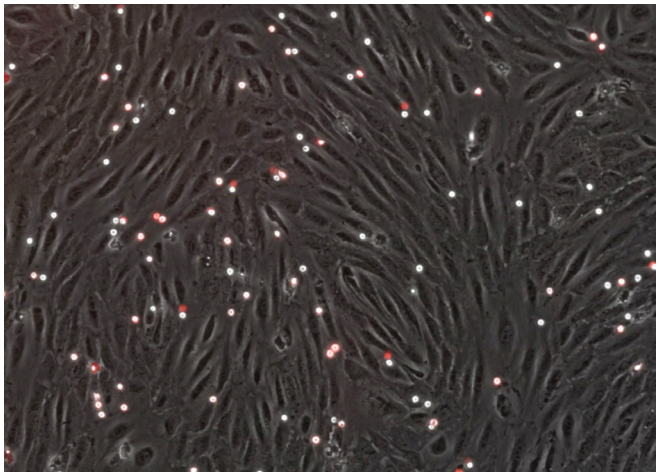

Supplementary Video 1.
Neutrophil TEM through inflamed endothelium. Fluorescently labelled neutrophils (green = control; red = ARPC1B-deficient patient) were flowed over TNF-a inflamed HUVECs for 45 minutes, see also Figure 1A. Scale bar = 80 µm. Results are representative of 3 independent experiments.

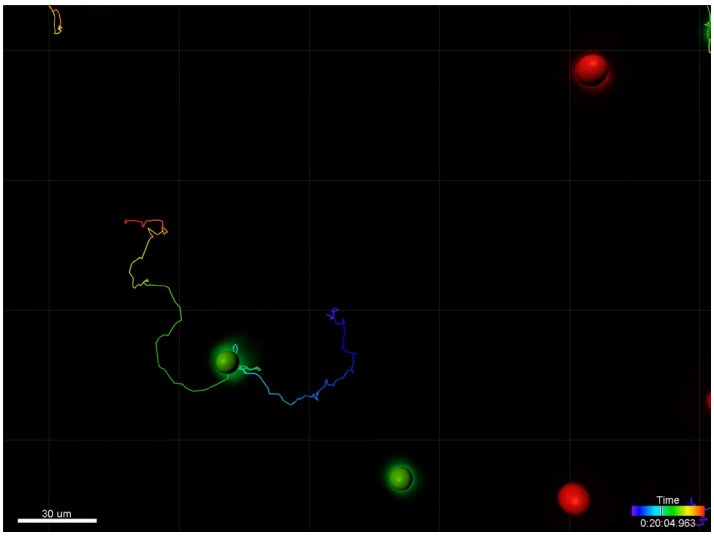

Supplementary Video 2.
Neutrophil migration in a collagen-I 3D matrix. Migration of neutrophils (green = control; red = ARPC1B-deficient patient) in a collagen-I 3D matrix upon C5a stimulation, see also Figure 2A. Neutrophil motility was assessed for a total of 50 minutes. Only control neutrophils show motility tracks as ARPC1B-deficient neutrophils were found to be non-motile. Heat bar = time in minutes. Results are representative of 3 independent experiments.

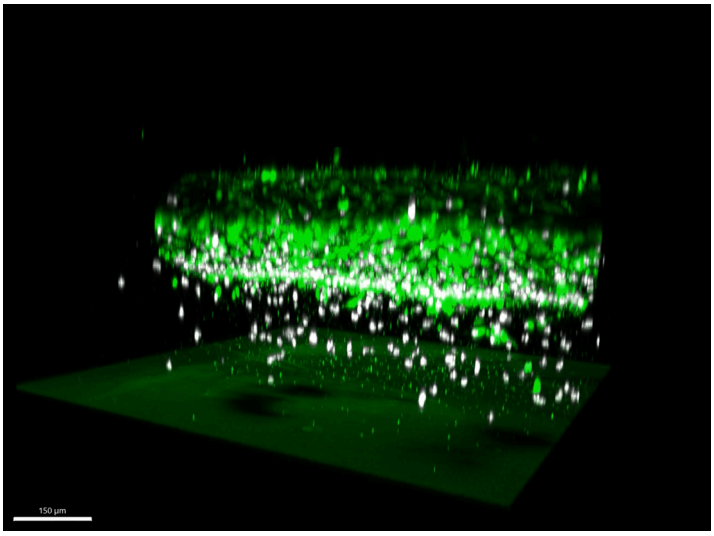

Supplementary Video 3.
Control neutrophil TEM in a vessel-on-a-chip. Neutrophils were injected in the vessel, whereupon they were allowed to adhere and migrate for 2.5 hours before the vessels were washed and fixed, see also Figure 2C. Scale bar = 150 µm. Results are representative of 6 vessels.

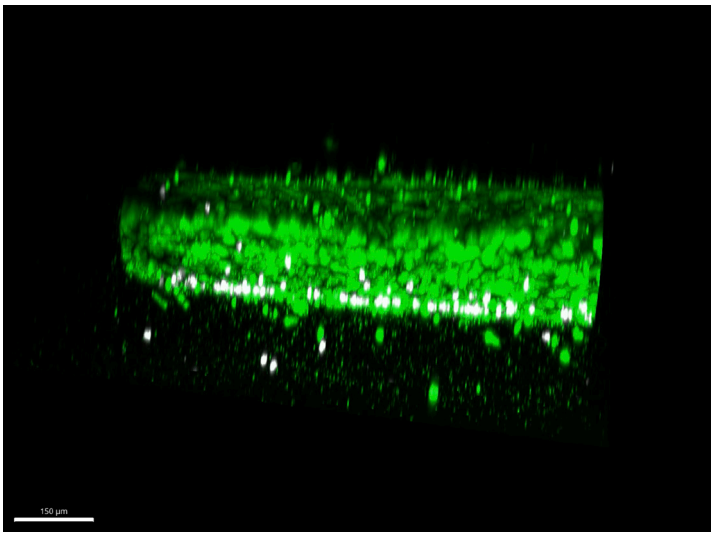

Supplementary Video 4.
ARPC1B-deficient neutrophil TEM in a vessel-on-a- chip. Neutrophils were injected in the vessel, whereupon they were allowed to adhere and migrate for 2.5 hours before the vessels were washed and fixed, see also Figure 2C. Scale bar = 150 µm. Results are representative of 6 vessels.

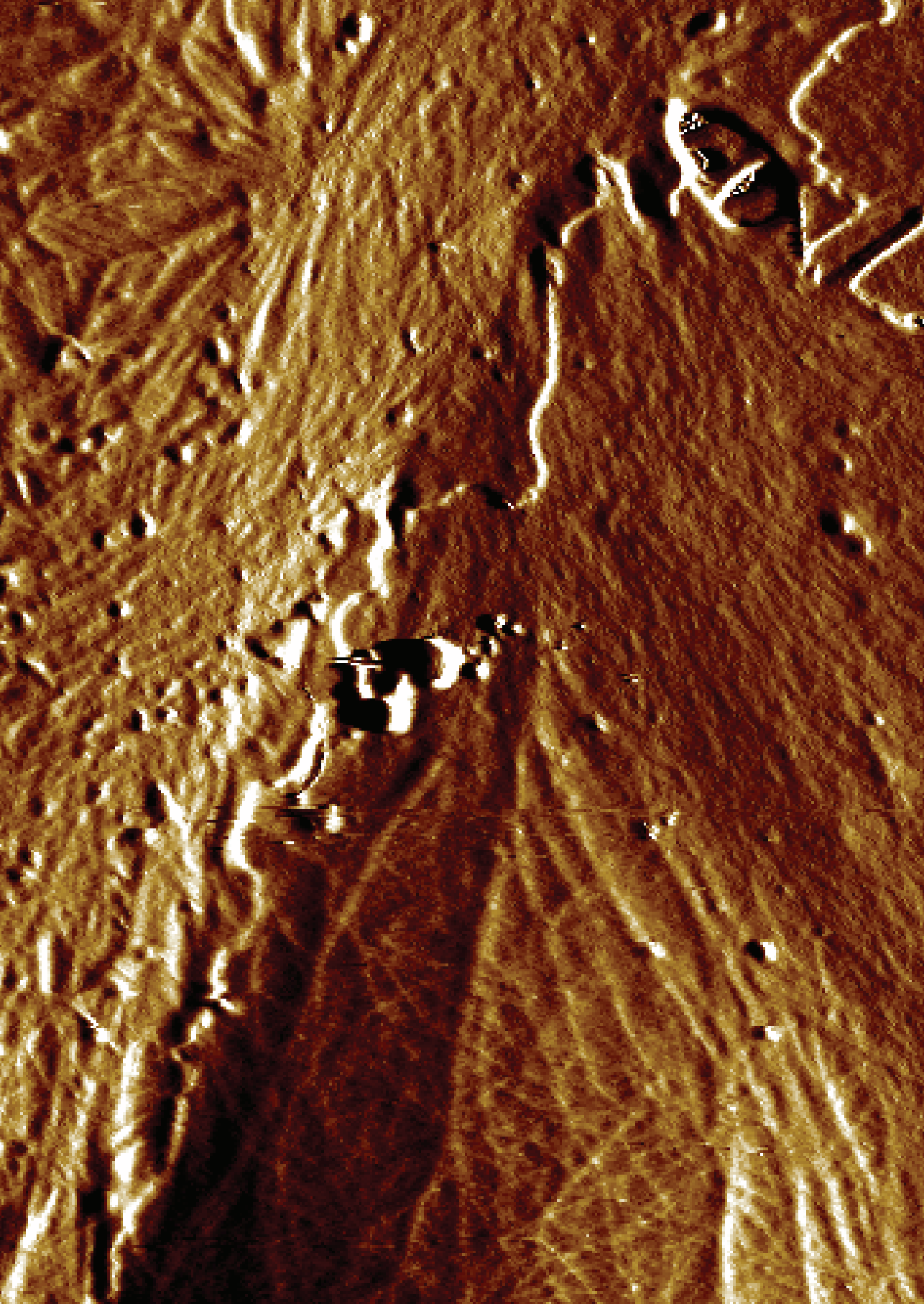

CHAPTER 8

Discussion

Leukocyte extravasation, also known as leukocyte transendothelial migration (TEM), under inflammatory conditions is a fascinating process. The interplay between the endothelium and the leukocyte ensures the exit happens at the right location in a rapid manner while maintaining the endothelial barrier function. In this thesis, we have focused on specific aspects of this complex cascade and developed a new model that mimics *in vivo* conditions to study this process *in vitro*. In this thesis we have worked on several aspects of the leukocyte extravasation cascade, in this chapter we will discuss how the different chapters work together to advance our understanding of this process, furthermore we will discuss questions that have not been answered in the individual chapters. In the first part of this discussion, we zoom in on the ICAM-1 adhesome, the part important for the interaction of the leukocyte with the endothelium. The second part of this discussion focuses on a broader perspective of leukocyte transendothelial migration in human physiology and discusses the use and development of new models for studying the integral leukocyte extravasation cascade.

THE ROLE OF ICAM-1 IN LEUKOCYTE EXTRAVASATION

Historically, ICAM-1 was described to be upregulated by the endothelium upon inflammation where it would serve as a ligand for leukocyte integrins. The integrins on the leukocytes would be activated during the selectin-mediated rolling through chemokine receptor triggering, and then the activated integrins would use high-affinity interaction with ICAM-1 to induce arrest and initiate crawling. This series of events is captured in the so-called multistep paradigm of leukocyte transendothelial migration, introduced by Butcher and Springer in the early 90s (Butcher, 1991; Springer, 1994). Since then, the role of ICAM-1 has been recognized in several other aspects of the TEM cascade. The interaction between leukocyte integrins and ICAM-1 is found to be initiated already during the rolling step, in particular during the slow-rolling step of the TEM cascade (Chesnutt et al., 2006; Kadono et al., 2002; Salas et al., 2004). Additionally, ICAM-1 has been shown to not merely be a passive integrin ligand, but an active signaling molecule. It was discovered that endothelial ICAM-1 clustering induces various intracellular signaling pathways (Muro et al., 2003; van Buul et al., 2010). These pathways lead to the recruitment of several actin adaptor proteins, local remodeling of the actin cytoskeleton, and even the recruitment of its family member VCAM-1 (Barreiro et al., 2008; Kanters et al., 2008; Schaefer et al., 2014).

Endothelial cells regulate their rigidity on environmental cues, such as substrate stiffness, which is different between vascular beds, and can increase dramatically under diseased conditions such as atherosclerosis (Zieman et al., 2005). Stiffer substrates induce contraction in endothelial cells which leads to stiffer endothelium and enhanced neutrophil extravasation (Huynh et al., 2011; Stroka & Aranda-Espinoza, 2011). The endothelial response to stiffer substrates leads to an increased recruitment of the ICAM-1-mediated adhesive

complex on stiffer substrates via activation of DLC-1 (Schimmel et al., 2018). The complex was named **the ICAM-1 adhesome** (Schimmel et al., 2018).

In **Chapter 3** of this thesis, we have deployed a state-of-the-art proteomics approach to take another look at the ICAM-1 adhesome. We have performed a mass spectrometry analysis of the ICAM-1 adhesome induced by anti-ICAM-1 antibody-coated beads to map all the proteins potentially associated with this complex. The mass spectrometry (MS) analysis of the ICAM-1 adhesome returned 93 positively enriched proteins, with many of these hits not yet linked to ICAM-1 or known to be involved in ICAM-1 clustering. This screen was followed up by investigating one of the most significant hits from this screen, CD44, and revealing its important function during cytotoxic T lymphocyte extravasation. CD44, also known as homing cell adhesion molecule (HCAM), is a transmembrane protein best known for binding hyaluronan which is a part of the glycocalyx (hyaluronic acid; HA) (Naor et al., 1997; Ponta et al., 2003). We confirmed the recruitment of CD44 to the ICAM-1 adhesome by western blot and showed that CD44 plays an important role in facilitating efficient CTL extravasation especially via the transcellular pathway. Our data shows that both ICAM-1 motility as well as chemokine presentation might be impaired in the absence of CD44.

Our data indicate that HA and CD44 is important to regulate efficient lateral ICAM-1 mobility and is required for the formation of ICAM-1-rich finger-like protrusions, known as filopodia. Recent findings indicate that HA bound to CD44 can act as a picket fence to restrict mobility of transmembrane proteins via their extracellular domain (Freeman et al., 2018). Furthermore this picket fence was shown to immobilize E-selectin in the membrane of endothelial cells via the spectrin cytoskeleton (Mylvaganam et al., 2020). In our work we show that knockdown of CD44 or removal of HA by hyaluronidase leads to an increased mobility of ICAM-1. Furthermore, both the alfa and beta subunits of spectrin are shown to be recruited to the ICAM-1 adhesome in the proteomics screen in Chapter 3. This strongly suggests that the picket fence is physically regulating recruitment of the ICAM-1 adhesome.

Besides the structural role of HA, it has also been described to bind chemokines and present them extracellularly to cells passing by (Kuschen et al., 1999; Tanaka et al., 1993). In Chapter 3 we degrade the HA matrix of the endothelium and detect an increased release of several chemokines confirming this hypothesis. Amongst these chemokines are CCL20 and CXCL10, potent inducers of CTL migration (Bromley et al., 2008). If we assume that ICAM-1 clustering is controlled by the picket fence, the recruitment of CD44 leads to the recruitment of chemokine-presenting HA to the ICAM-1 adhesome, thereby facilitating local integrin-activation. This could act as another signal to induce CTL diapedesis.

In **Chapter 4** we follow up on a second hit from the ICAM-1 adhesome screen; synaptosomal-associated protein 23 (SNAP-23). This protein guides the extravasation of secretory vesicles to the target membranes (Rothman, 1994). We found that clustering of ICAM-1 recruits SNAP23 and suggest that this recruitment of SNAP23 to the ICAM-1 adhesome leads to the local release of chemokine-containing vesicles that trigger CTLs to transmigrate via the transcellular migration route. In the absence of SNAP23-induced

local chemokine release, CTLs divert to migrating via the paracellular route. It has been a longstanding question why leukocytes would prefer one transmigration route over the other. Here we show that specific mechanisms are in place to trigger one specific pathway, i.e., SNAP23 triggers the transcellular pathway for T-cells. It is unclear why this is not happening for neutrophils, as neutrophils are known to cluster ICAM-1 as well and thereby SNAP23.

The work in **Chapter 3 and 4** has further expanded functions of the ICAM-1 adhesome to include signaling via the glycocalyx, secretory vesicle pathways, and chemokine signaling, binding all these pathways together. This highlights the importance of the ICAM-1 adhesome as a pivotal complex in the leukocyte cascade, which acts as a key checkpoint in the extravasation process.

UPDATING THE ICAM-1 ADHESOME

We followed up on only two out of the 93 hits from the mass spectrometry analysis of the ICAM-1 adhesome. Nevertheless, many of the additional hits from the ICAM-1 adhesome screen do not come unexpectedly. We additionally found proteins that control intermediate filaments and microtubules. Indeed, previous work showed a link to ICAM-1 (Kaatz et al., 2006; Nieminen et al., 2006). However, other protein groups that were strongly enriched in the adhesome compared to control were splicing factors that were not previously related to ICAM-1, such as serine and arginine-rich splicing factor (SRSF) 1 and SRSF7. These proteins are part of the spliceosome and are part of a small subset of the SR protein family that shuttles between the nucleus and cytoplasm of a cell (Cáceres et al., 1998; Cowper et al., 2001; Sapra et al., 2009). For these proteins, their localization in the nucleus is known, however, association with membrane structures such as the ICAM-1 adhesome has not been reported previously. Their association sparks the question of what their role in the ICAM-1 adhesome may be and whether ICAM-1 clustering alters their function. It is an attractive idea that transmigrating leukocytes would, via the ICAM-1 adhesome, alter the spliceosome and induce very rapid changes in expression profile. In this way, the leukocyte could very directly alter protein expression in the endothelium and induce the expression of proteins to alter the inflammatory status of the endothelium or signaling molecules. Future studies should clarify if such mechanisms support TEM.

Another interesting protein that was found to be present in the ICAM-1 adhesome is the membrane attack complex inhibitory protein (MAC-IP, CD59). This protein is known to inhibit the complement system from cell lysis. The interaction of CD59 and ICAM-1 may indicate a link between leukocyte extravasation and the complement system. This type of protein would not be expected to directly play a role in facilitating leukocyte extravasation, but might be recruited to prevent accidental damage to the endothelium during the process of leukocyte TEM. Our preliminary data confirmed the interaction of CD59 to ICAM-1 upon ICAM-1 clustering using cultured endothelial cells (Figure 1). Future experiments should

reveal if this interaction indeed functionally connects leukocyte extravasation with the complement system.

Another interesting protein that was precipitated in the ICAM-1 adhesome is CD73. CD73 is an enzyme that in humans is encoded by the NT5E gene and serves to convert AMP to adenosine. Our preliminary data confirmed the presence of this protein upon ICAM-1 clustering. Interestingly, CD73 contains binding sites for transcription factor AP-2, which is involved in endocytosis of VE-cadherin (Wessel et al., 2014). Moreover, CD73 mediates the hydrolysis of ADP to anti-inflammatory adenosine (Niemelä et al., 2004). Adenosine may have a crucial role in controlling the extent of inflammation, thereby rescuing vascular homeostasis. Our data indicate a potential link to endothelial ICAM-1 signaling.

It is clear that our MS screen has greatly expanded our knowledge on the proteins that can potentially be recruited to the ICAM-1 adhesome and thereby play an important role in TEM. The work presented in **Chapter 3 and 4** has added additional functions to the ICAM-1 adhesome during leukocyte extravasation and uncovered mechanisms that contribute to the crosstalk between leukocytes and the endothelium. It is interesting to realize that just one proteomics screen has led to all these new findings to the ICAM-1 adhesome (Figure 2). Over years of doing research on ICAM-1 function using more classical approaches, these proteins that are recruited to the ICAM-1 adhesome may not have been found otherwise. This makes a strong point for the application of new omics approaches to topics that are already studied for decades in the field, as they can shed new light on questions some might consider “finished” and open doors to new and interesting mechanisms.

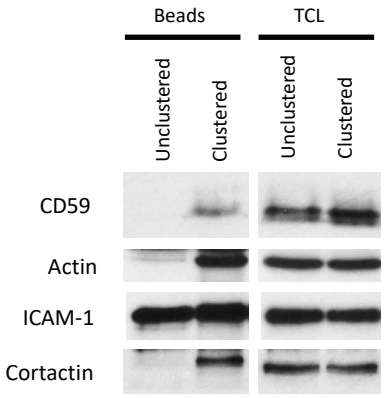

Figure 1. Western blotting of ICAM-1 adhesome stained for CD59,with actin and ICAM-1 as controls shows CD59 being recruited to the ICAM-1 adhesome.
ICAM-1 is clustered as described in **Chapter 3**. Total cell lysate (TCL) is used as an input control and beads are the magnetically washed anti-ICAM-1 beads and precipitated proteins. In the “clustered” condition beads were added to inflamed HUVEC and allowed to recruit the ICAM-1 adhesome for 30 minutes. In the “unclustered” condition, HUVEC were lysed before the beads were added.

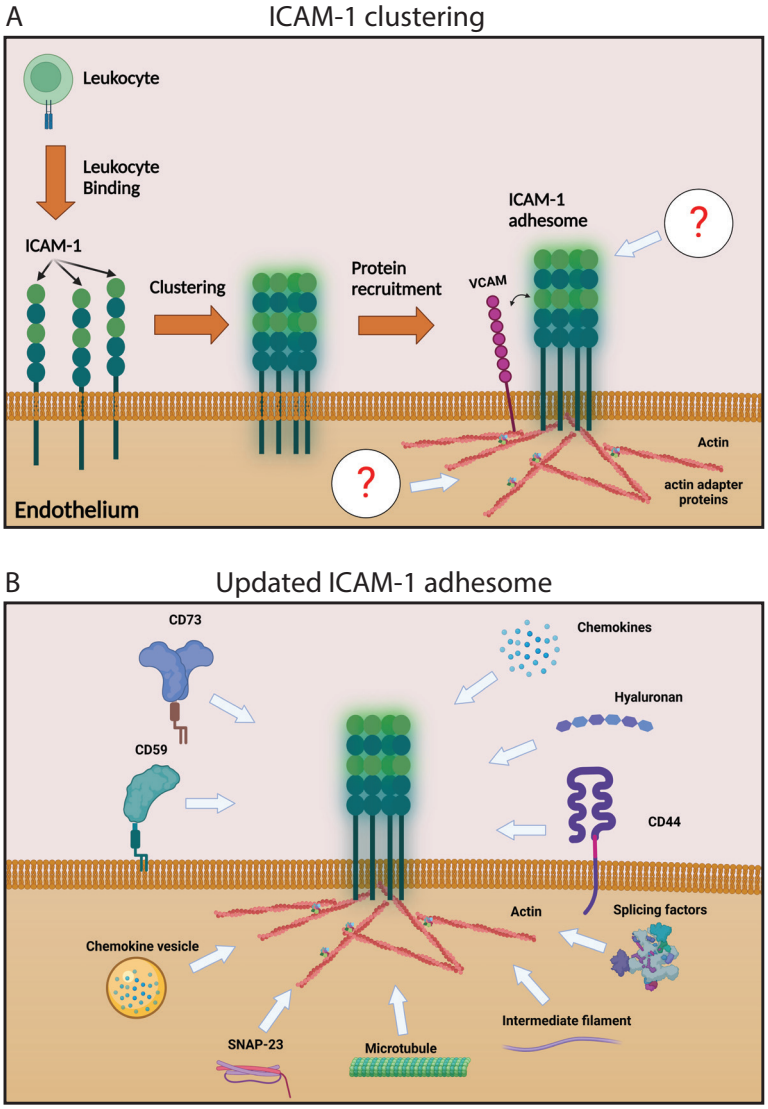

Figure 2. Schematic model of the ICAM-1 clustering process.
(A) ICAM-1 clustering by leukocytes induces the formation of the ICAM-1 adhesome leading to the recruitment of actin adapter proteins and rearrangement of the actin cytoskeleton. (B) Newly described members of the ICAM-1 adhesome complex include cytoskeletal components, transmembrane proteins, glycocalyx, secretory machinery, and vesicle components.

PERMEABILITY ASSAY

In **Chapter 6 and 7**, we show the potential of blood vessel-on-a-chip (BVOAC) devices to study the leukocyte TEM process. We show how we can use an existing BVOAC device and apply this to perform leakage and TEM assays in the same device. The barrier function of an endothelial monolayer, for example, is traditionally measured using electric cell-substrate impedance sensing (ECIS) or with fluorescently-labeled dextran in a Transwell system (Klems et al., 2020; Schimmel et al., 2020; Tiruppathi et al., 1992). These assays are very good at measuring barrier function, however, they are incompatible with microscopy. Therefore, the localization and timing of leaks are not detectable. The BVOAC device can be used to measure leakage using FITC-dextran with both confocal and widefield microscopy, thereby enabling real-time measurement of the leakage. This opens new possibilities to study the barrier function during leukocyte extravasation as a spatiotemporal process. Vascular leakage is one of the characteristics of inflammation, but it has been a longstanding question in the field if this leakage is caused or even accelerated by leukocyte extravasation. The hypothesis that leukocytes open the barriers to extravasate and thereby induce vascular leakage sounds plausible, however, vascular leakage and leukocyte extravasation have been shown to be uncoupled (He, 2010). The endothelium can limit leakage during leukocyte TEM using specific local pathways involving RhoA and Tie-2 signaling (Braun et al., 2020; Heemskerk et al., 2016). Introducing an assay to study this leakage as a spatiotemporal process will allow the field to further dissect the molecular pathways involved in this process. Adding leakage measurements to the leukocyte extravasation protocol using fluorescently-labeled endothelial cells and leukocytes only requires minimal alterations to the current protocol. Adding FITC-dextran to the leukocyte suspension combines the two assays and allows real-time imaging of the leakage during leukocyte extravasation. This experiment will pinpoint if the leakage is happening at all junctions or just at the sites where leukocytes transmigrate, or where leukocytes just interact with the endothelium. On top of that, it will show if the leakage occurs before, during, or after the diapedesis step, observations that are not possible with the current leakage assays.

PERSONALIZED MEDICINE

Another application where there is great potential for the BVOAC device is in the field of personalized medicine. Aimed at providing every patient with the most effective treatment for their specific disease and screening to avoid unwanted side effects of the treatment. Endothelial cells can be generated from peripheral blood from healthy donors or patients. These cells are named blood outgrowth endothelial cells (BOEC) and do not show any genetic modification (Martin-Ramirez et al., 2012). We have successfully used these BOEC to create BVOAC devices. This means that we can rebuild vessels lined with

patient's own endothelial cells. This opens possibilities to generate BVOAC from a donor and then study the transmigration of leukocytes of the same donor in the BVOAC system. The experiments would bypass any differences in, for example, human leukocyte antigen (HLA) types between the endothelium and the leukocytes. HLA mismatch between tissues and leukocytes will lead the leukocytes to become activated by the tissue and attack it, for example in graft-versus-host disease (Mickelson et al., 2000). HLA matching is generally ignored in *in vitro* transmigration studies using endothelial cells like HUVECs and primary leukocytes. Moreover, we can now start to use tailor-made vessels of the patient on a chip and use this to test different therapeutical approaches to determine which is most effective for this specific patient. This model could be developed even further to study other diseases that involve the vasculature and immune system, such as cancer. The role of the immune system is crucial to the effectiveness of cancer treatments. Therefore, it makes sense to speculate about further developing the BVOAC model to include a piece of tumor, derived from a biopsy or surgery. Doing this in a BVOAC system made from patient-derived BOEC and perfusing it with leukocytes from the patient would mimic the conditions in the patient closely. Different drugs and treatments could be tested in this system to select the most effective for this specific patient leading to more personalized treatment.

FURTHER IMPROVING THE BVOAC

Many factors regulate the behavior and functionality of endothelial cells, such as substrate stiffness, and chemical cues, such as growth factors. Another very important determinant of endothelial cell function is shear stress induced by flow (Baeyens et al., 2016; Hahn & Schwartz, 2009). Shear stress caused by laminar flow remodels endothelial cell-cell junctions and as a functional consequence improves the barrier function (Li et al., 2005; Polacheck et al., 2017). Defects in perfusion on the other hand have been implicated in various diseases such as stroke, myocardial infarction, and atherosclerosis (Ayata & Ropper, 2002; Dongaonkar et al., 2010; Hahn & Schwartz, 2009). Therefore, even though the BVOAC device is a strong improvement over the classical perfusion chambers in many aspects, the lack of flow is a significant drawback.

The LumeNext device used to generate BVOAC as described in chapter 6 and 7 unfortunately is not compatible with perfusion. Recently a new device for creating BVOAC was developed by the lab of Christopher Chen, called the human-engineered microvessel (hEMV) (Polacheck et al., 2019). This device is similar in design to the LumeNext device, both consisting of PDMS bonded to imaging glass with a diamond-shaped chamber accessible via 2 medium inlets and 2 matrix inlets. (Figure 3A) The major improvement of the hEMV design however is that the hEMV device can be perfused, even longer periods, i.e. hours to days. Because the device has a similar design to the LumeNext, the protocols developed in this thesis (**Chapter 6**) can be easily adapted to the hEMV chips. In fact, we reached out

to the Polacheck/Chen lab and were able to use these hEMV chips. Our preliminary data showed successful adaptation by creating a BVOAC in the hEMV chip and performing a neutrophil TEM assay under 1 dyn/cm^2 shear stress (Figure 3B). We were able to monitor all different steps of the TEM cascade, from rolling, and adhesion to crawling and actual diapedesis (Figure 3B). Thus, the hEMV device overcomes the biggest drawback of the BVOAC system, the lack of flow, and consolidates its claim to become the golden standard for *in vitro* leukocyte TEM studies.

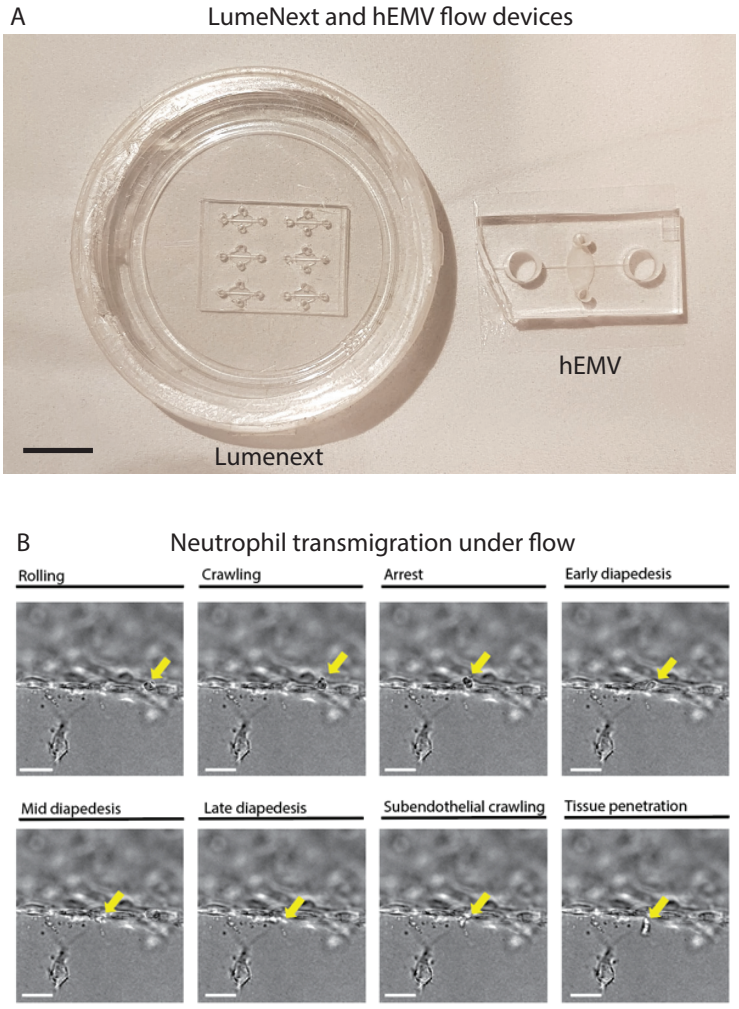

Figure 3. (A) Side-by-side image of a LumeNext and hEMV device for making BVOAC. The LumeNext device has 6 vessels on one chip but is incompatible with perfusion. The hEMV device has only a single vessel per chip, however larger medium inlets are suited for long-term controlled perfusion. (B) Stills from a video of an extravasating neutrophil in the hEMV device under 1 dyn/cm^2 shear stress. The direction of flow in the vessel is from the left side to the right side of the image. All steps from rolling under flow until migration into the matrix are indicated above the image.

ENDOTHELIUM INDUCES ARPC1B INDEPENDENT MIGRATION IN NEUTROPHILS

In **Chapter 7**, we applied the BVOAC model to study the migratory behavior of neutrophils from a patient with a deletion in the ARPC1B gene. During this project, we used three different parameters to characterize the migration behavior of these neutrophils and compare them to neutrophils from a healthy donor. From this study, it became clear that neutrophils that lack ARPC1B do cross the endothelium, albeit less efficient, but get stuck immediately after crossing, hence not capable of entering the tissue. In extra studies beyond the results presented in chapter 7, we explored this cellular behavior in more detail. Due to time restrictions, we did not include these data in the manuscript of chapter 7. Here, we present these data in this thesis because it shows how more advanced state-of-the-art models can lead to new findings.

When carefully analyzing the migratory behavior of the neutrophils with additional parameters, we observed what looked like a mismatch between the outcomes: Our initial results showed that neutrophils depleted from ARPC1B are impaired in both TEM as well as migration into the matrix. (Figure 4A) Interestingly, when these neutrophils were embedded directly in a collagen matrix and stimulated with C5a, we found that the control neutrophils generally migrated with an average speed of 0.08μm/sec, while ARPC1B-deficient neutrophils did not migrate or only “wobbled” and became polarized (Figure 4B). The speed of the ARPC1B deficient neutrophils is not zero since the polarization shifts the center of mass of the cell and is therefore detected as migration by the tracking algorithm. Careful assessment of the data, showed that ARPC1B-deficient neutrophils did not displace from their original position throughout the experiment. This is in strong contrast with the behavior of the ARPC1B-deficient neutrophils in the BVOAC experiment. These cells were clearly impaired, though a few ARPC1B-deficient neutrophils did migrate into the collagen, sometimes traveling more than 200 μm away from the vessel. This difference between no migration at all and migration over 200 μm puzzled us, as the collagen matrix used in both experiments was identical.

One of the differences between the two conditions is the presence of inflamed endothelium in the BVOAC experiment. This endothelium has been incubated overnight with TNFα to induce inflammation in the vessel, and during this time the endothelium starts producing and secreting proteins, including chemokines (Pober & Sessa, 2007). Based on this, we hypothesized that secreted proteins by inflamed endothelium may activate neutrophils that trigger the migration capacity independently from ARPC1B and trigger migration into the 3D matrix. This hypothesis was tested by harvesting supernatant from endothelial cells that were incubated with TNFα overnight and using this instead of C5a as a stimulus for neutrophils embedded in collagen-1 (figure 4C). Interestingly, the supernatant did trigger migration of ARPC1B-deficient neutrophils in collagen-1 as opposed to C5a, albeit less efficient than control neutrophils. Control neutrophils migrated when stimulated

either with C5a, TNFα, or HUVEC supernatant.

These preliminary data indicate that a factor produced and secreted by the inflamed endothelium can partially rescue the migration defects of the patient neutrophils and thus trigger an ARPC1B-independent pathway that drives cell migration. We believe this finding is of interest, as actin branching, mediated by the ARP protein complex, is essential for the formation of most cellular structures related to migration, including filopodia and lamellipodia(Chhabra & Higgs, 2007). These data suggest that the endothelium itself can trigger an unidentified signaling pathway in neutrophils that drives migration in an ARPC1B-independent manner.

Thus, identification of this migration pathway in neutrophils and potentially boosting the signaling may open a new strategy to promote ARPC1B-deficient neutrophils to migrate more efficiently across the endothelium towards the invading pathogens. Such findings may eventually help patients with ARPC1-mutations that suffer from chronic inflammation.

Additional data to identify the factors that trigger ARPC1B-deficient neutrophil migration may be found in **Chapter 4**. In this chapter, we have performed a chemokine screen on the supernatant of endothelial cells that were stimulated with TNFα for different time points, showing the release of multiple chemokines. These chemokines can be tested to trigger ARPC1B-deficient neutrophils to identify the specific chemokine inducing this ARPC1B independent mode of migration.

Historically, the endothelium was thought to merely convey the inflammatory signals from the tissue to the leukocytes in the bloodstream. The results presented in this thesis show that the endothelium has a much more active role in steering leukocyte extravasation through the vessel wall under inflammatory conditions: it can directly promote leukocyte migration, not only by triggering which transmigration route to take, trans- or paracellular, but also instruct leukocytes once they have crossed the endothelium and continue to migrate into the tissue. Such findings would have been impossible to make if we only would have been using the more simplified models. Thanks to the chip technology, we can now study the entire process of leukocyte extravasation and discover additional functions of the endothelium.

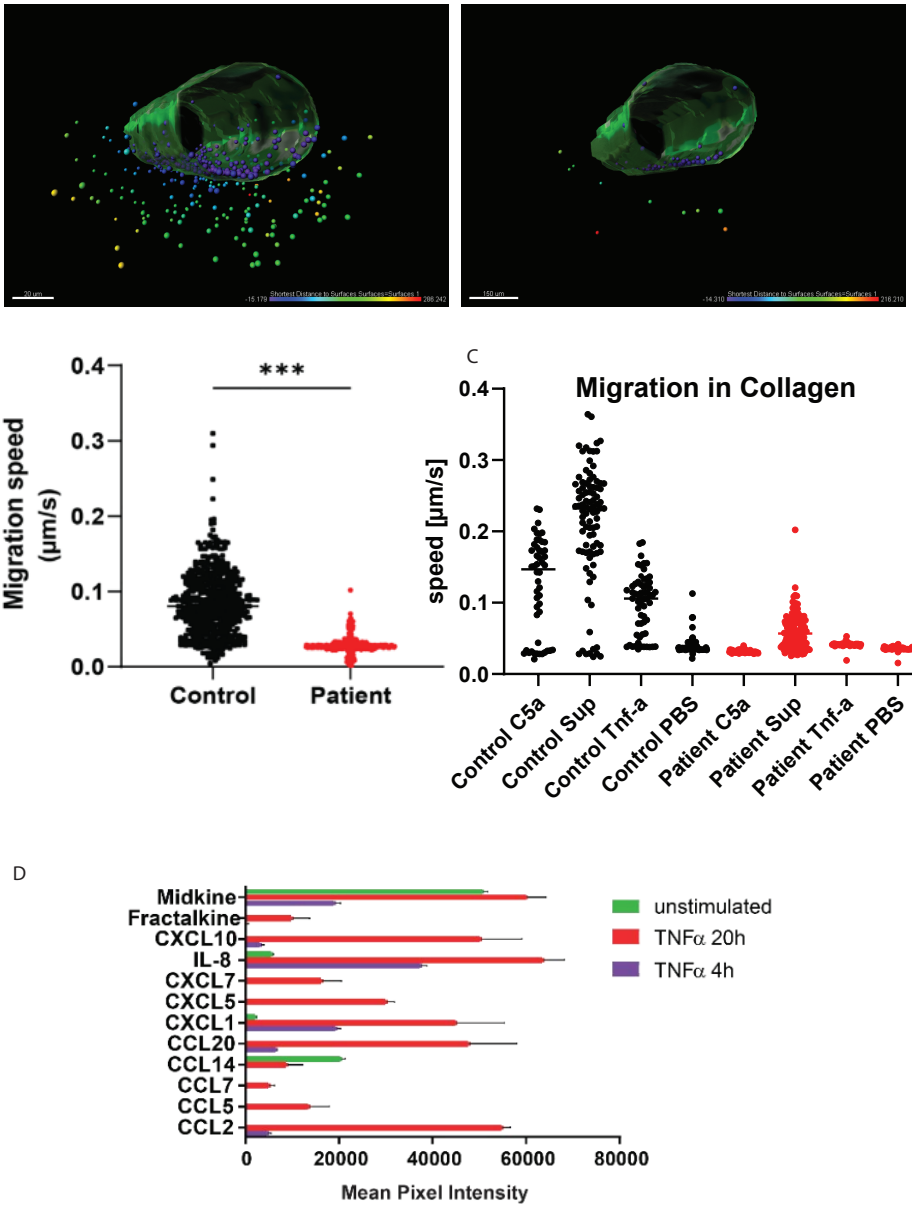

Figure 4. Partial rescue of ARPC1B deficient neutrophil migration defect in collagen using factors secreted by inflamed endothelial cells.
(A) neutrophils from a healthy donor and ARPC1B deficient donor after 2 hours in an inflamed BVOAC device. (B) The migration speed of C5a stimulated neutrophils in a collagen-1 matrix. (C) Patient and control neutrophil migration speed in collagen-1 matrix stimulated with either PBS, TNF, C5a, or supernatant of HUVEC stimulated with TNF. This graph represents data from a single experiment. Every dot represents the average speed of a single neutrophil. (D) Chemokines in the supernatant of HUVEC after 4 and 20 hours of TNF stimulation.

BETTER MODELS PRODUCE BETTER DATA

The work in this thesis can be roughly divided into two parts based on the methods used. The first part covers the proteomics screen of the ICAM-1 adhesome and the second part the blood vessel-on-a chip technology. Both parts study the process of leukocyte extravasation which has been studied for decades, more than a century even, and even though, we still uncovered new and exciting mechanisms, increasing our knowledge of this fascinating process.

It is clear that these new discoveries presented here were made possible only with the help of modern state-of-the-art tools. The first part uncovers several new pathways and adds many new subunits to a protein complex that has been studied for decades already. The second part develops a new model and uses this to characterize a migration defect in cells from a patient. This study revealed a much more active and unexpected role for the endothelium in activating leukocytes beyond immediate adhesive contact. An effect that without the blood vessel on a chip system would not have been detected.

Both these approaches highlight the importance of adopting new techniques such as advanced microscopy, omics approaches, and more advanced technologies such as organ-on-a chip systems into the workflow. Only by adopting these new techniques can we continue to discover new pathways for proteins and new functions for protein complexes, thereby unveiling unexpected interplay in more complex biological and physiological systems.

REFERENCES

Ayata, C., & Ropper, A. H. (2002). Ischaemic brain oedema. *Journal of Clinical Neuroscience*, *9*(2), 113–124. https://doi.org/10.1054/JOCN.2001.1031

Baeyens, N., Bandyopadhyay, C., Coon, B. G., Yun, S., & Schwartz, M. A. (2016). Endothelial fluid shear stress sensing in vascular health and disease. *The Journal of Clinical Investigation*, *126*(3), 821–828. https://doi.org/10.1172/JCI83083

Barreiro, O., Zamai, M., Yáñez-Mó, M., Tejera, E., López-Romero, P., Monk, P. N., Gratton, E., Caiolfa, V. R., & Sánchez-Madrid, F. (2008). Endothelial adhesion receptors are recruited to adherent leukocytes by inclusion in preformed tetraspanin nanoplatforms. *The Journal of Cell Biology*, *183*(3), 527–542. https://doi.org/10.1083/JCB.200805076

Braun, L. J., Stegmeyer, R. I., Schäfer, K., Volkery, S., Currie, S. M., Kempe, B., Nottebaum, A. F., & Vestweber, D. (2020). Platelets docking to VWF prevent leaks during leukocyte extravasation by stimulating Tie-2. *Blood*, *136*(5), 627–639. https://doi.org/10.1182/BLOOD.2019003442

Bromley, S. K., Mempel, T. R., & Luster, A. D. (2008). Orchestrating the orchestrators: chemokines in control of T cell traffic. *Nature Immunology 2008 9:9*, *9*(9), 970–980. https://doi.org/10.1038/ni.f.213

Butcher, E. C. (1991). Leukocyte-endothelial cell recognition: Three (or more) steps to specificity and diversity. *Cell*, *67*(6), 1033–1036. https://doi.org/10.1016/0092-8674(91)90279-8

Cáceres, J., Screaton, G., development, A. K.-G. &, & 1998, undefined. (1998). A specific subset of SR proteins shuttles continuously between the nucleus and the cytoplasm. *Genesdev.Cshlp.Org*. http://genesdev.cshlp.org/content/12/1/55.short

Chesnutt, B. C., Smith, D. F., Raffler, N. A., Smith, M. L., White, E. J., & Ley, K. (2006). Induction of LFA-1-dependent neutrophil rolling on ICAM-1 by engagement of E-selectin. *Microcirculation (New York, N.Y. : 1994)*, *13*(2), 99–109. https://doi.org/10.1080/10739680500466376

Chhabra, E. S., & Higgs, H. N. (2007). The many faces of actin: matching assembly factors with cellular structures. *Nature Cell Biology 2007 9:10*, *9*(10), 1110–1121. https://doi.org/10.1038/ncb1007-1110

Cowper, A. E., Cáceres, J. F., Mayeda, A., & Screaton, G. R. (2001). Serine-arginine (SR) protein-like factors that antagonize authentic SR proteins and regulate alternative splicing. *The Journal of Biological Chemistry*, *276*(52), 48908–48914. https://doi.org/10.1074/JBC.M103967200

Dongaonkar, R. M., Stewart, R. H., Geissler, H. J., & Laine, G. A. (2010). Myocardial microvascular permeability, interstitial oedema, and compromised cardiac function. *Cardiovascular Research*, *87*(2), 331–339. https://doi.org/10.1093/CVR/CVQ145

Freeman, S. A., Vega, A., Riedl, M., Collins, R. F., Ostrowski, P. P., Woods, E. C., Bertozzi, C. R., Tammi, M. I., Lidke, D. S., Johnson, P., Mayor, S., Jaqaman, K., & Grinstein, S. (2018). Transmembrane Pickets Connect Cyto- and Pericellular Skeletons Forming Barriers to Receptor Engagement. *Cell*, *172*(1–2), 305-317.e10. https://doi.org/10.1016/J.CELL.2017.12.023

Hahn, C., & Schwartz, M. A. (2009). Mechanotransduction in vascular physiology and atherogenesis. *Nature Reviews. Molecular Cell Biology*, *10*(1), 53–62. https://doi.org/10.1038/NRM2596

He, P. (2010). Leucocyte/endothelium interactions and microvessel permeability: coupled or uncoupled? *Cardiovascular Research*, *87*(2), 281–290. https://doi.org/10.1093/CVR/CVQ140

Heemskerk, N., Schimmel, L., Oort, C., van Rijssel, J., Yin, T., Ma, B., van Unen, J., Pitter, B., Huveneers, S., Goedhart, J., Wu, Y., Montanez, E., Woodfin, A., & van Buul, J. D. (2016). F-actin-rich contractile endothelial pores prevent vascular leakage during leukocyte diapedesis through local RhoA signalling. *Nature Communications*, *7*. https://doi.org/10.1038/NCOMMS10493

Huynh, J., Nishimura, N., Rana, K., Peloquin, J. M., Califano, J. P., Montague, C. R., King, M. R., Schaffer, C. B., & Reinhart-King, C. A. (2011). Age-related intimal stiffening enhances endothelial permeability and leukocyte transmigration. *Science Translational Medicine*, *3*(112). https://doi.org/10.1126/SCITRANSLMED.3002761

Kaatz, M., Berod, L., Lagadari, M., Fluhr, J. W., Elsner, P., & Norgauer, J. (2006). Microtubules regulate expression of ICAM-1 in epidermoid cells (KB cells). *Skin Pharmacology and Physiology*, *19*(6), 322–328. https://doi.org/10.1159/000095252

Kadono, T., Venturi, G. M., Steeber, D. A., & Tedder, T. F. (2002). Leukocyte Rolling Velocities and Migration Are Optimized by Cooperative L-Selectin and Intercellular Adhesion Molecule-1 Functions. *The Journal of Immunology*, *169*(8), 4542–4550. https://doi.org/10.4049/JIMMUNOL.169.8.4542

Kanters, E., van Rijssel, J., Hensbergen, P. J., Hondius, D., Mul, F. P. J., Deelder, A. M., Sonnenberg, A., van Buul, J. D., & Hordijk, P. L. (2008). Filamin B mediates ICAM-1-driven leukocyte transendothelial migration. *Journal of Biological Chemistry*, *283*(46), 31830–31839. https://doi.org/10.1074/JBC.M804888200/ATTACHMENT/9EF61D58-5668-4810-8385-B845EE2D5E28/MMC1.ZIP

Klems, A., van Rijssel, J., Ramms, A. S., Wild, R., Hammer, J., Merkel, M., Derenbach, L., Préau, L., Hinkel, R., Suarez-Martinez, I., Schulte-Merker, S., Vidal, R., Sauer, S., Kivelä, R., Alitalo, K., Kupatt, C., van Buul, J. D., & le Noble, F. (2020). The GEF Trio controls endothelial cell size and arterial remodeling downstream of Vegf signaling in both zebrafish and cell models. *Nature Communications 2020 11:1*, *11*(1), 1–20. https://doi.org/10.1038/s41467-020-19008-0

Kuschen, G. S. V., Coulin, F., Power, C. A., Proudfoot, A. E. I., Hubbard, R. E., Hoogewerf, A. J., & Wells, T. N. C. (1999). Glycosaminoglycans interact selectively with chemokines and modulate receptor binding and cellular responses. *Biochemistry*, *38*(39), 12959–12968. https://doi.org/10.1021/BI990711D

Li, Y. S. J., Haga, J. H., & Chien, S. (2005). Molecular basis of the effects of shear stress on vascular endothelial cells. *Journal of Biomechanics*, *38*(10), 1949–1971. https://doi.org/10.1016/J.JBIOMECH.2004.09.030

Martin-Ramirez, J., Hofman, M., van den Biggelaar, M., Hebbel, R. P., & Voorberg, J. (2012). Establishment of outgrowth endothelial cells from peripheral blood. *Nature Protocols 2012 7:9*, *7*(9), 1709–1715. https://doi.org/10.1038/nprot.2012.093

Mickelson, E. M., Petersdorf, E., Anasetti, C., Martin, P., Woolfrey, A., & Hansen, J. A. (2000). HLA matching in hematopoietic cell transplantation. *Human Immunology*, *61*(2), 92–100. https://doi.org/10.1016/S0198-8859(99)00151-2

Muro, S., Wiewrodt, R., Thomas, A., Koniaris, L., Albelda, S. M., Muzykantov, V. R., & Koval, M. (2003). A novel endocytic pathway induced by clustering endothelial ICAM-1 or PECAM-1. *Journal of Cell Science*, *116*(8), 1599–1609. https://doi.org/10.1242/JCS.00367

Mylvaganam, S., Riedl, M., Vega, A., Collins, R. F., Jaqaman, K., Grinstein, S., & Freeman, S. A. (2020). Stabilization of Endothelial Receptor Arrays by a Polarized Spectrin Cytoskeleton Facilitates Rolling and Adhesion of Leukocytes. *Cell Reports*, *31*(12). https://doi.org/10.1016/J.CELREP.2020.107798

Naor, D., Sionov, R. V., & Ish-Shalom, D. (1997). CD44: structure, function, and association with the malignant

process. *Advances in Cancer Research*, *71*, 241–319. https://doi.org/10.1016/S0065-230X(08)60101-3

Niemelä, J., Henttinen, T., Yegutkin, G. G., Airas, L., Kujari, A.-M., Rajala, P., & Jalkanen, S. (2004). IFN-alpha induced adenosine production on the endothelium: a mechanism mediated by CD73 (ecto-5'-nucleotidase) up-regulation. *Journal of Immunology (Baltimore, Md. : 1950)*, *172*(3), 1646–1653. https://doi.org/10.4049/JIMMUNOL.172.3.1646

Nieminen, M., Henttinen, T., Merinen, M., Marttila-Ichihara, F., Eriksson, J. E., & Jalkanen, S. (2006). Vimentin function in lymphocyte adhesion and transcellular migration. *Nature Cell Biology 2006 8:2*, *8*(2), 156–162. https://doi.org/10.1038/ncb1355

Pober, J. S., & Sessa, W. C. (2007). Evolving functions of endothelial cells in inflammation. *Nature Reviews. Immunology*, *7*(10), 803–815. https://doi.org/10.1038/NRI2171

Polacheck, W. J., Kutys, M. L., Tefft, J. B., & Chen, C. S. (2019). Microfabricated blood vessels for modeling the vascular transport barrier. *Nature Protocols*, *14*(5), 1425–1454. https://doi.org/10.1038/S41596-019-0144-8

Polacheck, W. J., Kutys, M. L., Yang, J., Eyckmans, J., Wu, Y., Vasavada, H., Hirschi, K. K., & Chen, C. S. (2017). A non-canonical Notch complex regulates adherens junctions and vascular barrier function. *Nature 2017 552:7684*, *552*(7684), 258–262. https://doi.org/10.1038/nature24998

Ponta, H., Sherman, L., & Herrlich, P. A. (2003). CD44: FROM ADHESION MOLECULES TO SIGNALLING REGULATORS. *NATURE REVIEWS | MOLECULAR CELL BIOLOGY*, *4*, 3. https://doi.org/10.1038/nrm1004

Rothman, J. E. (1994). Mechanisms of intracellular protein transport. *Nature 1994 372:6501*, *372*(6501), 55–63. https://doi.org/10.1038/372055a0

Salas, A., Shimaoka, M., Kogan, A. N., Harwood, C., von Andrian, U. H., & Springer, T. A. (2004). Rolling Adhesion through an Extended Conformation of Integrin αLβ2 and Relation to α I and β I-like Domain Interaction. *Immunity*, *20*(4), 393–406. https://doi.org/10.1016/S1074-7613(04)00082-2

Sapra, A. K., Änkö, M. L., Grishina, I., Lorenz, M., Pabis, M., Poser, I., Rollins, J., Weiland, E. M., & Neugebauer, K. M. (2009). SR protein family members display diverse activities in the formation of nascent and mature mRNPs in vivo. *Molecular Cell*, *34*(2), 179–190. https://doi.org/10.1016/J.MOLCEL.2009.02.031

Schaefer, A., Riet, J. te, Ritz, K., Hoogenboezem, M., Anthony, E. C., Mul, F. P. J., de Vries, C. J., Daemen, M. J., Figdor, C. G., van Buul, J. D., & Hordijk, P. L. (2014). Actin-binding proteins differentially regulate endothelial cell stiffness, ICAM-1 function and neutrophil transmigration. *Journal of Cell Science*, *127*(20), 4470–4482. https://doi.org/10.1242/JCS.154708/VIDEO-4

Schimmel, L., de Ligt, A., Tol, S., de Waard, V., & van Buul, J. D. (2020). Endothelial RhoB and RhoC are dispensable for leukocyte diapedesis and for maintaining vascular integrity during diapedesis. *Small GTPases*, *11*(3), 225. https://doi.org/10.1080/21541248.2017.1377815

Schimmel, L., van der Stoel, M., Rianna, C., van Stalborch, A.-M., de Ligt, A., Hoogenboezem, M., Tol, S., van Rijssel, J., Szulcek, R., Bogaard, H. J., Hofmann, P., Boon, R., Radmacher, M., de Waard, V., Huveneers, S., & van Buul, J. D. (2018). Stiffness-Induced Endothelial DLC-1 Expression Forces Leukocyte Spreading through Stabilization of the ICAM-1 Adhesome. *Cell Reports*, *24*(12), 3115–3124. https://doi.org/10.1016/J.CELREP.2018.08.045

Springer, T. A. (1994). Traffic signals for lymphocyte recirculation and leukocyte emigration: the multistep paradigm. *Cell*, *76*(2), 301–314. https://doi.org/10.1016/0092-8674(94)90337-9

Stroka, K. M., & Aranda-Espinoza, H. (2011). Endothelial cell substrate stiffness influences neutrophil

transmigration via myosin light chain kinase-dependent cell contraction. *Blood*, *118*(6), 1632–1640. https://doi.org/10.1182/BLOOD-2010-11-321125

Tanaka, Y., Adams, D. H., & Shaw, S. (1993). Proteoglycans on endothelial cells present adhesion-inducing cytokines to leukocytes. *Immunology Today*, *14*(3), 111–115. https://doi.org/10.1016/0167-5699(93)90209-4

Tiruppathi, C., Malik, A. B., del Vecchio, P. J., Keese, C. R., & Glaever, I. (1992). Electrical method for detection of endothelial cell shape change in real time: Assessment of endothelial barrier function. *Proceedings of the National Academy of Sciences of the United States of America*, *89*(17), 7919–7923. https://doi.org/10.1073/PNAS.89.17.7919

van Buul, J. D., van Rijssel, J., van Alphen, F. P. J., van Stalborch, A. M., Mul, E. P. J., & Hordijk, P. L. (2010). ICAM-1 clustering on endothelial cells recruits VCAM-1. *Journal of Biomedicine & Biotechnology*, *2010*. https://doi.org/10.1155/2010/120328

Wessel, F., Winderlich, M., Holm, M., Frye, M., Rivera-Galdos, R., Vockel, M., Linnepe, R., Ipe, U., Stadtmann, A., Zarbock, A., Nottebaum, A. F., & Vestweber, D. (2014). Leukocyte extravasation and vascular permeability are each controlled in vivo by different tyrosine residues of VE-cadherin. *Nature Immunology*, *15*(3), 223–230. https://doi.org/10.1038/NI.2824

Zieman, S. J., Melenovsky, V., & Kass, D. A. (2005). Mechanisms, pathophysiology, and therapy of arterial stiffness. *Arteriosclerosis, Thrombosis, and Vascular Biology*, *25*(5), 932–943. https://doi.org/10.1161/01.ATV.0000160548.78317.29

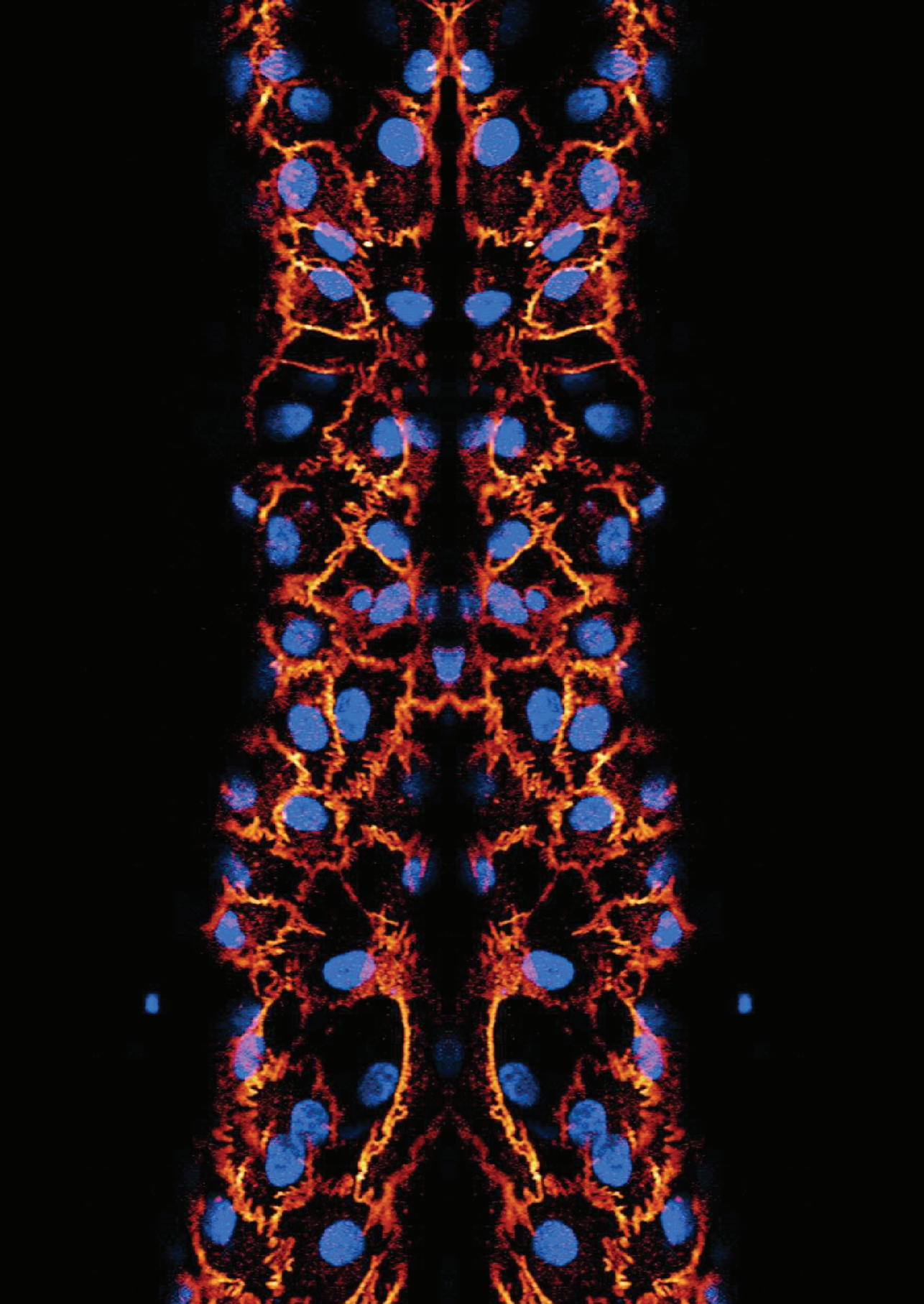

APPENDICES &

Summary
Samenvatting
List of publications
Acknowledgements

SUMMARY

Endothelial cells line the inside of blood vessels, providing a semi-permeable barrier that separates the blood from the surrounding tissues. Under inflammatory conditions, leukocytes are directed to exit the vasculature through this barrier to perform their function in the tissues and clean up invading pathogens. Inflammation is accompanied by the production of mediators by various types of cells that trigger pro-inflammatory signals. These signals can then activate the endothelium, causing it to become inflamed, increasing expression of several proteins. One of the key characteristics is the upregulation of adhesion molecules and the activation of several pathways that regulate actin cytoskeleton dynamics. These changes in the endothelium allow leukocytes to recognize inflamed areas in the human body. Through these changes, the endothelium guides the leukocytes to a suitable exit site to cross the vascular barrier and continue toward the site of infection. This process is known as leukocyte transendothelial migration (TEM), a multi-step process that performs a pivotal role not only in inflammatory reactions, but also in various physiological processes of the immune system. Impaired leukocyte extravasation prevents leukocytes from entering the tissue and clearing the infection, for example, in patients with leukocyte adhesion deficiency syndrome. Excessive leukocyte extravasation, on the other hand, can damage tissues in diseases, such as rheumatoid arthritis or COVID-19-induced lung damage. Therefore, we must obtain a complete understanding of this process so that we can develop better therapeutical interventions for conditions where this process is disturbed.

The actin cytoskeleton is an essential and dynamic part of the endothelial cell, constantly remodeling under the influence of extracellular stimuli and actin-binding proteins. These proteins control the turnover of actin and can induce the formation of high-tension actin stress fibers or branched meshes. During inflammation, the actin cytoskeleton remodels, thereby giving rise to various actin-based structures at the surface of the endothelial cell. These actin-based networks are essential for successful leukocyte extravasation and the determination of a suitable exit site. In **Chapter 2**, we give a comprehensive overview of the versatile role of the **endothelial actin cytoskeleton** under inflammatory conditions. Furthermore, we describe how leukocytes extravasate via the transcellular or paracellular route. The preference for one or the other depends on both the leukocyte subset and vascular bed. Finally, we give an overview of experimental data describing these different routes *in vivo* and *in vitro*.

During extravasation, adhering leukocytes bind adhesion molecules on the endothelium, such as intercellular adhesion molecule 1 (ICAM-1). This action leads to the clustering of the ICAM-1 molecules and triggers intracellular signaling pathways in the endothelium, known as the recruitment of the so-called ICAM-1 adhesome. In **Chapter 3**, we zoom in on the **ICAM-1 adhesome** and perform a cutting-edge proteomic screen revealing for the first time the full ICAM-1 adhesome. One of the prominent hits is **CD44**, a protein known for binding Hyaluronan, which is part of the endothelial glycocalyx. We confirm the recruitment of

CD44 to the ICAM-1 adhesome and show that depletion of this protein by RNA interference inhibits efficient cytotoxic T lymphocyte (CTL) extravasation. Further analysis revealed that ICAM-1 needs CD44 to be fully functional.

In **Chapter 4**, we study the function of another hit from the proteomic screen of the ICAM-1 adhesome; **SNAP-23**. We show how CTLs require stimulation by endothelial chemokines to perform extravasation via the transcellular pathway. Our data suggests that SNAP-23 guides chemokine-containing vesicles to be released at the ICAM-1-rich docking structure to locally activate integrins on CTLs, which stimulates the extravasation.

Unlike CTLs, neutrophils strongly prefer the paracellular route during extravasation. In **Chapter 5**, we use novel imaging methods to study the architecture of endothelial cell junctions to better understand how neutrophils traverse this barrier and why they prefer some exit sites over others. We describe that junctions between adjacent endothelial cells are formed by **overlapping plasma membrane regions**. Regions with increased overlap are enriched in PECAM-1, and transmigrating neutrophils prefer sites with wider PECAM-1-rich overlapping membranes.

In vitro research into leukocyte extravasation has generally been performed with endothelial cells cultured on stiff substrates such as glass or plastic. This is not comparable to the physiological environment, where the substrate consists of matrix proteins and is much softer. In **Chapter 6**, we use a **blood-vessel-on-a-chip** system where endothelial cells are grown in a tube shape in a collagen-1 hydrogel. Vessels created with this device have a barrier function, and the model can be used to study the complete leukocyte extravasation cascade from the lumen into the perivascular tissue.

In **Chapter 7**, we used this system to characterize neutrophils from a patient with a rare genetic defect and show an impaired migration phenotype. The patient has a defect in the **ARPC1B gene**, which encodes a subunit of the actin-binding ARP2/3 complex. This complex is crucial for proper actin branching, which drives various actin-based structures and, consequently, pathways that trigger cell migration. Using our blood-vessel-on-a-chip system, we discovered that neutrophils from this patient can cross the endothelium, but are subsequently unable to migrate into the perivascular tissue. Interestingly, without our model, we would not have been able to observe these migration dynamics, as the routine migration models are built up from a 2D environment and do not include the extracellular matrix space.

Chapter 8 summarizes the thesis and discusses some of the longstanding issues in the field. Moreover, in this chapter, we discuss potential **open questions** that arise from these studies.

NEDERLANDSE SAMENVATTING

Bloedvaten zijn bekleed met endotheelcellen die een semipermeabele barrière vormen die het bloed scheidt van de omliggende weefsels. Wanneer er een ontsteking optreedt, worden leukocyten (de witte bloedcellen) geactiveerd om door deze barrière heen de bloedvaten te verlaten om vervolgens hun rol in de weefsels uit te kunnen voeren en binnendringende ziekteverwekkers op te ruimen. Ontstekingen gaan gepaard met de productie van mediatoren door verschillende celtypes die pro-inflammatoire signalen opwekken. Deze signalen kunnen vervolgens het endotheel activeren, dat ontstoken raakt, waardoor de expressie van diverse eiwitten toeneemt. Dit leidt bijvoorbeeld tot het op reguleren van adhesiemoleculen en het activeren van signaleringsroutes binnenin de endotheelcel. Leukocyten kunnen door deze veranderingen van het endotheel ontstoken gebieden in het menselijk lichaam herkennen. Door deze veranderingen stuurt het endotheel de leukocyten naar een geschikte uitgangsplaats om de vasculaire barrière te passeren en verder te migreren naar de plaats van infectie. Dit proces staat bekend als leukocyt transendotheliale migratie (TEM), een proces dat naast een cruciale rol bij ontstekingsreacties, ook bij fysiologische processen van het immuunsysteem essentieel is. Als het TEM proces verstoord is, zorgt dat ervoor dat leukocyten niet bij de ontsteking kunnen komen om de infectie op te ruimen, bijvoorbeeld bij patiënten met een Leukocyten Adhesie Deficiëntie (LAD) syndroom. Overmatige extravasatie van leukocyten kan daarentegen ook leiden tot schade aan weefsels zoals bijvoorbeeld gebeurt bij reumatoïde artritis of door COVID-19 veroorzaakte longschade. Daarom is het essentieel dat we het TEM proces volledig begrijpen, zodat we betere therapeutische interventies kunnen ontwikkelen voor aandoeningen waarbij dit proces verstoord is.

Het actine-cytoskelet is een essentieel en dynamisch onderdeel van de functionerende endotheelcel en wordt voortdurend vernieuwd en aangepast onder invloed van extracellulaire stimuli. . In dit proces regelen actine-bindende eiwitten de vernieuwing en organisatie van actine en kunnen ze de vorming van actine-stressvezels waarop biofysische krachten staan of vertakte actine-gerelateerde netwerken induceren. Tijdens ontsteking wordt het actine-cytoskelet op een dusdanige manier aangepast, dat er op actine-gebaseerde structuren ontstaan aan het oppervlak van de endotheelcel. Deze structuren zijn belangrijk voor het kiezen van een geschikte uitgangsplaats en dragen daarmee bij aan een succesvolle passage van de leukocyten door de bloedvatwand. In **hoofdstuk 2** geven we een uitgebreid overzicht van de veelzijdige rol van het **endotheliale actine cytoskelet** onder ontstekingscondities. Verder beschrijven we hoe leukocyten uittreden via de transcellulaire of paracellulaire route. De voorkeur voor de route hangt zowel van de leukocytensubset af als van het vaatbed. Ten slotte geven we een overzicht van experimentele studies uit de literatuur die deze voorkeur *in vivo* en *in vitro* beschrijven.

Tijdens TEM binden leukocyten aan de adhesiemoleculen die op het endotheel tot expressie komen, zoals intercellulair adhesiemolecuul-1 (ICAM-1). Dit leidt tot het

bundelen van de ICAM-1-moleculen in het membraan van de endotheelcellen en activeert intracellulaire signaalroutes, een proces dat bekend staat als het rekruteren van het **ICAM-1-adhesoom**. In **hoofdstuk 3** zoomen we in op het ICAM-1-adhesoom met behulp van een geavanceerde screening op basis van massa spectometrie. Hiermee onthullen we voor de eerste keer het volledige ICAM-1-adhesoom. Een van de voornaamste vondsten is **CD44**, een eiwit dat bekend staat als de voornaamste receptor van hyaluronan; dit laatste is een suikerstructuur die op de endotheliale glycocalyx aanwezig is en dient als beschermingslaag rondom de cel. We hebben kunnen bevestigen dat CD44 naar het ICAM-1-adhesoom wordt gerekruteerd en dat depletie van dit eiwit door RNA-interferentie een efficiënte extravasatie van cytotoxische T-lymfocyten (CTLs) remt. Verdere analyse liet zien dat ICAM-1 afhankelijk is van CD44 om volledig functioneel te zijn.

In **hoofdstuk 4** bestuderen we de functie van een andere "treffer" van de eiwit screening van het ICAM-1-adhesoom; **SNAP-23**. We laten zien dat CTLs stimulatie door endotheliale chemokines nodig hebben om extravasatie via de transcellulaire route uit te kunnen voeren. Onze gegevens suggereren dat SNAP-23 blaasjes met chemokines naar het ICAM-1 adhesome stuurt, waar ze heel lokaal de integrines op de CTL activeren, en daarmee de extravasatie stimuleren.

In tegenstelling tot CTLs hebben neutrofielen een sterke voorkeur voor de paracellulaire route tijdens extravasatie. In **hoofdstuk 5** gebruiken we nieuwe imaging methodes om de structuur van endotheelcel juncties beter te bestuderen en zo uit te leggen hoe neutrofielen deze barrière passeren en waarom ze een voorkeur voor bepaalde uitgangsplekken hebben. We beschrijven dat aangrenzende endotheelcellen verbindingen vormen met **overlappende plasmamembranen**. De plekken waar deze plasmamembranen overlappen zijn positief voor PECAM-1 en transmigrerende neutrofielen hebben een voorkeur voor plaatsen met bredere PECAM-1-rijke overlappende membranen.

In vitro-onderzoek naar extravasatie van leukocyten wordt veelal gedaan met endotheelcellen die gekweekt zijn op stijve substraten zoals glas of plastic. Deze situatie is niet te vergelijken met de fysiologische omgeving waar de ondergrond uit matrixeiwitten bestaat en veel zachter is. In **hoofdstuk 6** gebruiken we een bloedvat-op-een-chip systeem waar endotheelcellen in de vorm van een buis in een collageen-gel groeien. Deze kunstmatige bloedvaten hebben een functionele barrière en het model kan worden gebruikt om het volledige TEM proces te bestuderen, van de binnenzijde van de vaatwand tot de tocht het weefsel in.

In **hoofdstuk 7** gebruiken we dit systeem om neutrofielen van een patiënt met een zeldzaam genetisch defect te bestuderen dat leidt tot gebrekkige migratie. De patiënt heeft een defect in het **ARPC1B gen**, dat codeert voor een onderdeel van het actinebindende ARP2/3-complex. Dit complex is cruciaal voor het vertakken van actine wat essentieel is voor verschillende cellulaire structuren die betrokken zijn bij leukocyt TEM. Dankzij ons bloed-vat-op-een-chip-systeem ontdekten we dat neutrofielen van deze patiënt wel het endotheel kunnen passeren, maar niet in staat zijn om in de perivasculaire weefsels door

te dringen. Deze observatie was niet mogelijk geweest zonder ons model, omdat de gebruikelijke migratiemodellen zijn opgebouwd in een 2D-omgeving zonder extracellulaire matrix.

Hoofdstuk 8 vat het proefschrift samen en bespreekt enkele nog openstaande onderwerpen van het vakgebied. Daarnaast bespreken we in dit hoofdstuk open vragen die uit deze onderzoeken naar voren komen.

LIST OF PUBLICATIONS

Arts, J. J. G., Mahlandt, E. K., Grönloh, M. L. B., Schimmel, L., Noordstra, I., Gordon, E., **van Steen, A. C. I.**, Tol, S., Walzog, B., van Rijssel, J., Nolte, M. A., Postma, M., Khuon, S., Heddleston, J. M., Wait, E., Chew, T. L., Winter, M., Montanez, E., Goedhart, J., & van Buul, J. D. (2021). Endothelial junctional membrane protrusions serve as hotspots for neutrophil transmigration. *ELife*, *10*. https://doi.org/10.7554/ELIFE.66074

Jeucken, K. C. M., van Rooijen, C. C. N., Kan, Y. Y., Kocken, L. A., Jongejan, A., **van Steen, A. C. I**., van Buul, J. D., Olsson, H. K., van Hamburg, J. P., & Tas, S. W. (2022). Differential Contribution of NF-κB Signaling Pathways to CD4 + Memory T Cell Induced Activation of Endothelial Cells. *Frontiers in Immunology*, *13*. https://doi.org/10.3389/FIMMU.2022.860327

Kempers, L*., Sprenkeler, E. G. G*., **van Steen, A. C. I.***, van Buul, J. D., & Kuijpers, T. W. (2021). Defective Neutrophil Transendothelial Migration and Lateral Motility in ARPC1B Deficiency Under Flow Conditions (Chapter 7). *Frontiers in Immunology*, *12*. https://doi.org/10.3389/FIMMU.2021.678030

Schoppmeyer, R., **van Steen, A. C. I.**, Kempers, L., Timmerman, A. L., Nolte, M. A., Hombrink, P., van Buul Correspondence, J. D., & van Buul, J. D. (2022). The endothelial diapedesis synapse regulates transcellular migration of human T lymphocytes in a CX3CL1- and SNAP23-dependent manner (Chapter 4). *CellReports*, *38*, 110243. https://doi.org/10.1016/j.celrep.2021.110243

van Steen, A. C. I.*, Kempers, L*., Schoppmeyer, R., Blokker, M., Beebe, D. J., Nolte, M. A., & van Buul, J. D. (2021). Transendothelial migration induces differential migration dynamics of leukocytes in tissue matrix (Chapter 6). *Journal of Cell Science*, *134*(21). https://doi.org/10.1242/JCS.258690

van Steen, A. C. I.*, van der Meer, W. J.*, Hoefer, I. E., & van Buul, J. D. (2020). Actin remodelling of the endothelium during transendothelial migration of leukocytes (Chapter 2). In *Atherosclerosis* (Vol. 0, Issue 0, pp. 1–9). Elsevier Ireland Ltd. https://doi.org/10.1016/j.atherosclerosis.2020.06.004

* authors contributed equally

ACKNOWLEDGEMENTS

Finally, one of the most important parts of the Thesis: the acknowledgments! Because working together and sharing ideas and knowledge is one of the most beautiful aspects of science. This is not just via the formal channels of publications and presentations and meetings, but also in informal conversations over a cup of coffee or a beer. In short, the work in this thesis would not have been possible without the help of many people whom I would like to thank for not only contributing directly to the thesis but also making science fun!

First of all, I would like to thank my promoter **Jaap** for giving me the opportunity to do a PhD in his group. I would like to thank you for the freedom you gave me and your enthusiasm for science. This has allowed me to develop myself in many areas and to do many fun projects. **Martijn**, my co-promoter, you only joined later in my PhD trajectory, and really helped me clarify the path towards the end. You always offered a listening ear and good input on the projects, besides the scientific input it was also very nice to have you on the team.

My OIO committee **Robin** and **Robbert**. Thank you for your support and feedback throughout the process, and the occasional comments on my project management were very helpful.

Then it's my turn to thank my paranymphs
Lanette, when you started in our group we soon started working together. You made quite the impression you came up with the groundbreaking idea to write down experiments and methods and plan things ahead of time. Eventually, that led to a beautiful collaboration and an interesting adventure to the USA. Good luck with your next adventure!

Joost, I really got to know you during our time at Helix. I always enjoy drinking a beer with you and having philosophical discussions. At the same time, you provide honest feedback and support when it is really needed, although sometimes not in the most tactful way. This always challenged me to think critically and consider different perspectives on topics.

Sofia, you started your PhD before I did and were there for almost my entire PhD. We visited quite several conferences together and I always enjoyed that a lot. Also when you successfully defended your thesis, that gave me the signal that I should start moving toward the end of my PhD journey.

Werner, you started working as my student and stayed to do your PhD at Sanquin. What an interesting internship that was. Trial and mostly error was the process while trying to get started with the vessel on a chip device. This led to a lot of kopstootjes at Radion at 3 PM on a Tuesday when all the vessels had collapsed for unknown reasons again.

Max, you were the last to join Jaaps Angels, and you were an amazing addition to the group. Your amazing work ethic and productivity really made the rest of us look bad. Having a discussion with you about science would always lead to productive and useful ideas.

I would like to thank the other members of our group over the years. **Jos**, you were always helpful and really helped me get started working in the lab, teaching me almost all of the techniques in the lab. **Rouven,** we worked together really well and made produced some very nice science. I always enjoyed our collaboration. **Anne-Marieke**, you were crucial to keeping the lab running at all times and always happy to help. **Andreas**, we came into contact because I was looking for a plasma asher but that turned into a very cool project. **Rianne,** I had a great time supervising you, your enthusiasm was contagious. I would like to further thank all the other members of the group over the years: **Lilian, Lotte, Aafke, Sebastian, Amber, Tatum and Marije.**

The Facility: **Erik**, **Mark**, and **Simon.** I still sometimes remember the horrible FACS experiments in my first year that would last into the night or the coffee breaks, back in the days of the coffee table. Thanks for all your help over the years. Corrie and Suzanne, thank you for all your help over the years and for bringing fun to all the parties! Floris and Arjan, thank you for your help with the MS experiment!

Over the years my PhD has brought me to collaborate with amazing people, most notably the people from UNC-Chapel Hill who have been patient with my stupid questions about their devices. Not just that, but they even facilitated our visit to North Carolina where we had a great time. Thank you very much **Bill**, **Stephanie**, **Chloe**, **Wen**, **Wesley**, **Yu** and **Tim**. Another collaboration I enjoyed working on was with **Kim** on the topic of NFκB signaling. Because we have different backgrounds it was fun to see how our simple flow experiment could really contribute to your story!

Over my PhD I have shared the lab with many people from other groups as well who I would like to thank for having patience with me! It was a lot of fun “working” with you. **Seline, Leonie,** thanks for making things fun in the office during the pandemic times. **Hugo,** I am very glad you decided to leave Y4 and joined us at Y3. **Bart** and **Dieke,** I had an amazing time going to parties with you!

That brings me to another aspect of Sanquin, the amazing drinks at U2, kunstborrels, tuinfeesten and Radion of course. Before the pandemic this was a significant aspect of Sanquin PhD life and I would like to thank all the people who made that a memorable time. Specifically **Max** and **Bogac**, I really hope we can have a beer together again sometime. **Dorien**, it was always nice chatting to you with a glass of wine. **Giota, Natasja, Casper, Carlijn** and all the others.

Daarnaast zou ik ook graag mijn vrienden willen bedanken van al die jaren terug. **Tjalling**, **Frederik**, **Peter Paul**, **Florian**, **Dennis**, **Franck** en **Marius**. De vakanties en dagenlang spellen spelen was echt een heerlijke tijd!

Natuurlijk wil ik ook graag mijn familie bedanken, **Tom**, **Jolijn**, **Maud**, **Marit** en **Pim**. Ontzettend bedankt voor al jullie steun en hulp. Ik vind het altijd geweldig om te zien hoe we elkaar kunnen ondersteunen als we hulp nodig hebben, of dat nou bij een thesis is of een verhuizing.

Ten slotte wil ik graag **Vera** bedanken. Bedankt dat jij er was om me te steunen. Het afronden van de PhD was een hele uitdaging en ik ben je heel erg dankbaar dat jij er tijdens deze tijd voor me was. Heel erg bedankt voor alles!